UNIVERSITY OF CALIFORNIA, SAN DIEGO

Mesozooplankton responses to climate variability and contributions to microbial export

A dissertation submitted in partial satisfaction

of the requirements for the Degree Doctor of Philosophy

in

Oceanography

by

Bellineth Valencia Ramírez

Committee in charge:

Professor Michael R. Landry, Chair
Professor Andrew E. Allen
Professor Mark D. Ohman
Professor Brian Palenik
Professor Jonathan B. Shurin

2017

The dissertation of Bellineth Valencia Ramírez is approved, and it is acceptable in quality and form for publication on microfilm and electronically:

Chair

University of California, San Diego

2017

TABLE OF CONTENTS

LIST OF FIGURES

Chapter 1

Chapter 2

Chapter 3

Chapter 4

Chapter 1 Appendix

Chapter 2 Appendix

Chapter 4 Appendix

LIST OF TABLES

Chapter 1

Chapter 2

Chapter 3

Chapter 4

Chapter 1 Appendix

Chapter 2 Appendix

Chapter 4 Appendix

ACKNOWLEDGEMENTS

It was a long way for me to get here and I have a lot of people to thank. This dream likely started when I was an undergraduate (many many years ago!) and my professor of "Introduction to marine biology" showed the best research institutions in marine science in his first class…. Since then, I wanted to learn from the best, always with the dream to fill those gaps in knowledge in the Colombian Pacific and do the best possible science with our limited resources. Although unfortunately I cannot say that these were the best years of my life, I can definitely say that I learned a lot, not only about oceanography, but also about life, and I am grateful because of that. Some people would say "be careful what you wish for".

I want to specially thank my advisor Mike Landry for his support and patience during my path through graduate school. Thanks Mike for believing in me. Thanks for encouraging me to look for novel approaches to develop my research, for guiding me to see the big picture when I only could see the details, and for encouraging me to think critically. Thanks for giving me the time that I needed to dedicate exclusively to my research, I am able to finish my PhD in a "shorter" time because of your support.

I would also like to specially thank my committee members, Mark Ohman, Andy Allen, Brian Pallenik, and John Shurin for challenging and encouraging me to think critically. Your questions, advice, and support were fundamental during this learning process.

I would like to thank my professors at Scripps. I felt honored to be part of your classes and I learned a lot from all of you. Specially, I would like to thank Mark Ohman, Peter Franks, and Paul Dayton, whose great classes and knowledge inspired me.

On this road, I met wonderful people and I still feel overwhelmed by the smart and talented students at UCSD. Ali Freibott, I would not have survived my first (and in general all) year in grad school without your help, support, advice, and patience! I could not have had a better lab and officemate. Thanks for being there in the crazy hours of work during the cruises and in the lab. We cried and laugh together. We both went through difficult moments in our lives and I am grateful that you were there when I needed it the most. Thanks for the long discussions to try to figure out the challenges in our research, and of course, thanks for helping me editing a lot of my papers!

I would also like to thank my friends Ali, Maitreyi Nagarkar, and Lauren Manck. Thanks guys for being there in this crazy road of grad school and for reminding me that there is still life out there! Thanks for being so patient when I was only seeing the dark, I was carrying a heavy weight (literally!); thanks for sticking in there when I was able to smile again :) Thanks to Donata Giglio and Emily Troemel, it's so random how life led our paths to cross, but I am infinitely grateful for your friendship and support.

Thanks to my cohort, Regina Guazzo, Jess Garwood, Abby Cannon, Lilly McCormick, Ben Whitmore, Matt Costa, Josh Jones, and Adam J Schlenger. Thanks guys for your help during the long hours of study! Specially, thanks to Jess for teaching me how to program!

My research would not have been possible without the infinite help, support, and advice of a lot of people at Scripps, both during the long days of work at sea, and in the lab.

Thanks to the past and present members of the Landry lab, Ally Pasulka, Andrew Taylor, Rasmus Swalethorp, Jennifer Beatty. I would especially like to thank Moira Décima, Lorena Linacre, and Ali for their friendship and support, and Andrés Gutiérrez and Mike Stukel for their help, support, and advice during the cruises.

Thanks to the members of the Ohman lab, for their help and support at sea, specially to Jenni Brandon, Ben, Cat Nickels, and Laura Lilly. Special thanks to Linsey Sala for teaching me to identify the copepods of the California Current.

Thanks to the members of the Allen lab, for their help and advice during the long hours of work at JCVI. I did not know anything about molecular analysis and I learned a lot from all my mistakes! Special thanks to Ariel Rabines and Hong Zheng for their patience, time, and advice, to Maxine Tan and Taylor Cole for their company in the lab, and John McCrow for his help with the bioinformatic analyses.

Thanks to the PI's, students, and staff of the California Current Ecosystem - Long Term Ecological Research (CCE-LTER) program. Thanks for your help during the P1408 and P1604 cruises. Thanks to the participants of the student cruise P1507, specially to Brandon Stephens and Angel Ruacho for your leadership.

Thanks to the people in the Scripps Graduate Office for their help and support.

A ti Alan, muchas gracias por tu compañía, apoyo y ayuda, así te hayas mamado al final del camino. Gracias por todos los momentos maravillosos. Gracias por el infinito esfuerzo que hiciste, por los múltiples viajes, por dejarlo todo por mí. Gracias por tu apoyo incondicional en esos largos años de ausencia, por ayudarme a sobrellevar mi depresión, sigo aquí gracias a ti. Gracias por insistirme en que este camino valía la pena cuando ya había decidido tirar la toalla y no me quedaban más fuerzas para continuar.

Gracias a mi familia por su apoyo incondicional y por presionarme a seguir estudiando, soy gracias a ellos, una de las pocas afortunadas que tuvieron la oportunidad de estudiar fuera del país. Infinitas gracias a mi hermanito, Johans Valencia, gracias Sini por tu compañía y apoyo.

Infinitas gracias a Erica Gutiérrez. Gracias amiga por acogerme en tu casa cuando solo quería huir y por tus múltiples viajes a San Diego cuando más necesitaba compañía. Gracias Moira por tu paciencia con mis múltiples preguntas, pero sobre todo por tu apoyo y amistad.

My PhD was partially funded by a scholarship (No. 529 - 2011) from the Colombian Administrative Department of Science, Technology and Innovation (COLCIENCIAS), as well as by National Science Foundation Grants OCE-0324666, -0926766 and -1260164. Thanks to the staff of COLFUTURO for their support through my PhD. The data for my research at station ALOHA were possible thanks to the Hawaii Ocean Time series program, which also partially funded my PhD studies and travel to conferences. My research at the California Current was possible thanks to the CCE-LTER program, which funded the cruises, molecular analyses, and travel to conferences. Part of my molecular analyses were funded by the Graduate Student Excellence Research Award of the Scripps Institution of Oceanography.

Below is the content of the dissertation, either published, submitted, or in preparation for submission. I was the primary investigator and author on all manuscripts in this dissertation.

Chapter 1, in full, is a reprint of materials as it appears in Valencia B, Landry MR, Décima M, and Hannides CCS. (2016). Environmental drivers of mesozooplankton variability in the North Pacific Subtropical Gyre. *Journal of Geophysical Research: Biogeosciences*. 121: 3131–3143, doi:10.1002/2016JG003544. The dissertation author was the primary investigator and author of this manuscript.

Chapter 2, in full, has been submitted for publication of the material as it may appear in Valencia B, Décima M, Landry MR. Environmental effects on mesozooplankton size structure and export flux at station ALOHA, North Pacific Subtropical Gyre. *Global*

Biogeochemical Cycles. The dissertation author was the primary investigator and author of this manuscript.

Chapter 3, in full, is currently being prepared for submission for publication of the material with the following co-authors: Valencia B, Freibott A, McCrow JP, Allen AE, Landry MR. The dissertation author was the primary investigator and author of this paper.

Chapter 4, in full, is currently being prepared for submission for publication of the material with the following co-authors: Valencia B, Stukel MR, Allen A, McCrow JP, Rabines A, Palenik B, Landry MR. The dissertation author was the primary investigator and author of this paper.

VITA

2006 Bachelor of Science, Biology, Universidad del Valle

2010 Master of Science, Marine Ecology, Centro de Investigación Científica y de Educación Superior de Ensenada

2016 Teaching Assistant in California Current Oceanography, Scripps Institution of Oceanography, University of California San Diego

2017 Doctor of Philosophy, Oceanography, Scripps Institution of Oceanography at the University of California San Diego

PUBLICATIONS

Valencia B, Giraldo A. (2009). A new species of the genus *Chelorchestia* (Amphipoda, Talitridae) from Palma Island, Malaga Bay, Pacific coast of Colombia. Crustaceana. 82: 1-10.

Valencia B, Giraldo A. (2009). Hyperiids (Crustacea: Amphipoda) along the northern margin of the eastern tropical Pacific of Colombia. Latin American Journal of Aquatic Research. 37: 265-273.

Giraldo A, **Valencia B** Ramírez D. (2011). Planktonic productivity and local oceanographic variability in Gorgona Island, eastern tropical Pacific of Colombia 2006. Bulletin of Marine and Coastal Research. 40: 185-201.

Valencia B, Giraldo A. (2011). Structure of hyperiid amphipod assemblages on Isla Gorgona, eastern tropical Pacific off Colombia. Journal of the Marine Biological Association of the United Kingdom. 92: 1489-1499.

Valencia B, Lavaniegos B, Giraldo A, Rodríguez-Rubio E. (2013). Temporal and spatial variation of hyperiid amphipod assemblages in response to hydrographic processes in the Panama Bight, eastern tropical Pacific. Deep-Sea Research. 73: 46-61.

Martín A, Díaz Y, Miloslavich P, Escobar-Briones E, Gerra-García JM, Ortiz M, **Valencia B,** Giraldo A, Klein E. (2013). Regional diversity of Amphipoda in the Caribbean Sea. International Journal of Tropical Biology and Conservation. 61: 1681-1720.

Valencia B, Herrera L, Giraldo A. (2014). Community structure and vertical distribution of the soft bottom macrofauna on Isla Gorgona, Colombian Pacific Ocean. International Journal of Tropical Biology and Conservation. 62: 169-188.

Giraldo A, **Valencia B**, Acevedo JD, Rivera M. (2014). Seasonal variation of phytoplankton and zooplankton on Isla Gorgona, Pacific Ocean of Colombia, and its relationship with some hydrographic variables. International Journal of Tropical Biology and Conservation. 62: 117-132.

Valencia B, Landry MR, Décima M, Hannides CCS. (2016). Environmental drivers of mesozooplankton biomass variability in the North Pacific Subtropical Gyre. Journal of Geophysical Research: Biogeosciences. 121: 3131-3143.

ABSTRACT OF THE DISSERTATION

Mesozooplankton responses to climate variability and contributions to microbial export

by

Bellineth Valencia Ramírez

Doctor of Philosophy in Oceanography

University of California, San Diego, 2017

Professor Michael R. Landry, Chair

Mesozooplankton are key components of pelagic ecosystems and the biological pump, providing a critical food web link between microbes and higher trophic levels and contributing to the passive and active fluxes of carbon and other elements from the ocean surface. Thus, elucidating mesozooplankton responses to climate variability and their contributions to export

flux are integral to understanding potential changes in carbon and energy cycling and transfers in the sea. In my dissertation, I examine the roles of mesozooplankton in the biological pump, in two contrasting, but both important, pelagic ecosystems of the North Pacific by addressing the following questions: 1) What large-scale climate forces modulate mesozooplankton fluctuations in the North Pacific Subtropical Gyre (NPSG)? and 2) How do mesozooplankton affect the contribution of certain microbes to export flux in the California Current System (CCS)?

I document that mesozooplankton biomass at station ALOHA in the NPSG increased by 173% from 1994 to 2013. Using generalized additive models, I show a strong coupling between mesozooplankton fluctuations and primary production, although lagged transport effects on biomass due to large-scale changes in gyre circulation are also evident. This result differs from the transport-dominated influences reported for North Pacific boundary currents. I also show that despite the variability of biomass and primary production at station ALOHA, the size structure of the mesozooplankton community and active export fluxes mediated by migrants have remained relatively uniform. Years with an increased contribution of smaller zooplankton to total biomass and decreased active flux may be related to strong El Niño events.

Using metabarcoding analysis of salps, doliolids, and sediment traps, I evaluate the contribution of mesozooplankton to vertical export of microbes in the CCS. I show that the protists detected in fecal pellets of salps and doliolids vary between species and sampling locations, and that only some mixed-layer microbes contribute significantly to sinking particles. Thus, pelagic tunicate feeding enhances the export of certain microbes within their fast-sinking fecal pellets. My results also indicate that digestion resistance may be an important mechanism by which small phytoplankton such as *Synechococcus* remain recognizable in material exported to the deep sea.

INTRODUCTION

The biological pump and the role of mesozooplankton

The oceans and its biota play a key role in the carbon cycle and help modulate increasing atmospheric carbon dioxide (CO_2) levels from the burning of fossil-fuels (Ducklow *et al.,* 2001; Sabine *et al.,* 2004). The biological pump includes the processes by which inorganic carbon (CO_2) is incorporated into organic particles by photoautotrophic organisms in the euphotic zone, the transformation of these particles by food web interactions, and their behaviorally-mediated transport, gravitational settling, and sequestration into the deep ocean (Longhurst and Harrison, 1989; Ducklow *et al.,* 2001). Elucidating the mechanisms that affect the function and variability of the biological pump is integral to understanding the cycling of carbon and other elements in the sea (Sanders *et al.,* 2014).

The structure of plankton communities affects the efficiency and magnitude of the biological pump and therefore, the proportion of CO_2 fixed during photosynthesis that is exported to the mesopelagic zone (Frost, 1984; Michaels and Silver, 1988; Ducklow *et al.,* 2001). High export of particulate organic matter tends to occur in eutrophic regions where the phytoplankton communities are dominated by large micro-sized cells (20–200 μm), rather than in oligotrophic waters dominated by small pico- (0.2–2.0 μm) and nano-sized cells (2.0–20 μm; Michaels and Silver, 1988; Ducklow *et al.,* 2001; Sanders *et al.,* 2014). However, our knowledge of which microbes contribute most to carbon export is still limited and the mechanisms affecting microbial contributions to export remains under debate (Richardson and Jackson, 2007; Stukel and Landry, 2010).

Mesozooplankton, a diverse group of organisms in the size range of 0.2–20 mm, play key roles in modulating the export of microbes out of the euphotic zone and are major players in the biological pump (Steinberg and Landry, 2017). Mesozooplankton act as links between microbes and higher trophic levels (e.g., Beaugrand *et al.,* 2003) and contribute to the gravitational settling of organic matter from the euphotic zone by packaging small cells into fast-sinking fecal pellets (e.g., Turner and Ferrante, 1979). Large mesozooplankton, high biomass, and high flux of large fecal pellets in mesotrophic regions lead to a more efficient biological pump compared to that of oligotrophic sites (Steinberg *et al.,* 2008; Wilson *et al.,* 2008). Furthermore, due to respiration and excretion at daytime mesopelagic depths, some mesozooplankton actively export dissolved compounds out of the euphotic zone during diel vertical migrations (e.g., Longhurst and Harrison, 1988).

The contributions of mesozooplankton to the biological pump are determined by the composition and relative abundances of different taxonomic groups (e.g., Wexels Riser *et al.,* 2002; Wilson *et al.,* 2008), which are influenced in turn by fluctuations in environmental conditions and changes in large-scale ocean circulation (Reid *et al.,* 1978; McGowan *et al.,* 1998; Beaugrand and Reid, 2003; Di Lorenzo *et al.,* 2013). In the North Pacific, long-term fluctuations in the mesozooplankton community structure and biomass are linked to the Pacific Decadal Oscillation (PDO, Mantua *et al.,* 1997) and the North Pacific Gyre Oscillation (NPGO, Di Lorenzo *et al.,* 2008). In the northeastern (Keister *et al.,* 2011; Chenillat *et al.,* 2012; Di Lorenzo and Ohman, 2013) and northwestern Pacific (Chiba *et al.,* 2006, 2013), fluctuations of the PDO and the NPGO are documented to affect primary productivity and mesozooplankton community structure due to changes in transport, vertical mixing, wind patterns, and strength and timing of upwelling (Di Lorenzo *et al.,* 2013). Relative to boundary current systems, much less

is known about mesozooplankton responses to changes in climate in the central oligotrophic gyres.

As contributions to long-term ecological programs in the central North Pacific (Hawaii Ocean Time series, HOT) and eastern North Pacific (California Current Ecosystem Long-Term Ecological Research, CCE-LTER), my dissertation addresses the following broad questions:

- What large-scale climate forces are the main drivers of mesozooplankton fluctuations in the North Pacific Subtropical Gyre, and how do they impact the contributions of mesozooplankton to the biological pump?

- How do the trophic interactions of mesozooplankton in the southern California Current System affect the contributions of certain phytoplankton groups to export flux?

Mesozooplankton in the oligotrophic North Pacific

The North Pacific Subtropical Gyre (NPSG) is the largest ecosystem in the ocean and was initially described as homogenous, stable, and predictable due to the apparent low spatiotemporal variability of the environmental conditions and plankton communities (Hayward *et al.,* 1983). As a result of the low nutrient availability in the euphotic zone, early studies recognized that productivity in the NPSG is low and largely recycled within the euphotic zone (Hayward *et al.,* 1983). Mesozooplankton were characterized by the lack of spatial, seasonal, and interannual changes (Hayward *et al.,* 1983), and community structure was thought to be regulated by *in situ* processes (Hayward and McGowan, 1979).

Although these studies elucidated important characteristics of the plankton communities in the NPSG, the conclusions with regard to ecosystem dynamics were based on sampling schemes that did not properly represent the spatiotemporal variability of the region (Karl, 1999).

Recognizing these limitations, with the goal of improving our understanding of the role of the NPSG in the cycling of carbon and other elements in the sea, systematic sampling at approximate monthly intervals started at station ALOHA (A Long-Term Oligotrophic Habitat Assessment) in 1988 with the initiation of the Hawaii Ocean Time series program (HOT; Karl and Lukas, 1996). The mesozooplankton component of the HOT program was added in 1994.

Contrary to the steady-state view, sampling at station ALOHA has demonstrated a clear seasonal cycle in the plankton community, characterized by a summertime increase in primary production (Dore *et al.,* 2008) and mesozooplankton biomass (Landry *et al.,* 2001). Likewise, a significant long-term increase in primary production (1988–2008) and mesozooplankton biomass (1994–2002) were documented by Saba *et al.* (2010) and Sheridan and Landry (2004), respectively. Variability in primary production was linked to fluctuations of the NPGO, with less consistent and weaker effects from the Multivariate ENSO index (MEI) and the PDO (Dave and Lozier, 2010; Saba *et al.* 2010). Chiaverano *et al.* (2013) reported a positive linear relationship between primary production and mesozooplankton biomass. However, our understanding of which large-scale climate forces modulate the temporal variability of mesozooplankton biomass in the NPSG has remained limited.

In addition to affecting mesozooplankton biomass, variability in primary production has been associated with changes in the size structure of mesozooplankton communities, which has implications for energy transfer efficiency in the food web and for export flux to the deep ocean (e.g., Rodríguez and Mullin, 1986a,b; Rykaczewski and Checkley, 2008; Garcia-Comas *et al.,* 2014). At station ALOHA, the primary producers are small and thus, direct mesozooplankton grazing impact is considerably low as they mainly prey upon nano and microzooplankton (Calbet and Landry, 1999). Although their food resources are limited, mesozooplankton contribute

directly to passive export flux in the NPSG by concentrating smaller prey into fast-sinking fecal pellets. The flux of fecal pellets contributes considerably to the particulate carbon flux, although the magnitude of the estimates depends on whether they are based on microscopical analyses of sediment traps (Wilson *et al.,* 2008) or empirical metabolic relationships (Roman *et al.,* 2002). In addition, mesozooplankton actively contribute to export of carbon and other elements from the euphotic zone through diel vertical migration, by feeding in surface waters at night and releasing metabolic by-products in mesopelagic waters during the day (Longhurst and Harrison, 1988, 1989). At station ALOHA, active export mediated by migrant mesozooplankton has been estimated to account for an additional 19%, 38%, and 78% on average of the carbon, nitrogen, and phosphorous collected in sediment traps (Al-Mutairi and Landry, 2001; Hannides *et al.,* 2009). However, to better characterize the role of mesozooplankton in the cycling of carbon and other elements in the NPSG, it is important to understand how mesozooplankton biomass, size structure, and export contributions respond to environmental variability in a changing ocean.

Mesozooplankton in the California Current System

As the eastern boundary current of the North Pacific, the California Current System (CCS) is a productive and dynamic coastal upwelling region characterized by contrasting oceanographic conditions (Hayward and Venrick, 1998; Checkley and Barth, 2009). In the seasonally productive inshore region, the phytoplankton community is diverse and dominated by large cells, such as diatoms and dinoflagellates. In the offshore region, the cells are small, abundance and biomass are low, and species composition more closely resembles the oligotrophic central North Pacific (Venrick, 2002; Taylor *et al.*, 2015). Although it is expected that large cells dominate export flux in the productive inshore region of the CCS, the relative

contributions of different phytoplankton groups to export across the environmental gradient is not yet known.

In addition to the contrasting inshore-offshore environmental conditions, variability at seasonal, interannual, and decadal scales in the CCS is reflected in changes in the composition of plankton communities, productivity, and particle export (McGowan *et al.,* 1998; Checkley and Barth, 2009; Lavaniegos and Ohman, 2007; Wilson *et al.,* 2013; Peterson *et al.,* 2017). Anomalously warm conditions (sea surface temperature anomalies > 2°C) prevailed in the region during the period of my dissertation research, from late 2013 to 2016. Initially, these anomalously warm waters extended southward from Alaska and affected the North Pacific, where it was known as the "blob" (Bond *et al.,* 2015). In the subsequent 2015-2016 El Niño event, the warm water conditions extended northward from the equatorial region (McClatchie *et al*., 2016). During warm events, productivity in the CCS tends to decrease and plankton communities shift towards a higher dominance of smaller tropical-subtropical and open-ocean taxa, affecting higher trophic levels (Chavez *et al.,* 2002; Peterson *et al.,* 2002; Keister *et al.,* 2011; Peterson *et al.,* 2017) and likely, the composition of the microbes contributing to export.

With the aim of understanding the mechanisms by which climate forcing affects pelagic ecosystems in the CCS, process cruise studies of the California Current Ecosystem – Long-Term Ecological Research (CCE-LTER) Program were carried out during the anomalous warm summer 2014 and spring 2016. The CCE-LTER has conducted systematic monitoring and experimental studies of long-term trends, ecosystem processes, and ecological modeling since 2004 (Ohman *et al.,* 2013). Because water-column and mesozooplankton samples as well as sinking particles in sediment traps are routinely collected during the cruises, the CCE-LTER

program provided an opportunity to evaluate how mesozooplankton trophic interactions affect microbial contributions to particle flux in a habitat with contrasting environmental conditions.

In the southern CCS, copepods generally dominate mesozooplankton biomass (Lavaniegos and Ohman, 2007); however, during the anomalously warm years of 2014-2016, conspicuous blooms of salps and doliolids occurred in the region. Pelagic tunicates (salps, doliolids, appendicularians, and pyrosomes) are important, although variable components of the mesozooplankton (Alldredge and Madin, 1982), but when swarms occur, they can greatly impact microbial communities both in the water column and on sinking particles (Madin, 1974; Silver and Bruland, 1981). Because pelagic tunicates are non-selective feeders, their diet generally reflects the microbial assemblages present in the water column (Madin, 1974; Silver and Bruland, 1981), and particles as small as picoplankton can be trapped in their mucous feeding nets and incorporated into fecal pellets (Silver and Bruland, 1981; Sutherland *et al.,* 2010). In turn, the mucous feeding net gets rolled into a dense mass that forms tabular fecal pellets that sink very fast, up to ~ 2.7 km d^{-1} in some salps (Bruland and Silver, 1981; Madin, 1982). Thus, pelagic tunicates represent an important export mechanism for small cells compared to other zooplankton groups (Madin, 1974, 1982; Bruland and Silver, 1981; Pfannkuche and Lochte, 1993). Together, due to their non-selective feeding, high rates of fecal pellet production, and fast-sinking pellets, pelagic tunicates contribute disproportionately to total carbon flux during blooms (Bruland and Silver, 1981; Iseki, 1981; Smith *et al.,* 2014). The blooms of salps and doliolids observed in the CCS during the anomalous warm years thus likely had an important impact on production, plankton size spectra, and export fluxes, creating a unique opportunity to assess the potential contributions of pelagic tunicates to microbial export.

Previous modeling, grazing experiments, and sediment trap analyses indicate that the microbes associated with the exported particles will likely reflect the species that are consumed by mesozooplankton and modified by differential digestion (Knauer *et al.,* 1979; Small *et al.,* 1987; Stukel and Landry, 2010; Stukel *et al.,* 2011, 2013, 2017), though some phytoplankton might also arrive via aggregate formation and direct sinking (Alldredge and Gotschalk, 1989). Phytoplankton exported from the euphotic zone are usually identified via microscopical analyses of the particles collected in sediment traps (e.g., Beaulieu and Smith, 1998) or via pigment analyses of samples from the euphotic and mesopelagic zones (e.g., Lomas and Moran, 2011). However, these methods only give a partial picture of all the taxa involved due to the difficulty of identifying cells that have been packaged in aggregates and mesozooplankton fecal pellets, and due to pigment degradation (Amacher *et al.,* 2013). Traditionally, only large photosynthetic microbes with heavy mineral tests, such as diatoms, were thought to significantly contribute to particle flux (Michaels and Silver, 1988). More recently, molecular techniques have been used to characterize the exported photosynthetic microbes, demonstrating that small phytoplankton in the pico- and nano-size ranges are often significantly associated with export flux (e.g., Amacher *et al.,* 2013; Guidi *et al.,* 2016). However, their relative importance to carbon flux and the mechanisms involved in their sinking, attachment to particle aggregates (Richardson and Jackson, 2007) in comparison with resistance to digestion within mesozooplankton guts (Stukel and Landry, 2010), are matters of debate.

To help elucidate which phytoplankton groups contribute disproportionately to particle flux across the contrasting environmental conditions in the CCS, I used metabarcoding analyses to a) characterize the microbes potentially exported due to mesozooplankton trophic interactions by comparing the microbial assemblages in the water column and in the guts and fecal pellets of

three species of salps (*Salpa aspera, Cyclosalpa affinis,* and *Pegea socia*) and one doliolid (*Doliolum denticulatum*), and to b) assess the microbes associated with sinking particles collected in sediment traps below the euphotic zone, in comparison to those associated with the food web in the overlying water column.

Dissertation outline

The goal of this dissertation is to examine the role of mesozooplankton in the biological pump in two contrasting, but both important, pelagic ecosystems of the North Pacific. The first half of the dissertation (Chapters 1-2) evaluates how changes in the environment modulate mesozooplankton biomass in the central North Pacific using the long-term biomass data collected at station ALOHA since 1994. The second half of the dissertation (Chapters 3-4) focuses on the roles of mesozooplankton in microbial export in the CCS based on sampling conducted during cruises in 2014 and 2016.

In Chapter 1, I evaluated the large-scale climate forces that modulate the temporal variability of mesozooplankton biomass at station ALOHA from 1994 to 2013. I found that annual variability of mesozooplankton biomass is significantly influenced by primary productivity, 4-year lagged NPGO, and 4-year lagged PDO. This study highlights a strong coupling between mesozooplankton fluctuations and primary production for subtropical waters, although lagged transport effects are also evident. Chapter 1 was published in full as Valencia B, Landry MR, Décima M, and Hannides CCS. (2016). Environmental drivers of mesozooplankton variability in the North Pacific Subtropical Gyre in the *Journal of Geophysical Research: Biogeosciences.* 121: 3131–3143, doi:10.1002/2016JG003544.

In Chapter 2, I evaluated how changing environmental conditions have affected mesozooplankton size structure and their potential contributions to export flux in the NPSG via

grazing and passive export in comparison with active vertical migration. I found that mesozooplankton size structure is significantly influenced by sea surface temperature, mainly driven by the strong 1997–1998 El Niño, and by primary production. This study highlights that increasing productivity led to greater evenness of the size spectra and a higher potential contribution of mesozooplankton fecal pellets to passive export flux. However, the biomass of diel migrants, and hence the active export of dissolved compounds, did not vary systematically with productivity. Chapter 2, in full, has been submitted for publication of the material as it may appear in Valencia B, Décima M, Landry MR. Environmental effects on mesozooplankton size structure and export flux at station ALOHA, North Pacific Subtropical Gyre. *Global Biogeochemical Cycles.*

In Chapter 3, entitled "The role of salps and doliolids in feeding and export of protists during two anomalously warm years in the California Current System", I used metabarcoding analysis to characterize the potential role of salps and doliolids in protist export. I found that in each species, the potential prey detected were significantly different than the protistan assemblages in the water column, among individuals collected at different locations, and between the guts and fecal pellets of individuals at the same location. However, these differences were largely due to changes in relative abundances rather than shifts in the prey detected. This study highlights that differences in digestion resistance of some taxa may explain the differences observed, which could be the result of the higher resolution of metabarcoding analysis compared to microscopy.

In Chapter 4, entitled "Microbial communities associated with sinking particles across an environmental gradient in the California Current System", I used metabarcoding analysis to evaluate the prokaryotic and protistan communities in the water column and in particles collected

in sediment traps in the CCS. I found that particle-associated microbial assemblages were distinctly different from the ambient water-column communities, and differences were also evident for protists across the ecosystem gradient. In addition, I found that only some mixed-layer microbes contributed significantly to sinking particles. This study highlights the need for better resolve taxon-specific contributions to sinking flux in terms of carbon versus DNA relative abundances.

Overall, using mesozooplankton biomass data, I documented the responses of the mesozooplankton community to the long-term increase in primary production in the NPSG. Understanding these responses is important (increase in mesozooplankton biomass, more even distribution of biomass across size classes, export flux mediated by mesozooplankton), considering that the future trends in productivity in the NPSG remain uncertain. Likewise, using metabarcoding analysis, I documented with an unprecedented detail the microbes potentially exported from the euphotic zone in the CCS. However, to better resolve taxon-specific contributions to upper-ocean productivity and particle export in terms of carbon, food-web studies are also necessary in addition to DNA relative abundances.

References

Alldredge AL, Madin LP. (1982). Pelagic Tunicates: Unique Herbivores in the Marine Plankton. BioScience **32:** 655–663.

Alldredge AL, Gotschalk CC. (1989). Direct observations of the mass flocculation of diatom blooms: characteristics, settling velocities and formation of diatom aggregates. Deep Sea Res Part I **36:** 159–171.

Al-Mutairi H, Landry MR. (2001). Active export of carbon and nitrogen at Station ALOHA by diel migrant zooplankton. Deep Sea Res Part II **48:** 2083–2103.

Amacher J, Neuer S, Lomas M. (2013). DNA-based molecular fingerprinting of eukaryotic protists and cyanobacteria contributing to sinking particle flux at the Bermuda Atlantic time-series study. Deep Sea Res Part II **93:** 71–83.

Beaugrand G, Reid PC. (2003). Long-term changes in phytoplankton, zooplankton and salmon related to climate. Glob Change Biol **9:** 801–817.

Beaugrand G, Brander KM, Lindley JA, Souissi S, Reid PC. (2003). Plankton effect on cod recruitment in the North Sea. Nature **426:** 661–664.

Beaulieu SE, Smith KL. (1998). Phytodetritus entering the benthic boundary layer and aggregated on the sea floor in the abyssal NE Pacific: Macro-and microscopic composition. Deep Sea Res II **45:** 781–815.

Bond NA, Cronin MF, Freeland H, Mantua N. (2015). Causes and impacts of the 2014 warm anomaly in the NE Pacific. Geophys Res Lett **42:** 3414–3420.

Bruland KW, Silver MW. (1981). Sinking rates of fecal pellets from gelatinous zooplankton (salps, pteropods, doliolids). Mar Biol **63**: 295–300.

Calbet A, Landry MR. (1999). Mesozooplankton influences on the microbial food web: direct and indirect trophic interactions in the oligotrophic open ocean. Limnol Oceanogr **44:** 1370–1380.

Chavez FP, Pennington JT, Castro CG, Ryan JP, Michisaki RP, Schlining B, Walz P, Buck KR, McFadyen A, Collins CA. (2002). Biological and chemical consequences of the 1997–1998 El Niño in central California waters. Prog Oceanogr **54:** 205–232.

Checkley DM, Barth JA. (2009). Patterns and processes in the California Current System. Prog Oceanogr **83:** 49–64.

Chenillat F, Rivière P, Capet X, Di Lorenzo E, Blanke B. (2012). North Pacific Gyre Oscillation modulates seasonal timing and ecosystem functioning in the California Current upwelling system. Geophys Res Lett **39:** L01606. doi:10.1029/2011GL049966.

Chiaverano LM, Holland BS, Crow GL, Blair L, Yanagihara AA. (2013). Long-term fluctuations in circalunar beach aggregations of the box jellyfish *Alatina moseri* in Hawaii, with links to environmental variability. PLoS ONE. **8:** e77039. doi:10.1371/journal.pone.0077039.

Chiba S, Tadokoro K, Sugisaki H, Saino T. (2006). Effects of decadal climate change on zooplankton over the last 50 years in the western subarctic North Pacific. Glob Change Biol **12:** 907–920.

Chiba S, Di Lorenzo E, Davis A, Keister JE, Taguchi B, Sasai Y, Sugisaki H. (2013). Large-scale climate control of zooplankton transport and biogeography in the Kuroshio-Oyashio Extension region. Geophys Res Lett **40:** 5182–5187.

Dave AC, Lozier MS. (2010). Local stratification control of marine productivity in the subtropical North Pacific. J Geophys Res **115:** C12032. doi:10.1029/2010JC006507.

Di Lorenzo E, Ohman MD. (2013). A double-integration hypothesis to explain ocean ecosystem response to climate forcing. Proc Natl Acad Sci U.S.A **110:** 2496–2499.

Di Lorenzo E, Schneider N, Cobb KM, Franks PJS, Chhak K, Miller AJ. (2008). North Pacific Gyre Oscillation links ocean climate and ecosystem change. Geophys Res Lett **35:** L08607. doi:10.1029/2007GL032838.

Di Lorenzo E, Combes V, Keister JE, Strub PT, Thomas AC, Franks PJ. (2013). Synthesis of Pacific Ocean climate and ecosystem dynamics. Oceanography **26:** 68–81.

Dore JE, Letelier RM, Church MJ, Lukas R, Karl DM. (2008). Summer phytoplankton blooms in the oligotrophic North Pacific Subtropical Gyre: Historical perspective and recent observations. Prog Oceanogr **76:** 2–38.

Ducklow HW, Steinberg DK, Buesseler KO. (2001). Upper ocean carbon export and the biological pump. Oceanography **14:** 50–58.

Frost BW. (1984). Utilization of phytoplankton production in the surface layer. In: Global Ocean Flux Study: Proceedings of a Workshop. Woods Hole, Massachusetts. National Academy Press. p. 125–135.

García-Comas C, Chang CY, Ye L, Sastri AR, Lee YC, Gong GC, Hsieh CH. (2014). Mesozooplankton size structure in response to environmental conditions in the East China Sea: How much does size spectra theory fit empirical data of a dynamic coastal area? Prog Oceanogr **121:** 141–157.

Guidi L, Chaffron S, Bittner L, Eveillard D, Larhlimi A, Roux S, Darzi Y, Audic S, Berline L, Brum JR, Coelho LP, Espinoza JCI, Malviya S, Sunagawa S, Dimier C, Kandels-Lewis S, Picheral M, Poulain J, Searson S, Tara Oceans Consortium Coordinators, Stemmann L, Not F, Hingamp P, Speich S, Follows M, Karp-Boss L, Boss E, Ogata H, Pesant S, Weissenbach J, Wincker P, Acinas SG, Bork P, de Vargas C, Iudicone D, Sullivan MB, Raes J, Karsenti E, Bowler C, Gorsky G. (2016). Plankton networks driving carbon export in the oligotrophic ocean. Nature **532:** 465–470.

Hannides CC, Landry MR, Benitez-Nelson CR, Styles RM, Montoya JP, Karl DM. (2009). Export stoichiometry and migrant-mediated flux of phosphorus in the North Pacific Subtropical Gyre. Deep Sea Res Part I. **56:** 73–88.

Hayward TL, McGowan JA. (1979). Pattern and structure in an oceanic zooplankton community. Amer Zool **19:** 1045–1055.

Hayward TL, Venrick EL. (1998). Nearsurface pattern in the California Current: coupling between physical and biological structure. Deep Sea Res II **45:** 1617–1638.

Hayward TL, Venrick EL, McGowan JA. (1983). Environmental heterogeneity and plankton community structure in the central North Pacific. J Mar Res **41:** 711–729.

Iseki K. (1981). Particulate organic matter transport to the deep sea by salp fecal pellets. Mar Ecol Prog Ser **5:** 55–60.

Karl DM. (1999). A sea of change: Biogeochemical variability in the North Pacific Subtropical Gyre. Ecosystems **2:** 181–214.

Karl DM, Lukas R. (1996). The Hawaii Ocean Time-series (HOT) program: Background, rationale and field implementation. Deep Sea Res **43:** 129–156.

Keister JE, Di Lorenzo E, Morgan CA, Combes V, Peterson WT. (2011). Zooplankton species composition is linked to ocean transport in the Northern California Current. Glob Chang Biol **17:** 2498–2511.

Knauer GA, Martin JH, Bruland KW. (1979). Fluxes of particulate carbon, nitrogen, and phosphorus in the upper water column of the northeast Pacific. Deep Sea Res Part I **26:** 97–108.

Landry MR, Al-Mutairi H, Selph KE, Christensen S, Nunnery S. (2001). Seasonal patterns of mesozooplankton abundance and biomass at Station ALOHA. Deep Sea Res II **48:** 2037–2061.

Lavaniegos BE, Ohman MD. (2007). Coherence of long-term variations of zooplankton in two sectors of the California Current System. Prog Oceanogr **75:** 42–69.

Lomas MW, Moran SB. (2011). Evidence for aggregation and export of cyanobacteria and nano-eukaryotes from the Sargasso Sea euphotic zone. Biogeosciences **8:** 203–216.

Longhurst AR, Harrison WG. (1988). Vertical nitrogen flux from the oceanic photic zone by diel migrant zooplankton and nekton. Deep Sea Res **35:** 881–889.

Longhurst AR, Harrison WG. (1989). The biological pump: profiles of plankton production and consumption in the upper ocean. Prog Oceanogr **22:** 47–123.

Madin LP. (1974). Field observations on the feeding behavior of salps (Tunicata: Thaliacea). Mar Biol **25:** 143–147.

Madin LP. (1982). Production, composition and sedimentation of salp fecal pellets in oceanic waters. Mar Biol **67:** 39–45.

Mantua NJ, Hare SR, Zhang Y, Wallace JM, Francis RC. 1997. A Pacific interdecadal climate oscillation with impacts on salmon production. B Am Meteorol Soc **78:** 1069–1079.

McClathchie S, Goericke R, Leising A, Auth T, Bjorkstedt E, Robertson RR, Brodeur RD, Du X, Daly HA, Morgan CA, Chavez FP, Debich AJ, Hildebrand J, Field J, Sakuma K, Jacox MG, Kahru M, Kudela R, Anderson C, Lavaniegos BE, Gomez-Valdes J, Jiménez-Rosenberg SPA, McCabe R, Melin SR, Ohman MD, Sala LM, Peterson B, Fisher J, Schroeder ID, Bograd SJ, Hazen EL, Schneider SR, Olightly RTG, Suryan RM, Gladics AJ, Loredo S, Porquez JM, Thompson AR, Weber ED, Watson W, Trainer V, Warzybok P, Bradley R, Jahncke J. (2016). State of the California Current 2015–16: Comparisons with the1997–98 El Niño. CalCOFI Rep **57:** 5–61.

McGowan JA, Cayan DR, Dorman LM. (1998). Climate-ocean variability and ecosystem response in the Northeast Pacific. Science **281:** 210–217.

Michaels AF, Silver MW. (1988). Primary production, sinking fluxes and the microbial food web. Deep Sea Res Part I **35:** 473–490.

Ohman MD, Barbeau K, Franks PJS, Goericke R, Landry MR, Miller AJ. (2013). Ecological transitions in a coastal upwelling ecosystem. Oceanography **26:** 210–219.

Peterson WT, Keister JE, Feinberg LR. (2002). The effects of the 1997–99 El Niño/La Niña events on hydrography and zooplankton off the central Oregon coast. Prog Oceanogr **54:** 381–398.

Peterson WT, Fisher JL, Strub PT, Du X, Risien C, Peterson J, Shaw CT. (2017). The pelagic ecosystem in the Northern California Current off Oregon during the 2014–2016 warm anomalies within the context of the past 20 years. J Geophys Res Oceans **122:** 7267–7290.

Pfannkuche O, Lochte K. (1993). Open ocean pelago-benthic coupling: cyanobacteria as tracers of sedimenting salp faeces. Deep Sea Res Part I **40:** 727–737.

Reid JL, Brinton E, Fleminger A, Venrick EL, McGowan JA. (1978). Ocean circulation and marine life. In Advances in oceanography. pp. 65–130. Springer US.

Richardson TL, Jackson GA. (2007). Small phytoplankton and carbon export from the surface ocean. Science **315:** 838–840.

Rodríguez J, Mullin MM. (1986a). Diel and interannual variation of size distribution of oceanic zooplanktonic biomass. Ecology **67:** 215–222.

Rodríguez J, Mullin MM. (1986b). Relation between biomass and body weight of plankton in a steady state oceanic ecosystem. Limnol Oceanogr **31:** 361–370.

Roman MR, Adolf HA, Landry MR, Madin LP, Steinberg DP, Zhang X. (2002). Estimates of oceanic mesozooplankton production: a comparison using the Bermuda and Hawaii time-series data. Deep Sea Res II **49:** 175–192.

Rykaczewski RR, Checkley DM. (2008). Influence of ocean winds on the pelagic ecosystem in upwelling regions. Proc Natl Acad Sci U.S.A **105:** 1965–1970.

Saba VS, Friedrichs MA, Carr ME, Antoine D, Armstrong RA, Asanuma I. (2010). Challenges of modeling depth-integrated marine primary productivity over multiple decades: A case study at BATS and HOT. Global Biogeochem Cycles. **24:** GB3020, doi:10.1029/2009GB003655.

Sabine CL, Feely RA, Gruber N, Key RM, Lee K, Bullister JL, Wanninkhof R, Wong CS, Wallace DWR, Tilbrook B, Millero FJ, Peng TH, Kozyr A, Ono T, Rios AF. (2004). The oceanic sink for anthropogenic CO_2. Science **305:** 367–371.

Sanders R, Henson SA, Koski M, Christina L, Painter SC, Poulton AJ, Riley J, Salihoglu B, Visser A, Yool A, Bellerby R, Martin AP. (2014). The biological carbon pump in the North Atlantic. Prog Oceanogr **129:** 200–218.

Sheridan CC, Landry MR. (2004). A 9-year increasing trend in mesozooplankton biomass at the Hawaii Ocean Time-series Station ALOHA. ICES J Mar Sci **61:** 457–463.

Silver MW, Bruland KW. (1981). Differential feeding and fecal pellet composition of salps and pteropods, and the possible origin of the deep-water flora and olive-green "cells". Mar Biol **62:** 263–273.

Small LF, Knauer GA, Tuel MD. (1987). The role of sinking fecal pellets in stratified euphotic zones. Deep Sea Res I **34:** 1705–1712.

Smith KL, Sherman AD, Huffard CL, McGill PR, Henthorn R, Von Thun S, Ruhl HA, Kahru M, Ohman MD. (2014). Large salp bloom export from the upper ocean and benthic community response in the abyssal northeast Pacific: Day to week resolution. Limnol Oceanogr **59:** 745–757.

Steinberg DK, Landry MR. (2017). Zooplankton and the ocean carbon cycle. Ann Rev Mar Sci **9:** 413–444.

Steinberg DK, Cope JS, Wilson SE, Kobari T. (2008). A comparison of mesopelagic mesozooplankton community structure in the subtropical and subarctic North Pacific Ocean. Deep Sea Res II **55:** 1615–1635.

Stukel MR, Landry MR. (2010). Contribution of picophytoplankton to carbon export in the equatorial Pacific: A reassessment of food web flux inferences from inverse models. Limnol Oceanogr **55:** 2669–2685.

Stukel MR, Landry MR, Benitez-Nelson CR, Goericke R. (2011). Trophic cycling and carbon export relationships in the California Current Ecosystem. Limnol Oceanogr **56:** 1866–1878.

Stukel MR, Ohman MD, Benitez-Nelson CR, Landry MR. (2013). Contributions of mesozooplankton to vertical carbon export in a coastal upwelling system. Mar Ecol Prog Ser **491:** 47–65.

Stukel MR, Aluwihare LI, Barbeau KA, Chekalyuk AM, Goericke R, Miller A J. (2017). Mesoscale ocean fronts enhance carbon export due to gravitational sinking and subduction. P Natl Acad Sci **114:** 1252–1257.

Sutherland KR, Madin LP, Stocker R. (2010). Filtration of submicrometer particles by pelagic tunicates. P Natl Acad Sci **107:** 15129–15134.

Taylor AG, Landry MR, Selph KE, Wokuluk JJ. (2015). Temporal and spatial patterns of microbial community biomass and composition in the Southern California Current Ecosystem. Deep Sea Res Part II **112:** 117–128.

Turner JT, Ferrante JG. (1979). Zooplankton fecal pellets in aquatic ecosystems. BioScience **29:** 670–677.

Venrick EL. (2002). Floral patterns in the California Current System off southern California: 1990-1996. J Mar Res **60:** 171–189.

Wexels Riser C, Wassmann P, Olli K, Pasternak A, Arashkevich E. (2002). Seasonal variation in production, retention and export of zooplankton faecal pellets in the marginal ice zone and the central Barents Sea. J Mar Sys **38:** 175–188.

Wilson SE, Steinberg DK, Buesseler KO. (2008). Changes in fecal pellet characteristics with depth as indicators of zooplankton repackaging of particles in the mesopelagic zone of the subtropical and subarctic North Pacific Ocean. Deep Sea Res Part II **55:** 1636–1647.

Wilson SE, Ruhl HA, Smith Jr. KL. (2013). Zooplankton fecal pellet flux in the abyssal northeast Pacific: A 15 year time-series study. Limnol Oceanogr **58:** 881–892.

CHAPTER 1

Environmental drivers of mesozooplankton biomass variability in the North Pacific Subtropical Gyre

AGU PUBLICATIONS

JGR

Journal of Geophysical Research: Biogeosciences

RESEARCH ARTICLE

10.1002/2016JG003544

Environmental drivers of mesozooplankton biomass variability in the North Pacific Subtropical Gyre

Bellineth Valencia[1], Michael R. Landry[1], Moira Décima[2], and Cecelia C. S. Hannides[3]

[1]Scripps Institution of Oceanography, University of California, San Diego, La Jolla, California, USA, [2]National Institute of Water and Atmospheric Research, NIWA, Wellington, New Zealand, [3]Department of Geology and Geophysics, University of Hawai'i at Mānoa, Honolulu, Hawaii, USA

Key Points:
- Fluctuations in primary production are the main drivers of variability of mesozooplankton biomass at station ALOHA
- NPGO is the main climate pattern modulating productivity at station ALOHA
- MEI and PDO effects on mesozooplankton biomass were weaker and less consistent

Supporting Information:
- Supporting Information S1

Correspondence to:
B. Valencia,
bellival@ucsd.edu

Citation:
Valencia, B., M. R. Landry, M. Décima, and C. C. S. Hannides (2016), Environmental drivers of mesozooplankton biomass variability in the North Pacific Subtropical Gyre, *J. Geophys. Res. Biogeosci.*, *121*, 3131–3143, doi:10.1002/2016JG003544.

Received 3 JUL 2016
Accepted 16 NOV 2016
Accepted article online 21 NOV 2016
Published online 28 DEC 2016

Abstract The environmental drivers of zooplankton variability are poorly explored for the central subtropical Pacific, where a direct bottom-up food-web connection is suggested by increasing trends in primary production and mesozooplankton biomass at station ALOHA (A Long-term Oligotrophic Habitat Assessment) over the past 20 years (1994–2013). Here we use generalized additive models (GAMs) to investigate how these trends relate to the major modes of North Pacific climate variability. A GAM based on monthly mean data explains 43% of the temporal variability in mesozooplankton biomass with significant influences from primary productivity (PP), sea surface temperature (SST), North Pacific Gyre Oscillation (NPGO), and El Niño. This result mainly reflects the seasonal plankton cycle at station ALOHA, in which increasing light and SST lead to enhanced nitrogen fixation, productivity, and zooplankton biomass during summertime. Based on annual mean data, GAMs for two variables suggest that PP and 3–4 year lagged NPGO individually account for ~40% of zooplankton variability. The full annual mean GAM explains 70% of variability of zooplankton biomass with significant influences from PP, 4 year lagged NPGO, and 4 year lagged Pacific Decadal Oscillation (PDO). The NPGO affects wind stress, sea surface height, and subtropical gyre circulation and has been linked to mideuphotic zone anomalies in salinity and PP at station ALOHA. Our study broadens the known impact of this climate mode on plankton dynamics in the North Pacific. While lagged transport effects are also evident for subtropical waters, our study highlights a strong coupling between zooplankton fluctuations and PP, which differs from the transport-dominated climate influences that have been found for North Pacific boundary currents.

1. Introduction

Time series data have been increasingly used over the past decade to shed new light on the impacts of natural cycles of environmental variability on marine plankton communities and to assess their potential vulnerabilities to climate change [*Beaugrand and Reid*, 2003; *Chiba et al.*, 2006, 2012; *Piontkovski et al.*, 2006; *Ji et al.*, 2010; *Garcia-Comas et al.*, 2011]. Zooplankton time series are particularly valuable in this regard because zooplankton relate to important food-web functions such as export and trophic transfer [*Steinberg et al.*, 2012] and because the week-to-month generation times and motility of pelagic animals integrate over the high-frequency and fine spatial scales of environmental variability [*Mackas and Beaugrand*, 2010].

In the North Pacific Ocean, investigations of the environmental drivers of zooplankton variability have principally focused on the eastern and western boundary currents [*Di Lorenzo et al.*, 2013]. In the California Current, abrupt changes in zooplankton biomass and community structure on interannual scales are strongly linked to fluctuations of El Niño–Southern Oscillation (ENSO) [e.g., *Peterson et al.*, 2002; *Lavaniegos and Ohman*, 2007], while decadal-scale variability appears to be mainly modulated by fluctuations in transport processes associated with the Pacific Decadal Oscillation (PDO) [*Peterson and Keister*, 2003; *Hooff and Peterson*, 2006; *Keister et al.*, 2011; *Di Lorenzo and Ohman*, 2013]. In the western Pacific boundary currents, transport processes also account for observed anomalies in zooplankton community [*Chiba et al.*, 2013], but these are driven by lagged responses to the North Pacific Gyre Oscillation (NPGO), a climate mode that reflects variations in North Pacific wind stress and sea surface height [*Di Lorenzo et al.*, 2008].

Relative to boundary currents of the North Pacific, much less is known about plankton community responses to climate variability in the central oligotrophic region, the North Pacific Subtropical Gyre (NPSG). Station ALOHA (A Long-term Oligotrophic Habitat Assessment), sampled approximately monthly since 1988 by the

Hawaii Ocean Time-series (HOT) program, is the only regularly studied location in the vast NPSG region [*Karl and Lukas*, 1996]. The station occupies a position slightly north of the Hawaiian Islands (22.45°N, 158°W), where connections to ENSO, PDO, and NPGO modes of climate variability have been advanced to explain decadal-scale variability of plankton dynamics in the region. *Corno et al.* [2007] suggested that ENSO and PDO influences on upper ocean stratification and nutrient delivery may regulate primary production and phytoplankton community composition at station ALOHA. *Bidigare et al.* [2009] similarly argued based on a coupled physical-biological model that observed increases in productivity, photosynthetic eukaryotes, and zooplankton biomass from 1990 to 2004 were a consequence of shifts in PDO and ENSO states from positive to negative in the late 1990s, which reduced stratification and increased nutrient mixing. In contrast, *Dave and Lozier* [2010] did not find a relationship between stratification and primary production in the HOT data set, but they did note, as did *Saba et al.* [2010], a significant correlation between NPGO forcing and primary production, although weaker correlations with the PDO and the Multivariate ENSO Index (MEI) were also reported.

Previous studies suggest a strong coupling of zooplankton biomass to primary production at station ALOHA [*Sheridan and Landry*, 2004; *Chiaverano et al.*, 2013]. Seasonally, zooplankton biomass peaks are observed during the summer months of highest productivity [*Landry et al.*, 2001]. A 9 year increase of mesozooplankton biomass from 1994 to 2002 [*Sheridan and Landry*, 2004] also coincided with the period of increasing productivity, as highlighted by *Bidigare et al.* [2009]. Based on these observations, we hypothesize that North Pacific climate modes drive mesozooplankton biomass variability in the NPSG principally through their bottom-up influences on primary productivity. In the present study, we develop generalized additive models (GAMs) to investigate this hypothesis using 20 years of monthly and annual mean zooplankton biomass data at station ALOHA. These analyses provide new insights on the contributions of climate variability to zooplankton fluctuations in the North Pacific.

2. Materials and Methods

2.1. Sampling and Laboratory Analysis

Zooplankton samples were collected on 198 cruises from 1994 to 2013 at station ALOHA as part of the Hawaii Ocean Time-series (HOT) program. Oblique tows were taken through the euphotic zone (tow depth: 161 ± 35 m, mean $\pm$ standard deviation (SD)) with a 1 m^2 plankton net from February 1994 to August 2005 and with a 1 m diameter ring net from November 2005 to the present. Both nets used 202 μm Nitex mesh and were equipped with a General Oceanic flowmeter across the net mouth to measure volume-filtered and a time-depth recorder (Brancker XL-200 or Vemco logger) attached to the net frame to measure depth of tow. On most cruises, three samples were collected during midday (1000–1400) and three during the midnight (2200–0200). Onboard, a Folsom-split subsample (1/2, 1/4, or 1/8) from each tow was wet sieved through five mesh sizes (5, 2, 1, 0.5, and 0.2 mm), and each fraction was concentrated onto preweighed 200 μm Nitex filters, rinsed with isotonic ammonium formate to remove salt, and flash frozen in liquid nitrogen as described by *Landry et al.* [2001].

In the laboratory, dry weight (DW) biomass of each size fraction was determined (Denver Instrument analytical balance, 0.01 mg) after thawing and oven drying (60°C, at least 24 h). Weighed biomass was corrected for the volume of the subsample split, the volume of water filtered (m^3), the tow depth (m), and is presented as areal biomass: g DW m^{-2}. Cruise DW means were calculated from the sums of the five size fractions in each tow and the average of day and night tows. Three cruises were excluded because both day and night samples were not collected. Carbon and nitrogen estimates were also determined as %DW for each size fraction on at least one day and one night tow per cruise by combusting a measured subsample of finely ground-dried zooplankton in a CHN elemental analyzer against known standards [*Landry et al.*, 2001]. Here we use only the mean ratios to convert DW trends to approximate C equivalents.

2.2. Long-Term Trend Analysis

Mesozooplankton biomass data (DW) were transformed ($\log_{10}$) prior to analysis to meet the assumption of normality (Shapiro-Wilk test, $w = 0.99$, $p = 0.06$). The biomass trend was evaluated by the generalized least squares (GLS) approach to account for positive autocorrelations of residuals, which in this case means removing the influence of past biomass on that measured at a given later time. In GLS, autocorrelation is

modeled by including an autocorrelation structure that removes the independence restriction on residuals [*Zuur et al.*, 2007, 2009]. The model was fit as

$$\log_{10}(\mathrm{DW}) = a + bX + \varepsilon_m, \quad (1)$$

where a and b are the model coefficients, intercept, and slope, respectively; X is the covariate; and ε_m are the residuals at time m modeled with an autoregressive process (AR1) as

$$\varepsilon_m = \rho\varepsilon_{m-1} + \eta, \quad (2)$$

where ρ is the correlation parameter between lagged residuals and η is an error term.

Results of a GLS without (linear regression model) and with an autocorrelation structure AR1 were compared based on the Akaike information criterion (AIC), which measures goodness of fit and model complexity [*Zuur et al.*, 2009]. The GLS model gave a lower AIC value than the linear regression model. Model validation was performed by evaluating the assumptions of homogeneity of variances, normality, and independence of data based on graphical analyses of the normalized residuals (Figure S1 in the supporting information). Fitted values and coefficients presented in figures and tables correspond to detransformed values. Data analysis was performed using R and the function "gls" in the nlme package [*Pinheiro et al.*, 2015].

In addition to the trend analysis of mesozooplankton biomass, anomalies were calculated in order to evaluate deviations from the long-term mean. For this, monthly biomass anomalies (A'_m) were computed as

$$A'_m = \log_{10}(\bar{A}_m) - \log_{10}(\bar{A}_i), \quad (3)$$

where $\bar{A}_m$ is the biomass for each month sampled (e.g., January 1998) and $\bar{A}_m$ is the long-term average biomass for month i (e.g., mean of all Januarys). Annual anomalies were calculated as the means of the monthly anomalies for each year [*Mackas et al.*, 2001; *O'Brien et al.*, 2013].

2.3. Environmental Data

From the set of environmental data collected at station ALOHA (HOT website: http://hahana.soest.hawaii.edu/hot/hot-dogs/index.html), we used chlorophyll *a* concentrations from the upper euphotic zone (mg m^{-2}; integrated: 0–50 m) and the deep chlorophyll maximum (mg m^{-2}; integrated: 75–125 m), primary production (g C m^{-2} d^{-1}; integrated: 0–150 m), and sea surface temperature (°C; mean: 0–10 m) as the locally measured variables most likely to be associated with temporal changes in mesozooplankton biomass. As in *Saba et al.* [2010], primary production was calculated as light minus dark bottle values from 1994 to 2000 and subsequently by subtracting 5% from the light bottle values.

For basin-wide indices of ocean-atmosphere variability in the NPSG, we used the Multivariate ENSO Index (MEI), the North Pacific Gyre Oscillation (NPGO), and the Pacific Decadal Oscillation (PDO). The MEI monitors El Niño–Southern Oscillation based on changes over the tropical Pacific in sea level pressure, zonal and meridional components of surface wind, sea surface temperature, surface air temperature, and total cloudiness fraction. Positive MEI values indicate El Niño events, and negative values indicate La Niña events. Bimonthly mean values of the MEI were obtained from http://www.esrl.noaa.gov/psd/enso/mei/. The NPGO is defined as the second dominant mode of variability of sea surface height in the northeast Pacific and reflects changes in the intensity of the North Pacific gyre circulation [*Di Lorenzo et al.*, 2008]. Positive values of the NPGO indicate stronger gyre circulation. Monthly mean values of the NPGO were obtained from http://www.o3d.org/npgo/. The PDO is defined as the first mode of North Pacific sea surface temperature variability [*Mantua et al.*, 1997]. Monthly mean values of the PDO were obtained from http://research.jisao.washington.edu/pdo/.

2.4. Mesozooplankton Biomass and Environmental Factors

We used generalized additive models (GAMs) to evaluate what factors might be driving the high- and low-frequency variabilities of mesozooplankton biomass at monthly and annual scales. The GAM is a nonlinear regression technique that fits smooth functions through data to model the relationships between response variables and covariates [*Wood*, 2006; *Zuur et al.*, 2009]. Because GAMs do not assume a particular type of response function, they represent an effective modeling approach for assessing the responses of plankton communities to environmental factors [e.g., *Irwin and Finkel*, 2008; *Llope et al.*, 2009; *Otto et al.*, 2014].

Table 1. Summary of Mesozooplankton Biomass, Primary Production, and Sea Surface Temperature at Station ALOHA From 1994 to 2013[a]

	n	Mean	SD[b]	Min	Max
Mesooplankton biomass (g DW m^{-2}; integrated: 0 to ~160 m)	195	0.97	0.36	0.64 (1997)	1.39 (2011)
Primary production (g C m^{-2} d^{-1}; integrated: 0–150 m)	188	0.51	0.13	0.41 (1998)	0.61 (2000)
Sea surface temperature (°C; mean: 0–10 m)	195	24.90	1.18	24.21 (1999)	25.54 (2004)

[a]Data of environmental factors include only the months in which zooplankton samples were collected. Parenthesis indicate the years in which the minimum (min) and maximum (max) values were found.
[b]SD denotes standard deviation.

Prior to GAM runs for the HOT data, collinearity between covariates was identified from the variance inflation factor (VIF) using a value of less than 3 as a cutoff for inclusion of covariates in the models. Although upper water-column stratification, computed as the change in potential density between 0–10 m and 140–150 m [*Lavaniegos and Ohman*, 2007], was initially considered as a covariate, it was highly collinear with SST and therefore was not included in the analyses. For monthly mean data, we modeled the effects of primary production ($\log_{10}$PP; g C m^{-2} d^{-1}), sea surface temperature (SST; °C), MEI, NPGO, and PDO on mesozooplankton biomass ($\log_{10}$ DW) as

$$\log_{10}(\mathrm{DW}) = a + b(\log_{10}\mathrm{PP}) + f_1(\mathrm{SST}) + f_2(\mathrm{MEI}.ml) + f_3(NPGO.ml) + f_4(\mathrm{PDO}.ml) + \varepsilon, \quad (4)$$

where a is the intercept, b is a linear function, fi are the thin-plate regression spline functions describing the effects of environmental factors on biomass, and the error term $\varepsilon \approx N(0, \sigma_2)$. The lagged response of the mesozooplankton biomass to the climate patterns denoted as l, was evaluated by running the models with no lag (m_0) and with lags of 1 (m_1), 2 (m_2), or 3 (m_3) months (Table S1 in the supporting information). Because mesozooplankton samples were not collected for all 12 months in most years, for each lag, the three indices were matched with the respective month in which zooplankton data were available.

Annual means were calculated for mesozooplankton biomass and environmental factors to describe low-frequency fluctuations. However, primary production and 1 year lagged NPGO (NPGO.$y1$) were highly collinear (VIF > 3) and thus not included in the same run (Table S1). Likewise, high collinearity was found between MEI and PDO of the same year (VIF > 3), and thus, two separate sets of models were run:

$$\log_{10}(\mathrm{DW}) = a + b(\mathrm{SST}) + f_1(\log_{10}\mathrm{PP}) + f_2(\mathrm{NPGO}.yl) + f_3(\mathrm{MEI}.yl) + \varepsilon, \quad (5)$$

$$\log_{10}(\mathrm{DW}) = a + b(\mathrm{SST}) + f_1(\log_{10}\mathrm{PP}) + f_2(\mathrm{NPGO}.yl) + f_3(\mathrm{PDO}.yl) + \varepsilon, \quad (6)$$

Similar to the monthly mean analyses, the annual mean models were run with no lag (y_0) and with lags of 1 (y_1), 2 (y_2), 3 (y_3), or 4 (y_4) years (Table S1). Although chlorophyll *a* concentration was included initially in both monthly and annual mean models, it was not significant in either case and is therefore left out of the results reported here. In addition to the full models for monthly and annual means, the effect of each covariate on mesozooplankton biomass variability was evaluated by running GAMs for each covariate separately.

For both monthly and annual mean models, overfitting of the smooth functions was reduced by restricting the effective degrees of freedom (edf ≤ 4). For cases where edf was equal to 1 (linear relationship), models were rerun including the covariate as a linear term, as for example with primary production in the monthly mean models and sea surface temperature in the annual mean models. Full models were run for each combination of lagged indices, and a stepwise backward approach was applied in which nonsignificant covariates ($p > 0.05$) were removed. After the ensemble of models was obtained, the best monthly and annual models were selected based on minimizing the generalized cross-validation (GCV) criterion that measures the degree of penalization during fitting [*Wood*, 2006].

Model validation was done by graphical analyses of the residuals to evaluate the assumptions of homogeneity of variances, normality, and independence, as well as the model fit to observed values (Figures S2 and S3). Influential observations were evaluated by the Cook's distance (>0.5). These analyses were performed using R and the function "gam" in the mgcv package [*Wood*, 2006].

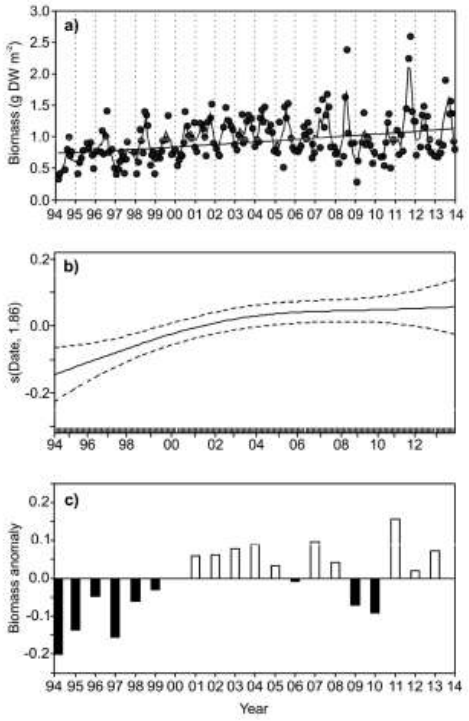

Figure 1. Mesozooplankton biomass (g DW m^{-2}) at station ALOHA from years 1994 to 2013. (a) Mean of day-night samples per cruise for the combined size fractions. Long-term increase in biomass is described by generalized least squares; the straight line corresponds to the detransformed predicted values ($n = 195$; intercept = 729 mg DW m^{-2}; slope = 20 mg DW m^{-2} yr^{-1}; 95% CI = 20–21 mg DW m^{-2} yr^{-1}; $p = 0.002$). Curved fit is a three-point moving average. (b) Biomass trend as described by generalized additive models; the solid line is the model fit, and the dashed lines are the 95% confidence intervals. (c) Biomass anomalies obtained as annual means of the monthly anomalies using transformed (log_{10}) dry weights.

3. Results

3.1. Temporal Variability in Mesozooplankton Biomass

Mesozooplankton biomass at station ALOHA averaged 0.97 g DW m^{-2} (±0.36 SD) and varied over 1 order of magnitude during the 20 year period analyzed (Table 1). Mean mesozooplankton biomass was 157% higher in 2013 (1.12 ± 0.41 g DW m^{-2}; mean ± SD) than at the beginning of the time series in 1994 (0.65 ± 0.24 g DW m^{-2}). Based on the GLS analysis, the long-term trend was significant with a mean rate of increase of 20 mg DW m^{-2} yr^{-1} (Figure 1a). To test if biomass has risen continuously over the study period, we ran a GAM of mesozooplankton biomass versus time that included an autocorrelation function AR1. Based on this analysis, mesozooplankton biomass increased rapidly during the first 10 years of the time series but has remained relatively constant since 2004 (Figure 1b). Annual biomass anomalies show negative values from 1994 to 1999 and mainly positive values since 2001, except during 2006 and 2009–2010. Strong negative anomalies like those registered from 1994 to 1997 have notably not occurred in the later time series data to date (Figure 1c).

3.2. Monthly Mean Model

The single function (two-variable GAM) of the monthly mean models that relates primary production, SST, NPGO, MEI, and PDO explained 22%, 14%, 11%, 8%, and 2% of mesozooplankton biomass variability, respectively (Table 2). Zooplankton biomass was not significantly associated with chlorophyll (Chl *a*) in the upper euphotic zone (0–50 m) or the deep chlorophyll maximum (Table 2). Based on the full GAM ensemble, the NPGO was the only climate index significantly related to mesozooplankton biomass, independent of a time lag up to 3 months (Table S2). The PDO was not significantly related to mesozooplankton biomass in any of the models, and the MEI was only significant when considered without lag (Table S2). The selected GAM for monthly mean data based on the GCV (and AIC > 2) indicates that local environmental factors, primary production, and SST, as well as basin-wide climate forcing, NPGO, and MEI (both indices without lag), are the most important environmental predictors of monthly changes in mesozooplankton biomass at station ALOHA (Table 3). Of these environmental factors, primary production accounts for about half of the variability explained by the model (Table 4). However, the final model explains less than 50% of total biomass variability (Table 3).

The relationship between mesozooplankton biomass and environmental factors in the final GAM for monthly mean data range from linear and positive for primary production (Figure 2a) and SST (Figure 2b) to nonlinear for the NPGO and the MEI, showing a saturated response for the NPGO (Figure 2c) and a complex response

Table 2. Two-Variable Generalized Additive Models With Monthly and Annual Mean Mesozooplankton Biomass at Station ALOHA Over the Period of 1994–2013[a]

Mean Monthly Model						Mean Annual Model					
	edf	R^2	DE (%)	GCV	*P* Value		edf	R^2	DE (%)	GCV	*P* Value
Chl.0–50m	1.9	0.01	1.8	0.0243	0.299	Chl.0–50m	1.00	0.09	14.1	0.0078	0.103
Chl.max	1.0	0.00	0.7	0.0244	0.239	Chl.max	1.00	0.00	5.2	0.0087	0.332
logPP	1.0	**0.22**	22.0	0.0194	**<0.001**	logPP	1.32	**0.43**	47.0	0.0050	**0.002**
SST	1.2	**0.14**	14.7	0.0209	**<0.001**	SST	1.00	0.03	7.7	0.0084	0.236
PDO.m0	1.0	**0.02**	2.7	0.0238	**0.023**	PDO.0	1.00	0.09	13.5	0.0079	0.110
PDO.m1	1.0	0.00	0.6	0.0244	0.302	PDO.y1	1.36	0.09	15.4	0.0080	0.154
PDO.m2	1.0	0.00	0.1	0.0245	0.697	PDO.y2	1.14	**0.22**	26.8	0.0068	**0.026**
PDO.m3	2.8	0.02	3.2	0.0242	0.254	PDO.y3	1.19	0.07	13.2	0.0081	0.242
						PDO.y4	1.00	−0.03	2.9	0.0089	0.475
NPGO.m0	2.3	**0.11**	11.8	0.0219	**<0.001**	NPGO.0	1.55	0.24	30.4	0.0068	0.075
NPGO.m1	1.9	**0.08**	8.9	0.0225	**<0.001**	NPGO.y1	1.29	**0.37**	41.6	0.0055	**0.010**
NPGO.m2	2.0	**0.08**	9.2	0.0225	**<0.001**	NPGO.y2	1.00	**0.32**	35.2	0.0059	**0.006**
NPGO.m3	2.1	**0.11**	12.0	0.0218	**<0.001**	NPGO.y3	1.00	**0.41**	44.1	0.0051	**0.001**
						NPGO.y4	1.13	**0.39**	42.8	0.0053	**0.004**
MEI.m0	3.8	**0.08**	9.6	0.0228	**0.001**	MEI.0	1.77	0.22	29.4	0.0070	0.086
MEI.m1	3.8	**0.07**	8.9	0.0230	**0.003**	MEI.y1	2.54	0.19	29.9	0.0077	0.158
MEI.m2	3.3	0.04	5.9	0.0236	0.061	MEI.y2	2.98	0.34	44.4	0.0064	0.048
MEI.m3	3.7	0.03	4.9	0.0240	0.058	MEI.y3	1.00	**0.17**	21.7	0.0072	**0.038**
						MEI.y4	1.00	0.15	19.2	0.0074	0.053

[a]Significant relationships are highlighted in bold. Chlorophyll values are averaged for the 0–50 m and 75–125 m depth strata. LogPP is log-transformed ($\log_{10}$) primary production, and SST is sea surface temperature. Pacific Decadal Oscillation (PDO), North Pacific Gyre Oscillation (NPGO), and Multivariate ENSO Index (MEI) are lagged 0, 1, 2, and 3 months for the monthly mean data and lagged 0, 1, 2, 3, and 4 years for the annual mean data. edf: effective degrees of freedom, DE: deviance explained, R^2: coefficient of determination, GCV: generalized cross validation.

for the MEI (Table 3 and Figure 2d). Mesozooplankton biomass is generally above the time series mean when primary production exceeds 0.48 g C m^{-2} d^{-1} (logPP = −0.32 g C m^{-2} d^{-1}) and SST is warmer than 25°C and below the mean when the NPGO index is negative (Figures 2a–2c). For the MEI, biomass varies relatively close to the mean when the index is neutral or negative and tends to decrease when the index is positive (MEI.m_0 > +1; Figure 2d).

3.3. Annual Mean Model

The single function (two-variable GAM) of the annual mean models that relates mesozooplankton biomass to primary production and 3 year lagged NPGO explained 43 and 41% of the biomass variability, respectively (Table 2). On the full GAM ensemble, annual biomass predictions were improved by averaging of the

Table 3. Relationship Between Mesozooplankton Biomass and Environmental Factors at Station ALOHA From 1994 to 2013[a]

Final Mean Monthly Model				Final Mean Annual Model			
	Estimate	SE	*P* Value		Estimate	SE	*P* Value
Intercept	−0.88	0.20	<0.001	Intercept	−0.05	0.01	<0.001
logPP	0.45	0.08	<0.001	NPGO.y4	0.05	0.01	0.001
SST	0.04	0.01	<0.001	PDO.y4	0.05	0.02	0.015
	edf		*P* Value		edf		*P* Value
NPGO.m0	2.74		<0.001	logPP	1.23		0.002
MEI.m0	3.75		0.004				
n	DE (%)	R^2	GCV	*n*	DE (%)	R^2	GCV
188	46	0.43	0.0147	20	75	0.70	0.0030

[a]Monthly and annual generalized additive model results are presented for the final models selected. logPP: $\log_{10}$ (primary production; g C m^{-2} d^{-1}), SST: sea surface temperature (°C), NPGO: North Pacific Gyre Oscillation (m_0: no lag, y_4: lag of 4 years), MEI.m0: Multivariate ENSO Index (no lag), PDO.y4: Pacific Decadal Oscillation (lag of 4 years), SE: standard error, edf: effective degrees of freedom, DE: deviance explained, R^2: coefficient of determination, GCV: generalized cross validation.

Table 4. Coefficient of Determination (R^2) for the Final Mean Monthly and Annual Models[a]

Mean Monthly Model			Mean Annual Model		
Covariate	R^2	%	Covariate	R^2	%
logPP, SST, NPGO.m0, MEI.m0	0.43	100	logPP, NPGO.y4, PDO.y4	0.70	100
logPP, SST, NPGO.m0	0.39	90	logPP, NPGO.y4	0.58	83
logPP, SST	0.32	75			
logPP	0.22	50	logPP	0.43	62
SST	0.14		NPGO.y4	0.39	
NPGO.m0	0.11		PDO.y4	−0.03	
MEI.m0	0.08				

[a]The percentage contribution to the variance explained by the final models is shown by omitting one covariate at a time, as well as by showing the effects of each individual covariate.

high-frequency month-to-month variability (Table S3). As with the monthly mean model, primary production was significant in all of the model combinations (Tables S2 and S3). From the set of annual mean models analyzed, two gave minor variations in GCV score (and AIC < 2). The first included nonlinear responses of mesozooplankton biomass to primary production and the 2 year lagged MEI. The second included mainly linear responses of biomass to primary production, the NPGO and the PDO, with both climate patterns lagged by 4 years (Table S3). Since the NPGO was significant in all monthly mean and in most of the annual mean models, it likely represents an important driver of variability of mesozooplankton biomass at station ALOHA. Hence, the model including the NPGO was selected to characterize the environmental factors that modulate mesozooplankton biomass at long temporal scales (Table 3).

In this selected model, the effects of primary production, the 4 year lagged NPGO, and the 4 year lagged PDO on biomass are mainly linear and positive and together account for 70% of the biomass variability (Table 3 and Figures 3a–3c). As in the monthly mean model, primary production accounts for most of the

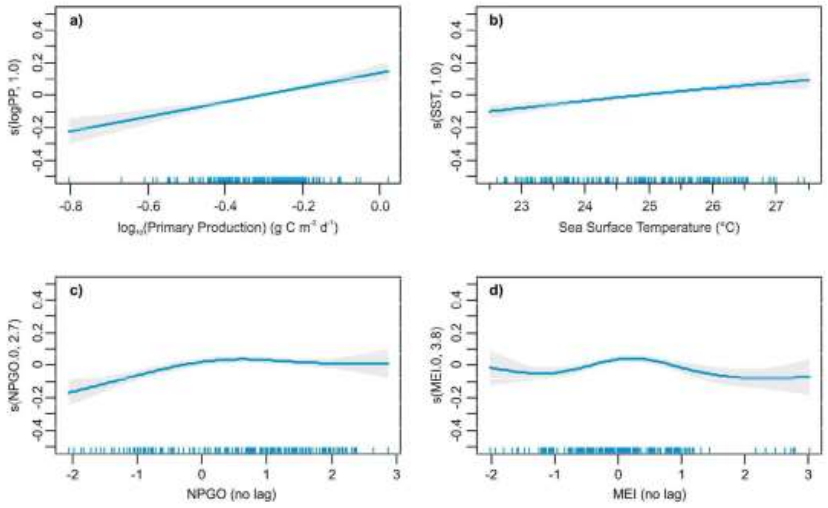

Figure 2. Relationships between monthly mean mesozooplankton biomass and environmental factors at station ALOHA. Partial regression plots represent the effects of four environmental factors on mesozooplankton biomass for the monthly mean generalized additive model selected. The *x* axes are the model covariates, and the tick marks represent each observation. The *y* axes represent the effects of covariates on predicted mesozooplankton biomass. The values are deviations from mean biomass and thus are centered. The numbers in parentheses are the effective degrees of freedom. The solid lines are the modeled trends (linear or smooth), and the shaded areas are the 95% confidence intervals. Predicted values of biomass are obtained by adding the deviations from each smooth function to the mean biomass.

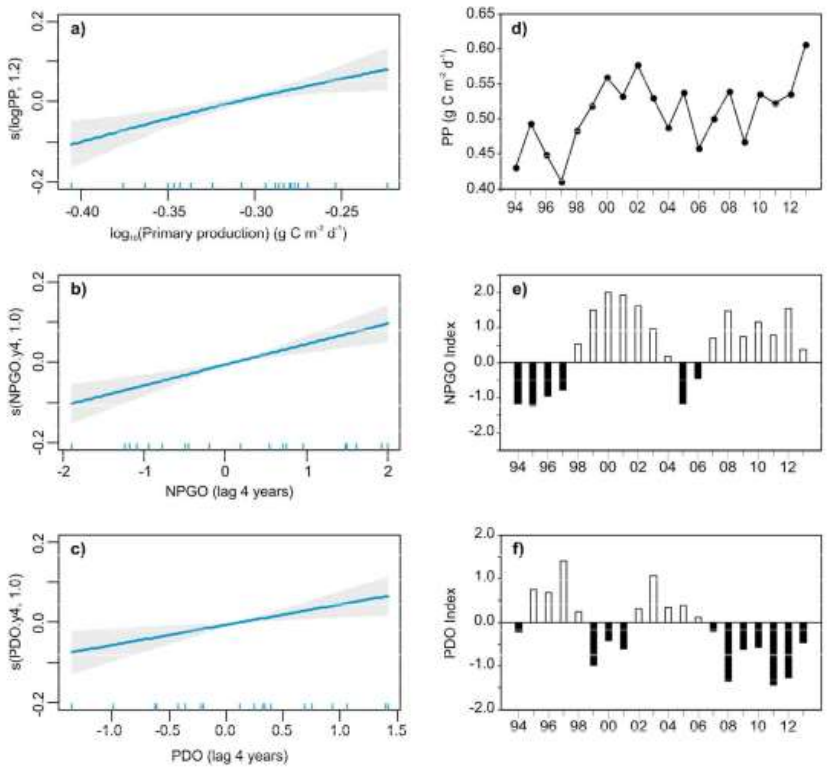

Figure 3. Relationships between annual mean mesozooplankton biomass and environmental factors at station ALOHA. Partial regression plots represent the effect of three environmental factors (primary production, NPGO, and PDO) on mesozooplankton biomass for the annual mean generalized additive model selected. Axes as described in Figure 3. Annual means of each covariate are shown on the right plot. PP: Primary production.

low-frequency variability of mesozooplankton biomass (62%), followed by the 4 year lagged NPGO, which explains 21%. Although the 4 year lagged PDO gave a negative coefficient of determination when the relationship with biomass was evaluated as a single function for each covariate (Table 2), indicating that its individual effect on biomass was insignificant, it explained 17% of biomass variability when considered in combination with primary production and the NPGO (Table 4). When the single function (two-variable GAM) that relates mesozooplankton biomass to the 4 year lagged PDO was plotted, the relationship was slightly negative, although variable (Figure S4), consistent with the generally opposite trends of the NPGO and PDO. Mesozooplankton biomass is generally above the mean when primary production exceeds 0.53 g C m^{-2} d^{-1} and when the 4 year lagged NPGO index is positive ($NPGO.y_4 > 0.2$; Figure 3).

Because the model that included primary production and the 2 year lagged MEI also performed well based on GCV and AIC, plots of the functions that relate mesozooplankton biomass to these two environmental factors are included in Figure S5. For this model, an influential observation was detected in the validation process (Cook's distance = 0.08 in 1997), suggesting that strong El Niño events might disproportionally have influenced the model results. According to this model, mesozooplankton biomass increases with primary production, but the increment decelerates at higher values of primary production. Nonetheless, when the association between biomass and primary production was assessed as a single function, the relationship was close to linear (edf: 1.32; Table 2), which is in agreement with the selected final model.

The lagged effect of the MEI was mainly negative; thus, biomass decreased when the index was positive (MEI. $y_0 > +0.5$; Figure S5).

4. Discussion

4.1. Plankton Variability in the North Pacific Subtropical Gyre (NPSG)

Although the NPSG was once viewed as system of pronounced constancy and homogeneity [*Hayward et al.*, 1983], time series sampling at station ALOHA has established that variability in plankton community dynamics occurs there at multiple scales [*Karl*, 1999; *Landry et al.*, 2001; *Sheridan and Landry*, 2004]. Seasonality at station ALOHA is characterized by increased sea surface temperature, stratification, and nitrogen fixation during summer, which is reflected in maxima of primary production and zooplankton biomass [*Landry et al.*, 2001; *Dore et al.*, 2008]. Episodic events such as winter storms, cyclonic mesoscale eddies, wind-driven Ekman pumping, and vertical transport of nitrate contribute to variability on shorter scales [*Karl*, 1999; *Dore et al.*, 2008; *Landry et al.*, 2008; *Johnson et al.*, 2010].

On longer time scales, *Sheridan and Landry* [2004] reported a decadal increase of mesozooplankton biomass in the NPSG based on the first 9 years of sampling at station ALOHA (1994–2002). The mean of day and nighttime biomass values give a rate of increase of 53 mg DW m^{-2} yr^{-1} (≈18 mg C m^{-2} yr^{-1}) over that time period. We show here that high biomass has persisted for an additional decade through 2013, but this has mainly occurred as the maintenance of the elevated values established prior to 2004, rather than an ongoing accumulation of zooplankton. Accordingly, the mean annual rate of change over the full 20 year period is substantially lower (20 mg DW m^{-2} yr^{-1} or 7 mg C m^{-2} yr^{-1}) than during the earlier sampling. Comparison with data from the CLIMAX program that monitored the NPSG from 1968 to 1974 has suggested that zooplankton biomass was likely lower then than at present, despite some ambiguities due to different locations and methodology [*Landry et al.*, 2001]. *Décima et al.* [2011] also found that mesozooplankton biomass in the eastern equatorial Pacific was significantly elevated in 2004–2005 cruises (80–90% higher) compared to similar measurements made during intensive U.S. Joint Global Ocean Flux Study investigations in the early 1990s. A similar switch from lower to higher zooplankton biomass occurred in the California Current System (CCS) during the late 1990s [*Lavaniegos and Ohman*, 2007]. There is thus some evidence to suggest long-term, basin-scale fluctuations in zooplankton biomass in the North Pacific, although the timelines and mechanisms that may connect them are not very clear.

Fluctuations in mesozooplankton biomass are strongly associated with primary productivity at station ALOHA [*Sheridan and Landry*, 2004; *Chiaverano et al.*, 2013]. *Steinberg et al.* [2012] reported a similar bottom-up relationship for a 17 year increase in zooplankton biomass in the Bermuda Atlantic Time-series Study (BATS) site in the subtropical North Atlantic. However, the rate (11 mg DW m^{-2} yr^{-1}) and overall percentage of biomass increase (61%) at BATS were lower than at station ALOHA, possibly reflecting differences in their autotrophic communities [*Steinberg et al.*, 2012] and food-web dynamics between the two regions [*Roman et al.*, 2002]. One additional relevant finding from the present analysis is the largely linear relationship between primary production and mesozooplankton biomass, which might not be expected for different reasons. Conventional thinking would suggest that higher productivity might be associated with an increase in larger phytoplankton and therefore more efficient coupling to mesozooplankton [*Landry*, 1977]. On the other hand, the fact that enhanced productivity at station ALOHA is linked to nitrogen-fixing cyanobacteria might be an argument for less efficient coupling due to unpalatable prey or perhaps increased aggregation and direct loss to sinking [*Hawser et al.*, 1992; *Bar-Zeev et al.*, 2013]. It would appear that neither of these mechanisms dominates to produce a nonlinear response of mesozooplankton biomass to enhanced productivity, which could simplify assumptions for regional modeling.

While the importance of primary production is highlighted in our analysis, it is equally useful to consider the variables that emerged as insignificant for predicting long-term increases or decreases of zooplankton biomass in the NPSG. These notably include the two variables—Chl *a* and SST—that are most commonly used from satellite observations to infer changes in the trophic states of open-ocean systems [*McClain*, 2009; *Boyce et al.*, 2010]. Similarly, *Dave and Lozier* [2010] found no relationships between primary production and stratification indices at station ALOHA. Thus, while much has been hypothesized about the effects of warming on stratification and their likely impacts on biomass, structure, and productivity of open-ocean food webs [*Behrenfeld et al.*, 2006; *Hoegh-Guldberg and Bruno*, 2010; *Doney et al.*, 2012], we see little evidence of SST

and Chl *a* providing meaningful information for predicting trends in annual means of zooplankton biomass in the NPSG over the past 20 years.

The lack of significant relationships with Chl *a* is at least partially explained by it being an imperfect index of phytoplankton biomass or nutritionally relevant carbon flux. For example, the Chl:C ratio of phytoplankton in the NPSG varies by almost a factor of 2 annually, being higher in winter when primary production is seasonally lowest [*Pasulka et al.*, 2013]. Chl *a* variability thus poorly reflects the annual cycle of phytoplankton biomass and production at station ALOHA. In addition, variability in Chl *a* concentration in surface waters, whether due to light or nutrient effects on the Chl:C ratio or to actual phytoplankton biomass differences, can be offset by effects on light penetration, which expand or contract the depth of the euphotic zone over which primary production occurs.

4.2. Links to Climate Variability

Sampling variability for mesozooplankton biomass estimates from individual HOT cruises is substantial relative to the approximate twofold ranges of seasonal and interannual variabilities at station ALOHA [*Landry et al.*, 2001]. As a consequence, the GAM of monthly averaged data has a much higher unexplained variability than the GAM based on annual means because it incorporates more of the cruise sampling uncertainties. As evident in the seasonal oscillations of zooplankton biomass in Figure 1a, results of the monthly GAM are clearly dominated by the seasonal plankton cycle at station ALOHA, in which elevated SST and high photon flux during summer months provide optimal conditions for N_2-fixing cyanobacteria and their associated diatoms [*White et al.*, 2007; *Dore et al.*, 2008; *Church et al.*, 2009; *Brzezinski et al.*, 2011]. Although some phytoplankton groups, such as prymnesiophytes and *Synechococcus*, have higher biomass levels in winter and spring [*Pasulka et al.*, 2013], both heterotrophic protists [*Pasulka et al.*, 2013] and mesozooplankton [*Landry et al.*, 2001] show similar patterns of summertime increase, suggesting a broad upward shift in trophic activity during summer. This sets seasonal plankton dynamics in the NPSG apart from the cycle observed at BATS, where the seasonal breakdown of stratification leads to a more classical bloom in late winter or spring [*Steinberg et al.*, 2012].

As shown by the GAM runs between annual means of zooplankton biomass and a single covariate at a time (Table 4), both primary production and NPGO each account for around 40% of annual biomass variability. In the full GAM for annual means, NPGO and primary production together explain 58% of zooplankton biomass variability. Thus, the result of the full model is consistent with the correlation between climate patterns and production reported at station ALOHA [*Dave and Lozier*, 2010; *Saba et al.*, 2010], where 1 year lagged primary production is correlated to the NPGO [*Dave and Lozier*, 2010]. The relationships between the NPGO and primary production and between NPGO and mesozooplankton biomass are linear and positive [*Dave and Lozier*, 2010; *Saba et al.*, 2010; *Chiaverano et al.*, 2013; this study], suggesting that both productivity and zooplankton biomass are enhanced by an intensified North Pacific Current, hence a stronger subtropical gyre circulation during positive phases of the NPGO [*Di Lorenzo et al.*, 2008]. Although a positive phase of the NPGO is associated with increasing stratification and downwelling in the subtropical gyre [*Di Lorenzo et al.*, 2008], according to *Dave and Lozier* [2010], the effect of the NPGO on the productivity at station ALOHA may be linked to changes in evaporation and freshwater input in the subtropical fronts where the North Pacific Tropical Water (NPTW), a water mass with a characteristic high-salinity signal found in subsurface waters at station ALOHA, is formed. Consistent with the hypothesis of the NPGO driving changes in productivity at station ALOHA due to the advection of modified waters from the source region, *Dave and Lozier* [2010] found a significant positive correlation between the NPGO and salinity in the middle and lower euphotic zone (50–150 m), with the strongest correlation occurring at 150 m and maximized at lags of 1 to 1.5 years. Even though the mechanism that links NPGO and plankton productivity at station ALOHA is still not clearly understood, the link may involve variability in diazotroph productivity, suggesting that if preformed nutrients vary with salinity at the NPTW source region, such mechanism could provide the boost to primary productivity at station ALOHA [*Dave and Lozier*, 2010]. Much of the zooplankton response to the NPGO thus appears to be associated with the impact on primary production, with a peak response lagging by 4 years.

Similar lagged responses of zooplankton to large-scale climate processes of 1 to 3 years have also been reported for the North Atlantic, where fluctuations of the North Atlantic Oscillation, an atmospheric forcing that modulates the intensity of the Atlantic gyres, affects advective processes between the eastern, western,

and central regions of the basin [*Piontkovski et al.*, 2006]. Given the week-to-month generation times of subtropical zooplankton, multiyear lagged correlations to climate mode variability clearly cannot be ascribed to the developmental delays of life history but rather suggest longer time delays due to altered circulation. Therefore, the additional lagged responses of zooplankton biomass to the NPGO must be due to other processes, such as advective influences on zooplankton populations or distributions, which do not manifest as direct impacts on primary productivity at station ALOHA. NPGO variability reflects fluctuations in wind-driven upwelling and circulation in the North Pacific [*Di Lorenzo et al.*, 2008], which impact productivity at different temporal scales (contemporaneous versus lagged). In their synthesis of climate impacts in the Pacific boundary currents, *Di Lorenzo et al.* [2013] observed that direct upwelling influences of the NPGO are mainly evident in the Southern California Current, while transport influences in the western Pacific arrive 2–3 years later, driven by westward propagating Rossby waves generated in the central and eastern North Pacific. Thus, the central region appears to play an important role mediating NPGO interactions between the eastern and western boundaries of the basin.

When lagged responses of mesozooplankton biomass are considered, a remarkable similarity is seen in the low-frequency fluctuations of the biomass and the NPGO. Positive phases of the NPGO (1998–2004 and 2007–2013) coincide with higher-than-average values of mesozooplankton biomass (2001–2008 and 2011–2013), except when biomass was low in 2006, whereas negative phases of the NPGO (1994–1997 and 2005–2006) generally coincide with lower-than-average biomass (1994–1999 and 2009–2010). *Chenillat et al.* [2012] considered the effects of negative (2005) and positive (2007) years of the NPGO on the productivity in the Southern CCS. In 2005 (NPGO−), an atypical delay in the upwelling onset and a late spring phytoplankton bloom had impacts extending to higher trophic levels, whereas atypical early upwelling favorable winds and an anomalously productive season occurred in 2007 (NPGO+). Those atypical years linked to NPGO variability in the CCS may also relate to lagged responses of mesozooplankton biomass at station ALOHA, where biomass was low in 2009 and considerably higher in 2011.

In addition to the NPGO, low-frequency fluctuations of zooplankton communities in the Pacific boundary currents are modulated by state of the PDO, but the effects are distinct and change in relative dominance with time [*Di Lorenzo et al.*, 2013]. Consistent with the weak negative correlation between primary production and the PDO for station ALOHA [*Dave and Lozier*, 2010; *Saba et al.*, 2010], we found a weak relationship between the PDO and annual mean zooplankton biomass. Negative years for the PDO occurred during 1999–2001 and 2007–2013, and mesozooplankton biomass was higher than average 4 years after those periods. However, 4 years following the positive PDO years of 1995–1998 and 2002–2006, mesozooplankton biomass was neither higher nor lower than average.

Similar to primary production [*Corno et al.*, 2007; *Dave and Lozier*, 2010], mesozooplankton biomass at station ALOHA shows a weak and inconsistent response to ENSO, with effects mainly apparent during the positive phase. From the monthly mean relationships, El Niño events appear to suppress the typical summer peak of mesozooplankton biomass, but that was only evident during some of the moderate (2005–2006 and 2009) to strong (1997–1998) events. For the annual mean data, the strongest negative anomalies coincided with El Niño events of 1994 and 1997–1998. As expected by the GAM, biomass was low 2 years after these events. However, mesozooplankton biomass was actually above the long-term mean during the 2002–2003 El Niño, even when lagged by 2 years. Therefore, despite the high proportion of biomass variability explained by the GAM that included primary production and the lagged MEI, the plankton responses are not consistent between events and may be masked by the effects of decadal forcing, as suggested by previous studies [*Corno et al.*, 2007; *Dave and Lozier*, 2010].

5. Conclusions

Of the 20 years of data analyzed here, new insights are shed on the environmental factors that affect mesozooplankton biomass variability in the oligotrophic NPSG. Primary production accounts for most of the variability in mesozooplankton biomass at both monthly and annual scales. The NPGO is the main climate pattern in modulating annual variability, with much less consistent and weaker effects of the MEI and the PDO. It remains to be seen how mesozooplankton biomass will respond to the strong El Niño of 2015–2016 and the likely phase change of the NPGO in 2014 [*Di Lorenzo et al.*, 2008; *NOAA*, 2016] (http://www.esrl.noaa.gov/psd/enso/mei/, 15 March 2016). Based on the model results found here, we predict

suppression of the summer mesozooplankton peak during the 2015 El Niño, while a few additional years of higher-than-average mesozooplankton biomass might be expected before the system shifts to lower values with the NPGO phase change. These future observations will serve to test the predictive power of the relationships found in this study.

Acknowledgments

This study would not have been possible without the hard work and dedication of the core HOT program group over the past two decades of time series cruises at station ALOHA. We specifically acknowledge David Karl and Matt Church for their leadership roles in the HOT Program, as well as the direct contributions of Karen Selph, Scott Nunnery, Stephanie Christensen, Rebecca Scheinberg, Colleen Allen, Melinda Simmons, and Blake Watkins to the HOT zooplankton collections and analyses. This work was supported by National Science Foundation grants OCE-0324666, OCE-0926766, and OCE-1260164. The Ph.D. research of B.V. was further supported by a scholarship (529-2011) from the Colombian Administrative Department of Science, Technology and Innovation (COLCIENCIAS). Mesozooplankton biomass data are available through the HOT website (http://hahana.soest.hawaii.edu/hot/hot-dogs/index.html).

References

Bar-Zeev, E., I. Avishay, K. D. Bidle, and I. Berman-Frank (2013), Programmed cell death in the marine cyanobacterium *Trichodesmium* mediates carbon and nitrogen export, *ISME J.*, *7*, 2340–2348.

Beaugrand, G., and P. C. Reid (2003), Long-term changes in phytoplankton, zooplankton and salmon related to climate, *Global Change Biol.*, *9*, 801–817.

Behrenfeld, M. J., et al. (2006), Climate-driven trends in contemporary ocean productivity, *Nature*, *444*, 752–755.

Bidigare, R. R., et al. (2009), Subtropical ocean ecosystem structure changes forced by North Pacific climate variations, *J. Plankton Res.*, *31*, 1131–1139.

Boyce, D. G., M. R. Lewis, and B. Worm (2010), Global phytoplankton decline over the past century, *Nature*, *466*, 591–596.

Brzezinski, M. A., J. W. Krause, M. J. Church, D. M. Karl, B. Li, J. L. Jones, and B. Updyke (2011), The annual silica cycle of the North Pacific Subtropical Gyre, *Deep Sea Res. I*, *58*, 988–1001.

Chenillat, F., P. Rivière, X. Capet, E. Di Lorenzo, and B. Blanke (2012), North Pacific Gyre Oscillation modulates seasonal timing and ecosystem functioning in the California Current upwelling system, *Geophys. Res. Lett.*, *39*, L01606, doi:10.1029/2011GL049966.

Chiaverano, L. M., B. S. Holland, G. L. Crow, L. Blair, and A. A. Yanagihara (2013), Long-term fluctuations in circalunar beach aggregations of the box jellyfish *Alatina moseri* in Hawaii, with links to environmental variability, *PLoS One*, *8*, e77039, doi:10.1371/journal.pone.0077039.

Chiba, S., K. Tadokoro, H. Sugisaki, and T. Saino (2006), Effects of decadal climate change on zooplankton over the last 50 years in the western subarctic North Pacific, *Global Change Biol.*, *12*, 907–920.

Chiba, S., S. Batten, K. Sasaoka, Y. Sasai, and H. Sugisaki (2012), Influence of the Pacific Decadal Oscillation on phytoplankton phenology and community structure in the western North Pacific, *Geophys. Res. Lett.*, *39*, L15603, doi:10.1029/2012GL052912.

Chiba, S., E. Di Lorenzo, A. Davis, J. E. Keister, B. Taguchi, Y. Sasai, and H. Sugisaki (2013), Large-scale climate control of zooplankton transport and biogeography in the Kuroshio-Oyashio Extension region, *Geophys. Res. Lett.*, *40*, 5182–5187, doi:10.1002/grl.50999.

Church, M. J., C. Mahaffey, R. M. Letelier, R. Lukas, J. P. Zehr, and D. M. Karl (2009), Physical forcing of nitrogen fixation and diazotroph community structure in the North Pacific Subtropical Gyre, *Global Biogeochem. Cycles*, *23*, GB2020, doi:10.1029/2008GB003418.

Corno, G., D. M. Karl, M. J. Church, R. M. Letelier, R. Lukas, R. R. Bidigare, and M. R. Abbott (2007), Impact of climate forcing on ecosystem processes in the North Pacific Subtropical Gyre, *J. Geophys. Res.*, *112*, C04021, doi:10.1029/2006JC003730.

Dave, A. C., and M. S. Lozier (2010), Local stratification control of marine productivity in the subtropical North Pacific, *J. Geophys. Res.*, *115*, C12032, doi:10.1029/2010JC006507.

Décima, M., M. R. Landry, and R. R. Rykaczewski (2011), Broad scale patterns in mesozooplankton biomass and grazing in the eastern equatorial Pacific, *Deep Sea Res. I*, *58*, 387–399.

Di Lorenzo, E., et al. (2008), North Pacific Gyre Oscillation links ocean climate and ecosystem change, *Geophys. Res. Lett.*, *35*, L08607, doi:10.1029/2007GL032838.

Di Lorenzo, E., and M. D. Ohman (2013), A double-integration hypothesis to explain ocean ecosystem response to climate forcing, *Proc. Natl. Acad. Sci. U.S.A.*, *110*, 2496–2499.

Di Lorenzo, E., et al. (2013), Synthesis of Pacific Ocean climate and ecosystem dynamics, *Oceanography*, *26*, 68–81.

Doney, S. C., et al. (2012), Climate change impacts on marine ecosystems, *Ann. Rev. Mar. Syst.*, *4*, 11–37.

Dore, J. E., R. M. Letelier, M. J. Church, R. Lukas, and D. M. Karl (2008), Summer phytoplankton blooms in the oligotrophic North Pacific Subtropical Gyre: Historical perspective and recent observations, *Prog. Oceanogr.*, *76*, 2–38.

Garcia-Comas, C., L. Stemmann, F. Ibanez, L. Berline, M. G. Mazzocchi, S. Gasparini, M. Picheral, and G. Gorsky (2011), Zooplankton long-term changes in the NW Mediterranean Sea: Decadal periodicity forced by winter hydrographic conditions related to large-scale atmospheric changes?, *J. Mar. Syst.*, *87*, 216–226.

Hawser, S. W., J. M. O'Neil, M. R. Roman, and G. A. Codd (1992), Toxicity of blooms of the cyanobacterium *Trichodesmium* to zooplankton, *J. Appl. Phycol*, *4*, 79–86.

Hayward, T. L., E. L. Venrick, and J. A. McGowan (1983), Environmental heterogeneity and plankton community structure in the central North Pacific, *J. Mar. Res.*, *41*, 711–729.

Hoegh-Guldberg, O., and J. F. Bruno (2010), The impact of climate change on the world's marine ecosystems, *Science*, *328*, 1523–1528.

Hooff, R. C., and W. T. Peterson (2006), Copepod biodiversity as an indicator of changes in ocean and climate conditions of the Northern California Current ecosystem, *Limnol. Oceanogr.*, *51*, 2607–2620.

Irwin, A. J., and Z. V. Finkel (2008), Mining a sea of data: Deducing the environmental controls of ocean chlorophyll, *PLoS One*, *3*, e3836, doi:10.1371/journal.pone.0003836.

Ji, R., M. Edwards, D. L. Mackas, J. A. Runge, and A. C. Thomas (2010), Marine plankton phenology and life history in a changing climate: Current research and future directions, *J. Plankton Res.*, *32*, 1355–1368.

Johnson, K. S., S. C. Riser, and D. M. Karl (2010), Nitrate supply from deep to near-surface waters of the North Pacific Subtropical Gyre, *Nature*, *465*, 1062–1065.

Karl, D. M. (1999), A sea of change: Biogeochemical variability in the North Pacific Subtropical Gyre, *Ecosystems*, *2*, 181–214.

Karl, D. M., and R. Lukas (1996), The Hawaii Ocean Time-series (HOT) program: Background, rationale and field implementation, *Deep-Sea Res. II*, *43*, 129–156.

Keister, J. E., E. Di Lorenzo, C. A. Morgan, V. Combes, and W. T. Peterson (2011), Zooplankton species composition is linked to ocean transport in the Northern California Current, *Global Change Biol.*, *17*, 2498–2511.

Landry, M. R. (1977), A review of important concepts in the trophic organization of pelagic ecosystems, *Helgoländer Wiss. Meeresunters.*, *30*, 8–17.

Landry, M. R., H. Al-Mutairi, K. E. Selph, S. Christensen, and S. Nunnery (2001), Seasonal patterns of mesozooplankton abundance and biomass at station ALOHA, *Deep Sea Res. II*, *48*, 2037–2061.

Landry, M. R., M. Decima, M. P. Simmons, C. C. Hannides, and E. Daniels (2008), Mesozooplankton biomass and grazing responses to Cyclone Opal, a subtropical mesoscale eddy, *Deep Sea Res. II*, *55*, 1378–1388.

Lavaniegos, B. E., and M. D. Ohman (2007), Coherence of long-term variations of zooplankton in two sectors of the California Current System, *Prog. Oceanogr., 75*, 42–69.
Llope, M., K. S. Chan, L. Ciannelli, P. C. Reid, L. C. Stige, and N. C. Stenseth (2009), Effects of environmental conditions on the seasonal distribution of phytoplankton biomass in the North Sea, *Limnol. Oceanogr., 54*, 512–524.
Mackas, D., and G. Beaugrand (2010), Comparisons of zooplankton time series, *J. Mar. Syst., 79*, 286–304.
Mackas, D. L., R. E. Thomson, and M. Galbraith (2001), Changes in the zooplankton community of the British Columbia continental margin, 1985–1999, and their covariation with oceanographic conditions, *Can. J. Fish. Aquat. Sci., 58*, 685–702.
Mantua, N. J., S. R. Hare, Y. Zhang, J. M. Wallace, and R. C. Francis (1997), A Pacific Interdecadal Climate Oscillation with impacts on salmon production, *Bull. Am. Meteorol. Soc., 78*, 1069–1079.
McClain, C. R. (2009), A decade of satellite ocean color observations, *Ann. Rev. Mar. Sci., 1*, 19–42.
NOAA (2016), Multivariate ENSO Index (MEI). [Available at www.esrl.noaa.gov/psd/enso/mei/, Accessed 15 March 2016.]
O'Brien, T. D., P. H. Wiebe, and T. Falkenhaug (2013), ICES zooplankton status report 2010/2011.
Otto, S. A., G. Kornilovs, M. Llope, and C. Möllmann (2014), Interactions among density, climate, and food web effects determine long-term life cycle dynamics of a key copepod, *Mar. Ecol. Prog. Ser., 498*, 73–84.
Pasulka, A. L., M. R. Landry, D. A. Taniguchi, A. G. Taylor, and M. J. Church (2013), Temporal dynamics of phytoplankton and heterotrophic protists at station ALOHA, *Deep Sea Res. II, 93*, 44–57.
Peterson, W. T., J. R. Keister, and L. R. Feinberg (2002), The effects of the 1997–99 El Niño/La Niña events on hydrography and zooplankton off the central Oregon coast, *Prog. Oceanogr., 54*, 381–398.
Peterson, W. T., and J. E. Keister (2003), Interannual variability in copepod community composition at a coastal station in the Northern California Current: A multivariate approach, *Deep Sea Res. II, 50*, 2499–2517.
Pinheiro, J., D. Bates, S. DebRoy, D. Sarkar, and R. Core Team (2015), nlme: Linear and nonlinear mixed effects models, *R package version, 3*, 1–123.
Piontkovski, S. A., T. D. O'Brien, S. F. Umani, E. G. Krupa, T. S. Stuge, K. S. Balymbetov, O. V. Grishaeva, and A. G. Kasymov (2006), Zooplankton and the North Atlantic Oscillation: A basin-scale analysis, *J. Plankton Res., 28*, 1039–1046.
Roman, M. R., H. A. Adolf, M. R. Landry, L. P. Madin, D. K. Steinberg, and X. Zhang (2002), Estimates of oceanic mesozooplankton production: A comparison using the Bermuda and Hawaii time-series data, *Deep Sea Res. II, 49*, 175–192.
Saba, V. S., et al. (2010), Challenges of modeling depth-integrated marine primary productivity over multiple decades: A case study at BATS and HOT, *Global Biageochem. Cycles, 24*, GB3020, doi:10.1029/2009GB003655.
Sheridan, C. C., and M. R. Landry (2004), A 9-year increasing trend in mesozooplankton biomass at the Hawaii Ocean Time-series station ALOHA, *ICES J. Mar. Sci., 61*, 457–463.
Steinberg, D. K., M. W. Lomas, and J. S. Cope (2012), Long-term increase in mesozooplankton biomass in the Sargasso Sea: Linkage to climate and implications for food web dynamics and biogeochemical cycling, *Global Biogeochem. Cycles, 26*, GB1004, doi:10.1029/2010GB004026.
White, A. E., Y. H. Spitz, and R. M. Letelier (2007), What factors are driving summer phytoplankton blooms in the North Pacific Subtropical Gyre?, *J. Geophys. Res., 112*, C12006, doi:10.1029/2007JC004129.
Wood, S. N. (2006), *Generalized Additive Models: An Introduction with R*, Chapman & Hall/CRC, Boca Raton, Fla.
Zuur, A. F., E. N. Ieno, and G. M. Smith (2007), *Analysing Ecological Data*, Springer, New York.
Zuur, A. F., E. N. Ieno, N. J. Walker, A. A. Saveliev, and G. M. Smith (2009), *Mixed Effects Models and Extensions in Ecology with R*, Springer, New York.

Chapter 1, in full, is a reprint of materials as it appears in Valencia B, Landry MR, Décima M, and Hannides CCS. (2016). Environmental drivers of mesozooplankton variability in the North Pacific Subtropical Gyre. *Journal of Geophysical Research: Biogeosciences*. The dissertation author was the primary investigator and author of this manuscript.

CHAPTER 2

Environmental effects on mesozooplankton size structure and export flux at station ALOHA, North Pacific Subtropical Gyre

Abstract

Using size-fractionated mesozooplankton biomass data collected over 23 years (1994–2016) of increasing primary production (PP) at station ALOHA, we evaluate how changing environmental conditions affect mesozooplankton size structure, trophic cycling, and export fluxes in the subtropical north Pacific. From Generalized Additive Model (GAM) analysis, size structure is significantly influenced by a non-linear relationship with sea surface temperature (SST) that is mainly driven by the strong 1997–1998 El Niño and a positive and linear relationship with PP. Increasing PP has more strongly enhanced the biomass of smaller (0.2-0.5 mm) and larger (>5 mm) mesozooplankton, increasing evenness of the biomass spectra, while animals of 2-5 mm, the major size class for vertically migrating mesozooplankton, show no long-term trend. Measured PP is sufficient to meet feeding requirements that satisfy zooplankton respiration and growth rates, as determined by commonly used empirical relationships based on animal size and temperature, consistent with a tightly coupled food web with one intermediate level for protistan consumers. Estimated fecal pellet production suggests an enhancing contribution of mesozooplankton to passive particle export relative to the material collected in 150-m sediment traps. In contrast, the biomass of vertically migrants does not vary

systematically with PP due to the varying responses of the different size classes. These results illustrate some complexities in understanding how varying environmental conditions can affect carbon cycling and export processes at the community level in open-ocean oligotrophic systems, and which need to be confirmed and better understood by process-oriented mechanistic study.

Introduction

The responses of mesozooplankton communities to environmental variability can alter the dynamics of pelagic food webs and the services that they provide. In dynamic regions of the oceans, for example, strong linkages have been demonstrated between climate-induced shifts in zooplankton size structure and the trophic fluxes to higher levels, including commercially important fishes such as cod, salmon, sardine, and anchovy (Ayón *et al.,* 2011; Beaugrand *et al.,* 2003, 2010; Peterson and Schwing, 2003; Rykaczewski and Checkley, 2008). Temporal trends to smaller zooplankton have also been suggested to drive change in biogeochemical cycling by decreasing the overall efficiency of the biological pump (Beaugrand *et al.,* 2010). While subtle trends in biomass and productivity have been documented for open-ocean oligotrophic regions, the long-term effects of climate on mesozooplankton communities and the processes they regulate have been much less explored compared to those in more productive habitats. This is surprising in light of the suggestion that the relative contributions of mesozooplankton to biogeochemical cycles in oligotrophic regions may exceed those in richer systems (Al-Mutairi and Landry, 2001; Calbet *et al.,* 2009; Isla *et al.,* 2004).

In this study, we evaluate how changes in environmental conditions at station ALOHA (A Long-Term Oligotrophic Habitat Assessment) in the North Pacific Subtropical Gyre (NPSG) affect the size structure of the mesozooplankton community and the resulting zooplankton roles

in carbon cycling and passive and active export fluxes from the euphotic zone. For this, we analyzed near monthly data of size-fractionated mesozooplankton biomass over a 23-year period in which North Pacific climate drivers (Pacific Decadal Oscillation - PDO, North Pacific Gyre Oscillation - NPGO, and El Niño cycles) have varied and primary production and total mesozooplankton biomass have generally increased (Valencia *et al.,* 2016). While relative constancy of plankton community structure has previously been assumed to be a characteristic of oligotrophic regions such as the NPSG (Quiñones *et al.,* 2003; Rodríguez and Mullin, 1986; Sprules and Barth, 2016), climate-related changes in the ratio of smaller to larger animals have the potential to affect the feeding requirement that support respiration and growth (Horne *et al.,* 2016; Sprules and Munawar, 1986), the relative production rates of smaller and larger fecal pellets (Paffenhöfer and Knowles, 1979; Wilson *et al.,* 2008), and the relative abundances of migrating and non-migrating zooplankton (Hannides *et al.,* 2009; Longhurst *et al.,* 1989; Steinberg *et al.,* 2012) – all with system-level biogeochemical implications. Here, we hypothesize that increasing primary productivity should be linked with a shift to increasing relative abundances of larger phyto- and zooplankton. Thus, while we might expect reduced biomass-specific rates of metabolism and growth (reduced contribution to euphotic-zone carbon cycling) as a consequence of larger mean zooplankton size, size structural changes should also enhance relative zooplankton contributions to passive (larger fecal pellets) and active export (larger zooplankton are more likely to migrate; Ohman and Romagnan, 2016). The data provide an opportunity to assess structural and functional responses of a subtropical zooplankton community to a natural multi-decadal change in system productivity, to determine the extent to which zooplankton responses scale proportionally or disproportionally relative to primary

production, and to establish their potential connections to the major modes of north Pacific climate variability.

Methods

Sampling and Laboratory Analyses

Zooplankton samples were collected on 225 cruises from February 1994 to August 2016 at station ALOHA (22.45°N, 158°W) as part of the Hawaii Ocean Time-series (HOT) program. Oblique tows were taken through the euphotic zone (tow depth: 162 ± 36 m, mean ± standard deviation (SD)) with a 1-m^2 plankton net from February 1994 to August 2005 and with a 1-m diameter ring net from November 2005 to the present. Comparisons of the two nets in a series of tows on the same cruise revealed no significant differences in areal estimates of zooplankton biomass for either day or night tows (Mann-Whitney test, $p > 0.05$); therefore, they are assumed to be equally efficient samplers in the time series. Both nets were made of 202-µm Nitex mesh and were equipped with a General Oceanic flowmeter across the net mouth to measure volume filtered and a time-depth recorder (Brancker XL-200 or Vemco logger) attached to the net frame to measure depth of tow. On most cruises, three tows were done during midday (1000–1400) and three during midnight (2200–0200). Onboard, a Folsom-split subsample (1/2, 1/4 or 1/8) from each tow was wet sieved through five mesh sizes (5, 2, 1, 0.505 and 0.202 mm), and each fraction was concentrated onto preweighed 200-µm Nitex filters, rinsed with isotonic ammonium formate to remove salt and frozen as described by Landry *et al.* (2001).

In the laboratory, dry weight (DW) biomass of each size class was determined (Denver Instrument analytical balance, 0.01 mg) after thawing and oven drying (60°C for at least 24h). Weighed biomass was corrected for the volume of the subsample split, the volume of water

filtered (m^3) and the tow depth (m), and is presented as areal biomass: g DW m^{-2}. When biomass in the 5 mm size class was zero and logarithmic transformations were needed for data analysis, as suggested by O'Brien *et al.* (2013), the sample was assigned a value of half of the minimum value in that fraction so as not to affect the trend. Cruise mean DWs were calculated from the sums of the five size classes for each tow and the averages of the day and night tows per cruise. Migrant mesozooplankton biomass was calculated as nighttime minus daytime DWs for the 221 cruises where paired day-night samples were collected. Negative migrant biomass due to higher values during the day occurred for eight cruises. These were not included in the trend analysis but are averaged in the calculations of active flux mediated by mesozooplankton migrations.

For most cruises, the ratios of carbon (C) and nitrogen (N) to DW content of mesozooplankton was determined for one day and one night tow and applied to the other tows on that cruise. Dried samples for each size class were ground to a fine powder, and a subsample (~ 1 mg) was weighed in preweighed tin capsules and then analyzed by combustion relative to acetanilide standards in a Perkin-Elmer CHN Elemental Analyzer or a Costech Elemental Combustion System. For cruises from October 2001 to October 2005 where no CN data were available, C biomass was obtained for each size class using the mean C:DW relationships for day and night tows (Appendix Table S2.1). Mesozooplankton biomass data from this study can be accessed at the HOT website: http://hahana.soest.hawaii.edu/hot/hot-dogs/index.html.

Biomass Size Structure

Temporal variability in mesozooplankton size structure was evaluated by comparing the slopes of the normalized biomass-size spectra (NB-SS) and size diversity among years. NB-SS slopes were obtained from least squares linear regressions (model 1) of normalized biomass ($Bx/\Delta x$) versus size class (x)

$$log_2\left(\frac{Bx}{\Delta x}\right) = b\, log_2(x) + a\,, \qquad (1)$$

where *Bx* is the DW of each size class *x*, *Δx* is the interval of each size class (0.303, 0.495, 1.0, 3.0, 5.0 mm), and *a* and *b* are respectively the y-intercept and slope of the best fit line. Regression model fit was evaluated by the coefficient of determination (r^2), which averaged 0.88 (range: 0.77–0.94). Size diversity was calculated using the Shannon-Wiener diversity index from the DWs in each size class using the 'diversity' function of vegan R package (Oksanen *et al.,* 2017).

$$H' = -\sum p_i\,(\ln pi)\,, \qquad (2)$$

where *pi* is the proportional biomass of size class *i*. Both the steepness of the NB-SS slope and the size diversity represent relative contributions of the size classes to total biomass (e.g., García-Comas *et al.,* 2014). We used mean DWs of paired day and night samples for these analyses (n = 221).

Temporal Trends of Biomass

The seasonal and long-term trend of mean mesozooplankton biomass (mean of paired day-night DWs) and migrant biomass (night minus day DW) were evaluated by generalized additive models (GAM). GAM is a non-linear regression technique that fits smooth functions through data to model the relationships between response variables and covariates without assuming a specific response function (Wood, 2006; Zuur *et al.,* 2009). In addition, the GAM structure can account for temporal autocorrelations of residuals, a usual characteristic of time series data. GAMs were run for each size class of mean mesozooplankton biomass and for total migrant biomass using untransformed data and assuming Gaussian distributed residuals.

$$DW_{iy} = a + f_1(Day.of.year_i) + f_2\left(Time_{iy}\right) + \varepsilon_{iy} \quad \text{where } \varepsilon_{iy} \sim N\left(0, \sigma_y^2\right), \quad (3)$$

where *DWiy* is mesozooplankton biomass of the *ith* cruise (*i* = 1 to 221) in year *y* (*y* = 1 to 23), *a* is the model intercept, and *f* are cubic (*f1*) and thin-plate (*f2*) regression spline functions describing the effects of covariates day of year and time on biomass, respectively. Residuals (ε_{iy}) were modeled using an auto-regressive process AR1 to account for positive autocorrelation in residuals and a VarIdent variance structure to allow different variances per year (Zuur *et al.,* 2009). Overfitting of the thin-plate smooth function was reduced by restricting the effective degrees of freedom (edf ≤ 4). Model validation was done by graphical analyses of the normalized residuals to evaluate the assumptions of normality, homogeneity of variances, and independence (Appendix Figure S2.1). We ran the GAMs in R using the function 'gamm' in the mgcv package (Wood, 2006).

Carbon Cycling in the Euphotic Zone

The potential impact of mesozooplankton on carbon cycling in the euphotic zone was estimated following an approach similar to that of Roman *et al.* (2002a). We first estimated zooplankton production (ZP) using an empirical growth rate relationship, then determined the food consumption (ingestion, I) needed to support that production using a gross growth efficiency of 20% (GGE = ZP:I). Egestion (E) of undigested carbon as fecal matter was estimated using an assimilation efficiency of 70% (i.e., E = 30% of I). Whereas Roman *et al.* (2002a) assumed a GGE of 30% for their calculations, we used a lower estimate to be more consistent with data-constrained inverse model results for the open-ocean equatorial Pacific (GGE ≈ 18%; Stukel and Landry, 2010) as well as the median efficiency (22%) reported for copepods over a wide range of food concentrations and temperatures (Straile, 1997).

Mesozooplankton production (ZP, mg C m^{-2} d^{-1}) was computed for each size class as the product of the carbon biomass (mg C m^{-2}) times calculated temperature-dependent growth rates (g: d^{-1}). Carbon biomass for each cruise was obtained by elemental analysis, whereas the intrinsic growth rates (g: d^{-1}) were calculated from the equation of Hirst and Lampitt (1998). Ingestion rates computed from ZP and GGE are compared to measured primary production on each cruise to assess the minimum portion of productivity needed to sustain mesozooplankton biomass, assuming direct herbivory. Likewise, to assess the potential contribution of mesozooplankton fecal pellets to the particulate carbon flux, the computed egestion rates were compared to measured particulate organic carbon flux collected in sediment traps at 150 m at station ALOHA (data from the HOT website). Annual rates (g C m^{-2} y^{-1}) of ingestion, fecal pellet production, and primary production were calculated by temporal integration according to the trapezoidal rule. Mean DW of paired day-night samples was used for all the calculations of this section (see Appendix 2 for further details on rate calculations).

Active and Passive Export Fluxes

Contributions of migrant mesozooplankton to the fluxes of dissolved inorganic carbon, nitrogen, and phosphorus due to respiration and excretion at mesopelagic depths were calculated following Hannides *et al.* (2009). Rates of respiration (µl O_2 ind^{-1} h^{-1}), ammonia excretion (µg N ind^{-1} h^{-1}), and phosphate excretion (µg P ind^{-1} h^{-1}) were determined as functions of the mean biomass per individual in each size class (Landry *et al.,* 2001; Appendix Table S2.2) and the temperature that migrants experience at daytime depths of 300-500 m (Table 1) using the metabolic relationships of Ikeda (1985) (see Appendix 2 for further details). Excretion rates of dissolved organic compounds were assumed to represent a constant fraction of the total carbon (24%, Steinberg *et al.,* 2000), nitrogen (32%, Steinberg *et al.,* 2002), and phosphorus

metabolized (47%, Pomeroy *et al.,* 1963). Migrant-mediated active flux of dissolved compounds was compared to the gravitational flux of particulate organic matter collected in sediment traps at 150 m, but only the months that matched the data available for migrant biomass were considered. Annual estimates of active (migrant-mediated) and passive fluxes (trap particles) were calculated by temporal integration according to the trapezoidal rule (g m^{-2} y^{-1}).

Environmental Effects on Size Structure and Migrant Biomass

We used GAMs to evaluate the effects of changes in local environmental conditions and large-scale climate patterns on mesozooplankton size structure and migrant biomass. Primary production (PP: integrated 0-150 m, g C m^{-2} d^{-1}), sea surface temperature (SST: mean 0-10 m, °C), the multivariate ENSO index (MEI), the Pacific Decadal Oscillation (PDO), and the North Pacific Gyre Oscillation (NPGO) were considered as covariates (eqs. 4 and 5). Local environmental data (PP and SST) were obtained from the HOT website, and climate indices were obtained from their respective websites: MEI (http://www.esrl.noaa.gov/psd/enso/mei/), PDO (http://research.jisao.washington.edu/pdo/), and NPGO (http://www.o3d.org/npgo/).

Before running the models, we identified collinearity from the variance inflation factor (VIF) for combinations of all variables, using values <3 as the cut-off for inclusion of covariates. The models were run for annual means. Because mesozooplankton were not sampled in all months over the 23 years analyzed, annual means of each environmental factor were calculated by including only the months that matched biomass data availability. Models were run as

$$ZSS_i = a + f_1(PP_i) + f_2(SST_i) + \varepsilon_i \quad \text{where } \varepsilon_i \sim N(0, \sigma^2), \quad (4)$$

$$MIG_i = a + f_1(PP_i) + f_3(index_i) + \varepsilon_i \quad \text{where } \varepsilon_i \sim N(0, \sigma^2), \quad (5)$$

where *ZSSi* is size structure in year *i*, *MIGi* is migrant biomass in year *i*, *a* is the intercept, *f* are thin-plate regression spline functions describing the effects of environmental factors on size structure and migrant biomass, *index* corresponds to MEI, PDO, and NPGO, and ε_i are the residuals. Overfitting of the smooth functions was reduced by restricting the effective degrees of freedom (edf ≤ 4). For cases where edf = 1 (linear relationship), models were re-run including the covariate as a linear term. We applied a stepwise backward approach to remove non-significant covariates ($p > 0.05$). After the ensemble of models was obtained for size structure and migrant biomass, the best model was selected by minimizing the generalized cross-validation (GCV) criterion that measures the degree of penalization during fitting (Wood, 2006).

Model validation was done by graphical analyses of the residuals to evaluate the assumptions of homogeneity of variances, normality and independence, as well as the model fit to observed values (Appendix Figures S2.2 and S2.3). Influential observations were evaluated by the Cook's distance (> 0.5). These analyses were done in R using the function 'gam' in the mgcv package (Wood, 2006).

Results

Biomass Size Structure

The percentages of daytime mesozooplankton biomass at station ALOHA are similar on average among the 0.2-0.5, 0.5-1 and 1-2 mm size classes (each 24 to 27% of total biomass), whereas the contributions of larger individuals to total biomass are lower (17% for 2-5 mm and 6% for >5 mm) (Figure 1a). Biomasses increase during nighttime in all size classes due to diel vertical migration, but the greatest increase occurs in the 1-2 and 2-5 mm fractions, resulting in a more even biomass distribution among the 0.2-0.5 to 2-5 mm fractions, each with 15-20% of the

total (Figure 1a and 1b). Among years, the biomass size structure shows relatively low variability, as seen in the distributions of NB-SS slopes and size diversity around their mean values (Figures 1c and 1d). Both the steepest NB-SS slope and the lowest size diversity occurred in 1999, indicating a shift in community size structure during that year (Figure 1c and d). The steeper NB-SS slopes in 1998–1999 suggest a relative increase in the contribution of smaller zooplankton. The decrease in size diversity from 1996 to 1999 suggest an increase in the dominance of one of the size classes, indicating that the distribution of biomass tended to be more uneven during those years.

A closer look at the temporal variability of each size class evaluated using GAMs confirms the described significant summertime increase in mesozooplankton biomass at station ALOHA (Appendix Table S2.3, Figure 2). However, in the long term, the trend varied between size classes: the smallest (0.2-0.5 mm) and largest (> 5 mm) increased linearly during the 23 years analyzed, the intermediate (0.5-1.0 and 1.0-2.0 mm) presented a saturated response, increasing linearly until about 2003–2004 and remaining relatively constant after that. The trend for the 2.0-5.0 mm size class was not significant (Appendix Table S2.3, Figure 2). Since we mainly focus here on the trends in mean biomass for each size class, the seasonal and long-term analyses for separate day and night biomass are presented in supporting information (Appendix Tables S2.3 and S2.4, Appendix Figure S2.4).

Carbon Cycling in the Euphotic Zone

Our computed contributions of mesozooplankton to carbon cycling in the euphotic zone via food consumption and fecal pellet production are lowest at the start of the time series in 1994 and highest by about 2 fold in 2011 (Table 1, Figure 3a). Not surprisingly, given their calculation from biomass values and the relatively low variability of the biomass structure

(Figures 1c and d), the rate estimates closely follow the biomass trend, which generally increased from 1994 to 2004, except for the abrupt decline in 1997. After 2004, however, annual variabilities of the rate estimates and biomass are higher, with substantial drops in 2006, 2009, and 2012 and peaks in 2007, 2011, and 2013 (Figure 3a). Although variable, estimates of mesozooplankton ingestion are positively associated with primary production (Figure 3b).

Mean mesozooplankton ingestion ranges from 25% (1995) to 47% (2011) of daily primary production, and the overall average is 33.7 ± 5.1% (± SD) (Figure 4a). The mean ratio of ingestion to primary production increased from 31% in 1994–2003 to 36% in 2004–2015; however, the long-term trend of the ratio is not significant ($p > 0.05$, Appendix Table S2.5). Computed estimates of mesozooplankton fecal pellet production average 191 ± 40% (± SD) of the particulate carbon collected in sediment traps at 150 m, varying from 168% in 1994–2003 to 213% in 2004–2014 (Table 2, Figure 4b). The mean relationship of fecal pellet production to passive flux has increased significantly over the study period ($p < 0.05$, Appendix Table S2.5, Figure 4b).

Migrant Biomass and Active Export Flux

Comparing the beginning (1994: 0.26 ± 0.14 g DW m^{-2}, mean ± SD) and end of the time series (2016: 0.51 ± 0.36 g DW m^{-2}), migrant mesozooplankton biomass at station ALOHA is two-fold higher after two decades of observation. However, biomass shows high variability both per month and year, with no clear seasonal patterns or long-term trends (Appendix Table S2.3, Figure 5). Average migrant biomass was lowest in 1997 (0.22 ± 0.11 g DW m^{-2}) and 2009 (0.24 ± 0.19 g DW m^{-2}), about one third of the maximum value in 2011 (0.67 ± 0.32 g DW m^{-2}). In contrast, both day and nighttime mesozooplankton biomasses increase significantly during summer months and over the two-decade time series (Appendix Tables S2.3 and S2.4, Appendix

Figure S2.4), as previously shown for the mean mesozooplankton biomass at station ALOHA (Valencia *et al.,* 2016).

Following migrant biomass variability, the active fluxes of dissolved inorganic compounds due to respiration and excretion at mesopelagic depths show strong interannual variability with the lowest contributions to export in 1997 and 2009 and the highest in 2007 and 2011 (Figure 6a). The passive fluxes of particulate carbon (C) and nitrogen (N) in 150-m sediment traps increased until 2003 and decreased slightly afterwards (Figure 6b and 6d). In contrast, the flux of particulate phosphorus (P) shows a stronger interannual variability, with a 6-year period of low values from 2004 to 2010, followed by a peak in 2012 (Figure 6f). Relative to the passive export of particulate matter, total migrant-mediated fluxes correspond to 17%, 17%, and 41% of the C, N and P fluxes, respectively (Table 2, Figures 6c, 6e, and 6g). The proportions of active/passive flux do not show significant temporal trends for any of the three elements ($p > 0.05$, Appendix Table S2.5); the mean proportions from 1994 to 2003 (C: 16.0%, N: 16.4%, P: 35.0%) are similar to those from 2004 to 2014 (C: 17.7%, N: 17.3%, P: 47.2%) for C and N, but an increase for P is noted (Figures 6c, 6e, 6g). Converting the flux estimates to molar units and calculating the elemental ratios give an average C:N:P of 251:31.9:1 (standard errors (SE) of C:P = 6.9 and N:P = 0.9) for passive flux and an average C:N:P of 101:13.3:1 (SE of C:P = 0.8 and N:P = 0.4) for the elemental fluxes from active migrant zooplankton. Turnover rates of N and P, calculated by dividing migrant-mediated active flux by migrant biomass (N from Table S1 and P from P:DW ratios from Hannides *et al.* (2009)) average 0.017 ± 0.002 d^{-1} ($\pm$ SD) and 0.021 ± 0.002 d^{-1}, respectively.

Environmental Relationships

Changes in relative size-class biomass contributions are best predicted by SST for the NB-SS slopes (Table 3 and Appendix Table S2.6-S2.7, Figure 7a) and by SST and PP for size diversity (Figure 7b and 7c). SST effects on both NB-SS slopes and size diversity are nonlinear. NB-SS slopes decrease rapidly below average when SST is below ~24.4°C (Figure 7a), and size diversity is lower than average when SST is below ~24.7°C (Figure 7b). Both results suggest that the contribution of larger zooplankton increases with SST until temperatures are ~24.7°C, thereafter staying more constant or declining slightly. Above 25.4°C, the contribution of smaller zooplankton may increase slightly, but the data are sparse for this part of the temperature range. In addition to SST, PP significantly drives change in zooplankton size diversity with a linear and positive relationship suggesting that higher PP leads to a more even distribution of biomass among the size classes (Figure 7c).

From the set of environmental factors (PP, MEI, PDO and NPGO) and lagged responses considered (up to 4 years), none are significant in explaining annual changes in migrant mesozooplankton biomass when two-variable GAMs are evaluated (Appendix Table S2.6). The only significant model is when PP and 3-year lagged PDO are considered together, suggesting that they are the main drivers of interannual changes in migrant biomass (Table 3 and Appendix Table S2.7). However, the relationships of both variables to migrant biomass are nonlinear and complex (Figure 8). According to the model, migrant mesozooplankton biomass is higher than the mean when PP ranges from ~ 470 to 540 mg C m^{-2} d^{-1} and lower at both higher and lower values of PP (Figure 8a). The relationship of migrant biomass with the 3-year lagged PDO shows a unimodal inverse response; migrant biomass is lower than the mean when PDO ranges from -0.5 to 1.0 and higher when the PDO index is lower or higher that that range (Figure 8b).

Discussion

Mesozooplankton Biomass Size Structure

In dynamic regions of the oceans, variability in system productivity is well demonstrated to modulate significant shifts in the size structure of zooplankton communities (Décima *et al.,* 2011; Manríquez *et al.,* 2012; Medellín-Mora *et al.,* 2016; Rykaczewski and Checkley, 2008). While the magnitudes of environmental variability are much smaller in the subtropical open oceans (Quiñones *et al.,* 2003; Rodríguez and Mullin, 1986; Sprules and Munawar, 1986), here we show that systematic changes in size structure can also occur in such systems. GAMs of the biomass variability for mesozooplankton size classes reveal subtle but significant differences in their responses to change over the 23 years of sampling at station ALOHA. For the 2.0-5.0 mm size class, the dominant size mode for migrant mesozooplankton, no temporal trend is evident. Intermediate size classes, 0.5-1.0 and 1.0-2.0 mm, show strong early responses to changing environmental conditions (Sheridan and Landry, 2004), but level off after about 2003–2004. In contrast, both the smallest (0.2-0.5 mm) and largest size classes (>5.0 mm) demonstrate positive linear increasing biomass over the full-time series. These differences result in a more even biomass distribution across size classes at the end of the sampling period than at the beginning (Appendix Figure S2.5), with both smaller and larger zooplankton increasing in relative importance.

Two indices of size structure, NB-SS slopes and size diversity, show significant effects of sea surface temperature (SST). Consistent with an expected decrease in adult body size due to temperature-enhanced metabolism and growth (Horne *et al.,* 2016), we found that smaller zooplankton increased when the water was warmer. However, because the relationship between size and SST is nonlinear, smaller zooplankton also increased with decreasing temperature. In

the Northwestern Pacific, Chiba *et al.* (2015) found a similar inverse relationship between copepod size and SST, which they attributed to concurrent variability in mixed-layer processes and productivity. Further, for the shelf region of the East China Sea, SST variability was not related to shifts in zooplankton size structure (NB-SS slope or size diversity) whereas food availability was important (García-Comas *et al.,* 2014). At station ALOHA, the SST-size relationship is most influenced by the period of 1996–1999, which includes the strong 1997–1998 El Niño and 1998–1999 La Niña, as well as the period of coolest SST and the lowest productivity in the data set. The persistence of these conditions over both El Niño and La Niña states probably explains the lack of a relationship between size structure and the MEI. In the equatorial Pacific, decreased zooplankton biomass and increased dominance of smaller zooplankton were associated with the 1992 El Niño event (White *et al.,* 1995).

Because we analyzed size structure by bulk biomass only, it is not clear if the strong increase in small and intermediate-sized zooplankton prior to 2004 reflects a change in community composition (i.e., smaller species), decreased adult size, or increased occurrence of juvenile stages. Previous studies have noted that zooplankton community composition in the NPSG can remain relatively constant despite abrupt changes in temperature (McGowan and Walker, 1985), community size structure (Rodríguez and Mullin, 1986), and total biomass (Landry *et al.,* 2001, 2008; McGowan and Walker, 1985). Therefore, variability in the size structure at station ALOHA does not necessarily imply a significant change in species dominance.

The positive linear relationship between PP and the size diversity index is consistent with the significant long-term increase in PP at station ALOHA (Saba *et al.,* 2010; Wilson *et al.,* 2015) and the linear (smaller and larger zooplankton) and saturated trends (intermediate

zooplankton) found for the size classes. However, this result contrasts with the expected positive linear relationship between PP and mean zooplankton size, by which higher food availability leads to a relative increase in larger zooplankton (Dam and Peterson, 1991; Hirst and Bunker, 2003). These more typical community responses have been shown to occur in mesoscale eddies in the NPSG (Landry *et al.,* 2008) and in the North Atlantic subtropical gyre (NASG) (Goldthwait and Steinberg, 2008), where shifts in phytoplankton size structure are reflected in increased mesozooplankton biomass and larger organisms. Our results also do not agree with the negative relationships between zooplankton size diversity and productivity in the East China Sea (García-Comas *et al.,* 2014) and Chilean upwelling systems (Medellín-Mora *et al.,* 2016), where shifts towards smaller zooplankton (juveniles) occur in response to productivity pulses. While we did not find a relationship (linear or nonlinear) between NB-SS slopes and PP, Sprules and Barth (2016) have observed that the NB-SS index is not always sensitive to productivity changes, as for example in the East China Sea (Garcia-Comas *et al.,* 2014).

On longer time scales, changes in the strength of alongshore currents associated with the PDO in the eastern North Pacific have been linked to shifts in the relative dominance of small-warm (PDO+) versus large-cold water copepods (PDO-) (Keister *et al.,* 2011). In the western North Pacific, Chiba *et al.* (2015) also suggested that shifts in copepod size structure result from changes in large-scale ocean circulation. In contrast to total zooplankton biomass (Valencia *et al.,* 2016), we did not find an effect of either the PDO or the NPGO on zooplankton size structure at station ALOHA. However, an analysis focused on species composition rather than bulk biomass could provide additional insights on mesozooplankton community responses to climate patterns in the NPSG.

Carbon Cycling in the Euphotic Zone

Although we express our estimates of mesozooplankton ingestion as a percentage of measured primary production, only a small portion of that is expected to come from direct herbivory due to the system's dominance by phytoplankton too small to be efficiently exploited by most mesozooplankton (Calbet and Landry, 1999; Calbet *et al.,* 2009). Isotopic evidence from the NPSG suggests that there is a 0.9 trophic level separation between primary producers and particle-feeding mesozooplankton, on average (Landry and Décima, 2017), indicative of their preferred feeding on protistan microzooplankton (Calbet and Saiz, 2005; Gifford, 1991). Consequently, one question that arises about the computed carbon cycling estimates for mesozooplankton at station ALOHA is whether their growth and energetic demands can be met by the measured rates of primary production given the trophic losses associated with carbon and energy transfer through an indirect multi-level food web. By construction (i.e., mesozooplankton production = 20% of their ingestion), up to 20% of the zooplankton feeding requirements could be satisfied by internal predation of their biomass production (ZP) by carnivorous or omnivorous taxa. If we assume that only half of ZP is eaten by carnivorous zooplankton, the rest going to other consumers like mesopelagic fishes, then growth and metabolic demands of suspension-feeding mesozooplankton equivalent to 30.3% (range 23-42%) of daily primary production (= 90% of our estimated mean ingestion rates) would need to be met by feeding on prey that comes indirectly from phytoplankton via an intermediate trophic step. Assuming a gross growth efficiency of ~30% (Straile, 1997) for protistan consumers, the effective transfer efficiency is 37% (0.9*0.3 + 0.1*1.0 = 0.37) for a 0.9 trophic level separation between phyto- and mesozooplankton. The flow to mesozooplankton should therefore require an average of 82% (range 61-114%) of primary production, which is not unreasonable for a tightly coupled open-

ocean food web. While this simple calculation does not validate all of the assumptions of our rates calculations, it does illustrate that the resulting estimates are internally consistent with what is known about productivity and trophic structure of the system. Primary production of the NPSG is clearly sufficient to support carbon requirements for respiration and growth of the mesozooplankton standing stock of the region at the rates suggested by the Ikeda (1985) and Hirst and Lampitt (1998) equations.

As expected from the mesozooplankton biomass pattern and the biomass-based empirical relationships (e.g., Calbet, 2001), ingestion and egestion rates increase with increasing PP. This has also been observed empirically in the responses of mesozooplankton biomass and grazing impact to enhanced productivity in mesoscale eddies in the NPSG (Landry *et al.,* 2008) and the NASG (Goldthwait and Steinberg, 2008). The temporal increase in productivity at station ALOHA is associated with increase in colonial and endosymbiotic nitrogen-fixing cyanobacteria (Karl *et al.,* 2001). Ingestion/egestion estimates are highly variable after 2004. Relative to other years, the decrease in ingestion/egestion in 2006 coincided with a decrease in biogenic silica concentrations (Brzezinski *et al.,* 2011), as well as with a change in the microbial community due to higher biomass of autotrophic eukaryotes and higher contribution of dinoflagellates to the heterotrophic biomass (Pasulka *et al.,* 2013). In 2012, anomalous upper water-column conditions in summer were characterized by low primary production and low diazotroph abundance (Wilson *et al.,* 2015), which likely affected food availability to the mesozooplankton.

As discussed above, increasing system productivity is expected to alter food-web size structure by selecting for larger phytoplankton (e.g., Landry, 2002; Thingstad, 1998). If the main effect is to enhance the efficiency of the direct trophic link between phyto- and zooplankton, one might expect increased productivity to lead to a disproportionate increase in the zooplankton

biomass supported by PP and therefore a disproportionate increase in the carbon cycling by zooplankton. If the main effect is to select for a significantly larger mean size of zooplankton, carbon cycling might decrease relative to PP due to lower biomass-specific rates of feeding and metabolism. Although our results do show a modest 16% increase in the ratio of potential mesozooplankton ingestion to PP between decades 1994–2003 and 2004–2015 (largely because of the high ratio in 2011), perhaps suggesting a possible direction of change, the trend analysis is not significant due to differences in the responses of size classes. Linear increases of the largest and smallest mesozooplankton size classes with PP will have opposing effects on biomass-specific rates, and the 2nd largest size fraction (2-5 mm animals) has no significant temporal trend. The resulting trend in the ingestion ratio (Figure 4a) therefore most resembles the biomass trends for intermediate (0.5-2 mm) size fractions, leveling off or declining after an early increase. We can conclude from this analysis that complexities in zooplankton size structure responses to varying PP tend to mute rather than amplify the effects on mesozooplankton roles in carbon cycling. If this is the case for a period of increasing PP, we might expect to first order a similar resistance to change during possible future periods of declining productivity.

Mesozooplankton and Export Flux

Mesozooplankton contribute to export flux from the euphotic zone in two important ways: 1) by their production of fecal pellets or egesta that become part of the passively sinking particle field and 2) by their active transport and loss of organic matter to depth by metabolism and mortality during diel vertical migrations. Similar to the result of Steinberg *et al.* (2012) for the Bermuda Atlantic Time Series (BATS), the potential contribution of mesozooplankton fecal egesta to particulate organic carbon (POC) flux has increased significantly at station ALOHA. This is because measured sediment trap flux has decreased slightly over the study period while

mesozooplankton biomass has increased substantially. On average, our calculated rates of fecal pellet production account for 191% of the sinking export flux of POC collected at the base of the euphotic zone (150 m), consistent with previous estimates for the subtropical (Roman *et al.,* 2002a) and equatorial Pacific (Dam *et al.,* 1995a). The pellet production estimates could be high because temporal changes in assimilation efficiencies were not considered (see Roman *et al.,* 2002a). The high ratio of fecal pellet production to measured POC flux could also reflect trap undersampling due to hydrodynamics (Butman, 1986) or missed pulses of POC export in the short-term (~ 3 days/month) trap deployments (see Karl *et al.,* 2012). However, the pellet production estimates are not necessarily inconsistent with the trap measurements because most of the pellets produced by smaller zooplankton are recycled in the euphotic zone (e.g., Roman *et al.,* 2002a; Urrere and Knauer, 1981; Wilson *et al.,* 2008).

In contrast to corresponding estimates for both daytime and nighttime mesozooplankton biomass, migrant biomass does not show a significant seasonal pattern or long-term trend, despite being higher in 2016 than at the beginning of the time series in 1994. This is due mainly to the lack of a systematic change in the 2-5 mm size class, which accounts for most migrant biomass. Previously, Hannides *et al.* (2009) documented an increase in migrant biomass and migrant-mediated export flux at station ALOHA from1994–2005, which suggests that more recent conditions (e.g., food availability, predation, physical environment) have become less favorable. Likewise, our results contrast with the long-term increase in migrant mesozooplankton biomass at BATS documented by Steinberg *et al.* (2012) from 1994–2010. At station ALOHA, the years of lowest migrant biomass, 1997 and 2009, were both El Niño years (1997–1998, 2009–2010) with the lowest total zooplankton biomass (Valencia *et al.,* 2016). The 1997–1998 El Niño corresponded to the canonical eastern-Pacific event, whereas the 2009–2010

El Niño was described as a central-Pacific event with differing ocean and atmospheric expressions (Di Lorenzo *et al.,* 2013). Although the size distributions of zooplankton biomass differed between these two events, both showed a low contribution of the >5 mm size class (Appendix Figure S2.5).

Annual changes in migrant mesozooplankton biomass are mainly explained by fluctuations in PP and 3-year lagged PDO; however, the response is nonlinear and complex (Figure 8). In the range in which the relationship between migrant biomass and PP is positive, the model suggests that increased system productivity transfers up the food web, enhancing the mesozooplankton contribution to metabolic fluxes in the mesopelagic zone. In the adjacent equatorial Pacific region, migrant biomass and grazing impact correlate positively with food availability, in particular, the peak concentrations of auto- and heterotrophic microplankton, as well as mean total microplankton biomass in the euphotic zone and mixed layer (Décima *et al.,* 2011). However, our model also suggests that there is a range in which the relationship between PP and migrant biomass is negative (~510 < PP < 570 mg C m^{-2} d^{-1}), consistent with the inverse relationship described between active flux mediated by migrant mesozooplankton and trophic state (e.g., Isla *et al.,* 2015; Longurst *et al.,* 1989; Roman *et al.,* 2002b). The positive-to-negative shift in the relationship between mesozooplankton migrant biomass and PP at station ALOHA may be due to a change in migrant community structure, perhaps driven by predation pressure. Likewise, the positive (PDO.y3 > +1) and negative (PDO.y3 < -1) effects of the PDO suggest that other variables not evaluated in this study, possibly covarying with the PDO, might be driving the relationship. As expected, the contribution of migrant active flux relative to the gravitational flux of particles collected in sediment traps was lower when migrant biomass was low (1997 and 2009, both El Niño years).

Despite the different temporal trends reported by Hannides *et al.* (2009) compared to this study, the relative magnitudes of migrant-mediated fluxes of carbon (17%), nitrogen (17%) and phosphorus (41%) compared to passive particulate flux are similar. Because most PP in oligotrophic regions is recycled in the euphotic zone (Eppley and Peterson, 1979; Karl, 1999), the active flux mediated by migrant mesozooplankton has been shown to represent an important contribution to the total export flux in the North Atlantic (Dam *et al.,* 1995b; Isla *et al.,* 2004; Steinberg *et al.,* 2000, 2002, 2012) and the North Pacific (Al-Mutairi and Landry, 2001; Hannides *et al.,* 2009; this study). In addition, because the NPSG is considered a phosphate-limited region (Karl *et al.,* 2001), migrant mediated phosphate flux at station ALOHA is particularly important (Hannides *et al.,* 2009), which is evident in comparing the elemental ratios (C:N:P) of the particulate (251:32:1) and active fluxes (101:13:1). As highlighted by Hannides *et al.* (2009), our results suggest that migrant mesozooplankton release more of their ingested phosphorus than nitrogen. It is notable, however, that while the computed N:P excretion ratios for mesozooplankton are only slightly less than the 16:1 expected for Redfield, the ratios for sinking particles is double the Redfield value. This is indicative of a P-limited system that efficiently recycles P in the euphotic zone relative to N, which is available in excess due to N_2 fixation (Karl, 1999). Despite the limitations of estimating fluxes from empirical relationships, it is clear that the migrant contributions to export flux and stoichiometry in oligotrophic regions should be included in biogeochemical models to better understand all of the biological influences on elemental fluxes from the surface to the deep ocean.

Conclusions

Because mesozooplankton can be viewed as temporal integrators of lower trophic level cycling in ocean food webs, the past two decades of increasing primary production at station ALOHA provides an opportunity to assess how variability in NPSG productivity can affect food web function and relationships. We show that the measured production rates can meet the respiration and growth requirements of NPSG mesozooplankton as determined by commonly used empirical relationships, consistent with a tightly coupled production-grazing food web with approximately one intermediate trophic step, on average, between phyto- and mesozooplankton (Landry and Décima, 2017). While total biomass and food consumption of mesozooplankton increase with increasing primary production, the effects on carbon cycling are not significantly disproportionate to PP due to complexities in the size structure responses. There is however a disproportionate enhancement of the potential mesozooplankton contribution via fecal pellet production to passive particulate export from the euphotic zone. In contrast, the biomass associated with vertically migrating mesozooplankton shows a dome-shape response to increasing primary production, leading to no significant change in the ratio of migrant-mediated active flux to measured passive export in sediment traps. We show that this is due to the altered size structure of mesozooplankton biomass, which has become more even across size classes with increasing system productivity. The future trend in NPSG productivity remains uncertain, potentially involving stratification effects that reduce phytoplankton biomass and select for picophytoplankton (e.g., Doney *et al.,* 2012) or, conversely, temperature and CO2 effects that further enhance diazotrophy (Hutchins *et al.,* 2007), and there is no assurance that even a reversal of the current trend of increasing PP will return the system to its previous state in all respects. Despite these uncertainties, the current results provide crude predictions of

relationships that might occur in the future, but which need to be confirmed and better understood by process-oriented mechanistic study.

Acknowledgments

This study would not have been possible without the hard work and dedication of the core HOT program group over the past two decades of time series cruises at station ALOHA. We specifically acknowledge David Karl and Matt Church for their leadership roles in the HOT Program, as well as the direct contributions of Cecelia C.S. Hannides, Karen Selph, Scott Nunnery, Stephanie Christensen, Rebecca Scheinberg, Colleen Allen, Melinda Simmons, and Blake Watkins to the HOT zooplankton collections and analyses. This work was supported by National Science Foundation grants OCE-0324666, OCE-0926766, and OCE-1260164. The Ph.D. research of B.V. was further supported by a scholarship (529-2011) from the Colombian Administrative Department of Science, Technology and Innovation (COLCIENCIAS). Mesozooplankton biomass data used in this study are available through the HOT website (http://hahana.soest. hawaii.edu/hot/hot-dogs/index.html).

Chapter 2, in full, has been submitted for publication of the material as it may appear in Valencia B, Décima M, Landry MR. Environmental effects on mesozooplankton size structure and export flux at station ALOHA, North Pacific Subtropical Gyre. *Global Biogeochemical Cycles.* The dissertation author was the primary investigator and author of this manuscript.

Table 2.1. Summary of the environmental conditions used to calculate mesozooplankton growth, respiration and excretion rates from 1994 to 2015 at station ALOHA. Euphotic zone estimates of the potential contributions of mesozooplankton to carbon cycling via ingestion and fecal pellet production are also presented. Mean ± standard deviation (SD). n = 22

	Mean ± SD	Range
Primary production (mg C m^{-2} d^{-1})	516 ± 53	410 - 609
Sea surface temperature (°C)	24.9 ± 0.3	24.2 - 25.5
Temperature 0-100 m (°C)	24.4 ± 0.3	23.8 - 24.8
Temperature 300-500 m (°C)	9.6 ± 0.3	8.8 - 10.2
Ingestion (mg C m^{-2} d^{-1})	170 ± 34	107 - 247
Fecal pellet production (mg C m^{-2} d^{-1})	51 ± 10	32 - 74

Table 2.2. Passive and active fluxes of carbon, nitrogen, and phosphorus (mg m^{-2} d^{-1}) at station ALOHA. Passive fluxes are from particulate matter collected in sediment traps deployed at 150 m from 1994 to 2014. Active fluxes are migrant-mediated export of dissolved inorganic and organic compounds due to zooplankton metabolism at mesopelagic depths from 1994 to 2015. Egestion corresponds to fecal pellets produced by mesozooplankton in the euphotic zone (Section 3.2). Mean ± standard deviation (SD).

	Carbon	Nitrogen	Phosphorus
Passive flux (n = 21)	27.51 ± 3.58	4.07 ± 0.60	0.31 ± 0.08
Active flux (n = 22)			
Inorganic	4.24 ± 1.17	0.63 ± 0.17	0.11 ± 0.03
Organic	1.34 ± 0.37	0.30 ± 0.08*	0.10 ± 0.03
Active/Passive flux (%)	17 ± 4	17 ± 4	41 ± 16
Egestion/Passive flux (%)	191 ± 40	-	-

* Dissolved organic nitrogen (DON) excretion using Steinberg *et al.* (2002) relationship that assumes DON represents 32% of the total dissolved nitrogen (TDN) excreted. Due to uncertainties in the relationship DON:TDN, values are also presented using Le Borgne and Rodier (1997) relationship that assumes DON represents 53% of TDN excretion, 0.71 ± 0.20 mg N m^{-2} d^{-1}.

Table 2.3. Effect of environmental factors on biomass size structure and migrant biomass of mesozooplankton at station ALOHA from 1994 to 2015. Generalized Additive Model results are presented for the final models selected. Biomass size structure was evaluated by calculating the slope of least square linear regressions between normalized biomass-size spectrum (NB-SS Slope) and by the Shannon-Wiener (Size Diversity) index. Migrant biomass (mg DW m^{-2}) correspond to the difference between day and night mesozooplankton dry weight estimates. Results of the effect of each environmental factor on the response variables (two variable GAM) (Table S6) and non-significant models (Table S7) are presented in supporting information. PP: primary production (mg C m^{-2} d^{-1}), SST: sea surface temperature (°C), NPGO: north Pacific gyre oscillation, PDO.y3: Pacific decadal oscillation lagged 3 years. SE: standard error, edf: effective degrees of freedom, r^2: coefficient of determination, DE: deviance explained. n = 22

Response variable	Parametric terms				Smooth terms				
		Estimate	SE	P value	Covariate	edf	P value	r^2	DE (%)
NB-SS Slope	Intercept	-1.27	0.01	< 0.001	SST	3.64	< 0.001	0.70	74.8
Size Diversity	Intercept	1.39	0.04	< 0.001	SST	2.46	0.004	0.60	66.7
	PP	0.24	0.09	0.012					
Migrant Biomass	Intercept	0.41	0.01	< 0.001	PP	3.98	0.002	0.61	72.9
					PDO.y3	2.50	0.020		

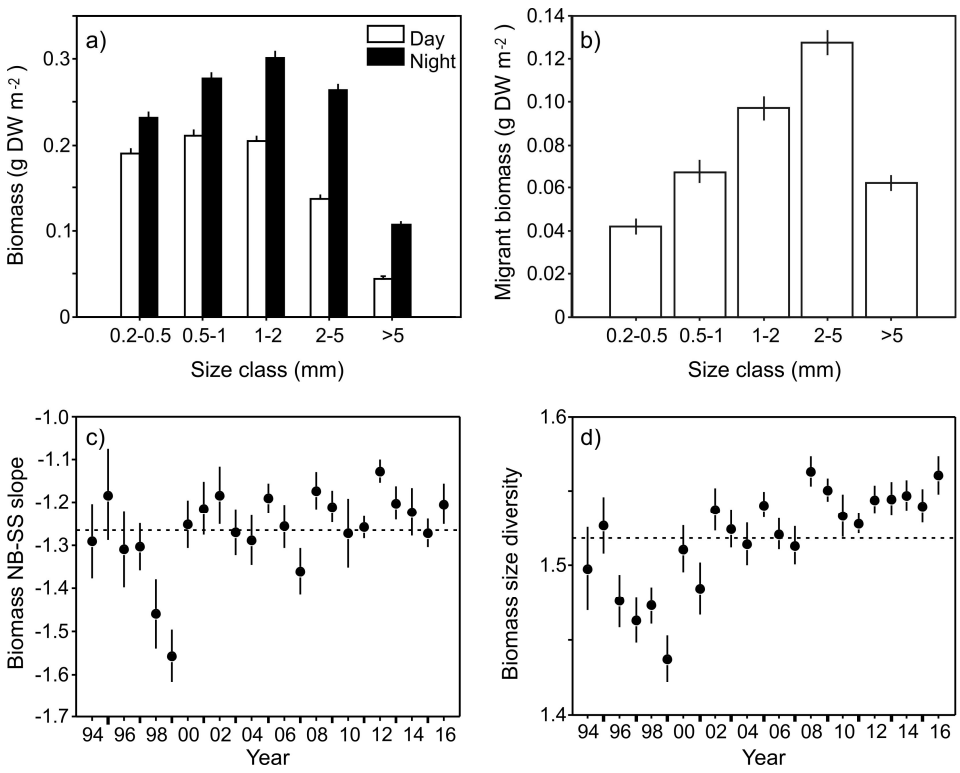

Figure 2.1. Mesozooplankton biomass size structure at station ALOHA from 1994 to 2016. (**a**) Day and night biomass and (**b**) migrant biomass in each size class. Biomass size structure was evaluated by (**c**) changes in the slope of the normalized biomass-size spectrum (NB-SS) and (**d**) changes in the Shannon-Wiener size diversity index. Mean slope and size diversity are indicated by a dashed line. Bars and dots correspond to the mean ± SE.

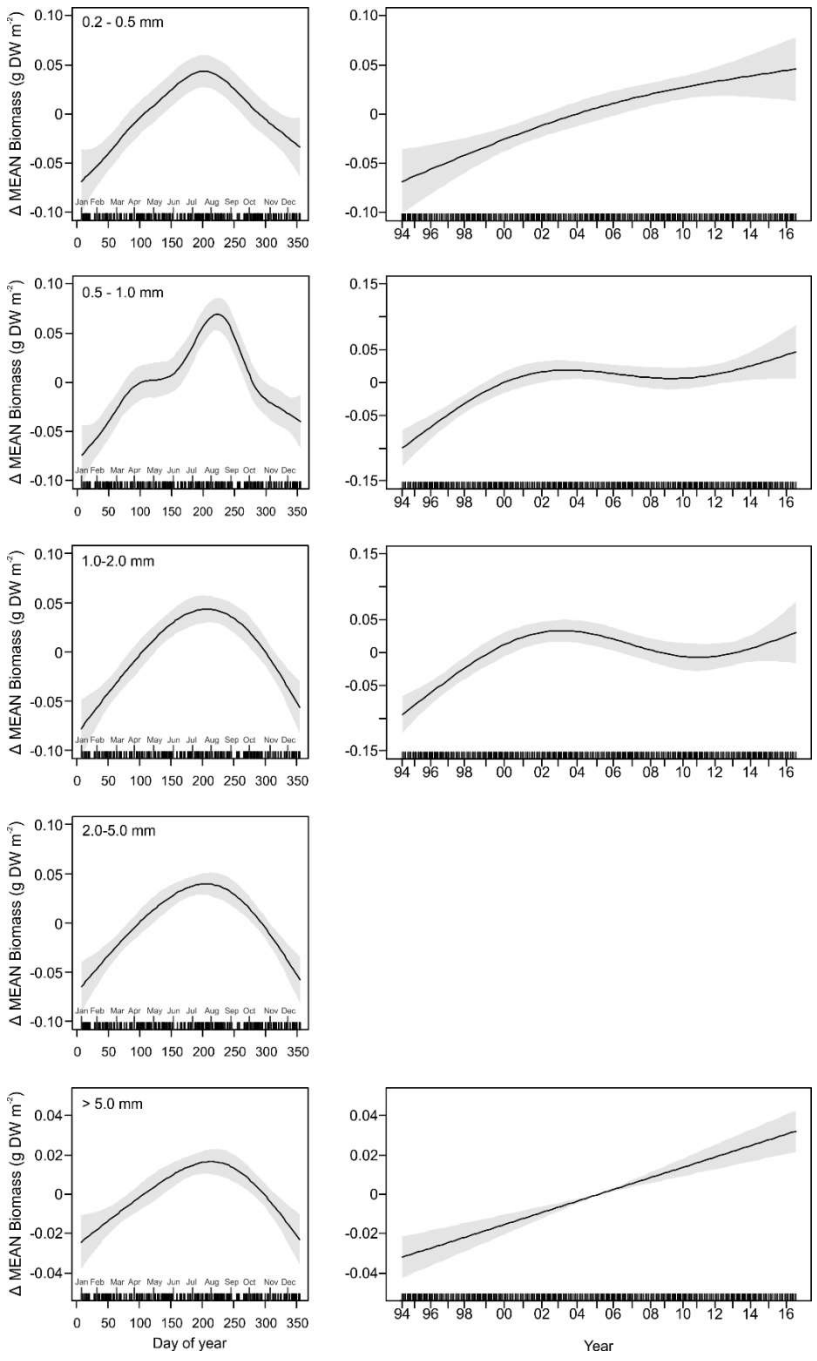

Figure 2.2. Temporal trends of each size class for mean mesozooplankton biomass (mean of paired day-night DW) at station ALOHA from 1994 to 2016. Partial regression plots represent the modeled seasonal and long-term trends of biomass using GAMs (see Table S3). X-axes are the model covariates (day of year and date) and the tick marks represent each observation. Y-axes represent the effects of covariates on predicted mesozooplankton biomass. Y-axes values are deviations from mean biomass and thus are centered. Numbers in parentheses are the effective degrees of freedom. Solid lines are the modeled trends and shaded areas are the 95% confidence intervals. Predicted values are obtained by adding the deviations from each smooth function to the mean.

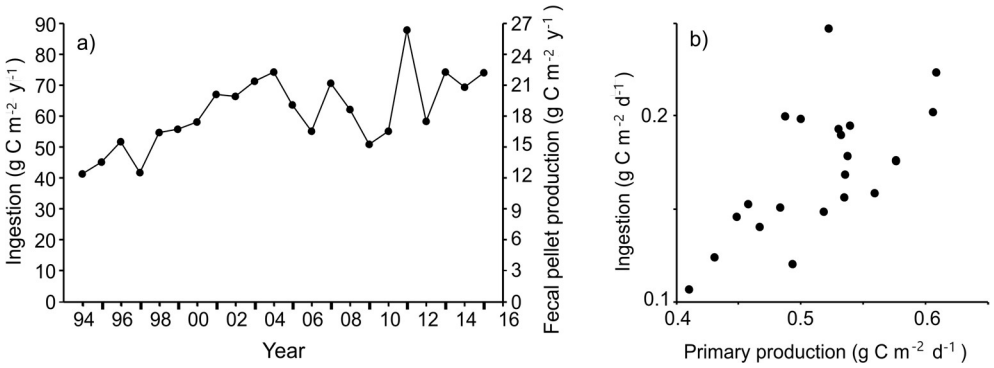

Figure 2.3. Estimates of mesozooplankton ingestion impact and fecal pellet production at station ALOHA from 1994 to 2015. (a) Interannual variability of ingestion and fecal pellet production. (b) Relationship between mesozooplankton ingestion estimates and primary production (rs = 0.63, p = 0.002).

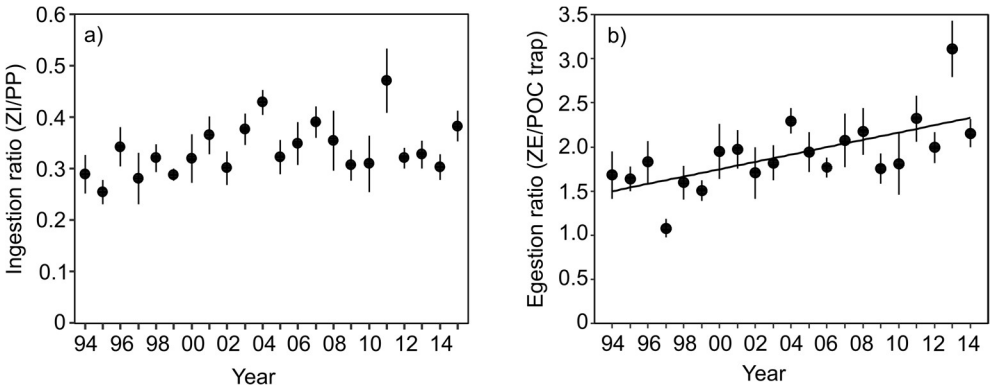

Figure 2.4. Temporal trends in annually averaged ratios of (**a**) mesozooplankton ingestion relative to primary production (ZI/PP) and (**b**) mesozooplankton fecal pellet production (ZE) relative to passive particulate organic carbon (POC) collected in 150-m sediment traps at station ALOHA. The significance of the trends was evaluated by GAMs. The trend of the ratio ZI/PP is not significant (p = 0.10, Table S5). The increase in the ratio ZE/POC trap is significant (p < 0.05, Table S5).

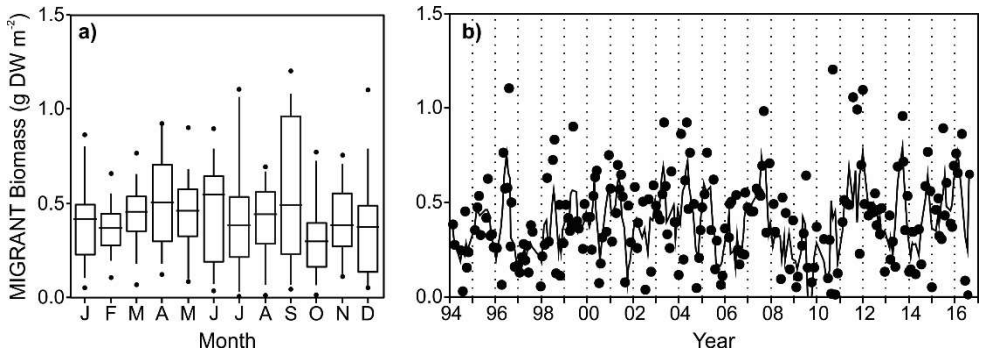

Figure 2.5. Temporal variability of migrant mesozooplankton biomass at station ALOHA from 1994 to 2016 evaluated using a GAM. Model results suggest that there is no significant seasonal pattern or long-term trend (Table S3, $p > 0.05$). (**a**) Monthly variability of migrant biomass. Boxes and whiskers correspond to 25-75th and 5-95th percentiles, respectively. The horizontal line represents the median and the circles represent outliers. (**b**) Interannual variability of migrant biomass. Fitted line is a three-point moving average. Results of the temporal analysis of day and night zooplankton biomass are presented in supporting information (Table S3, Figure S1).

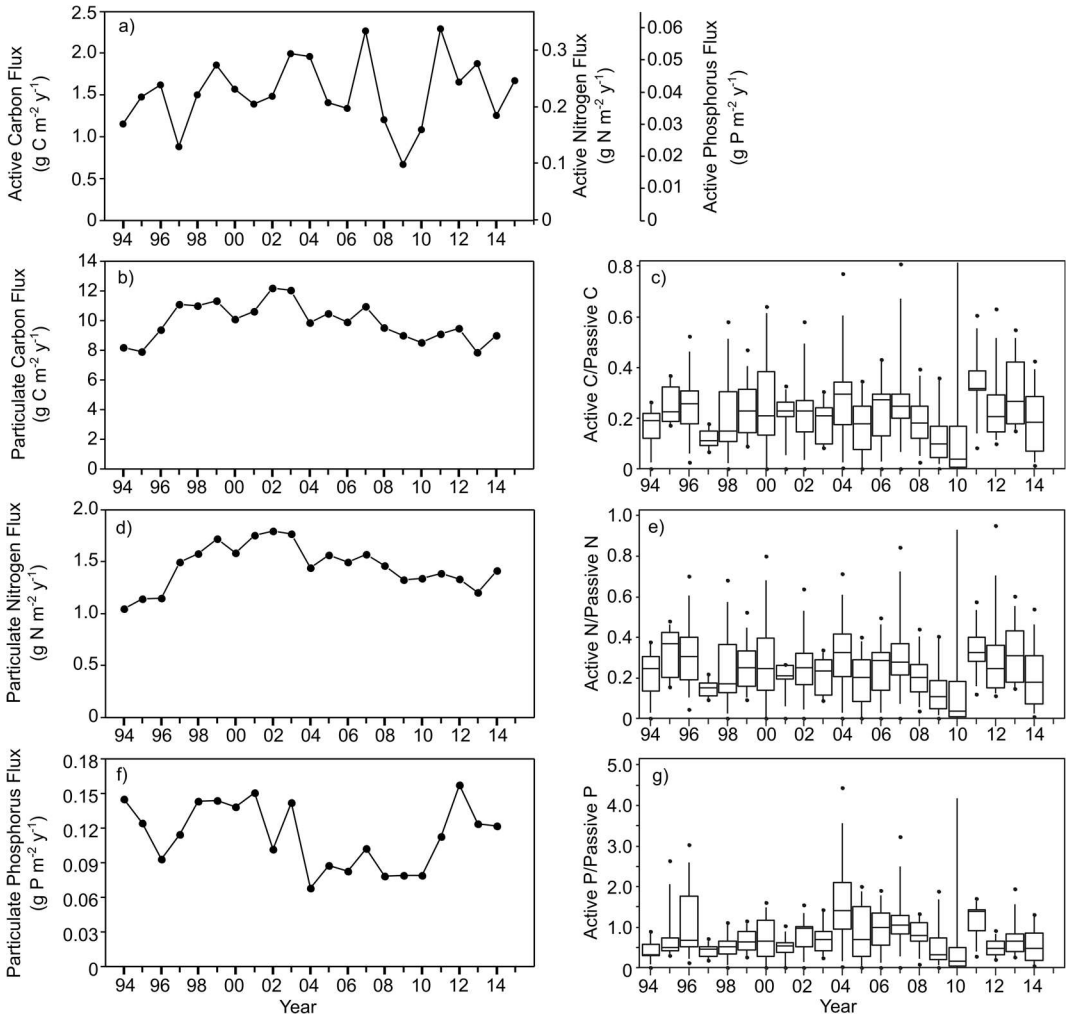

Figure 2.6. Active and passive flux (g m^{-2} y^{-1}) of carbon (C), nitrogen (N), and phosphorus (P) at station ALOHA. Active flux mediated by migrating mesozooplankton corresponds to the dissolved metabolic byproducts of respiration and excretion at mesopelagic depths (inorganic compounds). Although the magnitudes of the active fluxes of C, N and P differ, their temporal trends are the same because all were calculated as a function of mesozooplankton biomass and temperature following the equations proposed by Ikeda (1985). Passive flux corresponds to particulate organic matter collected at 150 m in sediment traps. Boxplots show the proportions of total migrant-mediated active flux (dissolved inorganic and organic compounds) to the passive flux of particles collected in sediment traps. Boxes and whiskers correspond to 25-75th and 5-95th percentiles, respectively. The horizontal lines represent the median and the circles represent outliers.

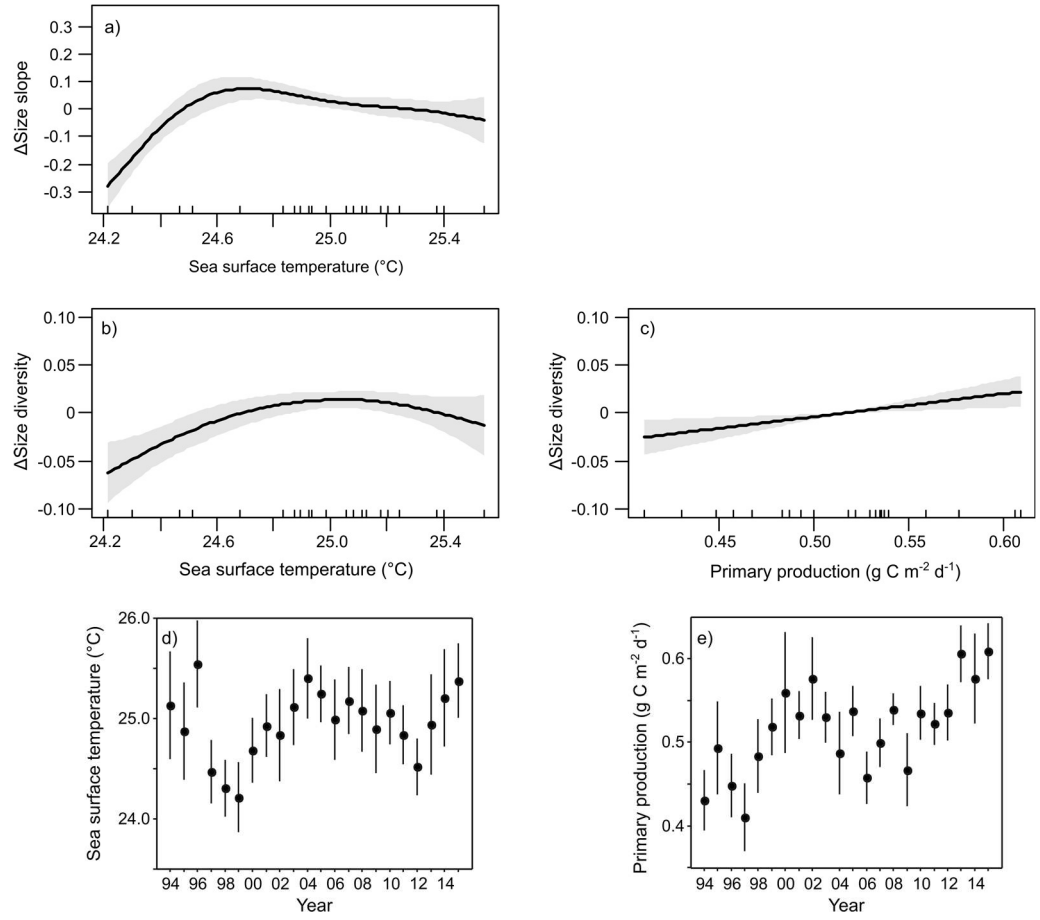

Figure 2.7. Relationships between mesozooplankton biomass size structure and environmental factors at station ALOHA evaluated using GAMs. Partial regression plots (**a**-**c**) represent the effects of environmental factors on the NB-SS slope (size slope) and size diversity for the generalized additive models selected. Axes as described in Figure 2. Interannual variability (mean ± SE) of sea surface temperature (**d**) and primary production (**e**).

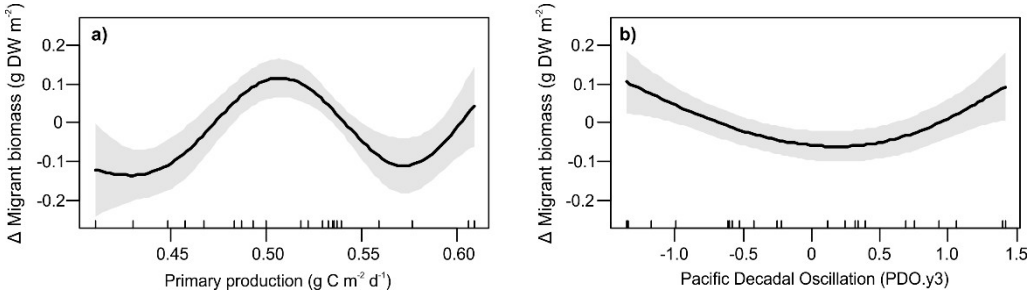

Figure 2.8. Relationships between migrant mesozooplankton biomass and environmental factors at station ALOHA. Partial regression plots represent the effect of (**a**) primary production and (**b**) PDO lagged by 3 years on biomass for the GAM selected. Axes as described in Figure 2.

References

Al-Mutairi, H., & Landry, M. R. (2001). Active export of carbon and nitrogen at Station ALOHA by diel migrant zooplankton. Deep-Sea Researcch II, 48, 2083-2103.

Ayón, P., Swartzman, G., Espinoza, P., & Bertrand, A. (2011). Long-term changes in zooplankton size distribution in the Peruvian Humboldt Current System: Conditions favoring sardine or anchovy. Marine Ecology Progress Series, 422, 211-222.

Beaugrand, G., Brander, K. M., Lindley, J. A., Souissi, S., & Reid, P. C. (2003). Plankton effect on cod recruitment in the North Sea. Nature, 426, 661-664.

Beaugrand, G., Edwards, M., & Legendre, L. (2010). Marine biodiversity, ecosystem functioning, and carbon cycles. Proceedings of the National Academy of Sciences. U.S.A, 107, 10120-10124.

Butman, C. A. (1986). Sediment trap biases in turbulent flows: results from a laboratory flume study. Journal of Marine Research, 44, 645-693.

Brzezinski, M. A., Krause, J. W., Church, M. J., Karl, D. M., Li, B., Jones, J. L., & Updyke, B. (2011). The annual silica cycle of the North Pacific Subtropical Gyre. Deep Sea Research I, 58, 988-1001.

Calbet, A. (2001). Mesozooplankton grazing effect on primary production: A global comparative analysis in marine ecosystems. Limnology and Oceanography, 46, 1824-1830.

Calbet, A., & Landry, M. R. (1999). Mesozooplankton influences on the microbial food web: Direct and indirect trophic interactions in the oligotrophic open ocean. Limnology and Oceanography, 44, 1370-1380.

Calbet, A., & Saiz, E. (2005). The ciliate-copepod link in marine ecosystems. Aquatic Microbial Ecology, 38, 157-167.

Calbet, A., Atienza, D., Henriksen, C. I., Saiz, E., & Adey, T. R. (2009). Zooplankton grazing in the Atlantic Ocean: A latitudinal study. Deep-Sea Research II, 56, 954-963.

Chiba, S., Batten, S. D., Yoshiki, T., Sasaki, Y., Sasaoka, K., Sugisaki, H., & Ichikawa, T. (2015). Temperature and zooplankton size structure: Climate control and basin-scale comparison in the North Pacific. Ecology and Evolution, 5, 968-978.

Dam, H. G., & Peterson, W. T. (1991). In situ feeding behavior of the copepod Temora longicornis: Effects of seasonal changes in chlorophyll size fractions and female size. Marine Ecology Progress Series, 71, 113-123.

Dam, H. G., Zhang, X., Butler, M., & Roman, M. R. (1995a). Mesozooplankton grazing and metabolism at the equator in the central Pacific: Implications for carbon and nitrogen fluxes. Deep-Sea Research II, 42, 735-756.

Dam, H. G., Roman, M. R., & Youngbluth, M. J. (1995b). Downward export of respiratory carbon and dissolved inorganic nitrogen by diel-migrant mesozooplankton at the JGOFS Bermuda time-series station. Deep-Sea Research I, 42, 1187-1197.

Décima, M., Landry, M. R., & Rykaczewski, R. R. (2011). Broad scale patterns in mesozooplankton biomass and grazing in the eastern equatorial Pacific. Deep-Sea Research I, 58, 387-399.

Di Lorenzo, E., Combes, V., Keister, J. E., Strub, P. T., Thomas, A. C., Franks, P. J., Ohman, M. D., Furtado J. C., Bracco, A., Bograd, S. J., Peterson, W. T., Schwing, F. G., Chiba, S., Taguchi, B., Hormazabal, S., Parada, C. (2013). Synthesis of Pacific Ocean climate and ecosystem dynamics. Oceanography, 26, 68-81.

Doney, S. C., Ruckelshaus, M., Duffy, J. E., Barry, J. P., Chan, F., English, C. A., Galindo, H. M., Grebmeier, J. M., Hollowed, A. B., Knowlton, N., Polovina, J., Rabalais, N. N., Sydeman, W. J., Talley, L. D. (2012). Climate change impacts on marine ecosystems. Annual Review of Marine Science, 4, 11-37.

Eppley, R. W., & Peterson, B. J. (1979). Particulate organic matter flux and planktonic new production in the deep ocean. Nature, 282, 677-680.

García-Comas, C., Chang, C. Y., Ye, L., Sastri, A. R., Lee, Y. C., Gong, G. C., & Hsieh, C. (2014). Mesozooplankton size structure in response to environmental conditions in the East China Sea: How much does size spectra theory fit empirical data of a dynamic coastal area? Progress in Oceanography, 121, 141-157.

Gifford, D. J. (1991). The Protozoan-metazoan trophic link in pelagic ecosystems. Journal of Eukaryotic Microbiology, 38, 81-86.

Goldthwait, S. A., & Steinberg, D. K. (2008). Elevated biomass of mesozooplankton and enhanced fecal pellet flux in cyclonic and mode-water eddies in the Sargasso Sea. Deep Sea Research II, 55, 1360-1377.

Hannides, C. C. S., Landry, M. R., Benitez-Nelson, C. R., Styles, R. M., Montoya, J. P., & Karl, D. M. (2009). Export stoichiometry and migrant-mediated flux of phosphorus in the North Pacific Subtropical Gyre. Deep-Sea Research I, 56, 73-88.

Hernández-León, S., & Ikeda, T. (2005). Zooplankton respiration. In P. Del Gorgio & P. Williams (Eds.), Respiration in Aquatic Systems (pp. 57-82). Oxford University Press, New York.

Hirst, G. A., & Lampitt, S. R. (1998). Towards a global model of in situ weight-specific growth in marine planktonic copepods. Marine Biology, 132, 247-257.

Hirst, A. G., & Bunker, A. J. (2003). Growth of marine planktonic copepods: Global rates and patterns in relation to chlorophyll a, temperature, and body weight. Limnology and Oceanography, 48, 1988-2010.

Horne, C. R., Hirst, A. G., Atkinson, D., Neves, A., & Kiørboe, T. (2016). A global synthesis of seasonal temperature–size responses in copepods. Global Ecology and Biogeography, 25, 988-999.

Huntley, M. E., Lopez, M. D. G., Zhou, M., & Landry, M. R. (2006). Seasonal dynamics and ecosystem impact of mesozooplankton at station ALOHA based on optical plankton counter measurements. Journal of Geophysical Research, 111, C05S10, doi:10.1029/2005JC002892.

Hutchins, D. A., Fu, F. X., Zhang, Y., Warner, M. E., Feng, Y., Portune, K., Bernhardt, P. W., Mulholland, M. R. (2007). CO_2 control of Trichodesmium N_2 fixation, photosynthesis, growth rates, and elemental ratios: Implications for past, present, and future ocean biogeochemistry. Limnology and Oceanography, 52, 1293-1304.

Ikeda, T. (1985). Metabolic rates of epipelagic marine zooplankton as a function of body mass and temperature. Marine Biology, 85, 1-11.

Isla, J. A., Llope, M., & Anadón, R. (2004). Size-fractionated mesozooplankton biomass, metabolism and grazing along a 50°N–30°S transect of the Atlantic Ocean. Journal of Plankton Research, 26, 1301-1313.

Isla, A., Scharek, R., & Latasa, M. (2015). Zooplankton diel vertical migration and contribution to deep active carbon flux in the NW Mediterranean. Journal of Marine Systems, 143, 86-97.

Karl, D. M. (1999). A sea of change: Biogeochemical variability in the North Pacific Subtropical Gyre. Ecosystems, 2, 181-214.

Karl, D. M., Bidigare, R. R., & Letelier, R. M. (2001). Long-term changes in plankton community structure and productivity in the North Pacific Subtropical Gyre: The domain shift hypothesis. Deep-Sea Research II, 48, 1449-1470.

Karl, D. M., Church, M. J., Dore, J. E., Letelier, R. M., & Mahaffey, C. (2012). Predictable and efficient carbon sequestration in the North Pacific Ocean supported by symbiotic nitrogen fixation. Proceedings of the National Academy of Sciences. U.S.A, 109, 1842-1849.

Keister, J. E., Di Lorenzo, E., Morgan, C. A., Combes, V., & Peterson, W. T. (2011). Zooplankton species composition is linked to ocean transport in the Northern California Current. Global Change Biology, 17, 2498-2511.

Landry, M. R. (2002). Integrating classical and microbial food web concepts: evolving views from the open-ocean tropical Pacific. Hydrobiologia, 480, 29-39.

Landry, M. R., & Décima, M. (2017). Protistan microzooplankton and the trophic position of tuna: quantifying the trophic link between micro- and mesozooplankton in marine foodwebs. ICES Journal of Marine Science, fsx006, doi:10.1093/icesjms/fsx006.

Landry, M. R., Al-Mutairi, H., Selph, K. E., Christensen, S., & Nunnery, S. (2001). Seasonal patterns of mesozooplankton abundance and biomass at Station ALOHA. Deep-Sea Research II, 48, 2037-2061.

Landry, M. R., Décima, M., Simmons, M. P., Hannides, C. C., & Daniels, E. (2008). Mesozooplankton biomass and grazing responses to Cyclone Opal, a subtropical mesoscale eddy. Deep-Sea Research II, 55, 1378-1388.

Longhurst, A. R., Bedo, A., Harrison, W. G., Head, E. J. H., Horne, E. P., Irwin, B. & Morales, C. (1989). NFLUX: a test of vertical nitrogen flux by diel migrant biota. Deep-Sea Research A, 36, 1705-1719.

Manríquez, K., Escribano, R., & Riquelme-Bugueño, R. (2012). Spatial structure of the zooplankton community in the coastal upwelling system off central-southern Chile in spring 2004 as assessed by automated image analysis. Progress in Oceanography, 92-95, 121-133.

McGowan, J. A., & Walker, P. W. (1985). Dominance and diversity maintenance in an oceanic ecosystem. Ecology Monographs, 55, 103-118.

Medellín-Mora, J., Escribano, R., & Schneider, W. (2016). Community response of zooplankton to oceanographic changes (2002–2012) in the central/southern upwelling system of Chile. Progress in Oceanography, 142, 17-29.

O'Brien, T. D., Wiebe, P. H., & Falkenhaug, T. (2013). ICES zooplankton status report 2010/2011.

Oksanen, J., Blanchet, F. G., Friendly, M., Kindt, R., Legendre, P., McGlinn, D., Minchin, P. R., O'Hara, R. B., Simpson, G. L., Solymos, P., Stevens, M. H. H., Szoecs, E., Wagner, H. (2017). vegan: Community ecology package. R package version 2.4-3.

Omori, M., & Ikeda, T. (1984). Methods in Marine Zooplankton Ecology, John Wiley.

Paffenhöfer, G. A., & Knowles, S. C. (1979). Ecological implications of fecal pellet size, production and consumption by copepods. Journal of Marine Research, 37: 35-49.

Pasulka, A. L., Landry, M. R., Taniguchi, D. A., Taylor, A. G., & Church, M. J. (2013). Temporal dynamics of phytoplankton and heterotrophic protists at station ALOHA. Deep-Sea Research II, 93, 44-57.

Peterson, W. T., & Schwing, F. (2003). A new climate regime in northeast pacific ecosystems. Geophysical Reserch Letters, 30, 1896, doi:10.1029/2003GL017528.

Pinheiro, J., Bates, D., DebRoy, S., Sarkar, D., & R Core Team. (2015). nlme: Linear and nonlinear mixed effects models. R package version 3.1-123.

Pomeroy, L. R., Mathews, H. M., & Min, H. S. (1963). Excretion of phosphate and soluble organic phosphorus compounds by zooplankton. Limnology and Oceanography, 8, 50-55.

Quiñones, R. A., Platt, T., & Rodríguez, J. (2003). Patterns of biomass-size spectra from oligotrophic waters of the Northwest Atlantic. Progress in Oceanography, 57, 405-427.

Rodríguez, J., & Mullin, M. M. (1986). Diel and interannual variation of size distribution of oceanic zooplanktonic biomass. Ecology, 67, 215-222.

Roman, M. R., Adolf, H. A., Landry, M. R., Madin, L. P., Steinberg, D. K., & Zhang, X. (2002a). Estimates of oceanic mesozooplankton production: a comparison using the Bermuda and Hawaii time-series data. Deep-Sea Research II, 49, 175-192.

Roman, M. R., Dam, H. G., Le Borgne, R., & Zhang, X. (2002b). Latitudinal comparisons of equatorial Pacific zooplankton. Deep-Sea Research II, 49, 2695-2711.

Rykaczewski, R. R., & Checkley, D. M. (2008). Influence of ocean winds on the pelagic ecosystem in upwelling regions. Proceedings of the National Academy of Sciences. U.S.A, 105, 1965-1970.

Saba, V. S., Friedrichs, M. A., Carr, M. E., Antoine, D., Armstrong, R. A., Asanuma, I., Aumont, O., Bates, N. R., Behrenfeld, M. J., Bennington, V., Bopp, L., Bruggeman, J., Buitenhuis, E. T., Church, M. J., Ciotti, A. M., Doney, S. C., Dowell, M., Dunne, J., Dutkiewicz, S., Gregg,

W., Hoepffner, N., Hyde, K. J. W., Ishizaka, J., Kameda, T., Karl, D. M., Lima, I., Lomas, M. W., Marra, J., McKinley, G. A., Melin, F., Moore, J. K., Morel, A., O'Reilly, J., Salihoglu, B., Scardi, M., Smyth, T. J., Tang, S., Tjiputra, J., Uitz, J., Vichi, M., Waters, K., Westberry, T. K., Yool, A. (2010). Challenges of modeling depth-integrated marine primary productivity over multiple decades: A case study at BATS and HOT. Global Biogeochemical Cycles, 24, GB3020, doi:10.1029/2009GB003655.

Sheridan, C. C., & Landry, M. R. (2004). A 9-year increasing trend in mesozooplankton biomass at the Hawaii Ocean Time-series Station ALOHA. ICES Journal of Marine Science, 61, 457-463.

Sprules, W. G., & Munawar, M. (1986). Plankton size spectra in relation to ecosystem productivity, size, and perturbation. Canadian Journal of Fisheries and Aquatic Sciences, 43, 1789-1794.

Sprules, W. G., & Barth, L. E. (2016). Surfing the biomass size spectrum: Some remarks on history, theory, and application. Canadian Journal of Fisheries and Aquatic Sciences, 73, 477-495.

Steinberg, D. K., Cope, J. S., Wilson, S. E., & Kobari, T. (2008). A comparison of mesopelagic mesozooplankton community structure in the subtropical and subarctic North Pacific Ocean. Deep-Sea Research II, 55, 1615-1635.

Steinberg, D. K., Carlson, C. A., Bates, N. R., Goldthwait, S. A., Madin, L. P., & Michaels, A. F. (2000). Zooplankton vertical migration and the active transport of dissolved organic and inorganic carbon in the Sargasso Sea. Deep-Sea Research I, 47, 137-158.

Steinberg, D. K., Goldthwait, S. A., & Hansell, D. A. (2002). Zooplankton vertical migration and the active transport of dissolved organic and inorganic nitrogen in the Sargasso Sea. Deep-Sea Research I, 49, 1445-1461.

Steinberg, D. K., Lomas, M. W., & Cope, J. S. (2012). Long-term increase in mesozooplankton biomass in the Sargasso Sea: Linkage to climate and implications for food web dynamics and biogeochemical cycling. Global Biogeochemical Cycles, 26, GB1004, doi:10.1029/2010GB004026.

Straile, D. (1997). Gross growth efficiencies of protozoan and metazoan zooplankton and their dependence on food concentration, predator-prey weight ratio, and taxonomic group. Limnology and Oceanography, 42, 1375-1385.

Stukel, M. R., & Landry, M. R. (2010). Contribution of picophytoplankton to carbon export in the equatorial Pacific: A reassessment of food web flux inferences from inverse models. Limnology and Oceanography, 55, 2669-2685.

Thingstad, F. T. (1998). A theoretical approach to structuring mechanisms in the pelagic food web. Hydrobiologia, 363, 59-72.

Urrère, M. A., & Knauer, G. A. (1981). Zooplankton fecal pellet fluxes and vertical transport of particulate organic material in the pelagic environment. Journal Plankton Research, 3, 369-387.

Valencia, B., Landry, M. R., Décima, M., & Hannides, C. C. S. (2016). Environmental drivers of mesozooplankton biomass variability in the North Pacific Subtropical Gyre. Journal of Geophysical Research Biogeosciences. 121, 3131-3143.

White, J. R., Zhang, X., Welling, L. A., Roman, M. R., & Dam, H. G. (1995). Latitudinal gradients in zooplankton biomass in the tropical Pacific at 140 W during the JGOFS EqPac study: Effects of El Niño. Deep-Sea Research II, 42, 715-733.

Wilson, S. E., Steinberg, D. K., & Buesseler, K. O. (2008). Changes in fecal pellet characteristics with depth as indicators of zooplankton repackaging of particles in the mesopelagic zone of the subtropical and subarctic North Pacific Ocean. Deep-Sea Research II, 55, 1636-1647.

Wilson, S. T., Barone, B., Ascani, F., Bidigare, R. R., Church, M. J., del Valle, D. A., Dyhrman, S. T., Ferron, S., Fitzsimmons, J. N., Juranek, L. W., Kolber, Z. S., Letelier, R. M., Martinez-Garcia, S., Nicholson, D. P., Richards, K. J., Rii, Y. M., Rouco, M., Viviani, D. A., White, A. E., Zehr, J. P., Karl, D. M. (2015). Short-term variability in euphotic zone biogeochemistry and primary productivity at Station ALOHA: A case study of summer 2012. Global Biogeochemical Cycles, 29, 1145-1164.

Wood, S. N. (2006). Generalized additive models: An introduction with R. Chapman & Hall/CRC, USA.

Zuur, A. F., Ieno, E. N., Walker, N. J., Saveliev, A. A., & Smith, G. M. (2009). Mixed effects models and extensions in ecology with R, Springer, New York.

CHAPTER 3

The role of salps and doliolids in feeding and export of protists during two anomalously warm years in the California Current System

Abstract

Salps and doliolids are important components of pelagic communities due to their high filtration rates and production of fast sinking fecal pellets. In the southern California Current System, blooms of three salp species, *Salpa aspera*, *Cyclosalpa affinis*, and *Pegea socia*, and the doliolid *Doliolum denticulatum* occurred during anomalously warm conditions of 2014-2016. Proliferation of the pelagic tunicates created a unique opportunity to evaluate and compare their gut contents and fecal pellets relative to water-column protistan assemblages using 18S rDNA metabarcoding. Parasitic alveolates, apicomplexans and syndiniales, accounted for 40 to 60% of the protistan sequences identified in the four species. Dinoflagellate sequences still dominated when known parasites were removed from the analyses, but prasinophytes also emerged as important prey for *S. aspera* and *C. affinis* in summer 2014, and heterotrophic stramenopiles for *P. socia* and *D. denticulatum* in spring 2016. For each species, the prey sequences differed significantly from protistan assemblages in the water column, among individuals collected at different locations, and between the guts and fecal pellets of individuals at the same location. Prey composition also differed significantly in co-occurring tunicates (*S. aspera* and *C. affinis* in 2014; *P. socia* and *D. denticulatum* in 2016), although they were generally more similar than individuals of the same species at different locations. Our results contrast with previous findings from microscopical analyses suggesting that prey of pelagic tunicates reflect the relative

abundances of microbial assemblages in the water column, although the differences were due to changes in protist composition or relative abundances rather than major shifts in prey detected. Clade I *Synechococcus* dominated in tunicate guts and fecal pellets compared to dominance of clade IV in the mixed layer, and appears to be differentially transferred to depth in tunicate pellets. Even for relatively passive filter feeders like salps and doliolids, complications from parasites and differential prey digestibility make the interpretations of dietary selectivity and microbial contributions to export far from straightforward.

Introduction

The pelagic tunicates salps and doliolids are important but variable components of marine zooplankton communities (Alldredge and Madin, 1982). When these gelatinous filter feeders occur in swarms, their efficient grazing can remove a large proportion of primary production and greatly impact microbial communities (Perissinotto and Pakhomov, 1998). In addition, their fast sinking fecal pellets (e.g., ~ 2.7 km/d for salps) and carcasses are major routes of carbon export from the euphotic zone to the deep sea (Bruland and Silver, 1981; Iseki, 1981; Madin, 1982; Smith *et al*., 2014; Takahashi *et al.,* 2015). Both salps and doliolids are considered non-selective feeders (Madin, 1974; Silver and Bruland, 1981), and micro-sized prey (20–200 μm) account for most of their carbon uptake (Sutherland *et al*., 2010). However, particles in the nano- (2–20 μm) and pico-plankton (<2 μm) size range can also be trapped in their mucous nets and incorporated into fecal pellets (Harbison and McAlister, 1979; Bruland and Silver, 1981; Katechakis *et al.,* 2004; Sutherland *et al*., 2010). Thus, compared to other major mesozooplankton groups, salps and doliolids represent an important export mechanism for very small cells (Madin, 1974, 1982; Bruland and Silver, 1981; Pfannkuche and Lochte, 1993).

Most knowledge about salp and doliolid feeding is restricted to micro-sized prey characterized by microscopical analyses of fecal pellets (Madin, 1974; Silver and Bruland, 1981), which provides little to no information about smaller microbes. Recently, molecular techniques have been used as an alternative method to obtain high-resolution information about zooplankton diet (e.g., Nejstgaard *et al*., 2003). For pelagic tunicates, these techniques have elucidated differences in diet composition between salp species (Metfies *et al*., 2014), as well as differences in digestability of doliolid prey (Frischer *et al*., 2014).

In the California Current System (CCS), conspicuous blooms of salps occurred in summer 2014 and doliolids in spring 2016, likely favored by the anomalously warm conditions (sea surface temperature anomalies > 2°C) and ocean circulation that prevailed in the region from late 2013 to 2016. Initially, these conditions were a result of a warm water anomaly that extended southward from Alaska and affected the North Pacific, where it was known as the "blob" (Bond *et al.,* 2015). In the subsequent 2015-2016 El Niño event, the warm water conditions extended northward from the equatorial region (McClatchie *et al*., 2016). These blooms, following the long-term decline documented by Lavaniegos and Ohman (2007), provided a unique opportunity to investigate the impacts of pelagic tunicates on microbial communities.

In this study, we used metabarcoding analysis to identify the prey species consumed by three species of salps, *Salpa aspera, Cyclosalpa affinis*, and *Pegea socia*, and one doliolid, *Doliolum denticulatum*. We also evaluated the potential role of these species in export via their fast-sinking fecal pellets. Although the four species of tunicates have been documented in the CCS previously, only *S. aspera* has been characterized as a persistent component of the region's zooplankton (Lavaniegos and Ohman, 2003). *C. affinis* and *P. socia* tend to occur more

frequently during cool phases of the Pacific Decadal Oscillation (PDO) (Lavaniegos and Ohman, 2003), thus their presence during warm-water conditions in 2014-2106 was unusual. *D. denticulatum* generally occurs during warm phases due to its predominantly subtropical distribution. Based on microscopical analysis and the passive filter-feeding behaviors of pelagic tunicates, we hypothesized that feeding would differ among individuals of the same species occurring at different sites, but tend to be similar in individuals of different species when they co-occured. Likewise, we hypothesized that the microbial composition of guts and fecal pellets, presumably representing taxon-specific contributions to export out of the euphotic zone, would largely reflect relative microbial abundances in the water column.

Materials and methods

Sample collection for metabarcoding

Zooplankton samples and environmental data were collected in the southern California Current System (CCS) as part of the CCE-LTER process cruises P1408 (11 August – 02 September 2014) and P1604 (19 April – 12 May 2016) onboard the R/V *Melville* and R/V *Sikuliaq*, respectively (Figure 1). During each cruise, water parcels with relatively homogeneous conditions were selected based on satellite images of sea surface temperature and chlorophyll, following surveys with a Moving Vessel Profiler (e.g., Ohman *et al.,* 2013). At each location, referred to as an experimental cycle, we followed water parcels for 3-5 days by tracking a surface drifter with a holey sock drogue attached at 15 m depth. As we followed the drifter, the euphotic zone (0.1% surface irradiance) was characterized by taking profiles twice a day (02:00 and 12:00) with a Conductivity Temperature Depth (CTD) profiler in a Niskin-bottle rosette. Discrete water samples were collected at 6-8 depths and analyzed for chlorophyll (Chl*a*),

nutrients, primary production, and molecular analysis. Complete protocols for the collection and processing of environmental samples as well as cruise data are available at the CCE-LTER website (http://oceaninformatics.ucsd.edu/datazoo/catalogs/ccelter/datasets).

Salps and doliolids were collected between 20:30 and 22:30 by shallow (~ 50 m) and short (~ 5 min) zooplankton tows with a 1-m diameter ring net (202-µm Nitex mesh). Solitary individuals and aggregates of *Salpa aspera* and *Cyclosalpa affinis* were collected during summer 2014, while aggregates of *Pegea socia* and blastozooids and oozoids of *Doliolum denticulatum* (L. Sala, pers. com.) were collected during spring 2016. After the tows, zooplankton samples were diluted with surface water in 5-gallon buckets, and aggregates or solitary individuals were carefully removed, rinsed with filtered sea water, wrapped in aluminum foil, and frozen at -80°C. The elapsed time between retrieval of samples on deck and freezing of individuals was approximately 5 minutes. To establish which protists passed undigested through the guts of salps and doliolids, some individuals were incubated for approximately 4 hours in 5-gallon buckets of filtered seawater. At the end of the incubation, the fecal pellets produced by the zooplankton were collected and both the individuals and pellets were immediately frozen (-80°C). A summary of the individuals analyzed per species is presented in Table 1. Additionally, 280 ml samples were collected from the mixed layer in summer 2014 and from the mixed layer, base of the euphotic zone, and 150 m in spring 2016 to analyze the potential prey available in the water column. These samples were filtered through 25-mm diameter 0.2-µm Supor membrane filters (Pall Corporation), placed in 2-ml cryogenic vials, flash-frozen in liquid nitrogen, and stored at -80°C.

Library construction and sequencing

Sample preparation for DNA extraction consisted of three steps. First, the guts of salps and doliolids were dissected using sterilized forceps and blades (ethanol-flamed). Second, the dissected guts were transferred to 1.5-ml tubes and ground with sterilized micro-pellet pestles. Finally, a portion of the homogenized guts was transferred to a new 1.5-ml tube. DNA was extracted with the DNeasy Blood & Tissue Kit (Qiagen) for zooplankton samples (gut subsamples and fecal pellets) and the NucleoMag 96 Plant kit (Macherey Nagel) for water column samples. For both kits, the manufacturer's instructions were followed. DNA was eluted to 100 µl for zooplankton samples and to 50 µl for the water column. The extracted DNA was stored at -80°C until amplification, typically within 1-5 days.

The eukaryotic communities in the water-column samples and in the guts and fecal pellets of analyzed animals were characterized by polymerase chain reaction (PCR) by amplifying the V9 region of the18S rDNA gene using primers 1389F (TTGTACACACCGCCC) and 1510R (CCTTCYGCAGGTTCACCTAC). Primers contained Illumina adaptors, a linker, and barcoded indices. Amplification was done using the Q5 high-fidelity PCR kit in a 25-µl reaction volume. The PCR thermal protocol consisted of an initial denaturation of 30 s at 98°C, 30 amplification cycles of 10 s at 98°C, 30 s at 56°C, and 30 s at 72°C, followed by a final extension of 2 min at 72°C, and held at 4°C until collection. The band size of the amplicons was visualized on a 1% agarose gel. PCR products were purified using Agencourt AMPure Beads XP and the concentration was quantified using PicoGreen dsDNA Quantitation Reagent.

A total of 88 purified PCR products were pooled for sequencing as follows: *Salpa aspera* (guts = 16, pellets = 10), *Cyclosalpa affinis* (guts = 12, pellets = 5), *Pegea socia* (guts = 14, pellets = 4), *Doliolum denticulatum* (guts = 12, pellets = 2), and water column (n = 13) (Table 1).

The PCR products were pooled in equimolar amounts (~ 10 ng μl^{-1}) in 1.5 ml Eppendorf tubes and were sequenced using a dual-barcode index on an Illumina MiSeq platform at the Institute for Genomic Medicine (IGM, University of California, San Diego).

Bioinformatic analyses

Initial quality control of the raw sequence reads was carried out using a workflow written by John P. McCrow (https://github.com/allenlab/rRNA_pipeline) that filtered the sequence reads, clustered Operational Taxonomic Units (OTU), and classified the OTUs according to taxonomy associated with the SSU-rRNA. Briefly, paired-end reads were aligned using PEAR (Zhang *et al.,* 2014) and quality trimmed to Phred score 30 (Q30 minimum average in sliding window of size 2 bp). Possible chimeras were found and filtered using USEARCH (Edgar 2010). Amplicons were clustered using SWARM into OTUs (Mahé *et al.,* 2014), and taxonomic assignments were made using the best hit from GLSEARCH36 (Pearson, 2016) with the PR2 reference database and taxonomic updates from the Tara Oceans-W2 (de Vargas *et al.,* 2015).

The initial filtered OTU table was processed further before statistical analyses. Additional quality control was carried out following these steps: 1) sequence reads assigned to non-eukaryote taxa (archaeal, bacterial, organelle, and unassigned) and OTUs with only 1 sequence read in the entire data set (singletons) were removed; 2) OTUs that were assigned to the same species but occurred multiple times in the OTU table were merged (merged over-split OTUs); 3) OTUs assigned only to supergroup level (e.g., Opisthokonta_X, Stramenopiles_X), Class Streptophyta (land plants), or fungi (potential contamination) were removed. This final OTU table was used for characterizing the protists communities in guts and fecal pellets of salps and doliolids.

Synechococcus sequence analysis and classification

Because pelagic tunicates might be an important export mechanism for picophytoplankton, particularly cyanobacteria (e.g., Pfannkuche and Lochte, 1993), we also evaluated the occurrence of *Synechococcus* strains in their fecal pellets by sequencing the 16S-23S rRNA internal transcribed spacer (ITS1F - CTTGGTCATTTAGAGGAAGTAA, ITS4R - TCCTCCGCTTATTGATATGC). The relative abundances of *Synechococcus* strains were evaluated for *Pegea socia* and *Doliolum denticulatum,* with six gut and two fecal pellet DNA samples from each species. Amplification, sequencing, and bioinformatics processing, including de-noising, chimera detection, and OTU clustering, of *Synechococcus* sequences, was carried out at RTL Genomics (Lubbock, Texas). The OTUs were assigned at a 97% cutoff, and OTU classification was carried out using MOTHUR (Schloss *et al*., 2009) and a *Synechococcus* ITS database from Choi *et al*. (2014). OTUs assigned to the same strain were merged.

Data analyses

We characterized the protists in the tunicate guts and fecal pellets by calculating the frequency of occurrence of each protist per sample type. We then evaluated the differences in protists detected among salp and doliolid species using multivariate analyses based on the Bray-Curtis dissimilarity index. Prior to analysis, sequence reads were merged by genus or lowest taxonomic level assigned. Because most sequences were ascribed to apicomplexan and syndiniales, both alveolate parasites, these were removed from the dataset. The remaining protists contributing >1% to the relative abundances in any sample were selected for analyses. For this subset of protists, the relative abundances per sample were recalculated and square-root transformed to minimize the impact of the most abundant taxa. Cluster significance was established by similarity profile analysis (SIMPROF), and protists differentiating the clusters

were identified by similarity percentage analysis (SIMPER). Multivariate analyses were done in R using the packages 'vegan' (Oksanen *et al.,* 2017) and 'clustsig' (Whitaker and Christman, 2015).

Results

Sequence analyses

The contribution of protistan sequences to total eukaryotes varied considerably within and between species of salps and doliolids, averaging 38% overall. Protist sequences ranged from 0.3 to 82% in *Salpa aspera* (mean = 30%, Figure 2), from 2.6 to 99% in *Cyclosalpa affinis* (mean = 59%, Figure 2), from 0.1 to 86% in *Pegea socia* (mean = 27%, Figure 3), and from 0.7 to 96% in *Doliolum denticulatum* (mean = 42%, Figure 3). In most samples, the sequences were dominated by metazoans and mainly corresponded to either the genus of tunicate analyzed or to calanoid copepods (Figures 2 and 3). In the water column, contributions from protistan sequences averaged 67% in summer 2014 (range = 6–98%) and 66% in spring 2016 (range = 33–87%). The broad range in the percentage contribution of protist sequences in summer 2014 was due to the dominance of copepod sequences in the mixed layer sample (93%) collected during Cycle 1 of that cruise. In summer 2014, two salp fecal pellets were collected from sediment traps deployed at 150 m in cycles 2 and 3 and analyzed. In these two samples, protistan sequences averaged 73% of total eukaryotes.

Rarefaction curves were constructed to determine if the number of sequence reads were sufficient to characterize the diversity of protists detected in guts and fecal pellets (Figure 4). In

general, the curves of merged-species versus number of sequence reads did not reach an asymptote for any of the samples, indicating that only a fraction of the potential protist diversity was characterized. A total of 207 protist genera (or lowest taxonomic level assigned) were identified from metabarcoding analysis in the four tunicate species. The highest number of genera was detected from *S. aspera* (150 total) and the lowest from *P. socia* (91 total, Table 2). Most protist genera were common among the four species (Table 2).

General patterns of protists detected in four species of pelagic tunicates

Alveolate sequences dominated in the guts and fecal pellets of all four tunicate species (Figure 5). This group was also dominant in most water-column samples, except for the mixed layer in Cycle 2 during summer 2014 and Cycle 3 during spring 2016, where chlorophytes (Archaeplastida) were the dominant group. Although they had much lower contributions, chlorophytes and stramenopiles in *S. aspera* and stramenopiles in *P. socia* were also important components of the protists detected (Figure 5). In Cycle 2, alveolates and chlorophytes had similar relative abundances in the fecal pellets analyzed from sediment traps, whereas the pellets collected from Cycle 3 were dominated by alveolates (Figure 5).

A closer look at the protistan composition revealed that alveolate dominance was mainly due to the high relative abundances of apicomplexans and syndiniales, which represented in most cases between 40% to 60% of the reads (Figures 6-10). These two protistan groups also occurred frequently in the four tunicate species (Tables 3-6). Sequences of apicomplexans were assigned mainly to Cephaloidophoroidea, whereas sequences of syndiniales were generally MALV-I clade 1 and MALV-I clade 4. For *S. aspera* and *C. affinis*, relative abundances of syndiniales were slightly higher or comparable to those of apicomplexans (Figures 6 and 7). In contrast, for *P. socia* and *D. denticulatum,* apicomplexan reads were generally more abundant

than those of syndiniales (Figures 9-10). Apicomplexans also dominated protistan reads in the salp fecal pellets collected from sediment traps during summer 2014 in Cycle 3 (Figure 8). High frequencies were also detected in protists assigned to the prasinophyte Prasino-Clade-7B1 for *S. aspera* (Table 3), the dinoflagellate *Gonyaulax* and the stramenopiles MAST-1C and MOCH-3 for *P. socia* (Table 5), and the dinoflagellates *Lepidodinium*, *Pelagodinium*, *Scrippsiella*, and an uncultured taxon for *D. denticulatum* (Table 6). In the case of *C. affinis*, several protists (i.e., dinoflagellates, prymnesiophytes, and stramenopiles) were detected in all samples analyzed, and gave the highest frequencies of occurrence (Table 4). Because apicomplexans and syndiniales are known parasites of protists and invertebrates, these were omitted from subsequent analyses.

Protists detected in guts and fecal pellets of pelagic tunicates

Evaluated by hierarchical cluster-SIMPROF analyses, the compositions and relative abundances of protists detected in the four tunicate species were significantly different than the protistan assemblages in the water column (Figures 11 and 12). Consequently, we focused our analysis on the clusters corresponding to protists detected in the tunicates only, which show, in general, that the prey varied among species and that differences were also evident among sampling locations (Figure 11). Likewise, SIMPER analysis suggests that the differences were largely due to subtle changes in protistan community composition or relative abundances, rather than abrupt changes in the types of prey detected (Figure 12).

Salpa aspera **and** *Cyclosalpa affinis*

In *S. aspera* fecal pellets from Cycle 1 (summer 2014), the highest relative abundances were for sequences assigned to the dinoflagellates *Alexandrium*, *Karlodinium*, *Protoperidinium*, and an uncultured species, the prasinophyte Prasino-Clade-7B1, and the diatom *Thalassiosira* (Group 10, Figures 11 and 12). These samples clustered closed to fecal pellets from the same

species in Cycle 2 of the same year, where *Alexandrium* dominated, with lower contributions of an uncultured dinoflagellate, Prasino-Clade-7B1, and *Thalassiosira* (Group 11). Although samples of *S. aspera* guts from Cycle 1 did not cluster together or with other samples, the sequences detected in one of the samples was most similar to those in fecal pellets of this same species from Cycles 1 and 2 (Groups 10 and 11). Guts of *S. aspera* in this sample had high contributions of the dinoflagellates *Karlodinium*, *Alexandrium*, and *Blastodinium,* as well as Prasino-Clade-7B1 (Figures 11 and 12).

Where *S. aspera* and *C. affinis* co-occurred in 2104 Cycle 3, prey of the two species were significantly different in their gut composition, but not in their fecal pellets. However, the gut compositions of these two species in Cycle 3 were more similar than those for other samples of the same species from Cycles 1, 2, 4 and 5 (Figures 11 and 12). In the guts of *S. aspera* (Cycle 3), the prey sequences were dominated by *Karlodinium*, with important contributions by *Blastodinium,* an uncultured dinoflagellate, Prasino-Clade-7B1, and the stramenopiles MAST-1C and *Pelagomonas* (Group 14). In the guts of *C. affinis*, both *Karlodinium* and *Blastodinium* had high relative abundances, but Prasino-Clade-7B1 and *Pelagomonas* had lower contributions (Group 13). In the salp fecal pellets from Cycle 3, mainly from *S. aspera,* most sequences were assigned to the prasinophyte Prasino-Clade-7B1, followed by *Karlodinium, Alexandrium*, and the uncultured dinoflagellate (Group 15).

At the two offshore sampling locations in 2014 (Cycles 4 and 5), relative prey abundances for *C. affinis* were similar among guts (Group 17) and fecal pellets (Group 18). Dinoflagellates were the main components in both guts and pellets and significant differences between the two were mainly due to differences in the relative abundances of dinoflagellate genera. In *C. affinis* guts, abundances of *Blastodinium,* an uncultured dinoflagellate, and

Karlodinium were similar, with minor contributions from *Scrippsiella* (Group 17). The fecal pellets were dominated by *Blastodinium*, an uncultured dinoflagellate, *Karlodinium*, with a minor contribution from the prymnesiophyte *Emiliania* (Group 18, Figures 11 and 12).

Doliolum denticulatum **and** *Pegea socia*

Samples from the guts of *D. denticulatum* collected offshore (Cycle 2) in spring 2016 (Group 19, Figures 11 and 12) clustered closest to the offshore 2014 samples from *C. affinis* (Groups 17 and 18). The highest sequence abundances in Group 19 from *D. denticulatum* guts were assigned to *Karlodinium,* an uncultured dinoflagellate, and MAST-1C stramenopiles. Protist assemblages from the mixed layer and euphotic zone base at the offshore site in spring 2016 (Group 4), containing high relative abundances of *Karlodinium* and an uncultured species, were also more similar to those from the mixed layer at the offshore sites in summer 2014 (Group 3). In contrast, guts and fecal pellets of *D. denticulatum* and *P. socia* collected in Cycle 3 (summer 2016) clustered in totally separate groups (Groups 20-25) than the guts of *D. denticulatum* in Cycle 2 (summer 2016) (Group 19, Figures 11 and 12). In guts and fecal pellets of *D. denticulatum* (Cycle 3 summer 2016), sequences assigned to *Scrippsiella* had the highest relative abundances, followed by *Pelagodinium* and MAST-1C and MOCH-3 stramenopiles in the guts (Group 20), and by *Pelagodinium, Karlodinium,* an uncultured dinoflagellate, and the ciliate *Tokophrya* in the pellets (Group 22).

Protists detected in *P. socia* varied among individuals, which could be a result of the analysis of single guts for this large salp species instead of multiple guts as with the doliolid. In the cluster where more samples of *P. socia* were grouped together, the sequences were dominated by MAST-1C, with minor contributions of *Scrippsiella* (Group 25). In the other group for *P. socia* guts, MOCH-3 had the highest relative abundances, followed by

Blastodinium, Scrippsiella, and an uncultured dinoflagellate (Group 23). In the pellets of *P. socia*, most sequences were assigned to an unidentified diatom (Bacillariophyceae_X), followed by MOCH-3, *Scrippsiella*, and an uncultured dinoflagellate (Group 24, Figures 11 and 12).

Salp fecal pellets analyzed from sediment traps

Protistan composition in the two salp fecal pellets collected in sediment traps from Cycles 2 and 3 during summer 2014 were similar to each other and to the mixed layer of Cycle 2 (Groups 7 and 8, Figures 11 and 12). In these samples, protist sequences were dominated by the prasinophyte Prasino-Clade-7B1.

Synechococcus **strains**

Nine *Synechococcoccus* strains were detected in the guts and fecal pellets of *P. socia* and *D. denticulatum* (Figure 13). In both species, sequences assigned to clade I dominated in guts and fecal pellets, followed by clade IV and clade XXX_GLB64471. Compared to the water column, the relative abundances of *Synechococcus* strains in *P. socia* and *D. denticulatum* were more similar to the deep euphotic zone and 150 m than to the mixed layer, where sequences were dominated by clade IV (Figure 13).

Discussion

The dense blooms of salps and doliolids that occurred in the California Current System (CCS) during the anomalously warm years of 2014-2016 provided an opportunity to characterize the protistan assemblages ingested, egested and exported by three species of salps, *Salpa aspera, Cyclosalpa affinis,* and *Pegea socia¸* and one doliolid, *Doliolum denticulatum*. Although we focus here on the protistan components of diet, the sequences in most samples were dominated

by metazoans, mainly copepods and tunicates, some of which may have been due to incidental engulfment in the net cod ends during collection. We note, however, that copepod remains have been observed in salp fecal pellets collected in situ by scuba divers (Madin, 1974), indicating that they could be a normal part of tunicate diets. That would certainly be the case for smaller and easily captured stages, such as nauplii and eggs. The overwhelming dominance of tunicate sequences in some individuals may also indicate animals that were not feeding at the time of collection, as has been observed previously for migrating salps in the subarctic Pacific, which come to surface waters at night to reproduce (Purcell and Madin, 1991). Parasitism, prey digestibility, and matching the stomach contents of animals to the depth strata where they feed emerge as key issues for interpreting measurements of relative sequence abundances in terms of feeding preferences and export contributions.

Major groups of protistan parasites

Using metabarcoding techniques, we detected 207 genera of protists in the guts and fecal pellets of the four pelagic tunicates analyzed, covering a wide range of taxa. Compared to previous microscopy and pigment analyses, in which only major categories of microbes were identified, these results considerably expand characterizations of dietary breadth for salps and doliolids (e.g., Madin, 1974; Silver and Bruland, 1981; Ahmad Ishak *et al.,* 2017). Nonetheless, rarefaction curves indicate that only a fraction of the diversity of protists ingested and egested was detected. Alveolates were the dominant group in the guts and fecal pellets of the four species, mainly due to the high relative abundances of sequences assigned to the apicomplexan Cephaloidophoroidea and syndiniales. Cephaloidophoroidea are poorly known gregarines that parasitize the intestines of crustaceans, including copepods (Rueckert *et al*., 2011), and syndiniales parasitize invertebrates and protists (Guillou *et al*., 2008). If these parasites were

inside prey ingested naturally rather than incidentally during net tows, then pelagic tunicates could represent an important mechanism for exporting parasites efficiently out of the euphotic zone, and potentially to infection of coprophagous zooplankton in the underlying mesopelagic environment. It is also possible that the apicomplexans were parasites of the tunicates themselves, as has been documented by microscopical observations of large gregarines (range: 116–200 μm) in the guts of *Salpa thompsoni* in the Southern Ocean (Wallis *et al*., 2017), and also in *Salpa aspera* and *S. maxima* (Clopton, 2002). The effects of such parasites on the physiologies and ecologies of salps are unknown, but their presence could have important implications for food-web interactions and net carbon transfers when tunicate blooms occur.

Although we removed sequences of apicomplexans and syndiniales for subsequent analysis because they are not considered prey ingested by the tunicates, we did include sequences of *Blastodinium*, a dinoflagellate parasite with high relative abundances in *C. affinis* (Figure 7). *Blastodinium* spp. are known to infect the guts of copepods, but their dinospores, resembling small thecate dinoflagellates (5–18 μm), can be abundant in the water column (Alves-de-Souza *et al.,* 2011). In the present study, they were relatively rare in water-column samples, substantially enriched in tunicate guts and declining in pellets (Figures 6-7), indicating their presence mainly as gut parasites.

General patterns within and among tunicate species

Based on microscopy, pigment, and stable isotope analyses, the diet of pelagic tunicates is expected to reflect the relative proportions of the protists available in the water column (Madin, 1974; Silver and Bruland, 1981; Alldredge and Madin, 1982; Vargas and Madin, 2004; Ahmad Ishak *et al.,* 2017). However, our metabarcoding results show significant differences among protistan assemblages in the water column and in the tunicate guts and fecal pellets. This

result could be influenced by the vertical resolution of the samples collected (i.e., only mixed-layer samples in 2014), with the tunicates potentially feeding in different depth strata. Even with samples of the natural prey assemblages at three depth strata in 2016 Cycle 3, it is difficult to explain the high incidence of *Scrippsiella*, *Gonyaulax*, MAST-1C and MOCH-3 stramenopiles in the guts and pellets of *P. socia* and *D. denticulatum*, when none are abundant in any of the water samples (Figures 9 and 10). In addition, since metabarcoding characterizes prey taxa in more detail than methods formerly employed, it is more sensitive to resolving differences that have previously escaped detection. In the present study, we ascribe those differences mainly to variations in the relative abundances of a few protistan genera.

Consistent with the results of Metfies *et al.* (2014), who analyzed gut contents of the salps *Salpa thompsoni* and *Ihlea racovitzai* by metabarcoding, we found significant differences in protistan prey compositions among animals sampled at different locations. This was expected for the spatially variable CCS where significant differences *in situ* protistan assemblages are well documented by microscopical (e.g., Venrick, 2002; Taylor *et al.,* 2015) and metagenomic methods (e.g., Allen *et al.,* 2012; this study). Likewise, in agreement with Metfies *et al.* (2014), we found that the gut contents of co-occurring tunicate species (*S. aspera* and *C. affinis* in summer 2014 Cycle 3; *P. socia* and *D. denticulatum* in spring 2016 Cycle 3) were statistically different, even though in *S. aspera* and *C. affinis* gut contents showed some striking similarities. For example, both *S. aspera* and *C. affinis* showed similar relative abundances of *Karlodinium*, Clade 7B1 prasinophytes, and *Pelagomonas* in their guts, but in their pellets, the contributions of these same taxa decreased (*Karlodinium* and *Pelagomonas*) or increased (Clade 7B1 prasinophytes). Gut contents in *P. socia* and *D. denticulatum* presented a similar composition, but differences in relative abundances were more evident, with high dominance of *Scrippsiella* in

D. denticulatum and high dominance of MAST-1C in *P. socia*. Consequently, we did not find abrupt changes in protistan dietary compositions as reported Metfies *et al.* (2014), but rather, shifts in relative abundances. Recent results from Ahmad Ishak *et al.* (2017) have also shown minor differences in the compositions and size ranges of the protists ingested by co-occurring salp species, *Salpa fusiformis* and *Thalia democratica*.

One remarkable result comparing the two cruises in our study is the similarity in gut contents of *D. denticulatum* collected offshore in spring 2016 (Cycle 2) and those of *C. affinis* collected offshore in summer 2014 (Cycles 4 and 5). This similarity occurred despite the two-year difference, the different seasons, the substantial size difference between species (*C. affinis* are much larger than *D. denticulatum*), and the different feeding behaviors of salps and doliolids (i.e., continuous pumping of water by muscular movement in comparison with stationary feeding by cilia generated flow; Alldredge and Madin, 1982). In the CCS, Taylor *et al.* (2015) have documented little interannual variability in the proportional contribution of the major groups of microbes to total biomass in offshore waters, compared to the substantial variability in the inshore CCS. Our mixed-layer samples, with offshore microbial assemblages in summer 2014 (Cycles 4 and 5) similar to offshore assemblages in spring 2016 (Cycle 2), also reflect low interannual variability within the long period of anomalously warm conditions from 2014 to 2016. However, mixed-layer communities at inshore locations (Cycles 1-3 in summer 2014 and Cycle 3 in spring 2016) were very different. While *C. affinis* and *D. denticulatum* appear to feed similarly on offshore protistan assemblages, these species may still have differential impacts on carbon cycling and export due to differences in their filtration rates, which are higher for larger individuals (Vargas and Madin, 2004), and in the size and density of their fecal pellets, which are denser in salps than doliolids (Bruland and Silver, 1981).

Potential implications for protistan export

In considering the implications of our results for export, we assume that DNA sequences that are enhanced in tunicate guts and fecal pellets relative to their water-column abundances are associated with prey that contribute disproportionately to export. This is true to the extent that the recognizable prey DNA in tunicates is from cells that are less degraded by digestion, or that pass through the gut intact (Silver and Bruland, 1981; Fowler and Fisher, 1983; Koster *et al.,* 2011). It does not mean, however, that contributions to carbon export are proportional to the prey DNA in fecal pellets, since, given the canonical assimilation efficiency of 70% (Madin and Purcell, 1992; Bochdansky *et al.,* 1999), a substantial fraction (30%) of all ingested prey carbon will be passed to feces even in the absence of a DNA signature. Thus, fully digested prey that leave no DNA evidence could well dominate export if they are consumed in high enough quantities.

Dinoflagellates generally dominated the guts and fecal pellets of the four tunicate species in the present study, consistent with the high relative abundances of sequences assigned to this group in most water column samples. Metfies *et al.* (2014) found similar results for salps from the Lazarev Sea, but those analyses were dominated by uncultured dinoflagellate species, whereas our sequences were more readily ascribed to known groups. Although dinoflagellate sequences are likely over-represented due to their high copy number of 18S rDNA genes, microscopical analyses have shown that they represent an important, and often dominant, part of total microbial biomass in the CCS (Taylor *et al.,* 2015). Silver and Bruland (1981) also documented by transmission electron microscopy that thecate dinoflagellates remained typically intact in salp fecal pellets compared to coccolithophores and diatoms.

Of the dinoflagellates detected, sequences assigned to *Alexandrium* had the highest relative abundances in the guts and fecal pellets of *S. aspera* and were particularly enriched in fecal pellets in summer 2014 Cycle 2 (inshore). *Alexandrium* species are associated with harmful algal blooms, and salps containing *Alexandrium* cells have been linked to fish mortality (Mianzan *et al.,* 1997). Thus, the importance of *Alexandrium* in the guts and fecal pellets of *S. aspera* could have implications for the accumulation and transfer of toxins to higher trophic levels. Sequences assigned to *Karlodinium*, another harmful bloom dinoflagellate, were also abundant in the guts and fecal pellets of *S. aspera, C. affinis*, and *D. denticulatum* (mainly in spring 2016 Cycle 2). However, relative abundances of *Karlodinium* were typically higher in the guts rather than the fecal pellets, suggesting that these non-thecate dinoflagellates may have been less resistant to digestion, and thus, less efficiently exported compared to S*crippsiella*, which had high relative sequence abundances in the guts and fecal pellets of *P. socia* and, in particular, *D. denticulatum* (spring 2016 Cycle 3). Cell abundances of *Scrippsiella* tend to be higher in the CCS during early stages of upwelling or relaxation events (Du *et al.,* 2015). *D. denticulatu* also contained *Pelagodinium*, a symbiotic dinoflagellate of foraminiferans and rhizarians that can also be found as free-living cells (Decelle *et al.,* 2012). Similar relative abundances of *Pelagodinium* in the guts and fecal pellets of *D. denticulatum* (spring 2016 Cycle 3) suggest that they were secondarily ingested and poorly digested by the doliolids.

Consistent with microscopic analyses (e.g., Madin, 1974; Silver and Bruland, 1981), our results indicate that salps can be an important export mechanism for tiny cells. This was particularly evident in the analysis of salp fecal pellets collected in sediment traps during summer 2014, where relative abundances were dominated by environmental sequences assigned to the picoeukaryote Prasino-Clade-7B1 (Figure 8). For Cycle 3, the fecal pellets produced by

incubating freshly collected *S. aspera* and *C. affinis* in filtered water both showed relative abundances of Prasino-Clade-7B1 higher or similar to the mixed layer. For Cycle 2, however, prasinophyte sequences were dominant in the mixed layer in Cycle 2, but not in the fecal pellets of *S. aspera*, suggesting that they were not feeding in the mixed layer at the time of collection.

While *S. aspera* and *C. affinis* both clearly grazed and exported small prasinophytes in 2014, there is little evidence of *P. socia* and *D. denticulatum* having comparable impacts on the picoeukaryote *Ostreococcus,* which was very abundant in the mixed layer in spring 2016 Cycle 3. The absence of *Ostreococcus* sequences in the guts and fecal pellets of these two species suggests that they could have been too small to be efficiently grazed or too rapidly and completely digested to be measured as gut DNA. It is also possible that the tunicates collected for analyses were feeding out of the mixed layer at the time they were captured, although this is an unlikely explanation for the absence of *Ostreococcus* in sediment trap material over multi-day deployments during Cycle 3 (Valencia *et al*., in prep.). Compared to *Ostreococcus*, the heterotrophic stramenopiles MAST-1C (Figures 9 and 10) and MOCH-3 (Figure 10) show evidence of significant feeding (high relative abundances in guts) by *D. denticulatum* and *P. socia*, followed by rapid digestion (minor contributions in fecal pellets). *Thalassiosira*, with known digestion resistant species (Fowler and Fisher, 1983), and an unidentified diatom (Bacillariophyceae_X) were, respectively, disproportionately important in the guts of *S. aspera* in summer 2014 Cycles 1 and 2 (Figure 6) and in the fecal pellets of *P. socia* in spring 2016 (Figure 9), while making relatively minor contributions to the water-column communities for those cycles. *Karlodinium* generally declined in relative abundance from guts to fecal pellets for *S. aspera* and *C. affinis*, while prasinophyte clade 7B1 increased in relative abundance in fecal pellets for both species (Figures 6 and 7). These different patterns highlight the fact that even

among consumers that are thought to be relatively indiscriminate grazers in pelagic ecosystems, it is difficult to separate dietary selectivity from digestion resistance differences.

Synechococcus **strains**

Although the size range of prey ingested by the tunicate species in this study mainly includes nano- and micro-sized plankton, cells in the pico-size range, including cyanobacteria, can also be trapped in their mucous feeding nets (Katechakis *et al.,* 2004; Sutherland *et al.,* 2010). Pfannkuche and Lochte (1993) have shown, for example, from microscopical analyses that picocyanobacteria can be transferred to deep-sea sediments in salp fecal pellets. Here, we document for the first time that *Synechococcus* in the guts and fecal pellets of salps (*P. socia*) and doliolids (*D. denticulatum*) are mainly a single strain in clade I, although some contributions of clades IV and XXX GLB64471 were also found. Clades I and IV are the dominant *Synechococcus* strains in the water column in upwelling regions of the northeast (Sohm *et al.,* 2016) and southeast Pacific (Zwirglmaier *et al*., 2008), and they were the dominant strains in the water column of our samples. The similarity of *Synechococcus* strains in tunicate guts and fecal pellets to the relative abundances of strains in the deep euphotic zone and at 150 m, rather than the mixed layer (Figure 13), could have two explanations. While it could indicate that feeding was mainly occurring in the lower euphotic zone, analyses of protistan prey in the same animals offer no evidence to support that hypothesis (Figures 9 and 10). It is therefore more likely that viable *Synechococcus* cells, enriched in clade I, were transferred from the mixed layer to the deeper waters via the sinking and disintegration of tunicate fecal pellets. This implies that the dominance of clade I in guts and fecal pellets of the two tunicate species was due to a higher digestion resistance (Zwirglmaier *et al*., 2009). Regardless, our results indicate that strain-level

differences operating through trophic intermediaries can be important when considering the water-column distributions of *Synechococcus* strains and their contributions to microbial export.

Conclusions

Salps and doliolids are among the least discriminate, pure filter-feeders in pelagic ecosystems. Different species are consequently expected to function similarly in removing microbes from the water column and packaging them for export in their fast-sinking fecal pellets, more-or-less in proportion to the relative abundances of microbes in the environment. The unusual occurrence of bloom concentrations of four species in the CCS during anomalous warm water conditions in 2014-2016 provided an opportunity to evaluate and compare species relative to this expectation for a broad range of prey, using metabarcoding analyses. Differences were detected in the protistan prey composition of individuals of the same species collected at different locations, between guts and fecal pellets, and between species that co-occurred at the same sampling location. While these differences largely reflected variations in relative prey sequence abundances, they were complicated by the unexplained presence of prey in stomachs that did not appear in mixed-layer assemblages, and by presumptive taxon-specific differences digestion resistance, which cause Prasino-Clade-7B1, *Alexandrium*, *Synechococcus* clade I, and unidentified diatom (Bacillariophyceae_X), among others, to be relatively enhanced in tunicate guts and fecal pellets and presumably exported more efficiently from the euphotic zone. Our results also document that sequences assigned to gregarine apicomplexans are common in tunicate species, suggesting that parasitism could have a significant impact on pelagic food-webs during bloom events. Overall, these results highlight the fact that neither direct observations of

feeding selectivity alone nor dietary analysis by molecular methods are sufficient for understanding how variability in microbial assemblages affects export in zooplankton fecal pellets, which rather appear to depend on a complex interplay of prey and consumer characteristics that operate postcapture and during digestive processing and pellet transport.

Acknowledgements

We thank the captain and crew of the R/V *Melville* and R/V *Sikuliaq* for their help at sea. We are grateful to Mark Ohman for his leadership as Chief Scientist and to Ralf Goericke, Mike Stukel, Megan Roadman, Andrew Taylor, Andrés Gutierrez, Tom Kelly, and all the scientists who participated on the CCE-LTER P1408 and P1604 cruises and whose support made this study possible. Michael Stukel provided the salp fecal pellets collected from sediment traps. We specially acknowledge Maitreyi Nagarkar for her help during sample processing at sea and during bioinformatic analyses, and Jennifer Beatty for her help during sample processing in the lab. We thank Linsey Sala for identifying the salp and doliolid species. We thank Hong Zheng for her help with processing the molecular samples. This study was funded by the National Science Foundation grant OCE-1614359 to the CCE-LTER site. Analyses of molecular samples was partly funded by the Graduate Student Excellence Research Award of the Scripps Institution of Oceanography to B. Valencia. The Ph.D. research of B.Valencia was supported by a scholarship (529-2011) from the Colombian Administrative Department of Science, Technology and Innovation (COLCIENCIAS).

Chapter 3, in full, is currently being prepared for submission for publication of the material with the following co-authors: Valencia, B., Freibott, A., McCrow, J.P., Allen,

A.E., Landry, M.R. The dissertation author was the primary investigator and author of this paper.

Table 3.1. Samples analyzed for each species of salp and doliolid. Type: individuals collected directly from zooplankton tows (F), incubated in filtered sea water (I), or fecal pellets from incubated individuals (P). So: Solitary individuals, Ag: aggregates. n: number of individuals combined for metabarcoding analyses.

P1408 - *Salpa aspera*			
Cycle	Date sampled	Type	n
1	13.08.2014	I – Ag	2
		I – Ag	2
		I – Ag	2
		I – Ag	2
1	14.08.2014	P	
		P	
		P	
1	14.08.2014	F – Ag	1
		F – Ag	1
2	19.08.2014	I – Ag	1
		I – Ag	1
		I – Ag	1
2	19.08.2014	P	
		P	
		P	
3	23.08.2014	F – Ag	1
		F – Ag	1
		F – Ag	1
		F – Ag	1
		F – So	1
3	24.08.2014	I – Ag	1
		I – Ag	2
3	25.08.2014	P	
		P	
		P	
		P	

P1408 - *Cyclosalpa affinis*			
Cycle	Date sampled	Type	n
3	24.08.2014	F – Ag	1
		F – Ag	1
3	24.08.2014	I – So	1
		I – So	1
3	25.08.2014	P	
		P	
4	26.08.2014	F – So	1
		F – So	1
4	28.08.2014	I – Ag	1
		I – Ag	1
		I – Ag	1
4	28.08.2014	P	
		P	
5	30.08.2014	I – So	1
5	31.08.2014	P	
5	31.08.2014	F – So	1
		F – So	1

Table 3.1. Samples analyzed for each species of salp and doliolid. Continued

P1604 - *Doliolum denticulatum*				P1604 - *Pegea socia*			
Cycle	Date sampled	Type	n	Cycle	Date sampled	Type	n
2	01.05.2016	F	5	3	03.05.2016	F – Ag	1
		F	5			F – Ag	1
		F	5			F – Ag	1
3	04.05.2016	F	5			F – Ag	1
		F	5			F – Ag	1
		F	5			F – Ag	1
		F	5			F – Ag	1
		F	5			F – Ag	1
		F	5	3	03.05.2016	I – Ag	1
		F	5			I – Ag	1
		F	5			I – Ag	1
		F	5			I – Ag	1
3	05.05.2016	P				I – Ag	1
		P				I – Ag	1
				3	03.05.2016	P	
						P	
						P	
						P	

Table 3.2. Summary of the number of protist genera (or lowest taxonomic level assigned) from metabarcoding analyses of the guts and fecal pellets of salps and doliolids.

	Salpa aspera (Sal.asp)	*Cyclosalpa affinis* (Cyc.aff)	*Pegea socia* (Peg.soc)	*Doliolum denticulatum* (Dol.den)
Total	150	134	91	113
Unique	26	20	9	15
Shared		Sal.asp - Cyc.aff 104	Sal.asp - Peg.soc 75	Sal.asp - Dol.den 84
			Cyc.aff - Peg.soc 60	Cyc.aff - Dol.den 79
				Peg.soc - Dol.den 71

Table 3.3. Frequency of occurrence of protists in the guts and fecal pellets of *Salpa aspera* in summer 2014. Only genera or lowest taxonomic level assigned with frequencies >60% are listed.

Protist	Guts	Pellets	Protist	Guts	Pellets
Alveolata - Dinophyceae			**Chlorophyta**		
Alexandrium	56	90	*Picocystis*	62	50
Azadinium	50	80	Prasino-Clade-7A1	69	100
Biecheleria	69	100	Prasino-Clade-7B1	100	100
Blastodinium	75	100	Prasino-Clade-7B2	50	70
Uncultured	75	100	**Rhizaria**		
Fragilidium	12	80	Protaspa	50	80
Gonyaulax	31	70	Spumellaria	56	90
Heterocapsa	62	100	**Stramenopila**		
Karlodinium	69	100	MAST-1C	56	90
Lepidodinium	56	80	MAST-9A	50	70
Luciella	38	80	MOCH-3	62	80
Paulsenella	19	70	MOCH-5	62	100
Pelagodinium	69	100	*Aplanochytrium*	25	100
Pfiesteriaceae	50	80	*Pelagomonas*	62	100
Prorocentrum	62	100	Pelagophyceae	50	80
Protodinium	50	90	Thraustochytriaceae	38	100
Protoperidinium	56	80	**Stramenopila - Bacillariophyceae**		
Scrippsiella	69	90	*Ardissonea*	0	70
Stoeckeria	62	100	Bacillariophyceae	62	100
Alveolata - Syndiniales			*Thalassiosira*	44	90
MALV-I-Clade-1	94	100			
MALV-I-Clade-2	50	80			
MALV-I-Clade-3	56	100			
MALV-I-Clade-4	81	100			
MALV-I	69	100			
MALV-II-Clade-10-and-11	50	80			
MALV-II-Clade-16	56	80			
MALV-II	31	70			
Alveolata - Apicomplexa					
Cephaloidophoroidea	88	100			

Table 3.4. Frequency of occurrence of protists in the guts and fecal pellets of *Cyclosalpa affinis* in summer 2014. Only genera or lowest taxonomic level assigned with frequencies >60% are listed.

Protist	Guts	Pellets	Protist	Guts	Pellets
Alveolata - Dinophyceae			**Chlorophyta**		
Alexandrium	67	60	*Picocystis*	92	80
Azadinium	100	100	Prasino-Clade-7A1	100	100
Biecheleria	100	100	Prasino-Clade-7B1	75	100
Blastodinium	100	100	Prasino-Clade-7B2	100	100
Uncultured	100	100	Prasino-Clade-9B2	83	40
Fragilidium	25	80	**Haptophyta**		
Gonyaulax	75	80	*Emiliania*	17	80
Gymnodinium	92	80	**Rhizaria**		
Karlodinium	100	100	*Spumellaria*	33	80
Lepidodinium	100	100	**Stramenopila**		
Luciella	42	80	MAST-1C	83	40
Pelagodinium	100	100	MAST-9A	58	80
Pfiesteriaceae	33	100	MOCH-5	83	100
Polarella	67	80	*Aplanochytrium*	33	80
Prorocentrum	92	100	*Aureococcus*	67	20
Protodinium	75	60	*Pelagomonas*	100	100
Pyrocystis	17	80	Pelagophyceae	100	80
Scrippsiella	92	100			
Alveolata - Syndiniales					
MALV-I-Clade-1	100	100			
MALV-I-Clade-3	92	80			
MALV-I-Clade-4	100	100			
MALV-I	100	100			
MALV-II-Clade-10-and-11	67	80			
MALV-II-Clade-23	67	60			
MALV-II	67	60			
Alveolata - Apicomplexa					
Cephaloidophoroidea	100	100			

Table 3.5. Frequency of occurrence of protists in the guts and fecal pellets of *Pegea socia* in spring 2016. Only genera or lowest taxonomic level assigned with frequencies >60% are listed.

Protist	Guts	Pellets	Protist	Guts	Pellets
Alveolata - Dinophyceae			**Chlorophyta**		
Alexandrium	71	100	*Ostreococcus*	64	100
Biecheleria	86	100	*Nannochloris*	57	75
Blastodinium	86	100	Prasino-Clade-7A1	64	100
Uncultured	93	100	Prasino-Clade-7B1	79	100
Dinophysis	21	75	**Haptophyta**		
Gonyaulax	100	100	*Emiliania*	14	75
Heterocapsa	71	100	**Stramenopila**		
Karlodinium	86	100	MAST-1C	100	100
Lepidodinium	71	100	MOCH-3	100	100
Paulsenella	7	75	*Pelagomonas*	64	75
Pelagodinium	86	100	**Stramenopila - Bacillariophyceae**		
Prorocentrum	86	100	*Actinocyclus*	14	75
Protodinium	93	100	Bacillariophyceae	43	100
Pyrophacus	7	75	*Fragilariopsis*	0	100
Scrippsiella	93	100	*Minutocellus*	21	100
Symbiodinium	36	100	*Navicula*	0	75
Alveolata - Syndiniales			*Thalassiosira*	86	100
MALV-I-Clade-1	93	100			
MALV-I-Clade-2	71	50			
MALV-I-Clade-3	93	100			
MALV-I-Clade-4	93	100			
MALV-I	64	100			
MALV-II-Clade-10-and-11	50	100			
MALV-II-Clade-23	86	100			
MALV-III	57	75			
Alveolata - Apicomplexa					
Cephaloidophoroidea	100	100			
Vitrella	57	100			

Table 3.6. Frequency of occurrence of protists in the guts of *Doliolum denticulatum* in spring 2016. Only genera or lowest taxonomic level assigned with frequencies > 60% are listed.

Protist	Guts	Protist	Guts
Alveolata - Dinophyceae		**Chlorophyta**	
Biecheleria	92	*Ostreococcus*	67
Blastodinium	83	*Nannochloris*	83
Uncultured	100	Prasino-Clade-7A1	92
Gonyaulax	92	Prasino-Clade-7B1	83
Heterocapsa	83	**Stramenopila**	
Karlodinium	92	MAST-1C	100
Lepidodinium	100	MAST-3E	67
Pelagodinium	100	MAST-9C	75
Protodinium	75	MOCH-3	83
Scrippsiella	100	*Pelagomonas*	75
Symbiodinium	75	**Stramenopila - Bacillariophyceae**	
Alveolata - Syndiniales		*Thalassiosira*	75
MALV-I-Clade-1	100		
MALV-I-Clade-3	83		
MALV-I-Clade-4	100		
MALV-I-Clade-7	75		
MALV-I	83		
MALV-II-Clade-23	83		
MALV-II-Clade-8	75		
Alveolata - Apicomplexa			
Cephaloidophoroidea	100		

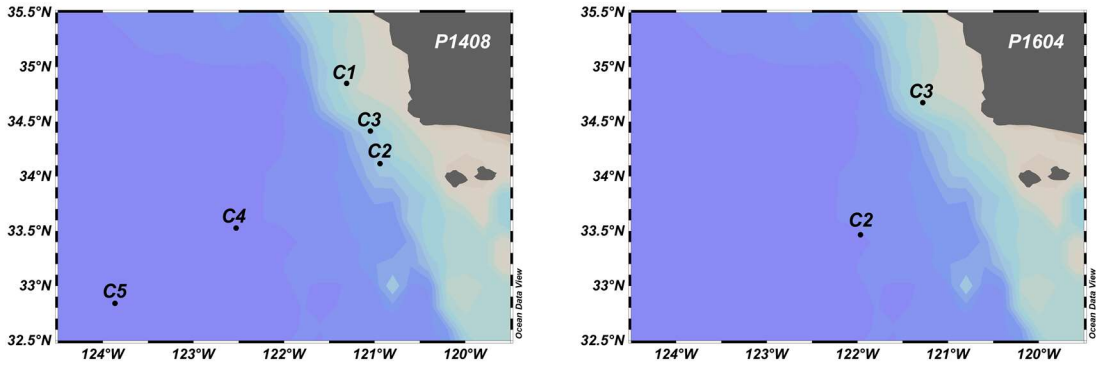

Figure 3.1. Map showing the locations of the experimental cycles (C) conducted in the California Current System during summer 2014 (P1408) and spring 2016 (P1604). Zooplankton samples were collected at each location. Prominent land feature in the figure is Point Conception, California.

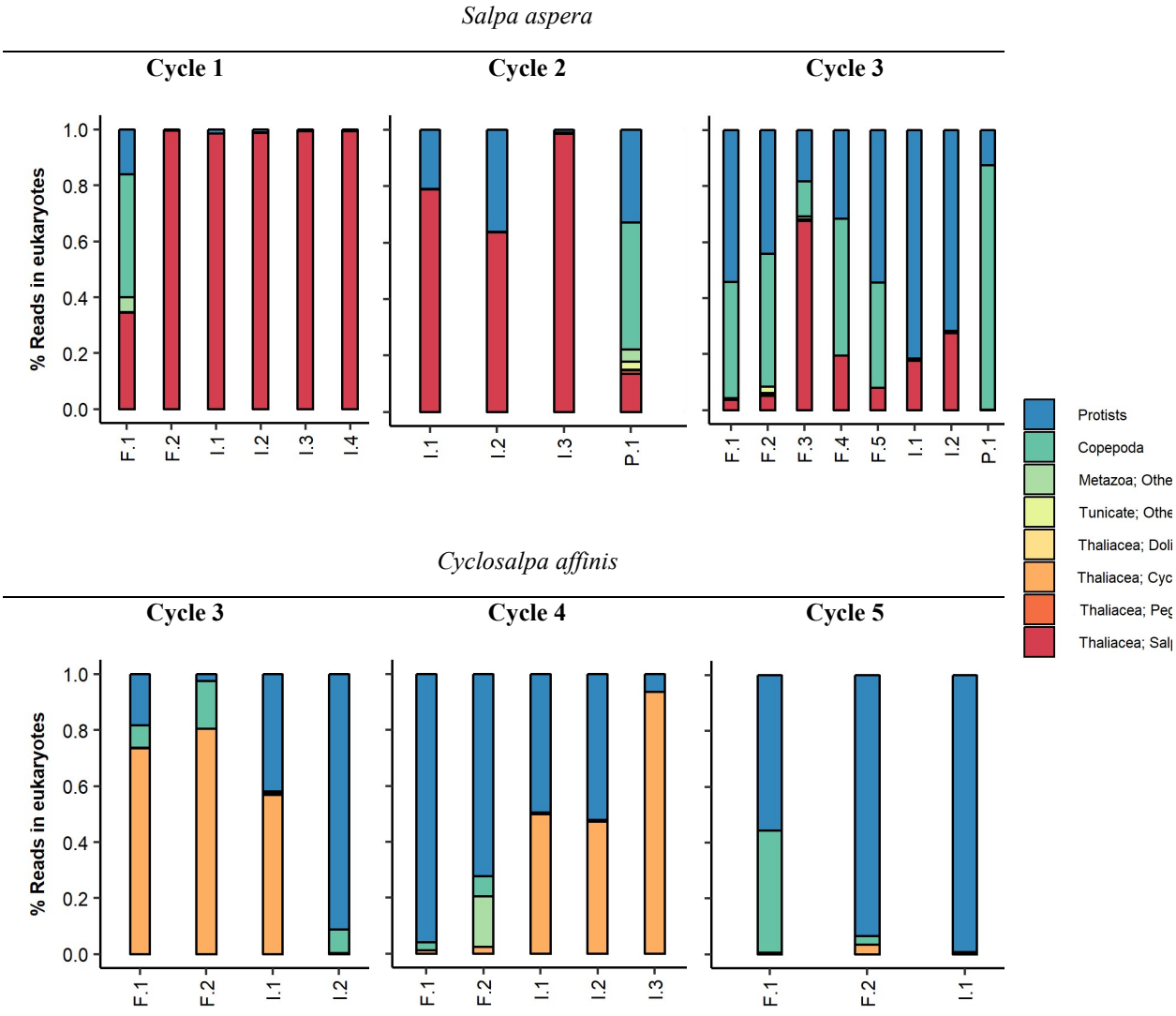

Figure 3.2. Proportion of sequence reads ascribed to protists and metazoans from guts (F: field collected, I: incubated in filtered seawater) and fecal pellets (P) of *Salpa aspera* and *Cyclosalpa affinis* in summer 2014.

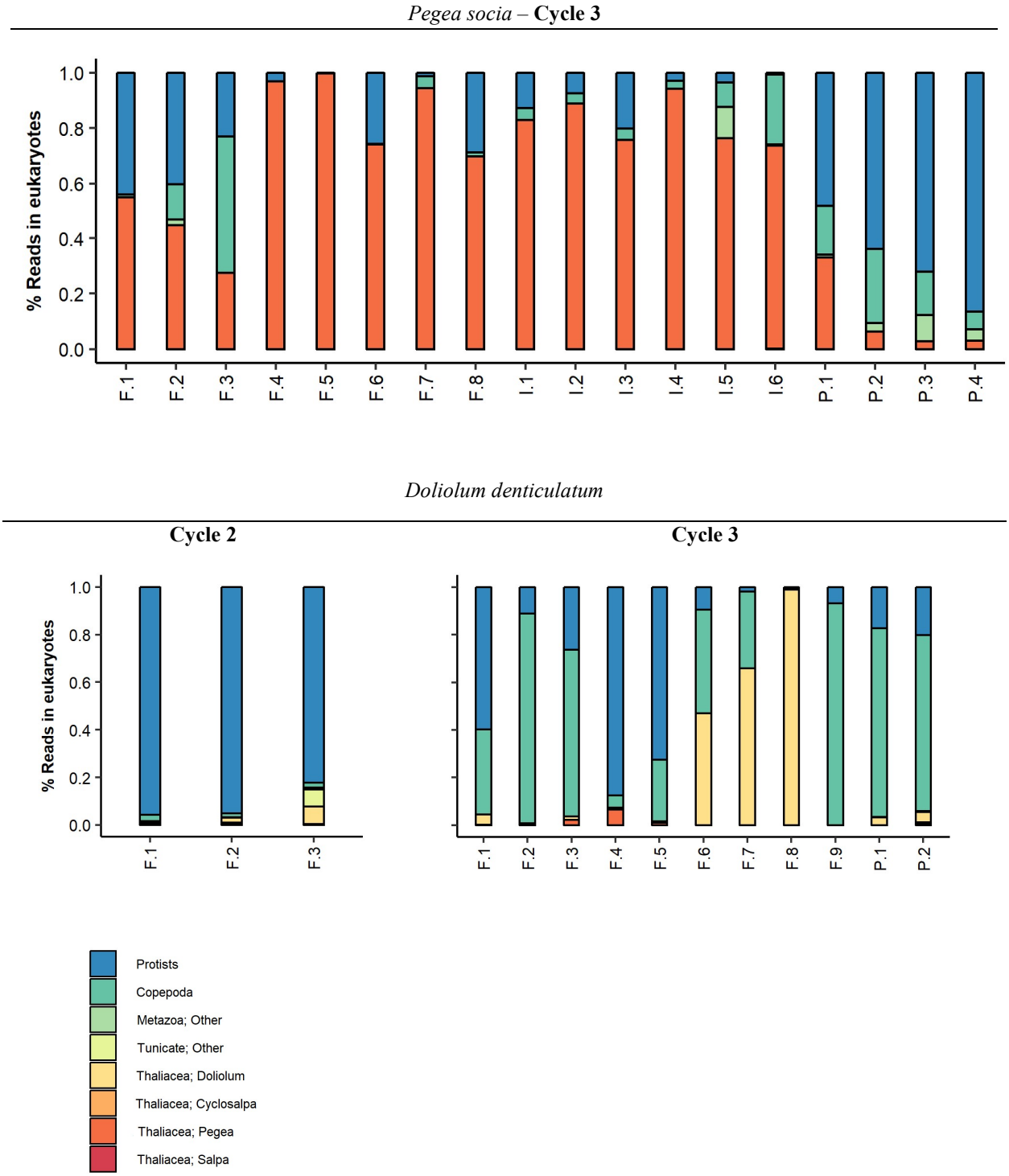

Figure 3.3. Proportion of sequence reads ascribed to protists and metazoans from guts (F: field collected, I: incubated in filtered seawater) and fecal pellets (P) of *Pegea socia* and *Doliolum denticulatum* in spring 2016. All individuals of *P. socia* were collected in Cycle 3.

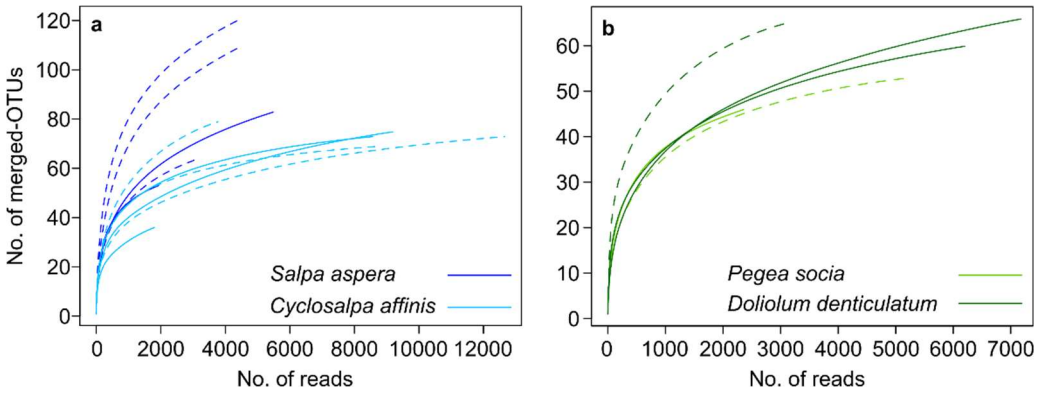

Figure 3.4. Rarefaction curves of protist OTUs identified in the guts and fecal pellets of salps and doliolids from metagenomic analysis. Dotted lines correspond to samples from fecal pellets.

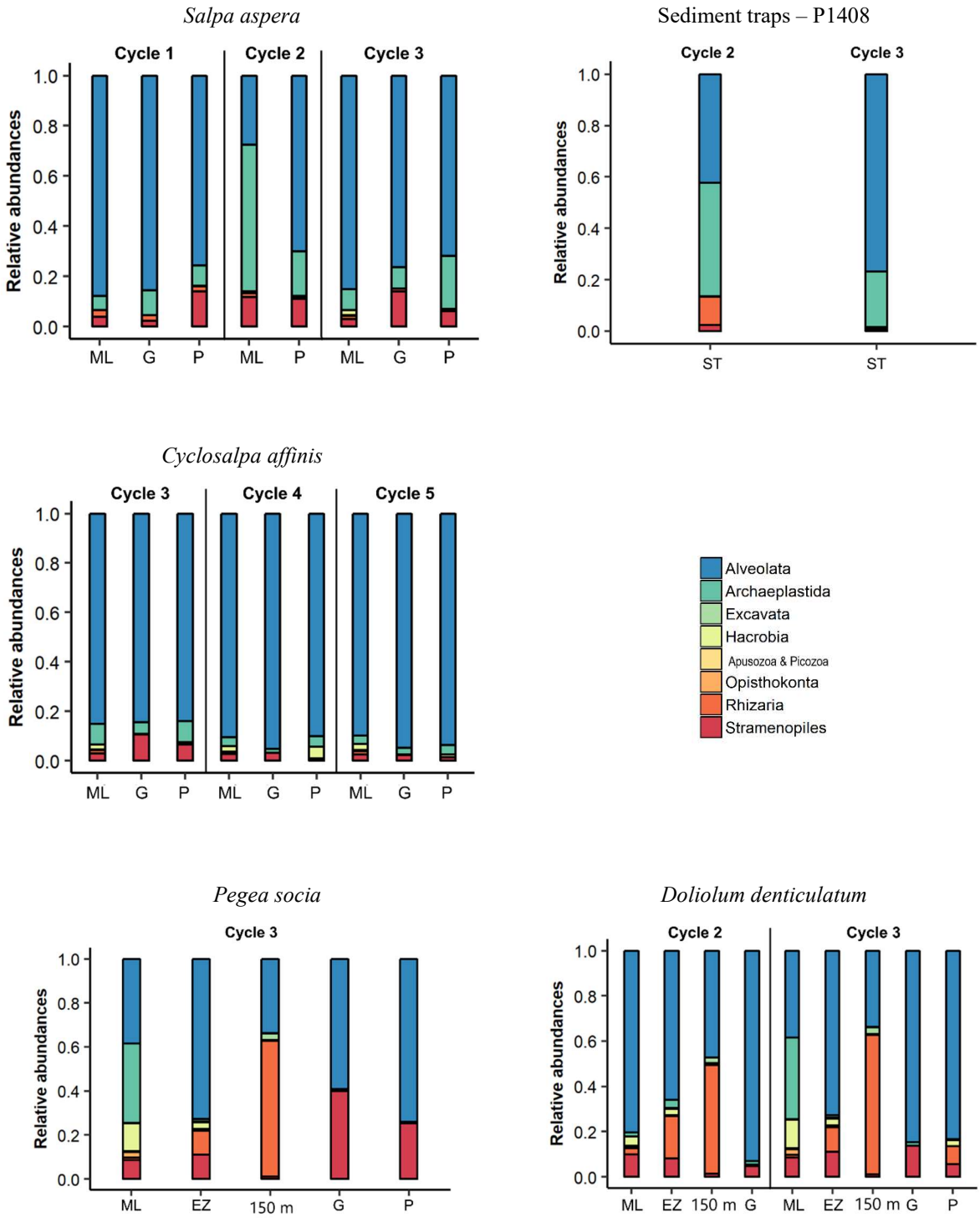

Figure 3.5. Relative abundances of major groups of protists detected from metabarcoding (18S rRNA) in guts (G) and fecal pellets (P) of salps and doliolids. Only data from individuals frozen immediately after collection are shown. Fecal pellets were collected from individuals incubated in filtered seawater. Cycle number (C) is indicated for each cruise; water-column samples are indicated as ML (mixed layer,) EZ (base of the euphotic zone) and DE (150 m). Two salp fecal pellets collected in sediment traps during summer 2014 were also analyzed.

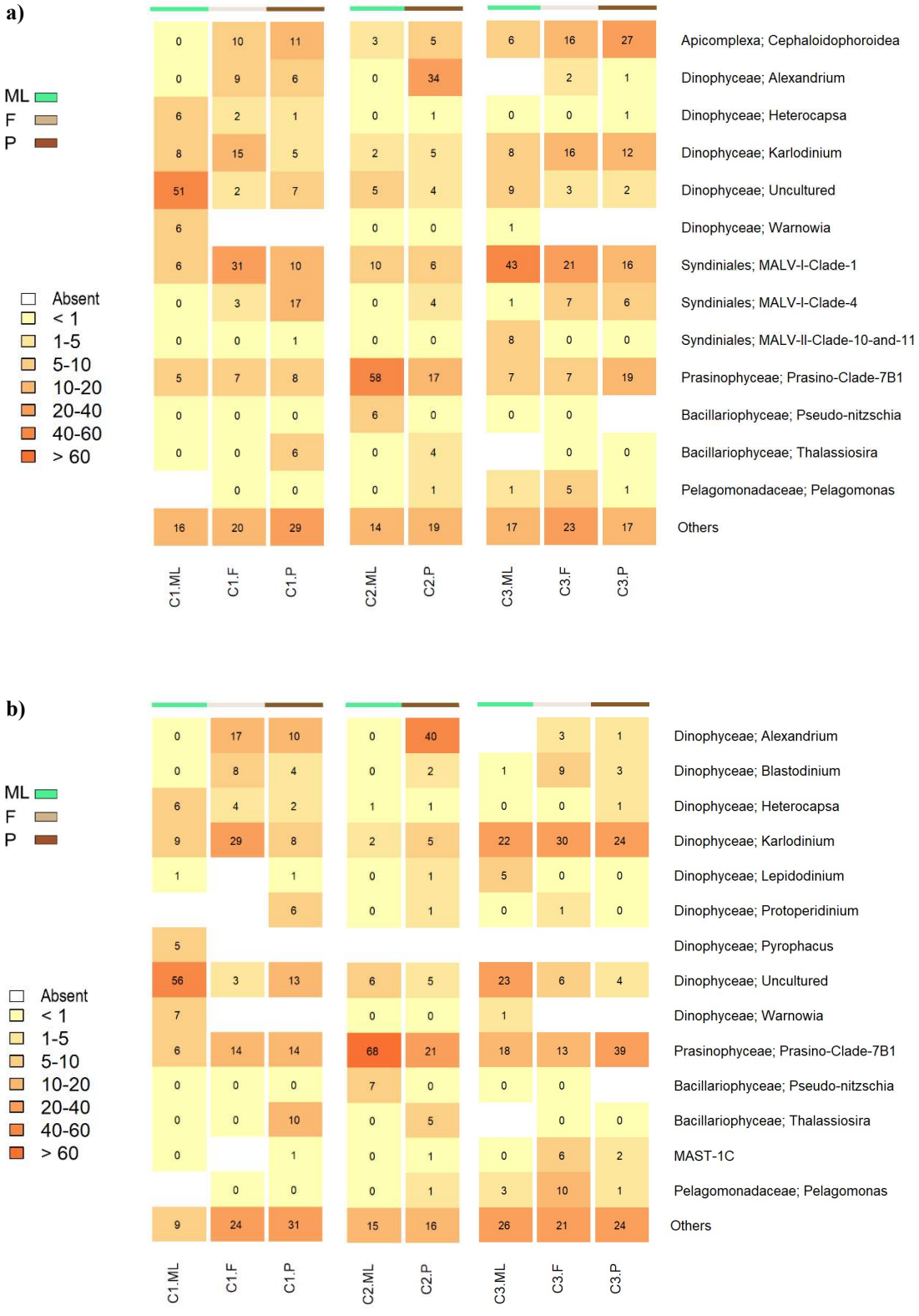

Figure 3.6. Relative abundance of protist reads in the water column (ML: mixed layer), guts (F: field collected), and fecal pellets (P) of *Salpa aspera* during summer 2014. **a)** All protists. **b)** Omitting sequence reads of apicomplexa and syndiniales. Only genera with relative abundances >5% are shown.

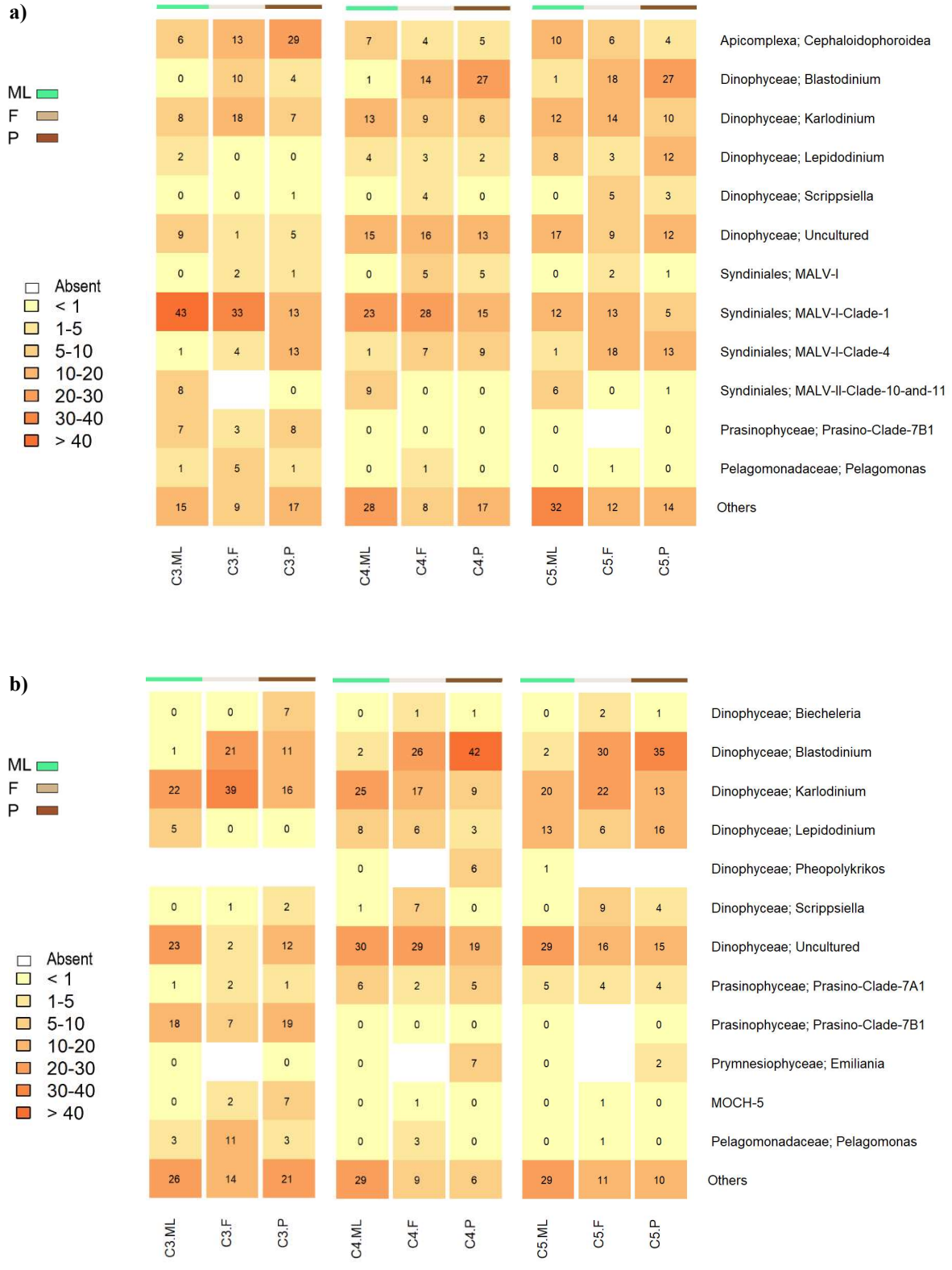

Figure 3.7. Relative abundance of protist reads in the water column (ML: mixed layer), guts (F: field collected), and fecal pellets (P) of *Cyclosalpa affinis* during summer 2014. **a)** All protists. **b)** Omitting sequence reads of apicomplexa and syndiniales. Only genera with relative abundances >5% are shown.

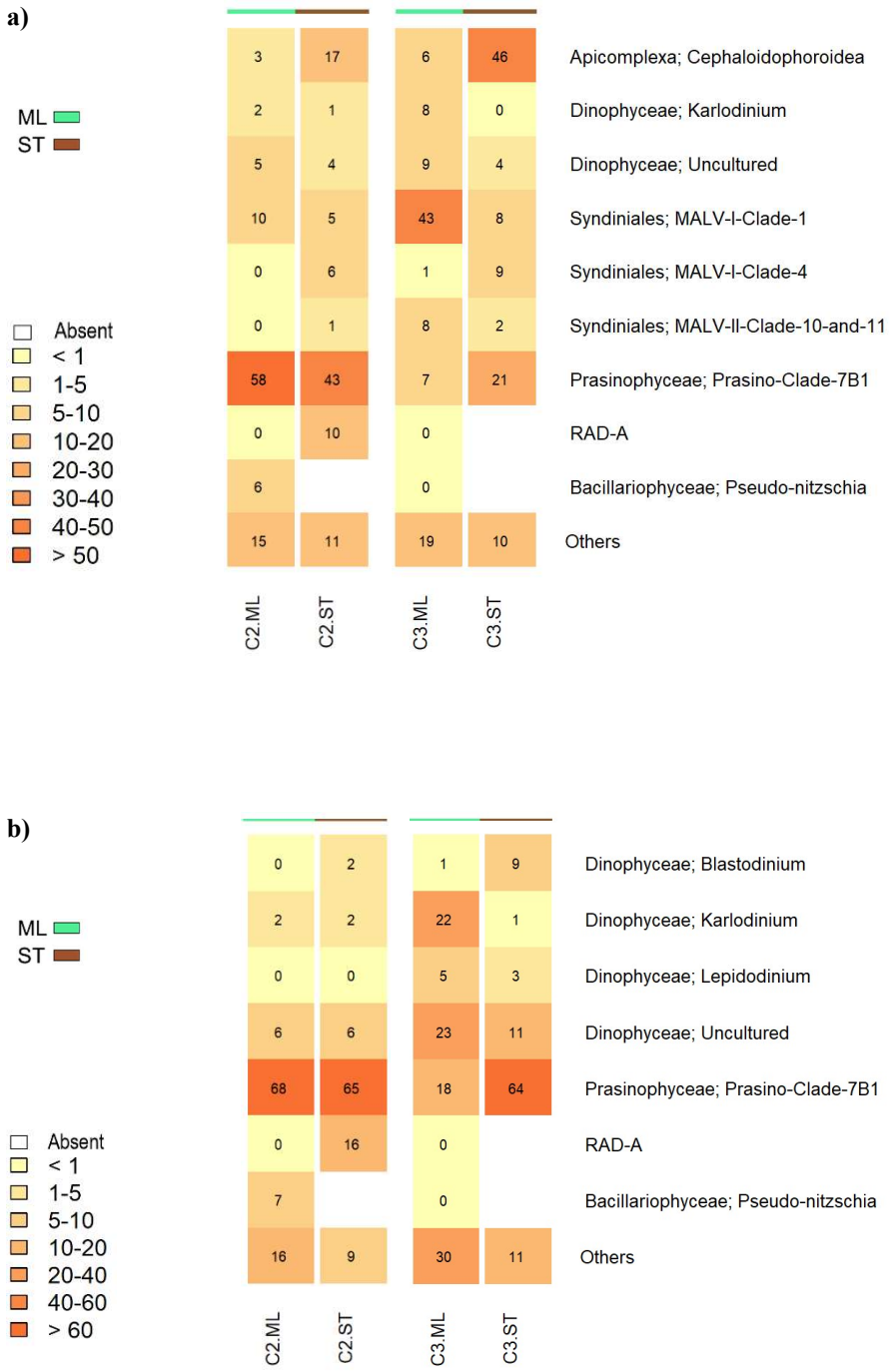

Figure 3.8. Relative abundance of protist reads in the water column (ML: mixed layer) and salp fecal pellets collected in sediment traps (ST) during summer 2014. **a)** All protists. **b)** Omitting sequence reads of apicomplexa and syndiniales. Only genera with relative abundances >5% are shown.

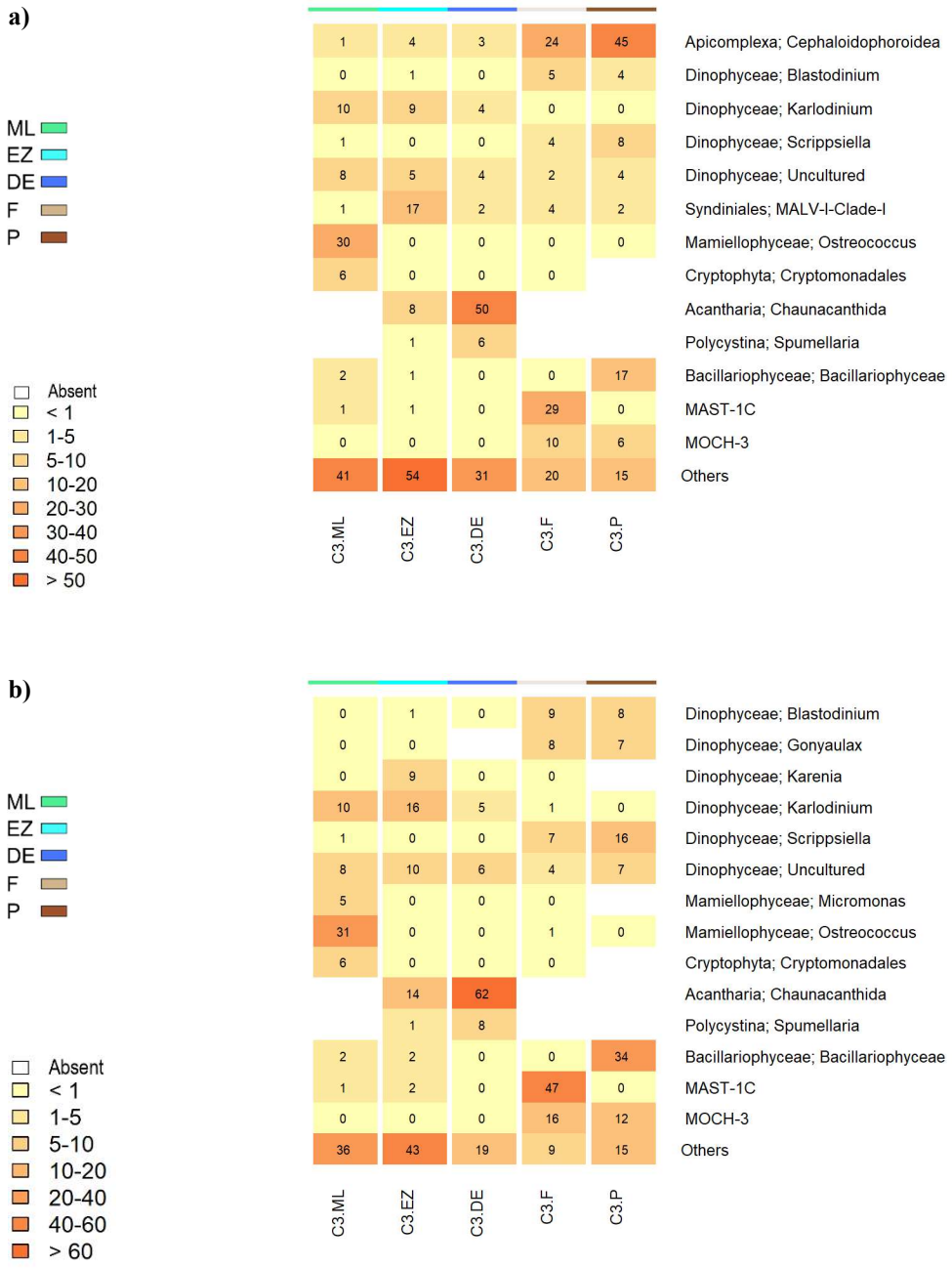

Figure 3.9. Relative abundance of protists reads in the water column, guts (F: field collected), and fecal pellets (P) of *Pegea socia* during spring 2016. **a)** All protists. **b)** Omitting sequence reads of apicomplexa and syndiniales. Only genera with relative abundances >5% are shown. ML: mixed layer, EZ: base of euphotic zone, DE: 150 m.

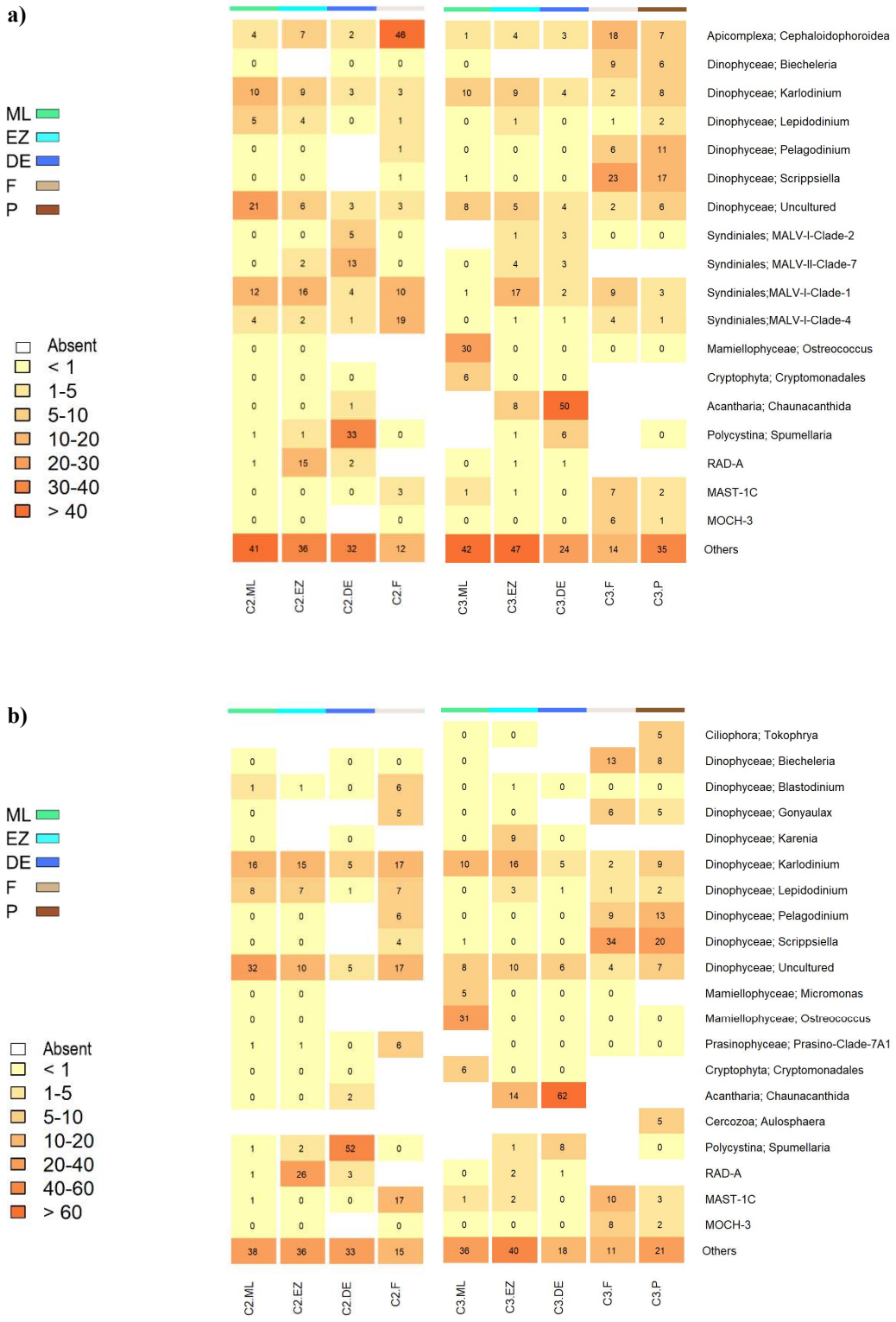

Figure 3.10. Relative abundance of protists reads in the water column, guts (F: field), and fecal pellets (P) of *Doliolum denticulatum* during spring 2016. **a)** All protists. **b)** Omitting sequence reads of apicomplexa and syndiniales. Only genera with relative abundances > 5% are shown. ML: mixed layer, EZ: base of euphotic zone, DE: 150 m.

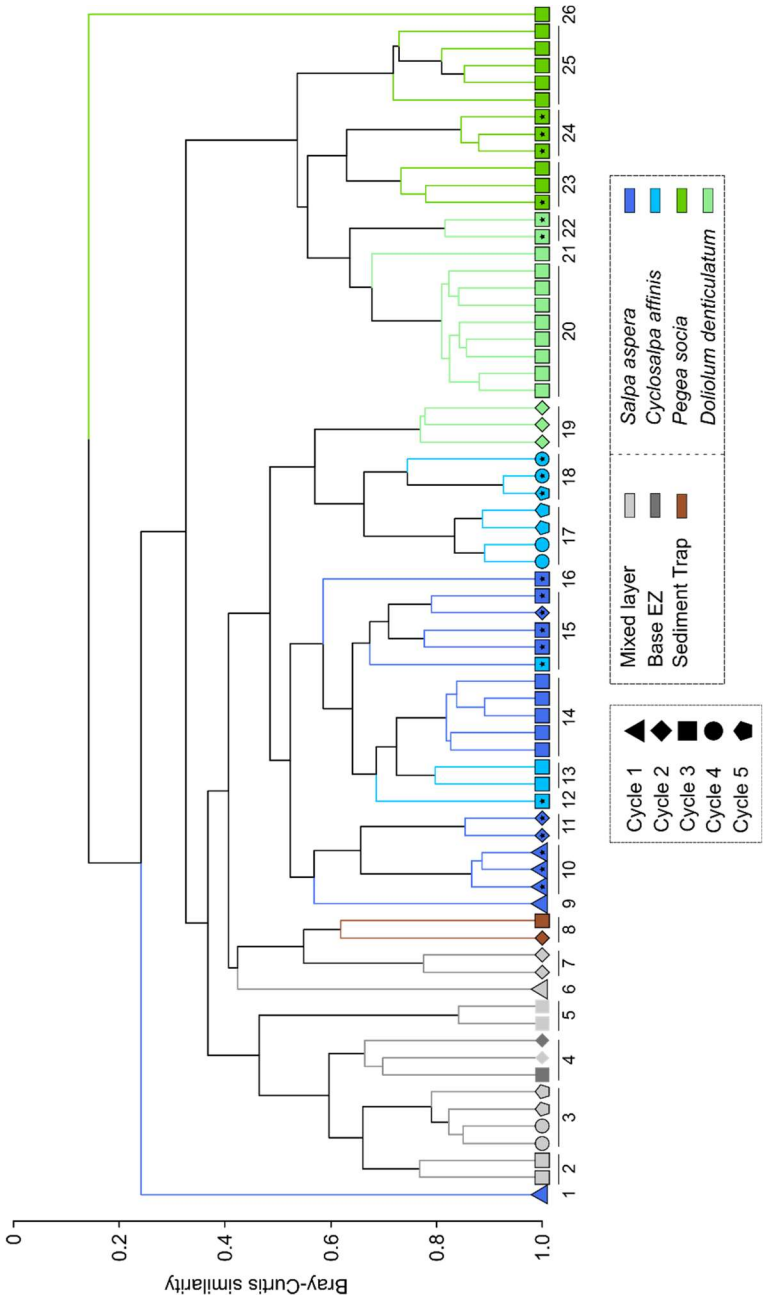

Figure 3.11. Structure of protist communities in guts and fecal pellets of three species of salps and one of doliolids evaluated by hierarchical cluster analysis. Analyses were done at the genus level and included only genera with relative abundances >1% in any sample (n = 99). Communities were grouped in 34 significant clusters (SIMPROF, $p < 0.05$, black lines in cluster). The number of clusters was reduced to determine the protists differentiating them by merging samples of a similar type (see Figure 12). Samples are color coded according to type and shape-coded according to site. Symbols with a star correspond to samples from fecal pellets. Cluster analysis included also water column samples from the mixed layer and base of the euphotic zone (Base EZ), as well as two salp fecal pellets collected in sediment traps in summer 2014. Symbols of water column samples with a black edge correspond to samples collected in summer 2014.

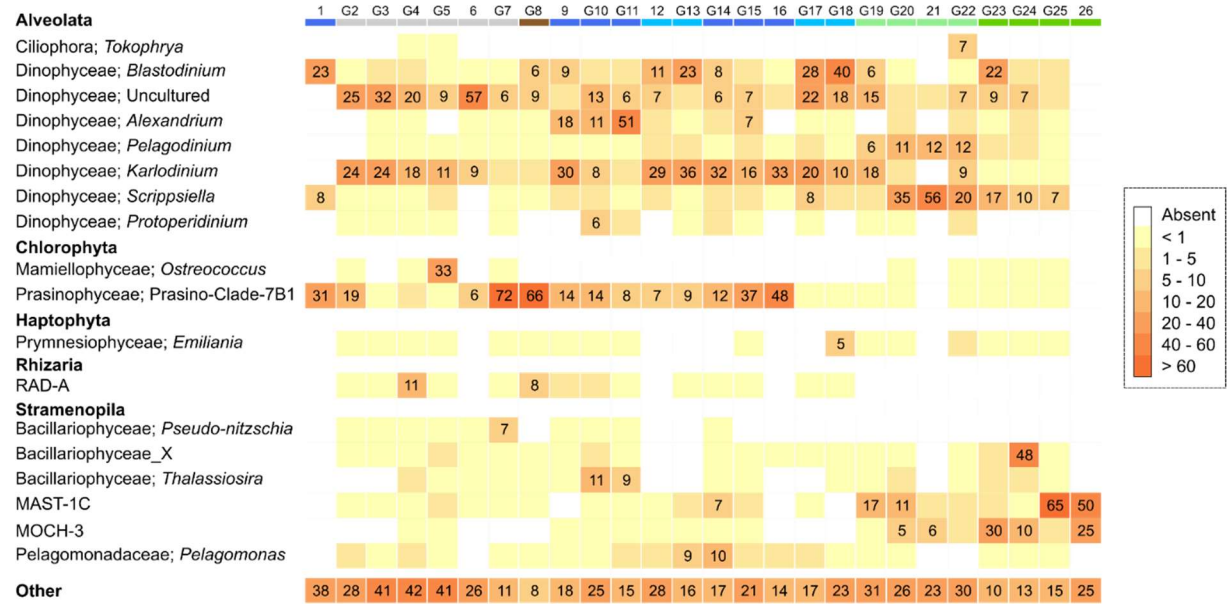

Figure 3.12. Protists differentiating the clusters of samples (see Figure 11) determined based on SIMPER analysis. Only a subset of protists and relative abundances >5% are shown in the heatmap.

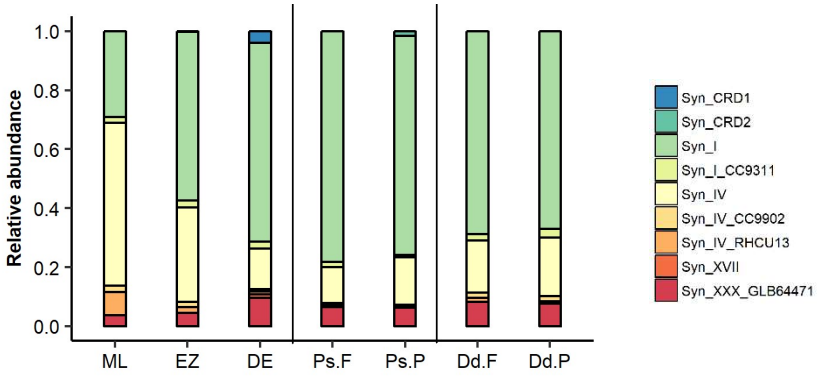

Figure 3.13. Sequence reads of *Synechococcus* strains detected with the ITS primer in guts (F: field collected) and fecal pellets (P) of *Pegea socia* (Ps) and *Doliolum denticulatum* (Dd). *Synechococcus* strains were also evaluated in the water column (ML: mixed layer, EZ: base of euphotic zone, DE: 150 m). Only samples from Cycle 3 (spring 2016) were analyzed.

References

Ahmad Ishak NH, Clementson LA, Eriksen RS, van den Enden RL, Williams GD, Swadling KM. (2017). Gut contents and isotopic profiles of *Salpa fusiformis* and *Thalia democratica*. Mar Biol **164:** 144.

Alldredge AL, Madin LP. (1982). Pelagic tunicates: unique herbivores in the marine plankton. BioScience **32:** 655–663.

Allen LZ, Allen EE, Badger JH, McCrow JP, Paulsen IT, Elbourne LDH, Thiagarajan M, Rusch DB, Nealson KH, Williamson SJ, Venter JC, Allen AE. (2012). Influence of nutrients and currents on the genomic composition of microbes across an upwelling mosaic. ISME J **6:** 1403–1414.

Alves-de-Souza C, Cornet C, Nowaczyk A, Gasparini S, Skovgaard A, Guillou L. (2011). *Blastodinium* spp. infect copepods in the ultra-oligotrophic marine waters of the Mediterranean Sea. Biogeosciences **8:** 2125–2136.

Bochdansky AB, Deibel D, Rivkin RB. (1999). Absorption efficiencies and biochemical fractionation of assimilated compounds in the cold water appendicularian *Oikopleura vanhoeffeni*. Limnol Oceanogr **44**: 415-424.

Bond NA, Cronin MF, Freeland H, Mantua N. (2015). Causes and impacts of the 2014 warm anomaly in the NE Pacific. Geophys Res Lett **42:** 3414–3420.

Bruland KW, Silver MW. (1981). Sinking rates of fecal pellets from gelatinous zooplankton (salps, pteropods, doliolids). Mar Biol **63**: 295–300.

Choi DH, Hoon noh J, Lee JH. (2014). Application of pyrosequencing method for investigating the diversity of *Synechococcus* subcluster 5.1 in open ocean. Microbes Environ **29:** 17–22.

Clopton RE. (2002). Phylum Apicoplexa Levine 1970: Order Eugregarinorida Léger, 1990. In: Lee JJ, Leedale G, Patterson D, Bradbury (eds) Illustrated guide to the protozoa, 2nd edn. Society of Protozoologists, Lawrence, pp 205–288.

Decelle J, Siano R, Probert I, Poirier C, Not F. (2012). Multiple microalgal partners in symbiosis with the acantharian *Acanthochiasma* sp. (Radiolaria). Symbiosis **58:** 233–244.

De Vargas C, Audic S, Henry N, Decelle J, Mahé F, Logares R, Lara E, Berney C, Bescot NL, Probert I, Carmichael M, Poulain J, Romac S, Colin S, Aury JM, Bittner L, Chaffron S, Dunthorn M, Engelen S, Flegontova O, Guidi L, Horak A, Jaillon O, Lima-Mendez G, Lukes J, Malviya S, Morard R, Mulot M, Scalco E, Siano R, Vincent F, Zingone A, Dimier C, Picheral M, Searson S, Kandels-Lewis S, Tara Oceans Coordinators, Acinas SG, Bork P, Bowler C, Gorsky G, Grimsley N, Hingamp P, Iudicone S, Not F, Ogata H, Pesant S, Raes J, Sieracki ME, Speich S, Stemmann L, Sunagawa S, Weissenbach J, Wincker P, Karsenti E. (2015). Eukaryotic plankton diversity in the sunlit ocean. Science **348:** 1261605, DOI: 10.1126/science.1261605.

Du X, Peterson W, O'Higgins L. (2015). Interannual variations in phytoplankton community structure in the northern California Current during the upwelling seasons of 2001-2010. Mar Ecol Prog Ser **519:** 75–87.

Edgar RC. (2010). Search and clustering orders of magnitude faster than BLAST. Bioinformatics **26:** 2460–2461.

Fowler SW, Fisher NS. (1983). Viability of marine phytoplankton in zooplankton fecal pellets. Deep Sea Res Part I **30:** 263–269.

Frischer ME, Sanchez CA, Walters TL, Thompson ME, Frazier LM, Paffenhöfer GA. (2014). Reliability of qPCR for quantitative gut content estimation in the circumglobally abundant pelagic tunicate *Dolioletta gegenbauri* (Tunicata, Thaliacea). Food Webs **1:** 18–24.

Guillou L, Viprey M, Chambouvet A, Welsh RM, Kirkham AR, Massana R, Scanlan DJ, Worden AZ. (2008). Widespread occurrence and genetic diversity of marine parasitoids belonging to Syndiniales (Alveolata). Environ Microbiol **10:** 3349–3365.

Harbison GR, McAlister VL. (1979). The filter-feeding rates and particle retention efficiencies of three species of Cyclosalpa (Tunicata, Thaliacea). Limnol Oceanogr **24:** 875–892.

Iseki K. (1981). Particulate organic matter transport to the deep sea by salp fecal pellets. Mar Ecol Prog Ser **5:** 55–60.

Katechakis A, Stibor H, Sommer U, Hansen T. (2004). Feeding selectivities and food niche separation of *Acartia clausi*, *Penilia avirostris* (Crustacea) and *Doliolum denticulatum* (Thaliacea) in Blanes Bay (Catalan Sea, NW Mediterranean). J Plankton Res **26:** 589–603.

Köster M, Sietmann R, Meuche A, Paffenhöfer GA. (2011). The ultrastructure of a doliolid and a copepod fecal pellet. J Plankton Res **33:** 1538–1549.

Lavaniegos BE, Ohman MD. (2003). Long-term changes in pelagic tunicates of the California Current. Deep Sea Res Part II **50:** 2473–2498.

Madin LP. (1974). Field observations on the feeding behavior of salps (Tunicata: Thaliacea). Mar Biol **25:** 143–147.

Madin LP. (1982). Production, composition and sedimentation of salp fecal pellets in oceanic waters. Mar Biol **67:** 39–45.

Madin LP, Purcell JE. (1992). Feeding, metabolism, and growth of *Cyclosalpa bakeri* in the subarctic Pacific. Limnol Oceanogr **37:**1236–1251.

Mahé F, Rognes T, Quince C, de Vargas C, Dunthorn M. (2014). Swarm: robust and fast clustering method for amplicon-based studies. PeerJ **2:** e593.

McClathchie S, Goericke R, Leising A, Auth T, Bjorkstedt E, Robertson RR, Brodeur RD, Du X, Daly HA, Morgan CA, Chavez FP, Debich AJ, Hildebrand J, Field J, Sakuma K, Jacox MG, Kahru M, Kudela R, Anderson C, Lavaniegos BE, Gomez-Valdes J, Jiménez-Rosenberg SPA, McCabe R, Melin SR, Ohman MD, Sala LM, Peterson B, Fisher J, Schroeder ID, Bograd SJ, Hazen EL, Schneider SR, Olightly RTG, Suryan RM, Gladics AJ, Loredo S, Porquez JM, Thompson AR, Weber ED, Watson W, Trainer V, Warzybok P, Bradley R, Jahncke J. (2016). State of the California Current 2015–16: Comparisons with the1997–98 El Niño. CalCOFI Rep **57:** 5–61.

Metfies K, Nicolaus A, Von Harbou L, Bathmann U, Peeken I. (2014). Molecular analyses of gut contents: Elucidating the feeding of co-occurring salps in the Lazarev Sea from a different perspective. Antarct Sc **26:** 545–553.

Mianzan HW, Pajaro M, Machinandiarena L, Cremonte F. (1997). Salps: possible vectors of toxic dinoflagellates?. Fish Res **29:** 193–197.

Nejstgaard JC, Frischer ME, Raule CL, Gruebel R, Kohlberg KE, Verity PG. (2003). Molecular detection of algal prey in copepod guts and fecal pellets. Limnol Oceanogr: Methods **1:** 29–38.

Ohman MD, Barbeau K, Franks PJS, Goericke R, Landry MR, Miller AJ. (2013). Ecological transitions in a coastal upwelling ecosystem. Oceanography **26:** 210–219.

Oksanen, J., Blanchet, F. G., Friendly, M., Kindt, R., Legendre, P., McGlinn, D., Minchin, P. R., O'Hara, R. B., Simpson, G. L., Solymos, P., Stevens, M. H. H., Szoecs, E., Wagner, H. (2017). vegan: Community ecology package. R package version 2.4-3.

Pearson WR. (2016). Finding protein and nucleotide similarities with FASTA. Curr. Protoc. Bioinform. **53:** 3.9.1-3.9.25. doi: 10.1002/0471250953.bi0309s53.

Perissinotto R, Pakhomov EA. (1998). The trophic role of the tunicate *Salpa thompsoni* in the Antarctic marine ecosystem. J Marine Syst **17:** 361–374.

Pfannkuche O, Lochte K. (1993). Open ocean pelago-benthic coupling: cyanobacteria as tracers of sedimenting salp faeces. Deep Sea Res Part I **40:** 727–737.

Purcell JE, Madin LP. (1991). Diel patterns of migration, feeding, and spawning by salps in the subarctic Pacific. Mar Ecol Prog Ser **73:** 211–217.

Rueckert S, Simdyanov TG, Aleoshin VV, Leander BS. (2011). Identification of a divergent environmental DNA sequence clade using the phylogeny of gregarine parasites (Apicomplexa) from crustacean hosts. PLoS One **6:** e18163.

Schloss PD, Westcott SL, Ryabin T, Hall JR, Hartmann M, Hollister EB, Lesniewski RA, Oakley BB, Parks DH, Robinson CJ, Sahl JW, Stres B, Thallinger GG, Van Horn DJ, Weber CF. (2009). Introducing mothur: Open-source, platform-independent, community-supported software for describing and comparing microbial communities. Appl Environ Microbiol **75:** 7537–7541.

Silver MW, Bruland KW. (1981). Differential feeding and fecal pellet composition of salps and pteropods, and the possible origin of the deep-water flora and olive-green “cells”. Mar Biol **62:** 263–273.

Smith KL, Sherman AD, Huffard CL, McGill PR, Henthorn R, Von Thun S, Ruhl HA, Kahru M, Ohman MD. (2014). Large salp bloom export from the upper ocean and benthic community response in the abyssal northeast Pacific: Day to week resolution. Limnol Oceanogr **59:** 745–757.

Sohm JA, Ahlgren NA, Thomson ZJ, Williams C, Moffett JW, Saito MA., Webb EA, Rocap G. (2016). Co-occurring *Synechococcus* ecotypes occupy four major oceanic regimes defined by temperature, macronutrients and iron. ISME J **10:** 333–345.

Sutherland KR, Madin LP, Stocker R. (2010). Filtration of submicrometer particles by pelagic tunicates. P Natl Acad Sci **107:** 15129–15134.

Takahashi K, Ichikawa T, Fukugama C, Yamane M, Kakehi S, Okazaki Y, Kubota H, Furuya K. (2015). In situ observations of a doliolid bloom in a warm water filament using a video plankton recorder: bloom development, fate, and effect on biogeochemical cycles and planktonic food webs. Limnol Oceanogr **60:** 1763–1780.

Taylor AG, Landry MR, Selph KE, Wokuluk JJ. (2015). Temporal and spatial patterns of microbial community biomass and composition in the Southern California Current Ecosystem. Deep Sea Res Part II **112:** 117–128.

Valencia B, Stukel MR, Allen AE, McCrow JP, Rabines A, Palenik B, Landry MR. (In prep). Microbial communities associated with sinking particles across an environmental gradient in the California Current System. To be submitted to Environ Microbiol.

Vargas CA, Madin LP. (2004). Zooplankton feeding ecology: clearance and ingestion rates of the salps *Thalia democratica*, *Cyclosalpa affinis* and *Salpa cylindrica* on naturally occurring particles in the Mid-Atlantic Bight. J Plankton Res **26:** 827-833.

Venrick EL. (2002). Floral patterns in the California Current System off southern California: 1990-1996. J Mar Res **60:** 171–189.

Wallis JR, Smith AJ, Kawaguchi S. (2017). Discovery of gregarine parasitism in some Southern Ocean krill (Euphausiacea) and the salp *Salpa thompsoni*. Polar Biol **40:** 1913–1917.

Whitaker D, Christman M. (2015). clustsig: Significant Cluster Analysis. R package version 1.1.

Zhang J, Kobert K, Flouri T, Stamatakis A. (2014). PEAR: A fast and accurate Illumina Paired-End reAd mergeR. Bioinformatics **30:** 614–620.

Zwirglmaier K, Jardillier L, Ostrowski M, Mazard S, Garczarek L, Vaulot D, Not F, Massana R, Ulloa O, Scanlan DJ. (2008). Global phylogeography of marine *Synechococcus* and *Prochlorococcus* reveals a distinct partitioning of lineages among oceanic biomes. Environ Microbiol **10:** 147–161.

Zwirglmaier K, Spence ED, Zubkov MV, Scanlan DJ, Mann NH. (2009). Differential grazing of two heterotrophic nanoflagellates on marine Synechococcus strains. Environ Microbiol **11:** 1767–1776.

CHAPTER 4

Microbial communities associated with sinking particles across an environmental gradient in the California Current System

Abstract

Using 16S/18S rRNA and ITS amplicon sequencing, we evaluate prokaryotic and protistan communities in the water column and on particles collected in sediment traps across an inshore-offshore environmental gradient in the California Current System. Particle-associated microbial assemblages were different from the ambient water-column communities. Diversity differences were also evident for protists, but less so for prokaryotes, across the inshore-offshore gradient. Gammaproteobacteria, dinoflagellates, and rhizarians were the dominant microbes associated with sinking particles at all sampling locations, with diatom contributions increasing significantly at the inshore mesotrophic site. Parasitic groups, syndiniales and apicomplexans, were also major particle-associated taxa. Only some mixed-layer microbes contributed significantly to sinking particles. For cyanobacteria, *Synechococcus* was significantly enriched on sinking particles relative to water-column community composition at the oligotrophic sampling locations, and clade I strains were consistently higher on sinking particles at all sites. Among protists, dinoflagellates contributed disproportionately to the particle-associated assemblages at oligotrophic and transition sites, while the diatom *Thalassiosira* was relatively enriched on particles at the inshore upwelling site. Our results highlight the need for trophic studies that better resolve taxon-specific contributions to upper-ocean productivity and particle export in terms of carbon-based fluxes in comparison with sequence relative abundances.

Introduction

The biological pump includes all of the processes that incorporate inorganic carbon into organic production, and then transform and transport it to the deep sea (Longhurst and Harrison, 1989; Ducklow *et al.,* 2001). The magnitude and efficiency of the pump are affected both by the structure and trophic interactions of plankton communities in the euphotic zone and by the activities of microbial and metazoan consumers that attenuate particle flux in the mesopelagic zone (Longhurst and Harrison, 1989; Ducklow *et al.,* 2001; Buesseler *et al.,* 2007; Stukel *et al.,* 2011). Only about 10% of global ocean productivity is estimated to be exported below the base of the euphotic zone (Siegel *et al*., 2014) and traditionally, large phytoplankton with mineral tests, such as diatoms, were believed to be responsible for most of this flux (Michaels and Silver, 1988). More recently, however, metabarcoding analyses have revealed that sequences of smaller pico- and nano-sized forms, such as *Synechococcus*, prasinophytes, and dinoflagellates, are strongly associated with particulate carbon export in oligotrophic systems (e.g., Amacher *et al.,* 2013; Guidi *et al.,* 2016). Nonetheless, the relative importance of different microbes to carbon fluxes under varying environmental conditions and the mechanisms driving their export remain poorly known (Richardson and Jackson, 2007; Stukel and Landry, 2010).

Process cruise studies of the California Current Ecosystem – Long-Term Ecological Research (CCE-LTER) Program provide an opportunity to evaluate how microbial assemblages vary in their contributions to particle flux in a habitat with contrasting environmental conditions. The inshore region of the California Current System (CCS) is a highly productive coastal upwelling habitat characterized by high biomass and dominance of larger primary producers, typically diatoms and dinoflagellates (Venrick, 2002; Taylor *et al.,* 2015). In contrast, the

offshore open-ocean region resembles the oligotrophic central gyres in low biomass and dominance of small cells. These differences also translate to the properties of exported particles, with zooplankton fecal pellets contributing most in the inshore region and amorphous aggregates offshore (Knauer *et al.,* 1979; Stukel *et al.,* 2013b). In addition to the contrasting inshore-offshore environmental conditions, variability at seasonal, interannual, and decadal scales in the CCS is reflected in changes in the composition of plankton communities, productivity, and particle export (McGowan *et al.,* 1998; Checkley and Barth, 2009; Lavaniegos and Ohman, 2007; Wilson *et al.,* 2013; Peterson *et al.,* 2017). In particular for this study, anomalously warm conditions (sea surface temperature anomalies > 2°C) prevailed in the region from late 2013 to 2016. Initially, these anomalously warm waters extended southward from Alaska and affected the North Pacific, where it was known as the "blob" (Bond *et al.,* 2015). In the subsequent 2015-2016 El Niño event, the warm water conditions extended northward from the equatorial region (McClatchie *et al*., 2016). In the CCS, productivity tends to decrease during El Niño events, and plankton communities shift towards a higher dominance of smaller subtropical and open-ocean taxa (Chavez *et al.,* 2002; Peterson *et al.,* 2002; Peterson *et al.,* 2017), which likely affects the microbial communities contributing to sinking particles.

Using metabarcoding to characterize microbial assemblages, we address two central questions: How does the structure of microbial communities differ between sinking particles and the water column across the CCS environmental gradient? How do specific microbial taxa differ in their contributions to exported particulate matter? Since previous metabarcoding analyses have identified the picocyanobacterium *Synechococcus* as an important component of export material (Amacher *et al.,* 2013; Guidi *et al*., 2016), we also investigated if specific *Synechococcus* strains are differentially enriched on particles relative to the water column. We

hypothesize: a) that the compositions of microbial communities on exported particles differ from those in the overlying water column, b) that microbial assemblages on sinking particles vary significantly across the ecosystem gradient, c) that certain water-column microbes are enriched on exported particles, and d) that *Synechococcus* contributions to sinking particles vary among its dominant strains. In addition, we expect diatoms on sinking particles to increase disproportionately with increasing productivity due to food-web enhancement (larger consumers, larger and faster sinking pellets, and late-bloom aggregations that sink directly).

Materials and Methods

Cruise plan

Samples and environmental data were collected in the southern California Current System (CCS) on the R/V Sikuliaq as part of the CCE-LTER process cruise P1604 (19 April - 12 May 2016). The aim of the cruise was to evaluate the effects of the anomalously warm conditions on the pelagic ecosystem due to the 2015-2016 El Niño event. Four water parcels with relatively homogeneous conditions were selected based on satellite images of sea surface temperature and chlorophyll, and following surveys with a Moving Vessel Profiler (e.g., Ohman *et al.,* 2013). The sampling locations are the offshore oligotrophic open-ocean waters (OO: Offshore Oligotrophic), the core water of the CCS (CC: California Current), the transition zone between the CC and inshore-mesotrophic waters (TZ: Transition Zone), and the mesotrophic, nutrient-rich waters influenced by seasonal upwelling (IN: Inshore) (Figure 1). Protocols for collection and processing of environmental samples as well as cruise data are available at the CCE-LTER website (http://oceaninformatics.ucsd.edu/datazoo/catalogs/ccelter/datasets).

Sample collection for metabarcoding

At each site, sinking particulate matter was collected using VERTEX-style sediment traps that were attached under a surface float with satellite telemetry and a holey sock drogue centered at 15 m depth (Knauer *et al.,* 1979; Stukel *et al.,* 2013b). Each deployment followed a water parcel for 3-5 days. The trap array consisted of 12 replicate particle interceptor traps deployed at both of two depths, the base of the euphotic zone (Zeu), which varied among deployments, and at 150 m. At each depth, two tubes were filled before deployment with either 2.2 liters of brine or a RNA later solution (Table S1; Appendix Table 4.1) to collect samples for metabarcoding (prokaryotes: 16S rRNA, *Synechococcus*: ITS, and eukaryotes: 18S rRNA). The brine solution consisted of 0.1 µm filtered seawater and 50 g l^{-1} of NaCl, creating a density interface to prevent mixing with *in situ* water. The RNA later, made as described by Fontanez *et al.* (2015), was used to minimize DNA degradation. Upon sediment trap recovery, the upper water was removed from each trap tube, and the remaining water was filtered through a 200-µm Nitex screen to remove zooplankton swimmers. Non-swimmer particles (>200 µm) were kept on the Nitex screen, frozen in liquid nitrogen, and stored at -80°C. Particles in the remaining water were concentrated onto 0.2 µm Sterivex filters, flash frozen, and stored at -80°C.

During deployments, samples from the mixed layer, the base of the euphotic zone, and 150 m were collected by CTD casts adjacent to the array to compare to microbial assemblages from the water column and trap-collected particles (Appendix Table S4.1). At each depth, 280 ml (200 µm Nitex screen) or 650 ml of seawater (500 µm Nitex screen) samples were filtered onto 0.2-µm Supor membrane filters (Pall). Then, the filters were flash frozen in liquid nitrogen and stored at -80°C until analysis.

DNA from water-column and trap samples was extracted using the NucleoMag 96 Plant kit (Macherey Nagel) following the manufacturer's instructions. Although DNA was extracted separately for the particles <200 μm and >200 μm, these were pooled for subsequent analysis. DNA was amplified by Polymerase Chain Reaction using the Q5 high-fidelity PCR kit (New England Biolabs). Prokaryotes were characterized by amplification of the V4-V5 regions of the 16S small subunit ribosomal RNA gene (SSU-rRNA) using primers 515F and 926R (Appendix Table S4.2). Eukaryotes were characterized by amplifying the V9 region of the18S rRNA gene using primers 1389F and 1510R (Appendix Table S4.2). *Synechococcus* strains were characterized by amplifying the 16S-23S rRNA internal transcribed spacer (ITS) using primers ITS1F and ITS4R (Appendix Table S4.2). For sediment traps samples that did not amplify during PCR, we used the OneStep™ PCR Inhibitor Removal Kit (Zymo Research) to remove inhibitory substances.

The PCR products were pooled in equimolar amounts (~10 ng μl^{-1}) and sequenced using a dual-barcode index on an Illumina MiSeq platform at the Institute for Genomic Medicine (IGM, University of California, San Diego). Initial quality control of the raw sequence reads was done using the workflow for read filtering, swarm Operational Taxonomic Unit (OTU) clustering, and taxonomic classification of the SSU-rRNA written by JP McCrow (https://github.com/allenlab/rRNA_pipeline). Amplification, sequencing, and bioinformatics processing (denoising, chimera detection, and OTU clustering) of *Synechococcus* sequences was carried out at RTL Genomics (Lubbock, Texas). Demultiplexed raw reads are available in the Archive under Accession Number. Additional processing details are in the Supplementary Information. The total number of sequence reads and OTUs are summarized for each primer set

in Appendix Table S4.3 and by sample types in S4.4 (prokaryotes), S4.5 (*Synechococcus*), and S4.6 (eukaryotes).

Statistical analyses

We evaluated differences in prokaryotic (16S) and eukaryotic (18S) assemblages at the genus or lowest assigned taxonomic level by multivariate analyses based on the Bray-Curtis dissimilarity index. Prior to analyses, the sequence reads were merged by genera (prokaryotes: 379, eukaryotes: 510), and only those contributing >1% to the relative abundances in any sample (prokaryotes: 79, eukaryotes: 97) were included in the analyses. For the genera selected, relative abundances per sample were recalculated and square-root transformed to reduce the impact of the most abundant microbes. Community differences were assessed by hierarchical clustering and ordination using non-metric multidimensional scaling (nMDS). Cluster significance was established by similarity profile analysis (SIMPROF), and microbes differentiating the clusters were identified by similarity percentage analysis (SIMPER). Multivariate analyses were done in R using the packages 'vegan' (Oksanen *et al.,* 2017) and 'clustsig' (Whitaker and Christman, 2015).

We used pairwise comparisons with the Fisher's exact test to evaluate differences in the contributions of taxa within individual microbial groups (prokaryotes, protists, and *Synechococcus* strains) to water-column communities and sinking particles. In addition, we used data from 16S plastid analyses in pairwise comparisons to assess the relative contributions of mixed-layer prokaryotic (cyanobacteria) and eukaryotic (protist) phytoplankton to sinking particles. For these comparisons, only the subset of taxa with relative abundances >5% in any mixed-layer sample were selected for analysis. For each genus or strain, sequence reads were

averaged for the mixed-layer and 150-m trap samples. A false discovery rate (FDR) threshold of 0.05 was considered significant.

Results

Environmental conditions and export fluxes

Our drifter experiments covered a seven-fold range in productivity (229–1659 mg C m^{-2} d^{-1}) and a six-fold range in sediment-trap carbon fluxes at 150 m (32–202 mg C m^{-2} d^{-1}) (Table 1). Environmental conditions in offshore oligotrophic (OO) and California Current waters (CC) were marked by deep mixed layers (50–80 m), low nutrients (0.02–0.08 µM nitrate), low chlorophyll (0.1–0.2 µg Chl*a* L^{-1}), and low primary production (PP, 229-276 mg C m^{-2} d^{-1}) (Table 1, Figure 1b-1e). In contrast, conditions in the transition zone (TZ) and inshore (IN) areas had shallower mixed layers (30 and 12 m, respectively) with elevated nutrients, Chl*a*, and PP compared to the offshore region (Table 1, Figure 1b-1e). Mixed-layer nitrate concentrations were highest in the TZ region (4.6 vs 2.1 µM), but Chl*a* and PP were greatest at the IN site (4.2 vs 1.2 µg L^{-1} and 1659 vs 868 mg C m^{-2} d^{-1}, respectively). These differences are typical of the gradient in ecosystem characteristics across the CCS and underlie the >6-fold difference in measured POC export fluxes in 150-m sediment traps between OO and IN deployments (Table 1).

Community composition from sequence analyses

Bacteria dominate the sequence reads for prokaryotes in trap samples (99.9% Bacteria; 0.1% Archaea), while metazoans account for more of the eukaryote reads (84% metazoans; 16% protists) (Appendix Tables S4.4 and S4.6, Appendix Figures S4.1 and S4.2). In water-column

samples, Bacteria sequences (92.6%) also dominate over Archaea, whereas protists account for most of the eukaryote reads (72%). Most of the metazoan sequences are ascribed to copepods (24 OTUs), especially the calanoids *Metridia* and *Calanus* spp., both important consumers and vertical migrators in CCS waters. Doliolid sequences are also present in water-column and trap samples (Appendix Figure S4.3) due to a bloom of *Doliolum denticulatum* during the study period, with highest densities in the TZ.

Compositions of prokaryote and protistan assemblages show clear shifts with depth in the water column but more sample-to-sample variability on sinking particles (Figure 2). Prokaryote sequences in the mixed layer are dominated by Bacteroidetes and Alphaproteobacteria at the inshore sites (TZ and IN) and by Alphaproteobacteria and Cyanobacteria at the offshore sites (OO and CCP). Archaea, Bacteroidetes, and Alphaproteobacteria are the main contributors at all sampling locations in the base of the euphotic zone (Zeu) and 150-m samples (Figure 2a). In contrast, Gammaproteobacteria, *Pseudoalteromonas* and *Vibrio*, dominate the sediment-trap sequences at all sampling locations (Appendix Figure S4.4), although relative abundances of Bacteroidetes, Alphaproteobacteria, and Cyanobacteria are high in OO and CCP samples from the brine-filled traps (Figures 2a and Appendix Figure S4.4). We did not find a consistent influence of trap fill solutions (brine and RNA later) on the microbial composition in sinking particles, possibly because our trap deployments were only for 3-5 days.

In mixed-layer samples, alveolates dominate protist sequences from the OO and CC sites, chlorophytes (Archeaplastida) are more important in the TZ, and alveolates and stramenopiles co-dominate at the IN site (Figure 2b). Rhizarians and alveolates are the main components in the Zeu and 150-m samples. In general, parasitic alveolates (apicomplexan and syndiniales) and rhizarians are the main protists associated with sinking particles, although their contributions

vary among sampling locations (Appendix Figure S4.5). In the CC traps, alveolate sequences assigned to the apicomplexan Cephaloidophoroidea dominate (except for rhizarians in one sample), while alveolates and rhizarians are important in the OO samples. In the IN traps, alveolates, rhizarians, and stramenopiles are all important (Figures 2b and Appendix Figure S4.5). At the TZ site, the large contribution of chlorophytes (Archaeplastida) to the water-column assemblage is not seen in the trap samples (Figure 2b).

Microbial community structure with depth and site

For the water-column samples, microbial community structure clusters mainly by depth, although mixed-layer assemblages also differ among sampling locations (Figures 3 and 4). For sinking particles, the protist communities cluster mainly by site, whereas little pattern is evident for prokaryotes. Because community structure results based on hierarchical cluster and ordination analysis (nMDS) were consistent, only plots of the clusters are presented here. nMDS plots for prokaryotes are in Appendix Figures S4.6a and for protists in S4.6b.

Prokaryotic communities in the mixed layer have high sequence abundances assigned to *Prochlorococcus*, SAR11 surface clade, and *Synechococcus* at the offshore sampling locations (Group 1: OO and CC). *Synechococcus* and *Roseobacter* are the main components at the inshore sampling locations (Group 2: TZ and IN) (Figure 3). An unclassified Thaumarchaeota has high sequence abundances in the deeper water column, followed by the Bacteroidetes clade NS5 (Group 3: OO, CC, and TZ) in the Zeu samples and by SAR11 at 150 m (Group 4: all sites). Prokaryotic communities in the trap samples are dominated by sequences assigned to Gammaproteobacteria *Pseudoalteromonas* and *Vibrio* (Groups 9-11). *Pseudoalteromonas, Prochlorococcus,* and Gammaproteobacteria clade BD1-7 are major components in Group 6

(two OO samples), whereas the Flavobacteria *Fluviicola* and *Pseudoalteromonas* are important components of Group 7 (one TZ and one IN sample).

Mixed-layer protistan communities show high sequence abundances of an uncultured dinoflagellate at the two offshore sampling locations (Group 2: OO and CC), the chlorophyte *Ostreococcus* in the TZ (Group 1), and diatoms (*Thalassiosira* and unclassified Bacillariophyceae) and chlorophytes (*Micromonas*) at the IN site (Group 6) (Figure 4). For the Zeu (Group 3: OO, CC, and TZ) and 150-m samples (Group 4: all sites), the main protistan sequences are rhizarians, with high relative abundances of the clade RAD-A in Group 3 and Chaunacanthida and Spumellaria in Group 4 (Figure 4). For trap samples, the protist community at the OO site (Group 5) clusters close to the mixed-layer (Group 2), the Zeu (Group 3), and 150-m (Group 4) samples, indicating strong compositional similarities to the water column. Likewise, the sequences from trap samples at the IN site (Group 8) cluster close to samples from the overlying mixed layer and the Zeu (Group 6). At the OO site in the traps, the dominant protist is an uncultured dinoflagellate that is not represented in the reference database (Group 5), whereas the apicomplexan Cephaloidophoroidea and the acantharean Chaunacanthida co-dominate in the CC (Groups 10 and 12). For the TZ, the Zeu samples cluster in Groups 5 and 8, whereas samples from 150 m cluster in Group 11, where sequences assigned to Cephaloidophoroidea are dominant. Inshore, the protists on sinking particles have high relative abundances of sequences assigned to the diatom *Thalassiosira* and syndiniales MALV III (Group 8).

Contributions of water-column microbes to sinking particles

To assess the importance of water-column microbes to sinking particles, we specifically looked at the contributions of only those taxa that were dominant in the water column (>5%

relative abundance in any mixed-layer sample). Among heterotrophic bacteria, pairwise comparisons reveal that only *Fluviicola* at the IN site show significant relative enrichment in the sediment traps (Appendix Table S4.7, Figure 5a). Contributions of most heterotrophic bacteria are significantly higher in the water column than on trap particles, although contributions of *Roseobacter* at the TZ and IN sites, the SAR11 surface clade in the TZ, and the Gammaproteobacteria clade OM60(NOR5) at the IN site are similar in the water column and on trap particles. Among phototrophic bacteria, the relative contributions of *Prochlorococcus,* a water-column dominant at the offshore sampling locations (OO and CC), are significantly higher in the water column (Appendix Table S4.7, Figure 5a). In contrast, relative abundances of *Synechococcus* are significantly higher on sinking particles at the offshore OO and CC sites, similar in the water column and trap particles in the TZ, and significantly higher in the water column at the IN site.

Among protistan taxa, a dominant but uncultured dinoflagellate is significantly higher on trap particles relative to mixed-layer abundances at the OO and TZ sites, but significantly lower in the CC (Appendix Table S4.8, Figure 5b). For *Karlodinium*, an important component of the mixed-layer communities at all sampling locations, relative contributions are significantly higher on trap particles in the TZ, lower in the CC, and similar at the IN site. Similarly, syndiniales MALV-I clade 1 is significantly enriched in trap particles at the offshore sites (OO and CC) but significantly lower at the IN site. The relative abundances of chlorophytes *Ostreococcus* and *Micromonas* are significantly higher in the mixed layer. For co-dominant diatoms at the IN site, the relative abundances of *Thalassiosira* are significantly higher on trap particles, whereas abundances of an unclassified Bacillariophyceae are significantly lower.

The analysis of plastid sequences allows comparison of the relative contributions of cyanobacteria and eukaryotic phytoplankton to sinking particles, whereas they cannot be directly compared from the separate 16S and 18S analyses. *Prochlorococcus* and *Synechococcus* dominate phytoplankton communities at the offshore OO and CC sites; however, only *Synechococcus* in the CC are relatively enriched on sinking particles compared to the mixed layer (Appendix Table S4.9, Appendix Figure S4.7). Among eukaryotic phytoplankton, Mamiellophyceae and prymnesiophytes are significantly enriched on sinking particles at the OO site. In the TZ, Mamiellophyceae show similar relative abundances in the water column and trap particles, and *Synechococcus* are significantly higher in the water column. Among water-column dominants at the IN site, only bacillariophytes have higher relative abundances in the trap samples. In contrast, *Synechococcus* relative abundances are significantly higher in the mixed layer, while Mamiellophyceae and prymnesiophytes are similar in the mixed layer and trap particles (Appendix Table S4.9, Appendix Figure S4.7).

Synechococcus strain analysis

Fourteen *Synechococcus* strains were found from sequencing the ITS region and clustering at the 97% identity level. The number of strains increased from inshore to offshore with all strains occurring at the OO site (Figure 6). Most sequences in the water column, sinking particles, and at all sampling locations were assigned to clades I and IV. Clade I relative abundances were significantly higher on sinking particles than in the water column, whereas clade IV relative abundances were significantly higher in the water column (Appendix Table S4.10, Figure 6). This pattern was consistent at all sampling locations even when abundances of the two clades were similar in the mixed layer and Zeu (OO and IN sites) or when the relative abundances of clade IV were higher in the mixed layer (CC and TZ) and Zeu (CC).

Discussion

Environmental conditions

The prolonged anomalous warm-water conditions that prevailed in the North Pacific from late 2013 to 2016 likely influenced the microbes contributing to sinking particles during our study. In the northern region of the California Current System (CCS), considerable changes in the plankton communities (protists and zooplankton) were documented by Peterson *et al.* (2017), who found an increase in taxa with tropical-subtropical affinities, increased species richness of dinoflagellates, and reduced plankton biomass. During our study in the southern region of the CCS, the presence of plankton with subtropical affinities was also evident (e.g., *Doliolum denticulatum*). However, the inshore-offshore distributions of the major groups of microbes in the water column were generally consistent with their normal ranges in the region. For example, the higher relative abundances of *Prochlorococcus* at the offshore sites (OO and CC) and of *Synechococcus* at the CC and TZ sites are consistent with their inshore-offshore biomass distributions documented by Taylor *et al.* (2015). Likewise, among protists primarily present in the mixed layer (Figure 5b), the dominance of dinoflagellates offshore and the importantance of both diatoms and dinoflagellates inshore (assuming that syndiniales were mostly within their hosts) agree with the inshore-offshore contributions of these groups to the protistan abundance and biomass in the CCS (Venrick, 2002; Taylor *et al.,* 2015). In addition, the high dominance of rhizarians deep in the water column is consistent with their increased importance to plankton biomass with depth (Biard *et al.*, 2016). Therefore, although surface waters in the southern CCS were warmer than normal (McClatchie *et al.,* 2016), our results suggest that the effects on water-column distributions of the major groups of microbes were not significant (see Freibott *et al.,*

2017). In addition, particulate organic carbon fluxes during this study at the OO, CC, and TZ sites were within the ranges previously documented in the CCS, whereas at the IN site, fluxes were actually higher (Stukel *et al.,* 2013b). Although the effects of the 2015-2016 El Niño on the specific microbes exported are uncertain due to the lack of a basis of comparison, they are likely representative of the range of conditions found in the region because our sampling was done when El Niño was in decline.

General patterns in microbial export and methodological considerations

Metabarcoding analyses of water-column and sediment trap samples collected across an environmental gradient in the CCS allow an unprecedented characterization of the contributions of microbial taxa to sinking particles. Our analyses indicate that most microbes associated with sinking particles can be grouped into three broad categories: 1) Particle-associated microbes that colonize sinking particles and derive their nutrition from the sinking organic matter (e.g. Gammaproteobacteria and Flavobacteriaceae, DeLong *et al.,* 1993; Fontanez *et al.,* 2015). 2) Organisms that live in the subsurface ocean and hence have a shorter distance to sink before they are collected in sediment traps, such as rhizarian taxa with siliceous or calcium carbonate skeletons that are abundant beneath the euphotic zone and likely feed on sinking particles (Biard *et al.,* 2016). This category may also include the reproductive stages of certain rhizarians such as acantharians that produce fast-sinking cysts (Bernstein *et al.,* 1987; Decelle *et al.,* 2013). 3) Organisms that are resistant to digestion and/or degradation of their genetic material. This category includes *Synechococcus* and *Thalassiosira*, which have both been shown to survive passage through zooplankton guts (Johnson *et al.,* 1982; Fowler and Fisher, 1983; Pfannkuche and Lochte, 1993). It may also include endosymbionts, gut microbes, and parasites (e.g.

syndiniales and apicomplexans) that have been found in our sediment traps and others (Amacher *et al.,* 2013; Guidi *et al.,* 2016).

Taken together, these results highlight some important concepts that must be considered when interpreting sequence analyses of sediment trap material in terms of the contributions of taxa from surface communities to export. First, degradation of nucleic acids can be rapid in a nitrogen- and phosphorus-limited ocean, while some organisms possess specific adaptations that lead to their preferential preservation. In addition, interpretation of community composition is affected by methodological limitations associated with DNA extraction and amplification biases, presence of extracellular DNA, and copy number of rDNA, which tend to overrepresent certain groups including dinoflagellates, ciliates, and rhizarians (all with high relative abundances in our samples). Hence, the export contributions of many organisms are difficult to determine from sediment trap DNA samples alone. Despite these difficulties, molecular approaches are powerful for analyzing microbial consortia associated with sinking particles and have highlighted the heterogeneity of sinking carbon in the ocean. While there are certainly some rapidly sinking particles (e.g., salp fecal pellets) that may escape remineralization, most sinking particles are likely continually re-worked as they sink through the water column. Thus, the nature of sinking particles changes with depth as particles are consumed and new compounds synthesized.

Microbes associated with sinking particles in the CCS

Our results agree with previous studies that have used metabarcoding analyses in oligotrophic and mesotrophic systems that show significant differences in the community structure of water-column and trap-collected microbes (Amacher *et al*., 2009, 2013; LeCleir *et al.,* 2014; Fontanez *et al.,* 2015). However, our results also indicate that environmental gradients can impact water-column and sinking-particle communities. Among heterotrophic bacteria,

sequences in the mixed layer were mainly represented by members of Flavobacteria (NS4 and NS5 clades, *Fluviicola*) and Alphaproteobacteria (SAR11, *Roseobacter*), some of which are important free-living (e.g., SAR11) or particle associated microbes (e.g., *Fluviicola, Roseobacter*) in pelagic ecosystems (DeLong *et al.,* 1993). SAR11 relative abundances tended to be higher offshore (OO and CC) and were rarely major components of sinking particles. Allen *et al.* (2012) also documented that SAR11 sequences were rarely found in the largest size-fractions analyzed (3.0–200 μm). Likewise, the higher relative abundances of *Roseobacter* in nutrient-rich waters is consistent with the results documented by Allen *et al.* (2012) in the CCS. Although *Roseobacter* are recognized as important colonizers of sinking particles (LeCleir *et al.,* 2014), during our study their relative abundances at the mesotrophic inshore sites (TZ and IN) were similar in the water column and sinking particles. Also at the IN site, *Fluviicola* was the only heterotrophic bacterium that was significantly enriched on sinking particles, likely because these are primarily particle-associated bacteria (Suzuki *et al*., 2017) that could have grown as the particles sank. Deeper in the water column, the increase in importance of Archaea with depth at all sites is consistent with their vertical distribution (Karner *et al.,* 2001), and with their general absence on sinking particles collected from sediment traps (Fontanez *et al.,* 2015). In contrast, sequences of heterotrophic bacteria associated with sinking particles were dominated by *Pseudoalteromonas* and *Vibrio* (Gammaproteobacteria). These bacteria are associated with sinking particles or eukaryote surfaces and have the enzymatic capabilities for degrading high molecular weight compounds (DeLong *et al.,* 1993; Fontanez *et al.,* 2015). In addition, *Pseudoalteromonas* are known to produce anti-bacterial compounds (Holmström and Kjelleberg, 1999), which may allow them to dominate on particles by inhibiting the growth of other bacteria.

The significantly higher relative abundances of *Prochlorococcus* in the mixed layer and *Synechococcus* on sinking particles at our offshore sites is consistent with results from oligotrophic systems (Amacher *et al*., 2013; Thiele *et al*., 2015). *Synechococcus* is the prokaryote most strongly associated with carbon export in open-ocean ecosystems (Amacher *et al.,* 2013; Thiele *et al.,* 2015; Guidi *et al.,* 2016). The contrasting contributions of *Prochlorococcus* and *Synechococcus* to sinking particles likely reflects differential resistance to digestion (Johnson *et al*., 1982; Guillou *et al*., 2001; Pfannkuche and Lochte, 1993; Stukel *et al*., 2013a). Microscopical analyses have shown abundant intact *Synechococcus* cells in mesozooplankton guts (Johnson *et al.,* 1982; Wilson and Steinberg, 2010; Stukel *et al*., 2013a) and fecal pellets (Silver and Bruland, 1981; Pfannkuche and Lochte, 1993), which can arise from feeding on aggregates or indirectly on microzooplankton that have consumed *Synechococcus*. Since amorphous aggregates are the main category of sediment trap material in offshore CCS waters (Stukel *et al*., 2013b), *Synechococcus* sinking may also occur as undigested cells in microzooplankton minipellets embedded in aggregates (e.g., Gowing and Silver, 1985). While aggregate formation by *Synechococcus* itself has been advanced to explain their higher relative abundances in exported material (Deng *et al*., 2016), the presence of *Synechococcus* in aggregates and fecal pellets in bathypelagic waters (Agusti *et al*., 2015) and deep-sea sediments (Pfannkuche and Lochte, 1993) suggests instead that trophic interactions are more important for *Synechococcus* export rather than their direct sinking.

Our results also indicate that *Synechococcus* export depends on the trophic state of the system. Their similar relative abundances in the water column and sinking particles at the TZ site may have been influenced by the large bloom of *Doliolum denticulatum*, which was particularly dense in the TZ. This small doliolid (~10 mm) is a filter-feeder that can efficiently

graze on small particles including picoplankton (Katechakis *et al*., 2004); thus, ingested *Synechococcus* cells would likely have remained intact in the doliolid fecal pellets. In contrast, at the IN site, *Synechococcus* relative abundances were significantly higher in the water column than in sinking particles, despite similar water-column abundances at the IN and OO sites, suggesting a less efficient transfer mechanism. In the CCS, the large copepod *Calanus pacificus* dominated the mesozooplankton community at the IN site, and its high selectivity for larger >10-μm protistan prey could have greatly reduced the uptake of *Synechococcus* cells or even their small flagellate consumers into fast sinking fecal pellets. Although this result seems to contradict recent sequence analyses suggesting that *Synechococcus* contributions in mesozooplankton guts including copepods can be considerable (Motwani and Gorokhova, 2013; Shoemaker and Moisander, 2017), the copepod species analyzed by these authors, *Acartia* and *Pleuromamma*, respectively, are less important components of the mesozooplankton communities at the IN site in the CCS. Therefore, composition of both the microbial (i.e., larger protists) and mesozooplankton communities, as well as differences in the relative abundances and feeding behaviors of the mesozooplankton can be important in modulating *Synechococcus* export across the CCS.

Despite differences in *Synechococcus* relative contributions to sinking particles across the CCS, most of its export can be attributed to clade I strains. Clades I and IV dominated in the water column at all sites, consistent with general findings for upwelling regions of the northeast (Sohm *et al.,* 2016) and southeast Pacific (Zwirglmaier *et al*., 2008). The significantly higher relative abundances of clade I in sinking particles across the CCS might reflect a greater resistance to digestion (Zwirglmaier *et al*., 2009), although it could also relate to Si content (Baines *et al.,* 2012; Brzezinski *et al.,* 2017) or aggregation properties (Deng *et al.,* 2015). In the

Sargasso Sea, *Synechococcus* clades II and III dominate the water column, and clade III contributions to export tend to be higher (De Martini *et al.,* 2016). Thus, these results highlight that strain-level differences may be important in explaining variability in the contributions of microbes to export under different environmental conditions.

Despite the high abundances of sequences of *Synechococcus* on sinking particles at oligotrophic sites in the CCS, its contributions relative to larger eukaryotic phytoplankton is the more critical issue for understanding how community structure affects efficiency of the biological carbon pump. In the central North Atlantic, Amacher *et al.* (2013) concluded that *Synechococcus* were overrepresented on sinking particles compared to *Prochlorococcus* and eukaryotic phytoplankton, including diatoms. Based on plastid data, which allow prokaryotic to eukaryotic phytoplankton to be compared more directly in the present study, *Synechococcus* contributions to sinking particles were significantly higher only at the CC site. In contrast, contributions of bacillariophytes were higher in trap particles at most CCS sites despite lower relative abundances of diatoms in the water column.

The protists on sinking particles were characterized by high relative abundances of alveolates (mostly dinoflagellates) and rhizarians at the OO site, consistent with their recognized importance on sinking particles (Amacher *et al*., 2009, 2013; Fontanez *et al.,* 2015) and carbon export in oligotrophic systems (Lampitt *et al*., 2009; Guidi *et al.,* 2016). Likewise, these groups are major components of protistan biomass in oligotrophic waters of the CCS (Taylor *et al.,* 2015; Biard *et al.,* 2016). The higher similarity between water-column and sinking-particle communities at the OO site, with high relative abundances of dinoflagellates and ciliates, suggest that processing of sinking particles by these taxa play a more important role in particle export in offshore waters compared to the more productive coastal sites.

In contrast to oligotrophic waters, the protists on sinking particles in the CC and TZ were dominated by the apicomplexan Cephaloidophoroidea and/or the acantharian Chaunacanthida. Acantharians are known for reproductive strategies that involve forming cysts, which sink rapidly due to their dense mineral composition (strontium sulfate) (Bernstein *et al*., 1987; Martin *et al*., 2010; Decelle *et al*., 2013). Because Chaunacanthida were important in the deeper water column at 150 m except at the CC, the high relative abundances of Chaunacanthida sequences in traps at this site could also reflect cyst sinking. We observed round structures similar to acantharian cysts in trap samples in the CC (Appendix Figure S4.8); however, these were considerably smaller (22–28 μm) than cysts collected in traps in the North Pacific (80–165 μm, Bernstein *et al*., 1987) and North Atlantic (200–1000 μm, Martin *et al*., 2010; Decelle *et al*., 2013).

Cephaloidophoroidea is a poorly known group of gregarine apicomplexans that parasitize the intestine of crustaceans, including copepods (Rueckert *et al*., 2011). The high relative abundances of apicomplexans in CC and TZ trap-collected particles coincide with the bloom of *D. denticulatum*. Due to the preferred particle sizes filtered by these doliolids (2.5–15 μm, Katechakis *et al*., 2004), it is unlikely that the parasites were acquired by feeding directly on copepods. Considering that other gregarine apicomplexans have been identified in guts of salps (Clopton 2002; Wallis *et al*., 2017), Cephaloidophoroidea possibly also parasitize doliolids. Because doliolids are passive filter-feeders, the proportions of appropriately sized microbes in their diet should be similar to those in the water column (Alldredge and Madin, 1982). Nonetheless, at the sites where doliolids were most abundant, microbial communities in the water column and on sinking particles showed the highest dissimilarities, suggesting substantial post-consumption transformations before particles were exported. The most notable contrast in

the TZ was the virtual absence of *Ostreococcus*, a dominant mixed-layer picophytoplankton, on the sinking particles. *Ostreococcus* and *Micromonas* are both important components of the water-column communities in nutrient-rich regions of the CCS (Allen *et al*., 2012). It is possible, however, that the very tiny cells of *Ostreococcus* (~1 μm) were not efficiently grazed by *D. denticulatum* (but see Katechakis *et al*., 2004). In contrast to *Ostreococcus,* the relative abundances of two dinoflagellates (an uncultured and *Karlodinium*) with lower contributions to the water-column assemblages were significantly higher on sinking particles. These dinoflagellates were likely grazed and transported in the doliolid fecal pellets.

Particle-associated microbes at the richer upwelling IN site had high relative abundances of dinoflagellates (syndiniales MALV I, MALV III, and *Karlodinium*) and diatoms (an unclassified Bacillariophyceae and *Thalassiosira*). The importance of MALV on sinking particles suggests that these parasites might have been transported within their eukaryotic hosts (Guillou *et al*., 2008). Although the mechanisms are not well understood, syndiniales, among parasites generally, appear to play important roles in modulating export flux (e.g., Amacher *et al.,* 2013; Guidi *et al.,* 2016). The mixotroph *Karlodinium* was in general a main component of the mixed-layer communities at all sites, but its contributions to sinking particles varied. *Karlodinium* are associated with harmful algal blooms, that while grazed by micro- (Johnson *et al*., 2003) and mesozooplankton (Berge *et al*., 2012), can affect the feeding rates and survival of consumers when present above certain density thresholds (Vaqué *et al*., 2006). In contrast to the large contributions of dinoflagellates at most sites, protist contributions to sinking particles compared to the water column at the mesotrophic IN site were characterized by significantly higher relative abundances of *Thalassiosira* spp. Microscopical analysis indicated that *Thalassiosira* cells are numerically important in mesotrophic CCS waters (Du *et al*., 2015), and

that diatoms in general often dominate biomass in the coastal upwelling region (Taylor *et al.,* 2015). Although three diatom taxa were important in the water-column community at the IN site (group 6 in Figure 4), only *Thalassiosira* was strongly represented in the sediment trap material. *Thalassiosira* is among the taxa found to remain viable and culturable for up to 10 days in sediment trap material and fecal pellets of copepods and euphausiids (Fowler and Fisher, 1983). Therefore, their sinking could have been due to grazing and transport in zooplankton fecal pellets, although post-bloom aggregate formation could have also played an important role (Alldredge and Gotschalk,1989; Stukel *et al*., 2013b). These differences indicate that taxon-specific characteristics, such as size, palatability, digestability, and/or rapid sinking as aggregates likely determine which diatoms remain recognizable by molecular methods in exported material. Overall, the stronger similarity between euphotic zone and trap particle communities at mesotrophic IN site suggests more efficient export of "fresh" carbon from the ocean's surface than at the other study sites, consistent with higher export expected for diatom-rich waters.

Conclusions

Metabarcoding analyses of water-column and sediment trap samples from the CCS confirm some general findings from other systems, such as the strong associations of Gammaproteobacteria, rhizarians, and dinoflagellates with particle export. Additionally, they provide new perspectives on variability within taxa and across gradients of ecosystem trophic state. For the former, we document differential sequence retention of *Thalassiosira* relative to co-occurring diatoms in sinking particles, and we show a consistent difference among *Synechococcus* clades in exported particles. There are substantial differences in microbial contributions to export from the water column between inshore mesotrophic and offshore

oligotrophic waters in the CCS that seem to align with differences in dominant grazing pathways (large copepods, doliolids, protistan microzooplankton) and export delivery mechanisms (fecal pellets versus amorphous aggregates). However, those associations are inferential and nonquantitative in the present study. One hypothesis that arises from these combined results is that relative recovery of sequences in exported particles is more a reflection of digestion resistance through variable trophic pathways than direct sinking of different taxa. Some groups, such as *Prochlorococcus*, *Ostreococcus*, and most diatoms, while abundant in the water column, might have rapidly lost their DNA signatures during digestive processing. Others, such as *Synechococcus* clade I, gut flora bacteria, and parasites seem to have properties that resist digestion, greatly amplifying their relative sequence abundances in sinking particles. As a consequence, understanding the implications of pelagic community structure on biological pump efficiency cannot be done by comparative sequence analysis alone. It will require food-web studies that account for the differences in taxon-specific carbon biomass and sequence relative abundances in comparing contributions to upper ocean productivity and the particulate matter leaving the euphotic zone.

Acknowledgements

We thank the captain and crew of the R/V Sikuliaq for their help at sea. We also thank Mark Ohman for his leadership as Chief Scientist, Ralf Goericke, Megan Roadman, Tom Kelly, and all the scientists that participated on the CCE-LTER P1604 cruise, whose support made this study possible. We specially acknowledge Ali Freibott and Maitreyi Nagarkar for their help during sample collection, processing, and bioinformatic analyses. We thank Hong Zheng for her help with processing the molecular samples. This study was funded by the National Science

Foundation grant OCE-1614359 to the CCE-LTER site. Analyses of molecular samples was partly funded by the Graduate Student Excellence Research Award of the Scripps Institution of Oceanography to B. Valencia. The Ph.D. research of B.Valencia was supported by a scholarship (529-2011) from the Colombian Administrative Department of Science, Technology and Innovation (COLCIENCIAS).

Chapter 4, in full, is currently being prepared for submission for publication of the material with the following co-authors: Valencia B, Stukel MR, Allen A, McCrow JP, Rabines A, Palenik B, Landry MR. The dissertation author was the primary investigator and author of this paper.

Table 4.1. Summary of environmental data during sediment trap drift deployments across a gradient of ecosystem conditions in the California Current System. PP = primary production (mg C m^{-2} d^{-1}), POC flux = export of particulate organic carbon (mg C m^{-2} d^{-1}), Temp = temperature (°C), Chl*a* = chlorophyll a (µg l^{-1}), NO_3 = nitrate (µg l^{-1}). Number of chlorophyll-nitrate measurements per depth and CTD casts were as follow: OO (n = 3, 4), CC (n = 7, 10), TZ (n = 6, 11), and IN (n = 7, 11).

Oligotrophic Offshore (OO)					
PP	Depth (m)	POC flux	Temp	Chl*a*	NO_3
229.0	0-50	-	15.11 ± 0.10	0.11 ± 0.02	0.02 ± 0.01
	100	72.1 ± 7.3	12.22 ± 0.05	0.16 ± 0.05	11.16 ± 1.68
	150	31.8 ± 4.9	9.51 ± 0.01		
California Current (CC)					
PP	Depth (m)	POC flux	Temp	Chl*a*	NO_3
275.7 ± 41.1	0-80	-	14.20 ± 0.11	0.19 ± 0.02	0.08 ± 0.04
	97	40.2 ± 3.8	13.18 ± 0.08	0.34 ± 0.06	4.94 ± 1.67
	147	37.0 ± 5.0	9.54 ± 0.03	-	-
Transition Zone (TZ)					
PP	Depth (m)	POC flux	Temp	Chl*a*	NO_3
868.0 ± 133.8	0-30	-	12.40 ± 0.18	1.10 ± 0.03	4.57 ± 0.25
	57	120.4 ± 9.7	11.24 ± 0.06	0.25 ± 0.06	13.21 ± 0.71
	147	77.4 ± 4.4	8.78 ± 0.01	-	-
Inshore (IN)					
PP	Depth (m)	POC flux	Temp	Chl*a*	NO_3
1658.7 ± 195.6	0-12	-	14.25 ± 0.06	4.06 ± 0.17	2.14 ± 0.49
	47	251.0 ± 8.3	10.39 ± 0.04	0.42 ± 0.06	24.27 ± 2.07
	147	202.3 ± 14.0	8.82 ± 0.04	-	-

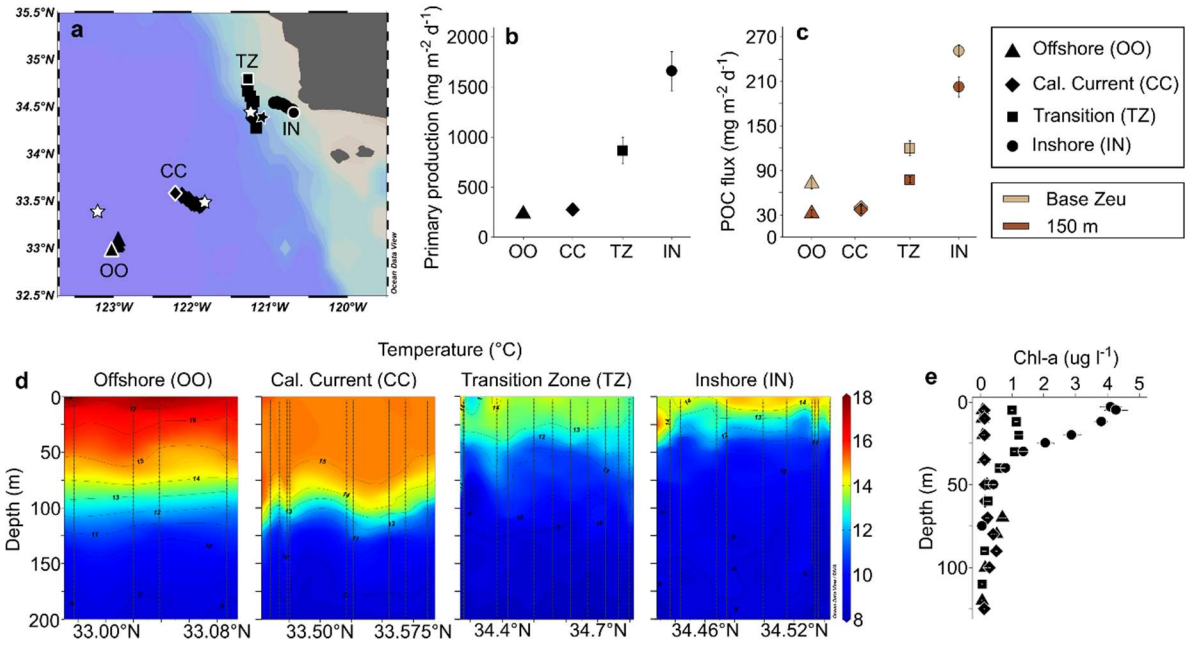

Figure 4.1. Map showing the sampling locations spanning an inshore-offshore gradient in environmental conditions across the California Current System. OO: Oligotrophic Offshore, CC: California Current, TZ: Transition Zone, IN: Inshore. **(a)** Paths of the free-drifting sediment trap arrays. At each site, sampling began with the deployment of the arrays and a CTD cast (symbols with white edge) and ended with the recovery of the sediment traps (white stars). Daily CTD casts, represented in the map by each symbol, were performed to characterize the water column as the arrays were followed. **(b)** Integrated primary production. **(c)** Particulate organic carbon (POC) flux measured in the sediment traps at the base of the euphotic zone (Zeu: light brown) and 150 m (dark brown). **(d)** Vertical sections of temperature. Dotted lines represent each CTD cast. **(e)** Mean vertical profiles of chlorophyll (Chl*a*). Symbols and deviations represent the mean ± standard error.

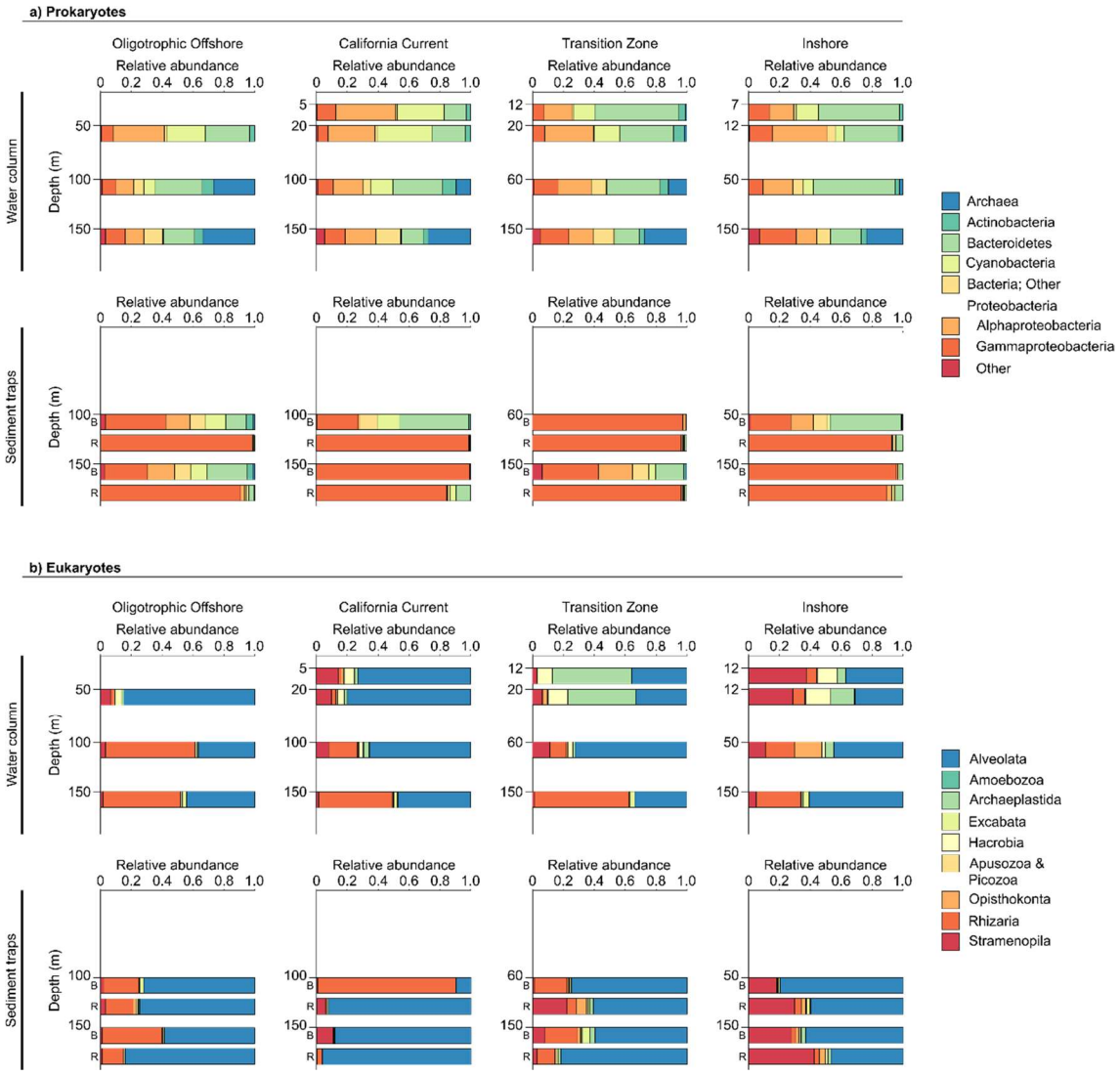

Figure 4.2. Major groups of microbes in the water column and sinking particles across an environmental gradient in the California Current System. **(a)** Prokaryotic phyla from 16S rRNA. **(b)** Eukaryotic supergroups from 18S V9 rRNA. Sinking particles were collected at two depths (base of the euphotic zone and 150 m) and trap tubes were filled with either a brine (B) or a RNA later solution (R).

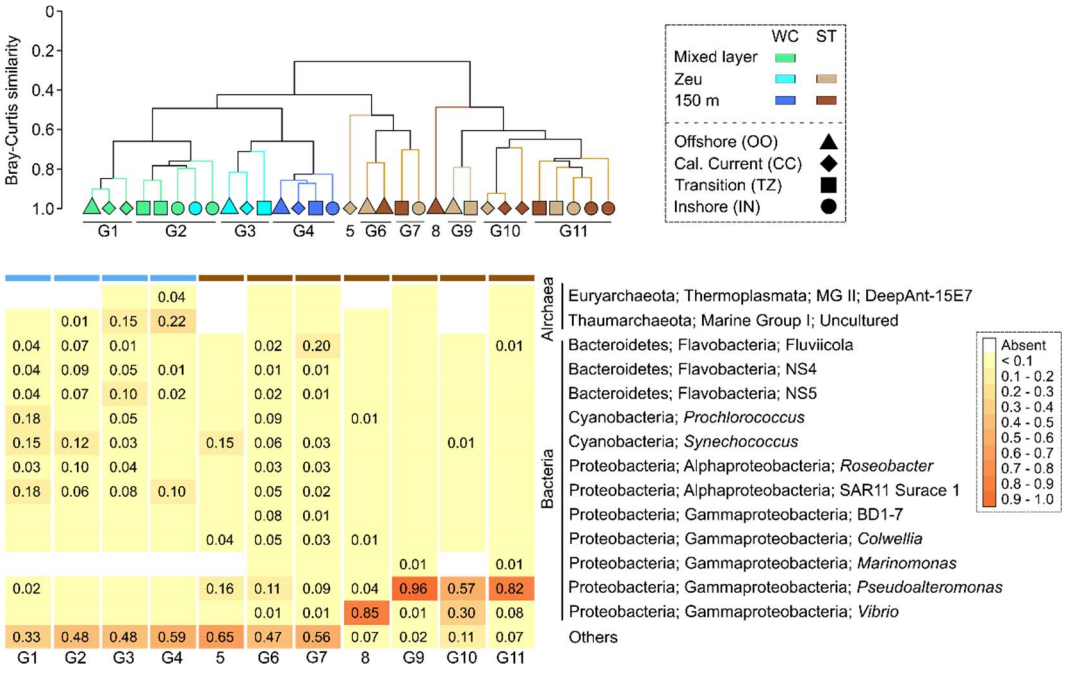

Figure 4.3. Structure of the prokaryotic communities in the water column and sinking particles across an environmental gradient in the California Current System. Communities were grouped in twenty significant clusters (SIMPROF, $p < 0.05$, black lines in cluster). Heatmaps are based on SIMPER analysis; only relative abundances >1% are shown. Colors indicate sample type (WC: water column, ST: sediment trap) and symbol shapes the sampling locations. The nMDS plot is presented in Figure S6a.

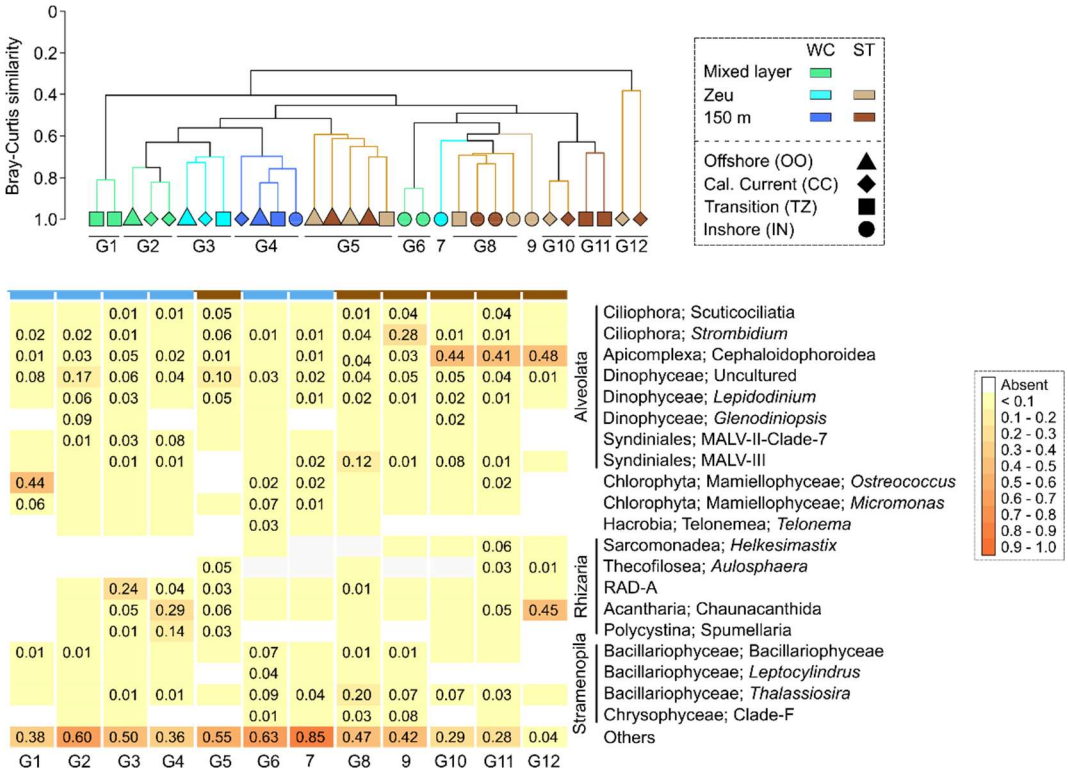

Figure 4.4. Structure of the protist communities in the water column and sinking particles across an environmental gradient in the California Current System. Communities were grouped in thirteen significant clusters (SIMPROF, $p < 0.05$, black lines in cluster). Heatmaps are based on SIMPER analysis; only relative abundances >1% are shown. Colors indicate sample type (WC: water column, ST: sediment trap) and symbol shapes the sampling locations. The nMDS plot is presented in Figure S6b.

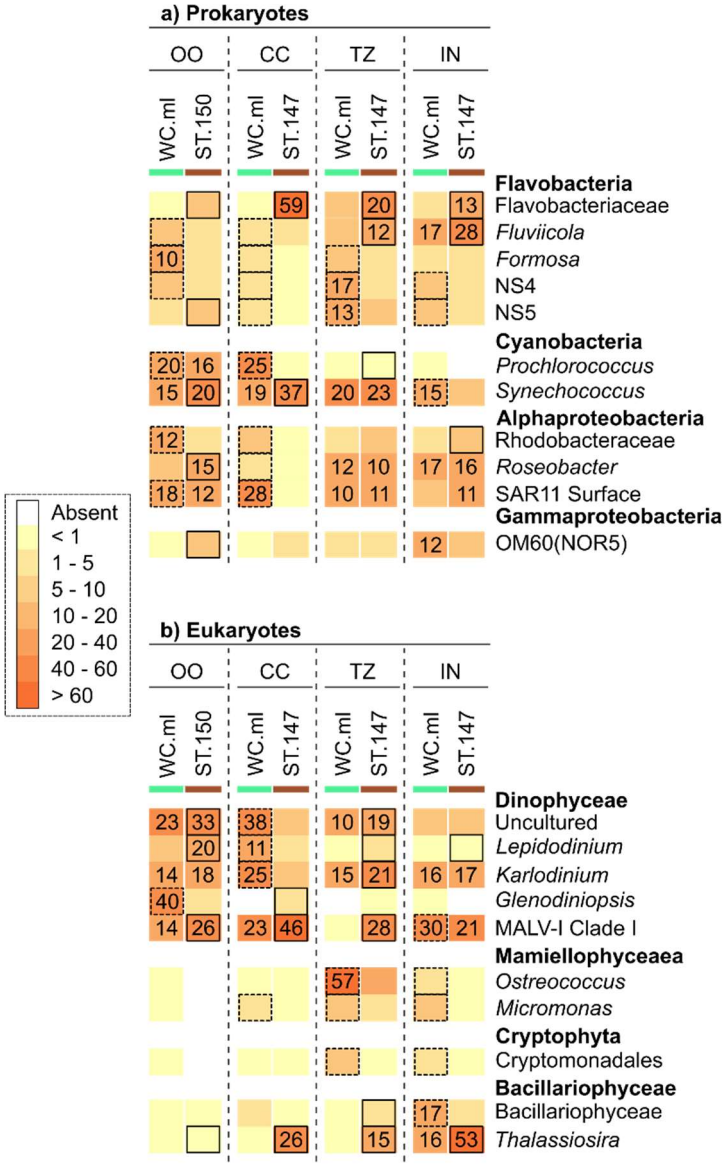

Figure 4.5. Contributions of microbes primarily present in the mixed layer to sinking particulate matter across the California Current System. Contributions were evaluated by pairwise comparisons using the Fisher exact test at the genus level for **(a)** prokaryotes and **(b)** eukaryotes. Percentages are indicated for contributions >10%. Squares indicate that relative abundances were significantly higher (FDR < 0.05, Tables S6 and S7) in sediment traps (ST, solid squares) or in the water-column mixed layer (WC.ml, dotted squares). OO: Oligotrophic Offshore, CC: California Current, TZ: Transition Zone, IN: Inshore.

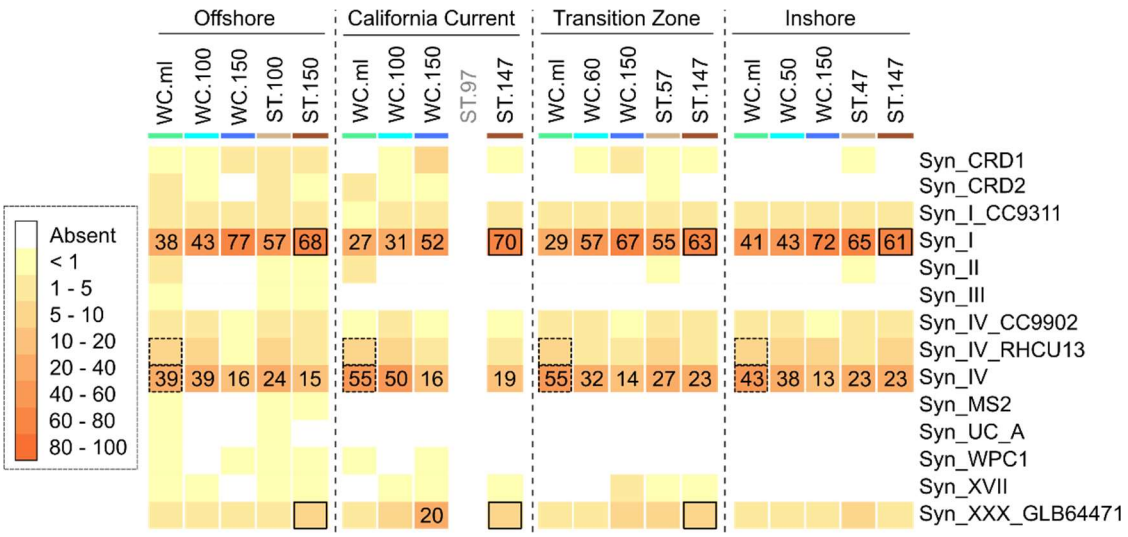

Figure 4.6. Percentages of *Synechococcus* strains in the water column and on sinking particles in the California Current System based on analysis of the ITS region. Contributions were evaluated by pairwise comparisons using the Fisher exact test. Percentages are indicated for contributions >10%. Squares indicate that relative abundances were significantly higher (FDR < 0.05, see Table S10 for results of all strains) in sediment traps (ST, solid squares) or in the water-column mixed layer (WC.ml, dotted squares). Sequence data were not available for the trap tube filled with the brine solution at the California Current (ST.97).

References

Alldredge AL, Madin LP. (1982). Pelagic Tunicates: Unique Herbivores in the Marine Plankton. BioScience **32:** 655–663.

Alldredge AL, Gotschalk CC. (1989). Direct observations of the mass flocculation of diatom blooms: characteristics, settling velocities and formation of diatom aggregates. Deep Sea Res Part I **36:** 159–171.

Allen LZ, Allen EE, Badger JH, McCrow JP, Paulsen IT, Elbourne LDH, Thiagarajan M, Rusch DB, Nealson KH, Williamson SJ, Venter JC, Allen AE. (2012). Influence of nutrients and currents on the genomic composition of microbes across an upwelling mosaic. ISME J **6:** 1403–1414.

Amacher J, Neuer S, Anderson I, Massana R. (2009). Molecular approach to determine contributions of the protist community to particle flux. Deep Sea Res Part I **56:** 2206–2215.

Amacher J, Neuer S, Lomas M. (2013). DNA-based molecular fingerprinting of eukaryotic protists and cyanobacteria contributing to sinking particle flux at the Bermuda Atlantic time-series study. Deep Sea Res Part II **93:** 71–83.

Agusti S, González-Gordillo JI, Vaqué D, Estrada M, Cerezo MI, Salazar G, Gasol JM, Duarte M. (2015). Ubiquitous healthy diatoms in the deep sea confirm deep carbon injection by the biological pump. Nat Commun **6:** DOI: 10.1038/ncomms8608.

Baines SB, Twining BS, Brzezinski MA, Krause JW, Vogt S, Assael D, McDaniel H. (2012). Significant silicon accumulation by marine picocyanobacteria. Nat Geosci **5:** 886–891.

Berge T, Poulsen LK, Moldrup M, Daugbjerg N, Hansen PJ. (2012). Marine microalgae attack and feed on metazoans. ISME J **6:** 1926–1936.

Bernstein RE, Betzer PR, Feely RA, Byrne RH, Lamb MF, Michaels AF. (1987). Acantharian fluxes and strontium to chlorinity ratios in the North Pacific Ocean. Science **237:** 1490–1495.

Biard T, Stemmann L, Picheral M, Mayo, N, Vandromme P, Hauss H, Gorsky G, Guidi L, Kiko R, Not F. (2016). In situ imaging reveals the biomass of giant protists in the global ocean. Nature **532:** 504–507.

Bond NA, Cronin MF, Freeland H, Mantua N. (2015). Causes and impacts of the 2014 warm anomaly in the NE Pacific. Geophys Res Lett **42:** 3414–3420.

Brzezinski MA, Krause JW, Baines SB, Collier JL, Ohnemus DC. (2017). Patterns and regulation of silicon accumulation in *Synechococcus* spp. J Phycol **53:** 746–761.

Buesseler KO, Lamborg CH, Boyd PW, Lam PJ, Trull TW, Bidigare RR, Bishop JKB, Casciotti KL, Dehairs F, Elskens M, Honda M, Karl DM, Siegel DA, Silver MW, Steinberg DK, Valdes J, Van Mooy B, Wilson S. (2007). Revisiting carbon flux through the ocean's twilight zone. Science **316:** 567–570.

Chavez FP, Pennington JT, Castro CG, Ryan JP, Michisaki RP, Schlining B, Walz P, Buck KR, McFadyen A, Collins CA. (2002). Biological and chemical consequences of the 1997–1998 El Niño in central California waters. Prog Oceanogr **54:** 205–232.

Checkley DM, Barth JA. (2009). Patterns and processes in the California Current System. Prog Oceanogr **83:** 49–64.

Choi DH, Hoon noh J, Lee JH. (2014). Application of pyrosequencing method for investigating the diversity of *Synechococcus* subcluster 5.1 in open ocean. Microbes Environ **29:** 17–22.

Clopton RE. (2002). Phylum Apicoplexa Levine 1970: Order Eugregarinorida Léger, 1990. In: Lee JJ, Leedale G, Patterson D, Bradbury (eds) Illustrated guide to the protozoa, 2nd edn. Society of Protozoologists, Lawrence, pp 205–288.

Decelle J, Martin P, Paborstava K, Pond DW, Tarling G, Mahé F, de Vargas C, Lampitt R, Not F. (2013). Diversity, ecology and biogeochemistry of cyst-forming Acantharia (Radiolaria) in the oceans. PLoS One **8:** e53598.

Decelle J, Romac S, Stern RF, Bendif EM, Zingone A, Audic S, Guiry MD, Guillou L, Tessier D, Le Gall F, Gourvil P, Dos Santos AL, Probert I, Vaulot D, de Vargas C, Christen R. (2015). PhytoREF: a reference database of the plastidial 16S rRNA gene of photosynthetic eukaryotes with curated taxonomy. Mol Ecol Resour **15:** 1435–45.

DeLong EF, Franks DG, Alldredge AL. (1993). Phylogenetic diversity of aggregate-attached vs. free-living marine bacterial assemblages. Limnol Oceanogr **38:** 924–934.

De Martini F, Neuer S, Hamill D, Robidart J, Lomas MW. (2016). Clade and strain specific contributions of *Synechococcus* and *Prochlorococcus* to the carbon export in the Sargasso Sea. In: Martini FD. Growth and grazing mortality of pico- and nano-phytoplankton and their role in the carbon export in the Sargasso Sea. Dissertation. Arizona State University.

Deng W, Cruz BN, Neuer S. (2016). Effects of nutrient limitation on cell growth, TEP production and aggregate formation of marine *Synechococcus*. Aquat Microb Ecol **78:** 39–49.

Deng W, Monks L, Neuer S. (2015). Effects of clay minerals on the aggregation and subsequent settling of marine Synechococcus. Limnol Oceanogr **60:** 805–816.

De Vargas C, Audic S, Henry N, Decelle J, Mahé F, Logares R, Lara E, Berney C, Bescot NL, Probert I, Carmichael M, Poulain J, Romac S, Colin S, Aury JM, Bittner L, Chaffron S, Dunthorn M, Engelen S, Flegontova O, Guidi L, Horak A, Jaillon O, Lima-Mendez G, Lukes J, Malviya S, Morard R, Mulot M, Scalco E, Siano R, Vincent F, Zingone A, Dimier C,

Picheral M, Searson S, Kandels-Lewis S, Tara Oceans Coordinators, Acinas SG, Bork P, Bowler C, Gorsky G, Grimsley N, Hingamp P, Iudicone S, Not F, Ogata H, Pesant S, Raes J, Sieracki ME, Speich S, Stemmann L, Sunagawa S, Weissenbach J, Wincker P, Karsenti E. (2015). Eukaryotic plankton diversity in the sunlit ocean. Science **348:** 1261605, DOI: 10.1126/science.1261605.

Du X, Peterson W, O'Higgins L. (2015). Interannual variations in phytoplankton community structure in the northern California Current during the upwelling seasons of 2001-2010. Mar Ecol Prog Ser **519:** 75–87.

Ducklow HW, Steinberg DK, Buesseler KO. (2001). Upper ocean carbon export and the biological pump. Oceanography **14:** 50–58.

Edgar RC. (2010). Search and clustering orders of magnitude faster than BLAST. Bioinformatics **26:** 2460–2461.

Fontanez KM, Eppley JM, Samo TJ, Karl DM, DeLong EF. (2015). Microbial community structure and function on sinking particles in the North Pacific Subtropical Gyre. Front Microbiol **6:** 469. doi: 10.3389/fmicb.2015.00469.

Fowler SW, Fisher NS. (1983). Viability of marine phytoplankton in zooplankton fecal pellets. Deep Sea Res Part I **30:** 263–269.

Freibott A, Rabines A, McCrow JP, Allen AE, Landry MR. (2017). Impacts of the 2014 Blob on microbial community dynamics in the southern California Current. In: Freibott AL. Plankton community composition and grazing dynamics in upwelling regions of the Pacific Ocean. Dissertation. University of California, San Diego.

Gowing MM, Silver MW. (1985). Minipellets: a new and abundant size class of marine fecal pellets. J Mar Res **43:** 395–418.

Guidi L, Chaffron S, Bittner L, Eveillard D, Larhlimi A, Roux S, Darzi Y, Audic S, Berline L, Brum JR, Coelho LP, Espinoza JCI, Malviya S, Sunagawa S, Dimier C, Kandels-Lewis S, Picheral M, Poulain J, Searson S, Tara Oceans Consortium Coordinators, Stemmann L, Not F, Hingamp P, Speich S, Follows M, Karp-Boss L, Boss E, Ogata H, Pesant S, Weissenbach J, Wincker P, Acinas SG, Bork P, de Vargas C, Iudicone D, Sullivan MB, Raes J, Karsenti E, Bowler C, Gorsky G. (2016). Plankton networks driving carbon export in the oligotrophic ocean. Nature **532:** 465–470.

Guillou L, Jacquet S, Chrétiennot-Dinet MJ, Vaulot D. (2001). Grazing impact of two small heterotrophic flagellates on *Prochlorococcus* and *Synechococcus*. Aquat Microb Ecol **26:** 201–207.

Guillou L, Viprey M, Chambouvet A, Welsh RM, Kirkham AR, Massana R, Scanlan DJ, Worden AZ. (2008). Widespread occurrence and genetic diversity of marine parasitoids belonging to Syndiniales (Alveolata). Environ Microbiol **10:** 3349–3365.

Holmström C, Kjelleberg S. (1999). Marine Pseudoalteromonas species are associated with higher organisms and produce biologically active extracellular agents. FEMS Microbiol Ecol **30:** 285–293.

Johnson PW, Huai-Shu X, Sieburth JM. (1982). The utilization of chroococcoid cyanobacteria by marine protozooplankters but not by calanoid copepods. Ann Inst Oceanogr Paris Nouv Ser **58:** 297–308.

Johnson MD, Rome M, Stoecker DK. (2003). Microzooplankton grazing on *Prorocentrum minimum* and *Karlodinium micrum* in Chesapeake Bay. Limnol Oceanogr **48:** 238–248.

Katechakis A, Stibor H, Sommer U, Hansen T. (2004). Feeding selectivities and food niche separation of *Acartia clausi*, *Penilia avirostris* (Crustacea) and *Doliolum denticulatum* (Thaliacea) in Blanes Bay (Catalan Sea, NW Mediterranean). J Plankton Res **26:** 589–603.

Karner MB, DeLong EF, Karl DM. (2001). Archaeal dominance in the mesopelagic zone of the Pacific Ocean. Nature **409:** 507–510.

Knauer GA, Martin JH, Bruland KW. (1979). Fluxes of particulate carbon, nitrogen, and phosphorus in the upper water column of the northeast Pacific. Deep Sea Res Part I **26:** 97–108.

Lampitt RS, Salter I, Johns D. (2009). Radiolaria: major exporters of organic carbon to the deep ocean. Global Biogeochem Cycles **23:** GB1010, doi:10.1029/2008GB003221.

Lavaniegos BE, Ohman MD. (2007). Coherence of long-term variations of zooplankton in two sectors of the California Current System. Prog Oceanogr **75:** 42–69.

LeCleir GR, DeBruyn JM, Maas EW, Boyd PW, Wilhelm SW. (2014). Temporal changes in particle-associated microbial communities after interception by nonlethal sediment traps. FEMS Microbiol Ecol **87:** 153–163.

Longhurst AR, Harrison WG. (1989). The biological pump: profiles of plankton production and consumption in the upper ocean. Prog Oceanogr **22:** 47–123.

Mahé F, Rognes T, Quince C, de Vargas C, Dunthorn M. (2014). Swarm: robust and fast clustering method for amplicon-based studies. PeerJ **2:** e593.

Martin P, Allen JT, Cooper MJ, Johns DG, Lampitt RS, Sanders R, Teagle DA. (2010). Sedimentation of acantharian cysts in the Iceland Basin: Strontium as a ballast for deep ocean particle flux, and implications for acantharian reproductive strategies. Limnol Oceanogr **55:** 604–614.

McClathchie S, Goericke R, Leising A, Auth T, Bjorkstedt E, Robertson RR, Brodeur RD, Du X, Daly HA, Morgan CA, Chavez FP, Debich AJ, Hildebrand J, Field J, Sakuma K, Jacox MG, Kahru M, Kudela R, Anderson C, Lavaniegos BE, Gomez-Valdes J, Jiménez-Rosenberg SPA, McCabe R, Melin SR, Ohman MD, Sala LM, Peterson B, Fisher J, Schroeder ID, Bograd SJ, Hazen EL, Schneider SR, Olightly RTG, Suryan RM, Gladics AJ, Loredo S, Porquez JM, Thompson AR, Weber ED, Watson W, Trainer V, Warzybok P, Bradley R, Jahncke J. (2016). State of the California Current 2015–16: Comparisons with the1997–98 El Niño. CalCOFI Rep **57:** 5–61.

McGowan JA, Cayan DR, Dorman LM. (1998). Climate-ocean variability and ecosystem response in the Northeast Pacific. Science **281:** 210–217.

Michaels AF, Silver MW. (1988). Primary production, sinking fluxes and the microbial food web. Deep Sea Res Part 1 **35:** 473–490.

Motwani NH, Gorokhova E. (2013). Mesozooplankton grazing on picocyanobacteria in the Baltic Sea as inferred from molecular diet analysis. PLoS ONE **8:** e79230. doi:10.1371/journal.pone.0079230.

Ohman MD, Barbeau K, Franks PJS, Goericke R, Landry MR, Miller AJ. (2013). Ecological transitions in a coastal upwelling ecosystem. Oceanography **26:** 210–219.

Oksanen, J., Blanchet, F. G., Friendly, M., Kindt, R., Legendre, P., McGlinn, D., Minchin, P. R., O'Hara, R. B., Simpson, G. L., Solymos, P., Stevens, M. H. H., Szoecs, E., Wagner, H. (2017). vegan: Community ecology package. R package version 2.4-3.

Pearson WR. (2016). Finding protein and nucleotide similarities with FASTA. Curr. Protoc. Bioinform. **53:** 3.9.1-3.9.25. doi: 10.1002/0471250953.bi0309s53.

Peterson WT, Keister JE, Feinberg LR. (2002). The effects of the 1997–99 El Niño/La Niña events on hydrography and zooplankton off the central Oregon coast. Prog Oceanogr **54:** 381–398.

Peterson WT, Fisher JL, Strub PT, Du X, Risien C, Peterson J, Shaw CT. (2017). The pelagic ecosystem in the Northern California Current off Oregon during the 2014–2016 warm anomalies within the context of the past 20 years. J Geophys Res Oceans **122:** 7267–7290.

Pfannkuche O, Lochte K. (1993). Open ocean pelago-benthic coupling: cyanobacteria as tracers of sedimenting salp faeces. Deep Sea Res Part I **40:** 727–737.

Quast C, Pruesse E, Yilmaz P, Gerken J, Schweer T, Yarza P, Peplies J, Glockner FO. (2013). The SILVA ribosomal RNA gene database project: improved data processing and web-based tools. Nucleic Acids Res **41:** D590–D596.

Richardson TL, Jackson GA. (2007). Small phytoplankton and carbon export from the surface ocean. Science **315:** 838–840.

Rueckert S, Simdyanov TG, Aleoshin VV, Leander BS. (2011). Identification of a divergent environmental DNA sequence clade using the phylogeny of gregarine parasites (Apicomplexa) from crustacean hosts. PLoS One **6:** e18163.

Schloss PD, Westcott SL, Ryabin T, Hall JR, Hartmann M, Hollister EB, Lesniewski RA, Oakley BB, Parks DH, Robinson CJ, Sahl JW, Stres B, Thallinger GG, Van Horn DJ, Weber CF. (2009). Introducing mothur: Open-source, platform-independent, community-supported software for describing and comparing microbial communities. Appl Environ Microbiol **75:** 7537–7541.

Shoemaker KM, Moisander PH. (2015). Microbial diversity associated with copepods in the North Atlantic subtropical gyre. FEMS Microbiol Ecol **91:** fiv064, doi: 10.1093/femsec/fiv064.

Siegel DA, Buesseler KO, Doney SC, Sailley SF, Behrenfeld MJ, Boyd PW. (2014). Global assessment of ocean carbon export by combining satellite observations and food-web models. Global Biogeochem Cycles **28:** 181–196.

Silver MW, Bruland KW. (1981). Differential feeding and fecal pellet composition of salps and pteropods, and the possible origin of the deep-water flora and olive-green "cells". Mar Biol **62:** 263–273.

Sohm JA, Ahlgren NA, Thomson ZJ, Williams C, Moffett JW, Saito MA., Webb EA, Rocap G. (2016). Co-occurring *Synechococcus* ecotypes occupy four major oceanic regimes defined by temperature, macronutrients and iron. ISME J **10:** 333–345.

Stukel MR, Landry MR. (2010). Contribution of picophytoplankton to carbon export in the equatorial Pacific: A reassessment of food web flux inferences from inverse models. Limnol Oceanogr **55:** 2669–2685.

Stukel MR, Landry MR, Benitez-Nelson CR, Goericke R. (2011). Trophic cycling and carbon export relationships in the California Current Ecosystem. Limnol Oceanogr **56:** 1866–1878.

Stukel MR, Décima M, Selph KE, Taniguchi DA, Landry MR. (2013a). The role of *Synechococcus* in vertical flux in the Costa Rica upwelling dome. Prog Oceanogr **112:** 49–59.

Stukel MR, Ohman MD, Benitez-Nelson CR, Landry MR. (2013b). Contributions of mesozooplankton to vertical carbon export in a coastal upwelling system. Mar Ecol Prog Ser **491:** 47–65.

Suzuki S, Kaneko R, Kodama T, Hashihama F, Suwa S, Tanita I, Furuya K, Hamasaki K. (2017). Comparison of community structures between particle-associated and free-living

prokaryotes in tropical and subtropical Pacific Ocean surface waters. Journal of Oceanography **73:** 383–395.

Taylor AG, Landry MR, Selph KE, Wokuluk JJ. (2015). Temporal and spatial patterns of microbial community biomass and composition in the Southern California Current Ecosystem. Deep Sea Res Part II **112:** 117–128.

Thiele S, Fuchs BM, Amann R, Iversen MH. (2015). Colonization in the photic zone and subsequent changes during sinking determine bacterial community composition in marine snow. Appl Environ Microbiol **81:** 1463–1471.

Vaqué D, Felipe J, Sala MM, Calbet A, Estrada M, Alcaraz M. (2006). Effects of the toxic dinoflagellate *Karlodinium* sp. (cultured at different N/P ratios) on micro and mesozooplankton. Sci Mar **70:** 59–65.

Venrick EL. (2002). Floral patterns in the California Current System off southern California: 1990-1996. J Mar Res **60:** 171–189.

Wallis JR, Smith AJ, Kawaguchi S. (2017). Discovery of gregarine parasitism in some Southern Ocean krill (Euphausiacea) and the salp *Salpa thompsoni*. Polar Biol **40:** 1913–1917.

Whitaker D, Christman M. (2015). clustsig: Significant Cluster Analysis. R package version 1.1.

Wilson SE, Steinberg DK. (2010). Autotrophic picoplankton in mesozooplankton guts: evidence of aggregate feeding in the mesopelagic zone and export of small phytoplankton. Mar Ecol Prog Ser **412:** 11–27.

Wilson SE, Ruhl HA, Smith Jr. KL. (2013). Zooplankton fecal pellet flux in the abyssal northeast Pacific: A 15 year time-series study. Limnol Oceanogr **58:** 881–892.

Zhang J, Kobert K, Flouri T, Stamatakis A. (2014). PEAR: A fast and accurate Illumina Paired-End reAd mergeR. Bioinformatics **30:** 614–620.

Zwirglmaier K, Jardillier L, Ostrowski M, Mazard S, Garczarek L, Vaulot D, Not F, Massana R, Ulloa O, Scanlan DJ. (2008). Global phylogeography of marine *Synechococcus* and *Prochlorococcus* reveals a distinct partitioning of lineages among oceanic biomes. Environ Microbiol **10:** 147–161.

Zwirglmaier K, Spence ED, Zubkov MV, Scanlan DJ, Mann NH. (2009). Differential grazing of two heterotrophic nanoflagellates on marine *Synechococcus* strains. Environ Microbiol **11:** 1767–1776.

CONCLUSIONS

Plankton communities play critical roles in transferring energy to higher trophic levels and modulating the cycles of carbon and other elements in the ocean (Longhurst and Harrison, 1989; Ducklow *et al.,* 2001). In my dissertation, I combined long-term data sets of mesozooplankton biomass, empirical equations, field measurements, and molecular techniques to investigate how these roles are affected by changes in the environment and the composition and relative abundances of different taxonomic groups. I based my research on two overarching questions: 1) What large-scale climate forces modulate mesozooplankton fluctuations in the North Pacific Subtropical Gyre? 2) How do the trophic interactions of mesozooplankton in the southern California Current System affect the contributions of certain phytoplankton groups to export flux? Here, I highlight the main results and novel contributions of my research working to answer these questions.

Mesozooplankton in the oligotrophic North Pacific

In Chapter 1, I used more than 20 years of approximately monthly data collected at station ALOHA to evaluate the environmental factors that modulate mesozooplankton biomass variability in the oligotrophic North Pacific Subtropical Gyre (NPSG). I found that primary production accounts for most of the variability in mesozooplankton biomass at both monthly and annual scales. The strong coupling between mesozooplankton fluctuations and primary production elucidated in this study differs from the transport-dominated influences that have been documented for North Pacific boundary currents (Hooff and Peterson, 2006; Keister *et al.,*

2011; Chiba *et al.,* 2013; Di Lorenzo and Ohman, 2013). Nevertheless, large-scale climate patterns also influenced annual variability of mesozooplankton biomass at station ALOHA, mainly due to lagged transport effects modulated by the North Pacific Gyre Oscillation (NPGO). Based on the model results from this study, I predicted a possible short-term decrease in mesozooplankton biomass as a response to the anomalously warm conditions of the 2015–2016 El Niño, but long-term positive biomass anomalies due to the lagged response to the NPGO.

The results from Chapter 1 offered new insights on the major environmental drivers affecting mesozooplankton biomass variability in the NPSG, but raised questions about how changes in the environment affect the structure and role of mesozooplankton in the biological pump. My analysis of the variability of mesozooplankton size structure in Chapter 2 suggested that the strong 1997–1998 El Niño was associated with an increase in smaller organisms at station ALOHA. In addition, I found that mesozooplankton biomass became more evenly distributed across size classes with increasing system productivity, largely due to increases in biomass of smaller (0.2–0.5 mm) and larger (>5 mm) organisms. Because no long-term trend in biomass was evident for the size class that accounts for most of the vertically migrating mesozooplankton (2–5 mm), the ratio of active flux mediated by migrants to passive export measured in sediment traps was not significantly different throughout the dataset. In contrast, I found that the potential contribution of mesozooplankton via fecal pellet production to passive particulate export measured in the traps showed a significant long-term increase.

Mesozooplankton in the California Current System

Mesozooplankton play a critical role in the biological pump by enhancing sinking of pico-, nano-, and micro-sized organisms within their fast-sinking fecal pellets (e.g., Schrader 1971; Madin, 1974; Turner and Ferrante, 1979), but this raises the question which microbes are

exported out of the euphotic zone by mesozooplankton? Microscopical analyses have given some insight into which microbes contribute to sinking particles; however, such analyses have been limited to taxa with hard shells such as diatoms and thecate dinoflagellates (see Amacher *et al.,* 2013). Therefore, in Chapters 3 and 4, I used metabarcoding analyses to elucidate the contributions of microbial taxa to export via mesozooplankton-mediated grazing and fecal pellets, processes that are influenced by the structure of both the mesozooplankton and microbial communities (e.g., Wexels Riser *et al.,* 2002; Wilson *et al.,* 2008).

My analyses of the protists ingested and egested by salps and doliolids (Chapter 3), and of the microbial assemblages associated with sinking particulate matter collected in sediment traps (Chapter 4) provided an unprecedented characterization of the potential microbes exported in the southern California Current System (CCS). I found that certain taxa, such as the prasinophyte Prasino-Clade-7B1, the dinoflagellate *Alexandrium*, an unidentified diatom (Bacillariophyceae_X), and strains of *Synechococcus* clade I, dominated the sequences in the fecal pellets of salps and doliolids. I also found that only certain mixed-layer microbes retained enough of their rDNA signatures to be recognized and contributed significantly to sinking particles. Strains of *Synechococcus* clade I were consistently high in the particles across sampling locations, and likely are the dominant clade in deep water due to transport in sinking pellets that degrade at depth. Among protists, dinoflagellates contributed disproportionately more at oligotrophic and transition sites, while the diatom *Thalassiosira* was enriched on particles at the inshore upwelling site. Based on these results, I inferred that these specific microbes likely resisted digestion within mesozooplankton guts. My analyses also highlighted that alveolate parasites assigned to gregarine apicomplexans and syndiniales were common in guts and fecal pellets of salps and doliolids, as well as on sinking particles collected in sediment

traps. These results suggest that parasitism could have a significant impact on food-web dynamics, which potentially affected the grazing impact and role in export flux of the salp and doliolid blooms during the study period.

Methodological considerations and future directions

The approximately monthly data of the Hawaii Ocean Time series (HOT) program enabled me to evaluate the environmental factors most likely linked to mesozooplankton biomass variability in the NPSG. However, the ocean faces unprecedented future changes and the responses of the mesozooplankton communities to these changes are complex and difficult to predict (e.g., Peterson and Schwing, 2003; Lavaniegos and Ohman, 2007; Rykaczewski and Checkley, 2008; Beaugrand *et al.,* 2010; Di Lorenzo and Ohman, 2013; Peterson *et al.,* 2017). In particular for the NPSG, mesozooplankton responses to future trends in productivity remain uncertain due to the potential increase in stratification favoring picophytoplankton in a warmer ocean (e.g., Doney *et al.,* 2012) or, conversely, due to the potential further enhancement of nitrogen fixing organisms (Hutchins *et al.,* 2007). Therefore, future observations are needed to test the predictive power of the strong relationship between mesozooplankton and productivity that I found here and to evaluate possible changes in the relative importance of different factors over time.

I found that fluctuations in environmental conditions can affect carbon cycling and export processes mediated by mesozooplankton in open-ocean oligotrophic systems. However, I based my calculations of mesozooplankton contributions to passive (fecal pellets) and active (excretion) fluxes on size-fractionated biomass, the growth rate equations of Hirst and Lampitt (1998), assumed gross growth efficiency (see Straile, 1997; Stukel and Landry, 2010), and the metabolic relationships of Ikeda (1985). This approach was necessary because direct

measurements of growth and excretion rates for the whole mesozooplankton community are very difficult to obtain and unavailable in the NPSG. Because my results provide only crude estimates of the relative contributions of mesozooplankton to passive and active fluxes, future studies need to be done by direct measurements and process-oriented mechanistic studies. Likewise, I based my analysis of mesozooplankton size structure on size-fractionated biomass, but it remains unclear if the increased evenness across size classes was due to changes in community composition (i.e., smaller species), a decrease in adult size, or an increase in the occurrence of juvenile stages.

Compared to microscopy, the high resolution of metabarcoding analysis enabled me to characterize which microbes were exported out of the euphotic zone in the CCS. However, uncertainties during amplification, sequencing, and bioinformatic analyses (e.g., primer bias, OTU clustering, taxonomic assignment), as well as the issue of gene copy number versus cell abundance, limit the strict interpretation of sequence data in terms of food-web dynamics. Likewise, although metabarcoding analyses illuminates which microbes were present in guts, fecal pellets, and sinking particles, it does not provide any information on microbial size or trophic roles, impeding the use of biovolume-to-carbon conversion factors that would shed some light on specific export efficiencies. Considering these methodological uncertainties, I based the interpretation of my results on relative abundances of sequence reads; thus, the relative contributions of various groups to export are nonquantitative. It is important to keep in mind that in the context of the biological pump, the currency needed to determine the relative importance of the microbes exported is in terms of carbon. Therefore, in addition to the relative abundances of DNA, carbon fluxes from food-web studies are also necessary to better resolve taxon-specific contributions to upper-ocean productivity and particle export.

An important finding from my dissertation is that the recovery of sequences in the fecal pellets of salps and doliolids, as well as in exported particles, may be more a reflection of digestion resistance than direct sinking of certain taxa. Some groups, such as *Synechococcus* Clade I, the prasinophyte Prasino-Clade-7B1, diatoms such as *Thalassiosira*, and parasites, appear to be resistant to digestion, greatly amplifying their relative sequence abundances in fecal pellets and sinking particles collected in the mesopelagic zone. Therefore, a necessary step to increase our understanding of the biological pump requires elucidating the role that degradation rate of prey DNA in mesozooplankton guts and that digestion resistance, even at the strain level, may play in upper-ocean food-web dynamics and carbon export. This knowledge will be particularly relevant to clarify uncertainties in the relative contributions of different microbes to zooplankton nutrition, in addition to carbon fluxes, under varying environmental conditions, together with their associated mechanisms (Richardson and Jackson, 2007; Stukel and Landry, 2010). Although this study was carried out during anomalously warm conditions due to a warm-water anomaly and El Niño, the inshore-offshore range in environmental conditions covered across the CCS offers insights into the possible responses of the ecosystem in terms of the role of mesozooplankton-mediated microbial export and the potential microbes exported.

References

Amacher J, Neuer S, Lomas M. (2013). DNA-based molecular fingerprinting of eukaryotic protists and cyanobacteria contributing to sinking particle flux at the Bermuda Atlantic time-series study. Deep Sea Res Part II **93:** 71–83.

Beaugrand, G, Edwards M, Legendre L. (2010). Marine biodiversity, ecosystem functioning, and carbon cycles. Proc Natl Acad Sci U.S.A **107:** 10120–10124.

Chiba S, Di Lorenzo E, Davis A, Keister JE, Taguchi B, Sasai Y, Sugisaki H. (2013). Large-scale climate control of zooplankton transport and biogeography in the Kuroshio-Oyashio Extension region. Geophys Res Lett **40:** 5182–5187.

Di Lorenzo E, Ohman MD. (2013). A double-integration hypothesis to explain ocean ecosystem response to climate forcing. Proc Natl Acad Sci U.S.A **110:** 2496–2499.

Doney SC, Ruckelshaus M, Duffy JE, Barry JP, Chan F, English CA, Galindo HM, Grebmeier JM, Hollowed AB, Knowlton N, Polovina J, Rabalais NN, Sydeman WJ, Talley LD. (2012). Climate change impacts on marine ecosystems. Ann Rev Mar Sci **4:** 11–37.

Ducklow HW, Steinberg DK, Buesseler KO. (2001). Upper ocean carbon export and the biological pump. Oceanography **14:** 50–58.

Hirst GA, Lampitt S R. (1998). Towards a global model of in situ weight-specific growth in marine planktonic copepods. Mar Biol **132:** 247–257.

Hooff RC, Peterson WT. (2006). Copepod biodiversity as an indicator of changes in ocean and climate conditions of the northern California current ecosystem. Limnol Oceanogr **51:** 2607–2620.

Hutchins, D. A., Fu, F. X., Zhang, Y., Warner, M. E., Feng, Y., Portune, K., Bernhardt, P. W., Mulholland, M. R. (2007). CO_2 control of Trichodesmium N_2 fixation, photosynthesis, growth rates, and elemental ratios: Implications for past, present, and future ocean biogeochemistry. Limnology and Oceanography, 52, 1293-1304.

Ikeda T. (1985). Metabolic rates of epipelagic marine zooplankton as a function of body mass and temperature. Mar Biol **85:** 1–11.

Keister JE, Di Lorenzo E, Morgan CA, Combes V, Peterson WT. (2011). Zooplankton species composition is linked to ocean transport in the Northern California Current. Glob Chang Biol **17:** 2498–2511.

Longhurst AR, Harrison WG. (1989). The biological pump: profiles of plankton production and consumption in the upper ocean. Prog Oceanogr **22:** 47–123.

Madin LP. (1974). Field observations on the feeding behavior of salps (Tunicata: Thaliacea). Mar Biol **25:** 143–147.

Peterson WT, Schwing F. (2003). A new climate regime in northeast pacific ecosystems. Geophys Res Lett **30:** 1896, doi:10.1029/2003GL017528.

Peterson WT, Fisher JL, Strub PT, Du X, Risien C, Peterson J, Shaw CT. (2017). The pelagic ecosystem in the Northern California Current off Oregon during the 2014–2016 warm anomalies within the context of the past 20 years. J Geophys Res Oceans **122:** 7267–7290.

Richardson TL, Jackson GA. (2007). Small phytoplankton and carbon export from the surface ocean. Science **315:** 838–840.

Rykaczewski RR, Checkley DM. (2008). Influence of ocean winds on the pelagic ecosystem in upwelling regions. Proc Natl Acad Sci U.S.A **105:** 1965–1970.

Schrader HJ. (1971). Fecal pellets: role in sedimentation of pelagic diatoms. Science **174:** 55–57.

Stukel MR, Landry MR. (2010). Contribution of picophytoplankton to carbon export in the equatorial Pacific: A reassessment of food web flux inferences from inverse models. Limnol Oceanogr **55:** 2669–2685.

Straile D. (1997). Gross growth efficiencies of protozoan and metazoan zooplankton and their dependence on food concentration, predator-prey weight ratio, and taxonomic group. Limnol Oceanogr **42:** 1375–1385.

Turner JT, Ferrante JG. (1979). Zooplankton fecal pellets in aquatic ecosystems. BioScience **29:** 670–677.

Wexels Riser C, Wassmann P, Olli K, Pasternak A, Arashkevich E. (2002). Seasonal variation in production, retention and export of zooplankton faecal pellets in the marginal ice zone and the central Barents Sea. J Mar Sys **38:** 175–188.

Wilson SE, Steinberg DK, Buesseler KO. (2008). Changes in fecal pellet characteristics with depth as indicators of zooplankton repackaging of particles in the mesopelagic zone of the subtropical and subarctic North Pacific Ocean. Deep Sea Res Part II **55:** 1636–1647.

APPENDIX 1

[Journal of Geophysical Research: Biogeosciences]

Supporting Information for

Environmental drivers of mesozooplankton biomass variability in the North Pacific Subtropical Gyre

Bellineth Valencia[1], Michael R. Landry[1], Moira Décima[2], and Cecelia C.S. Hannides[3]

1Scripps Institution of Oceanography, University of California San Diego, La Jolla, California.

2National Institute of Water and Atmospheric Research, NIWA, Wellington, New Zealand.

3Department of Geology and Geophysics, University of Hawaii, Honolulu, Hawaii.

Contents of this file

Introduction

This document includes the Generalized Additive Model (GAM) results for all the combinations of covariates evaluated to assess the effects of environmental factors on the monthly and annual variability of mesozooplankton biomass at Stn. ALOHA. For the final models selected, model validation results are presented based on graphical analyses of the residuals. In addition, GAM plots are presented for the alternative annual mean model.

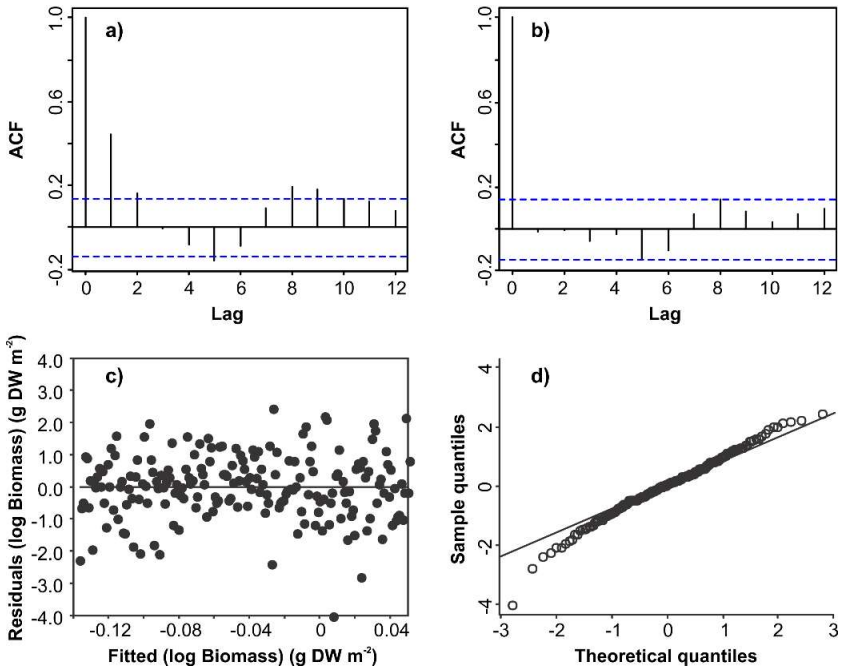

Appendix Figure S1.1. Model validation of the generalized least squares analysis including an autocorrelation structure AR1 to evaluate the long-term trend in mesozooplankton biomass (log10 dry weight) at Stn. ALOHA. a) Results of the autocorrelation coefficient (ACF) for the model without autocorrelation structure (ordinary least squares). b) Results of the ACF for the model including an AR1 structure in the residuals. c) Homogeneity of variances was assessed by plotting the normalized residuals versus the fitted values. d) Deviation from the normal distribution was assessed by a quantile-quantile plot.

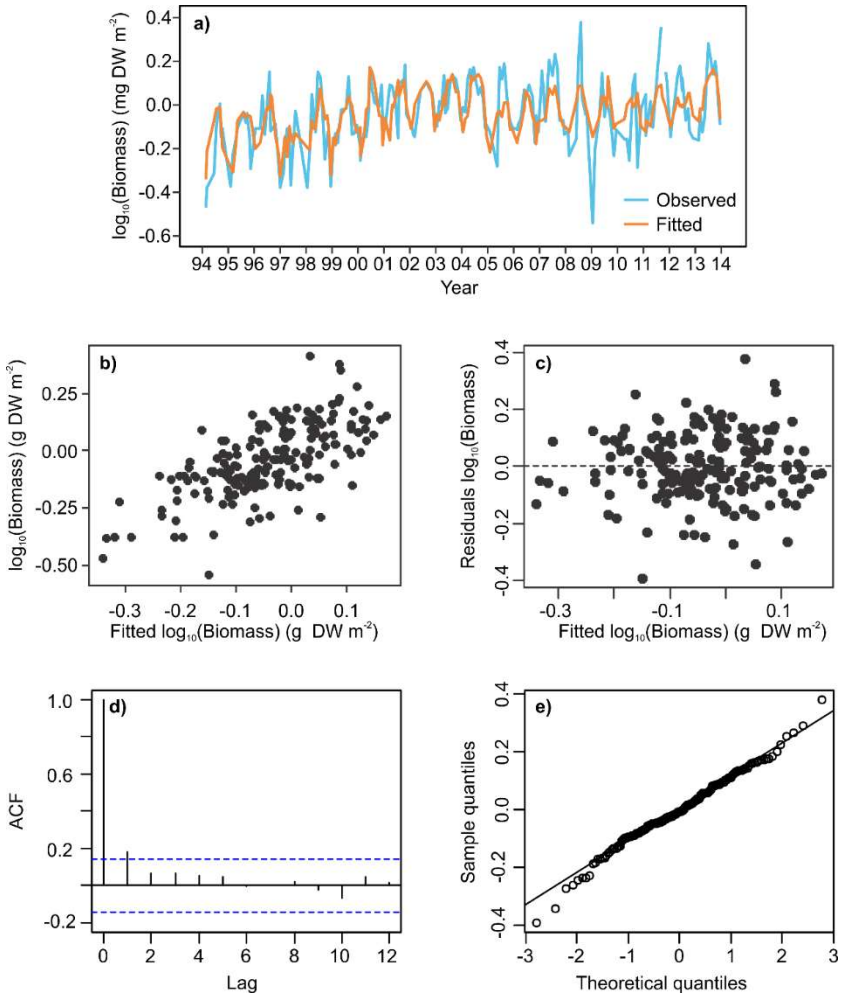

Appendix Figure S1.2. Model validation of the final monthly mean GAMs for mesozooplankton biomass at Stn. ALOHA. The fitness of the model was evaluated by plots of a) the observed and fitted values versus time and b) observed versus fitted values. c) Homogeneity of variances was assessed by plotting the residuals versus fitted values. d) Autocorrelation in the residuals was assessed by the plot of the autocorrelation function (ACF). e) Deviation from the normal distribution was assessed by a quantile-quantile plot.

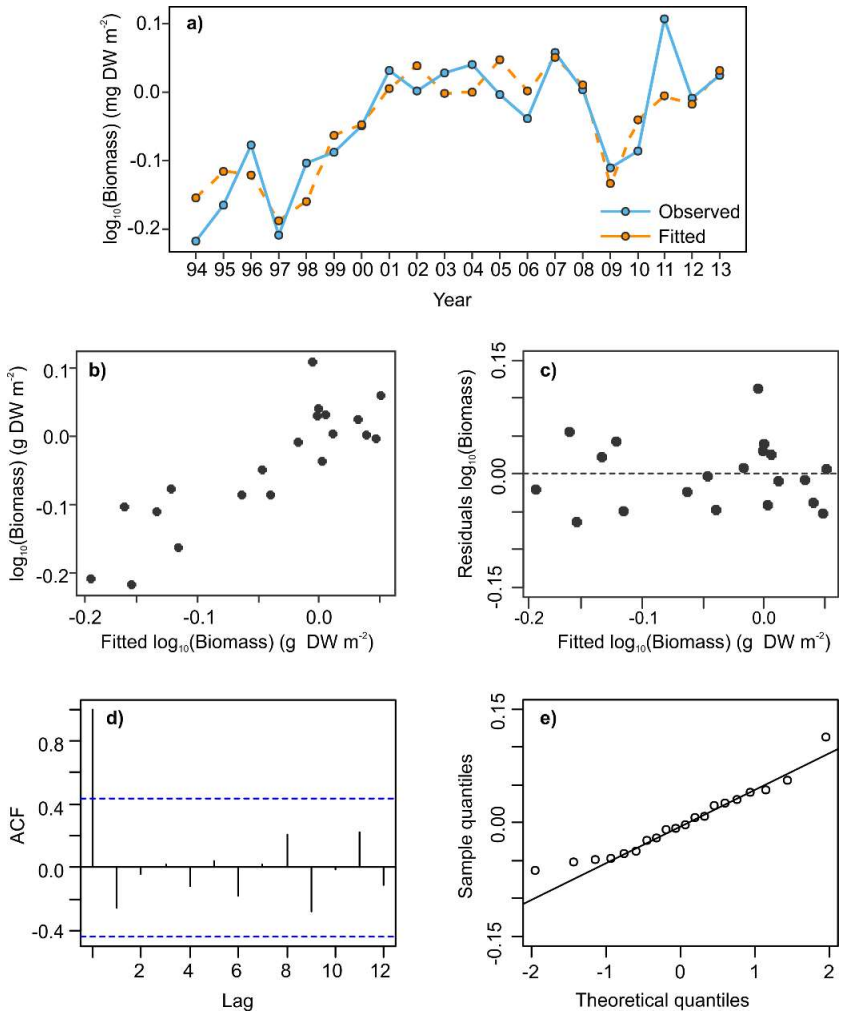

Appendix Figure S1.3. Model validation of the final annual mean GAMs for mesozooplankton biomass at Stn. ALOHA. The fitness of the model was evaluated by plots of a) the observed and fitted values versus time and b) observed versus fitted values. c) Homogeneity of variances was assessed by plotting the residuals versus fitted values. d) Autocorrelation in the residuals was assessed by the plot of the autocorrelation function (ACF). e) Deviation from the normal distribution was assessed by a quantile-quantile plot.

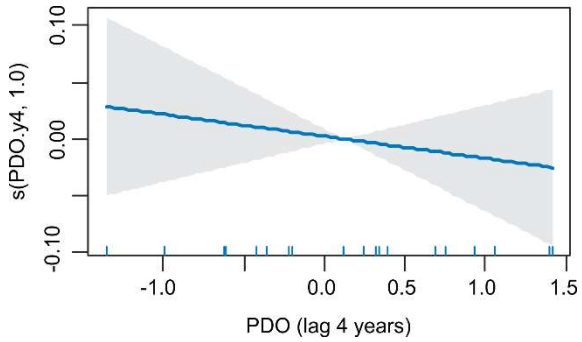

Appendix Figure S1.4. Annual mean of mesozooplankton biomass at Stn. ALOHA modeled with a GAM as function of 4-y lagged PDO only.

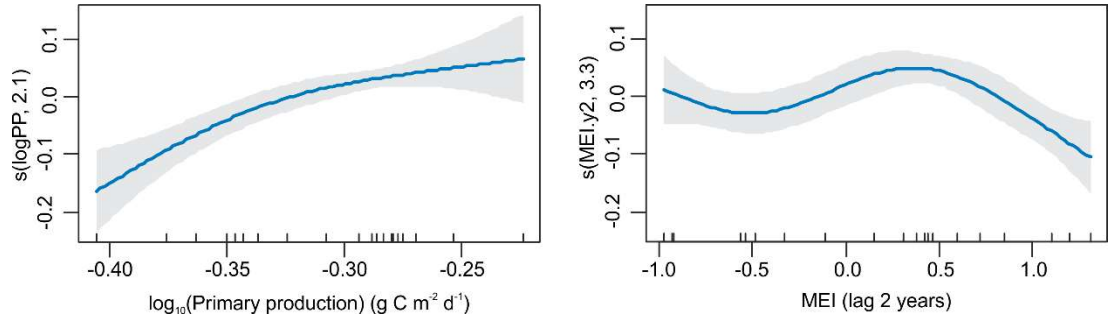

Appendix Figure S1.5. Generalized additive model functions for the alternative annual mean model to explain the relationship between mesozooplankton biomass and environmental factors at Stn. ALOHA. The model includes smooth functions for primary production and MEI. Results of the model are presented in Table S3.

Lag	Monthly mean models
None	$b(log_{10}PP) + f_1(SST) + f_2(MEI.m0) + f_3(NPGO.m0) + f_4(PDO.m0)$
1 month	$b(log_{10}PP) + f_1(SST) + f_2(MEI.m1) + f_3(NPGO.m1) + f_4(PDO.m1)$
2 months	$b(log_{10}PP) + f_1(SST) + f_2(MEI.m2) + f_3(NPGO.m2) + f_4(PDO.m2)$
3 months	$b(log_{10}PP) + f_1(SST) + f_2(MEI.m3) + f_3(NPGO.m3) + f_4(PDO.m3)$

Lag	Annual mean models
None	$b(SST) + f_1(log_{10}PP) + f_2(NPGO.y0) + f_3(MEI.y0)$
	$b(SST) + f_1(log_{10}PP) + f_2(NPGO.y0) + f_3(PDO.y0)$
1 year	$b(SST) + f_1(log_{10}PP) + f_2(MEI.y1)$
	$b(SST) + f_1(log_{10}PP) + f_2(PDO.y1)$
2 years	$b(SST) + f_1(log_{10}PP) + f_2(NPGO.y2) + f_3(MEI.y2)$
	$b(SST) + f_1(log_{10}PP) + f_2(NPGO.y2) + f_3(PDO.y2)$
3 years	$b(SST) + f_1(log_{10}PP) + f_2(NPGO.y3) + f_3(MEI.y3)$
	$b(SST) + f_1(log_{10}PP) + f_2(NPGO.y3) + f_3(PDO.y3)$
4 years	$b(SST) + f_1(log_{10}PP) + f_2(NPGO.y4) + f_3(MEI.y4)$
	$b(SST) + f_1(log_{10}PP) + f_2(NPGO.y4) + f_3(PDO.y4)$

Appendix Table S1.1. Generalized additive models (GAMs) run to evaluate the effect of environmental factors on mesozooplankton biomass at Stn. ALOHA. A stepwise backward approach was applied and models were re-run when non-significant covariates were found or when the effective degrees of freedom were equal to 1 (linear relationship). Two sets of models for each lag were run for annual data because the PDO and the MEI were highly collinear. Likewise, primary production and the NPGO were highly collinear with a lag of one year. *b* denotes linear terms whereas *f* denotes smooth functions. PP: $\log_{10}$(primary production), SST: sea surface temperature, MEI: Multivariate ENSO index, NPGO: North Pacific Gyre Oscillation, PDO: Pacific Decadal Oscillation.

No lag			Lag 1 month		
	Estimate	**p-value**		**Estimate**	**p-value**
Intercept	-0.88	<0.001	Intercept	0.11	<0.001
logPP	0.45	<0.001	logPP	0.50	<0.001
SST	0.04	<0.001			
	edf	**p-value**		**edf**	**p-value**
			SST	1.53	<0.001
NPGO.m0	2.74	<0.001	NPGO.m1	1.74	<0.01
MEI.m0	3.75	<0.01	MEI.m1		ns
PDO.m0		ns	PDO.m1		ns
DE (%)	**R^2**	**GCV**	**DE (%)**	**R^2**	**GCV**
46	0.43	0.0147	39	0.38	0.0157

Lag 2 months			Lag 3 months		
	Estimate	**p-value**		**Estimate**	**p-value**
Intercept	0.12	<0.001	Intercept	0.12	<0.001
logPP	0.52	<0.001	logPP	0.51	<0.001
	edf	**p-value**		**edf**	**p-value**
SST	1.82	<0.001	SST	1.40	<0.001
NPGO.m2	3.01	<0.01	NPGO.m3	2.26	<0.001
MEI.m2		ns	MEI.m3		ns
PDO.m2		ns	PDO.m3		ns
DE (%)	**R^2**	**GCV**	**DE (%)**	**R^2**	**GCV**
41	0.39	0.0156	41	0.40	0.0153

Appendix Table S1.2. Results of the monthly means GAMs. A stepwise backward approach was applied and only the significant models for each lag are presented. Final model selected reported in table 3 corresponds to the model with no lags. DE: deviance explained, n = 188

No lag (PDO)			No lag (MEI)		
	Estimate	**p-value**		**Estimate**	**p-value**
Intercept	-2.13	0.04	Intercept	-2.13	0.04
SST	0.08	0.04	SST	0.08	0.04
	edf	**p-value**		**edf**	**p-value**
log PP	2.82	0.02	log PP	2.82	0.02
NPGO.y0	3.34	0.02	NPGO.y0	3.34	0.02
PDO.y0		ns	MEI.y0		ns
DE (%)	**R^2**	**GCV**	**DE (%)**	**R^2**	**GCV**
83	0.73	0.0035	83	0.73	0.0035

Lag 1 year (PDO)			Lag 1 year (MEI)		
	Estimate	**p-value**		**Estimate**	**p-value**
Intercept	-0.04	0.01	Intercept	-0.04	0.01
SST		ns	SST		ns
	edf	**p-value**		**edf**	**p-value**
log PP	1.32	<0.01	log PP	1.32	<0.01
NPGO.y1		-	NPGO.y1		-
PDO.y1		ns	MEI.y1		ns
DE (%)	**R^2**	**GCV**	**DE (%)**	**R^2**	**GCV**
47	0.43	0.0050	47	0.43	0.0050

Appendix Table S1.3. Results of the annual means GAMs. Final model selected reported in Table 3 corresponds to the model that includes the 4-y lagged PDO. The model that includes the 2-y lagged MEI also performed well; however, the response of the biomass tended to be more complex (see Results and Figure S5). DE: deviance explained, n = 20.

Lag 2 years (PDO)			Lag 2 years (MEI)		
	Estimate	**p-value**		**Estimate**	**p-value**
Intercept	-0.04	0.01	Intercept	-0.04	<0.01
SST		ns	SST		ns
	edf	**p-value**		**edf**	**p-value**
log PP	1.32	<0.01	log PP	2.14	<0.01
NPGO.y2		ns	NPGO.y2		ns
PDO.y2		ns	MEI.y2	3.32	0.01
DE (%)	**R^2**	**GCV**	**DE (%)**	**R^2**	**GCV**
47	0.43	0.0050	82	0.74	0.0030

Lag 3 years (PDO)			Lag 3 years (MEI)		
	Estimate	**p-value**		**Estimate**	**p-value**
Intercept	-0.04	<0.01	Intercept	-0.04	0.01
SST		ns	SST		ns
	edf	**p-value**		**edf**	**p-value**
log PP	1.50	0.04	log PP	1.50	0.04
NPGO.y3	1.17	0.04	NPGO.y3	1.17	0.04
PDO.y3		ns	MEI.y3		ns
DE (%)	**R^2**	**GCV**	**DE (%)**	**R^2**	**GCV**
63	0.57	0.0041	63	0.57	0.0041

Appendix Table S1.3. Continued.

Lag 4 years (PDO)			Lag 4 years (MEI)		
	Estimate	**p-value**		**Estimate**	**p-value**
Intercept	-0.05	<0.001	Intercept	0.25	0.02
SST		ns	SST		ns
NPGO.y4	0.05	<0.01	log PP	0.95	0.01
PDO.y4	0.05	0.02	NPGO.y4	0.03	0.01
	edf	**p-value**		**edf**	**p-value**
log PP	1.23	<0.01	MEI.y4		ns
DE (%)	**R^2**	**GCV**	**DE (%)**	**R^2**	**GCV**
75	0.70	0.0030	62	0.58	0.0039

Appendix Table S1.3. Continued.

APPENDIX 2

Global Biogeochemical Cycles

Supporting Information for

Environmental Effects on Mesozooplankton Size Structure and Export Flux at Station ALOHA, North Pacific Subtropical Gyre

Bellineth Valencia[1], Moira Décima[2], and Michael R. Landry[1]

[1]Scripps Institution of Oceanography, University of California San Diego, La Jolla, California.

[2]National Institute of Water and Atmospheric Research, NIWA, Wellington, New Zealand.

Contents of this file

Introduction

This document includes the approaches for calculating mesozooplankton ingestion and egestion rates in the euphotic zone, as well as the contributions of migrant mesozooplankton to the active fluxes of carbon, nitrogen, and phosphorus. Table S1 summarizes the ratios carbon to dry weight (C:DW) and nitrogen to dry weight (N:DW) per size class used to calculate mesozooplankton growth rates in the euphotic zone and the turnover rates of carbon and nitrogen in the mesopelagic zone. Table S2 contains the estimated biomass per individual in terms of carbon and dry weight using the values published by Landry et al. (2001). The biomass per individual was then used to calculate mesozooplankton growth rate from the empirical equation of Hirst and Lampitt (1998), as well as to calculate respiration and excretion rates from the empirical equations of Ikeda (1985). This document also explains the considerations involved

for running the Generalized Additive Models (GAMs). Results of the GAMs are presented for: 1) the long-term trend of day, night, and migrant mesozooplankton biomass (Figures S1 and S4, Tables S3 and S4), 2) the long-term trend of each size class of mean mesozooplankton biomass (mean of paired day-night samples; Table S3), 3) the temporal trend of the proportion of ingestion to primary production and egestion to particulate organic carbon flux (Table S5), 4) the temporal trend of the proportion of active to passive flux (Table S5), and 4) the effect of environmental factors on size structure (Figure S2, Tables S6 and S7) and migrant biomass (Figure S3, Tables S6 and S7). For the final models selected, model validation is presented based on graphical analyses of the normalized residuals (Figures S1 to S3). Changes in migrant mesozooplankton biomass are presented for 1997 and 2009, both El Niño years (Figure S5).

Text S1. Rate estimates: Carbon cycling in the euphotic zone

The potential impact of mesozooplankton on carbon cycling in the euphotic zone was estimated following an approach similar to that of Roman et al. (2002a). We first estimated mesozooplankton production (*ZP*) using an empirical growth rate relationship, then determined the food consumption (ingestion, *I*) needed to support that production using a gross growth efficiency of 20% (GGE = *ZP:I*) (Straile, 1997; Stukel & Landry, 2010). Egestion (*E*) of undigested carbon as fecal matter was estimated using an assimilation efficiency of 70% (i.e., *E* = 30% of *I*). Thus, *I* = *ZP*/0.2 and *E* = 1.5 * *ZP*.

Mesozooplankton production (*ZP*, mg C m^{-2} d^{-1}) was computed for each size class as the product of the carbon biomass (mg C m^{-2}) times calculated temperature-dependent growth rates (*g*: d^{-1}). Carbon biomass for each cruise was obtained by elemental analysis, whereas the intrinsic growth rates (*g*: d^{-1}) were calculated from the equation of Hirst and Lampitt (1998)

$$log_{10}\, g = 0.0208 * T_{0-100} - 0.3221 * log_{10}\, BW - 1.1408, \quad (1)$$

which predicts the intrinsic growth rate of copepods, the dominant mesozooplankton (>80%) at station ALOHA (Landry et al., 2001), from environmental temperature ($T_{0\text{-}100}$: °C) and body carbon (*BW*, µg C ind^{-1}). For temperature, we used cruise mean values for the upper 100 m of the water column, where most of the mesozooplankton reside in the euphotic zone at station ALOHA (Huntley et al., 2006; Steinberg et al., 2008). For body carbon of individual animals, we used the mean estimates of Landry et al. (2001), which were determined by dividing the measured bulk carbon by the mesozooplankton abundance for each of the 5 mesh-screened size classes of 71 daytime and 73 nighttime tows collected at station ALOHA over the course of three years (Table S2, *BW*).

Text S2. Rate estimates: Active flux mediated by migrant mesozooplankton

Migrant mesozooplankton respiration (R_O: µl O2 ind^{-1} h^{-1}; eq. 2), ammonia excretion (E_{DIN}: µg N ind^{-1} h^{-1}; eq. 3), and phosphate excretion (E_{DIP}: µg P ind^{-1} h^{-1}; eq. 4) were determined for each size class using the empirical equations of Ikeda (1985). The rates were calculated as function of the biomass per individual (*mDWI*: mg DW ind^{-1}, Table S2) and the temperature ($T_{300\text{-}500}$: °C; mean 300–500 m) that migrants might experience at daytime depths (300–500 m). Similar to the approach followed by Al-Mutairi and Landry (2001), the biomass per individual was calculated by dividing the dry weight biomass (mg DW m^{-2}) by the abundance (ind m^{-2}) published for station ALOHA by Landry et al. (2001) (Table S2, *mDWI*).

$$ln\, R_o = -0.2512 + (0.7886 * \ln\, mDWI) + (0.0490 * T_{300-500}), \quad (2)$$

$$ln\, E_{DIN} = -2.8900 + (0.7616 * \ln\, mDWI) + (0.0511 * T_{300-500}), \quad (3)$$

$$ln\, E_{DIP} = -4.3489 + (0.7983 * \ln\, mDWI) + (0.0285 * T_{300-500}), \quad (4)$$

Respiration rates (R_O) were converted to carbon equivalents (R_C: mg C ind^{-1} h^{-1}) using the molar volume of an ideal gas at standard temperature and pressure (22.4 L mol^{-1}), the respiratory quotient, and the molecular weight of carbon (12 g C mol^{-1}). The respiratory quotient represents the molar ratio of carbon dioxide produced to oxygen consumed during the oxidation of organic matter, and a value of 0.97 was used, assuming protein-dominated metabolism (Hernández-León & Ikeda, 2005; Omori & Ikeda, 1984).

Once the rates per individual were calculated (g ind^{-1} h^{-1}), the daily contribution of all migrating mesozooplankton to the active export flux was determined (g m^{-2} d^{-1}) by assuming that migrants

metabolize during the daytime (12h) while they are at depth (300–500 m) and by multiplying each rate by the abundance of migrants in each size class (ind m^{-2}). For individual cruises, the number of animals in each size class were estimated by dividing the measured migrant biomass of each size class (mg DW m^{-2}) by the mean biomass estimate of individuals (Table S2, *mDWI*: mg DW ind^{-1}).

Text S3. Data analysis

The seasonal and long-term trend of day and night mesozooplankton biomass (untransformed data) from 1994 to 2016 were modeled using a generalized additive model (GAM) that assumed Gaussian distributed residuals

$$DW_{iy} = a + f_1(Day.of.year_i) + f_2(Time_{iy}) + \varepsilon_{iy} \quad \text{where } \varepsilon_{iy} \sim N(0, \sigma_y^2), \qquad (5)$$

where DW_{iy} is mesozooplankton biomass of the *ith* cruise (i = 1 to 223) in year y (y = 1 to 23), a is the model intercept, f are cubic (*f1*) and thin-plate (*f2*) regression splines functions describing the effects of the covariates day of year and time on biomass, respectively, and ε are the residuals modeled with an auto-regressive process AR1 and a variance structure VarIdent. The variance structure VarIdent allows to have a different variance per stratum (Zuur et al., 2009), which is appropriate considering that the spread of the biomass differs per year. Model results of the temporal analysis of biomass are presented in Table S3 and Figure S1.

Models run with a Gaussian distribution that included the variance structure had a tendency to overfit the data. Hence, we attempted to model the long-term trend in biomass assuming that residuals follow a Gamma distribution, which is appropriate for right-skewed data (Wood, 2006; Zuur et al., 2009). Model results assuming the Gamma and Gaussian distributions were similar in terms of the covariates that were significant and the general shape of the trends.

Because the long-term trends of day and night mesozooplankton biomass were significant, approximate segments of increase or decrease were visually identified after running the GAMs. The significance of the trend of those segments were evaluated by generalized least squares (GLS) models including an AR1 process to account for positive autocorrelation in residuals and a VarIdent variance structure to allow different variances per year (Zuur et al., 2009) (Table S4). Model validation for GAMs (Figure S2) and GLS was done by graphical analysis of the normalized residuals. GAMs and GLS models were performed in R using the function 'gamm' in the mgcv package (Wood, 2006) and the function "gls" in the nlme package (Pinheiro et al., 2015), respectively.

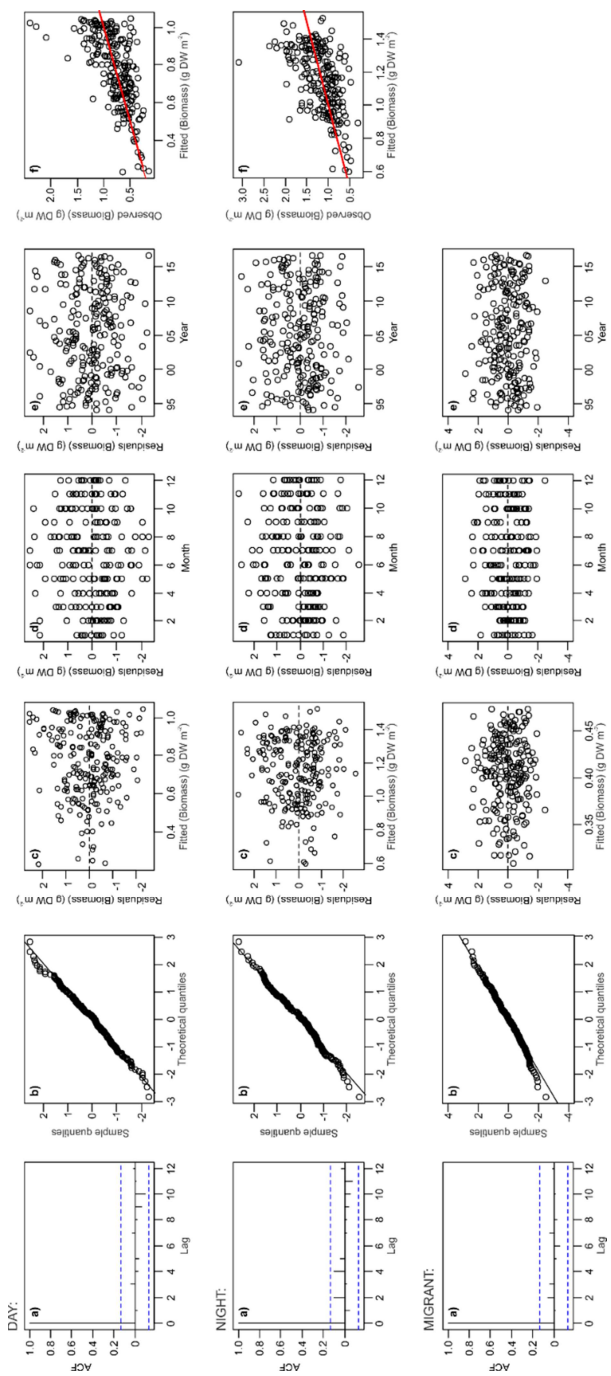

Appendix Figure S2.1. Model validation of the GAMs evaluating the temporal variability of day, night, and migrant mesozooplankton biomass at station ALOHA. Assumptions of the models were evaluated using the normalized residuals. a) Autocorrelation in the residuals was assessed by the plot of the autocorrelation function (ACF). b) Deviation from the normal distribution was assessed by quantile-quantile plots. c) Homogeneity of variances was assessed by plotting the residuals versus fitted values. d) and e) Independence was assessed by plotting the residuals versus each covariate, month and year. f) Model fit was assessed by plotting the observed versus fitted values.

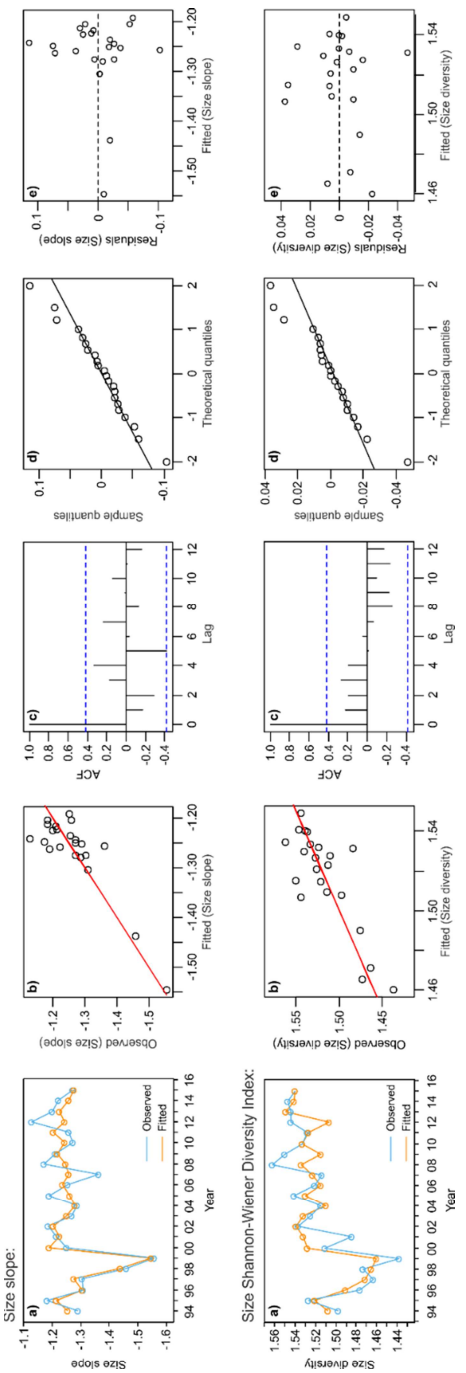

Appendix Figure S2.2. Model validation of the GAMs evaluating the effect of the environmental factors on mesozooplankton biomass size structure at station ALOHA. Assumptions of the models were evaluated using the deviance residuals. a) and b) Model fit was assessed by plotting the observed versus fitted values. c) Autocorrelation in the residuals was assessed by the plot of the autocorrelation function (ACF). d) Deviation from the normal distribution was assessed by quantile-quantile plots. e) Homogeneity of variances was assessed by plotting the residuals versus fitted values. Note heterogeneity in residuals in the model of the size slope.

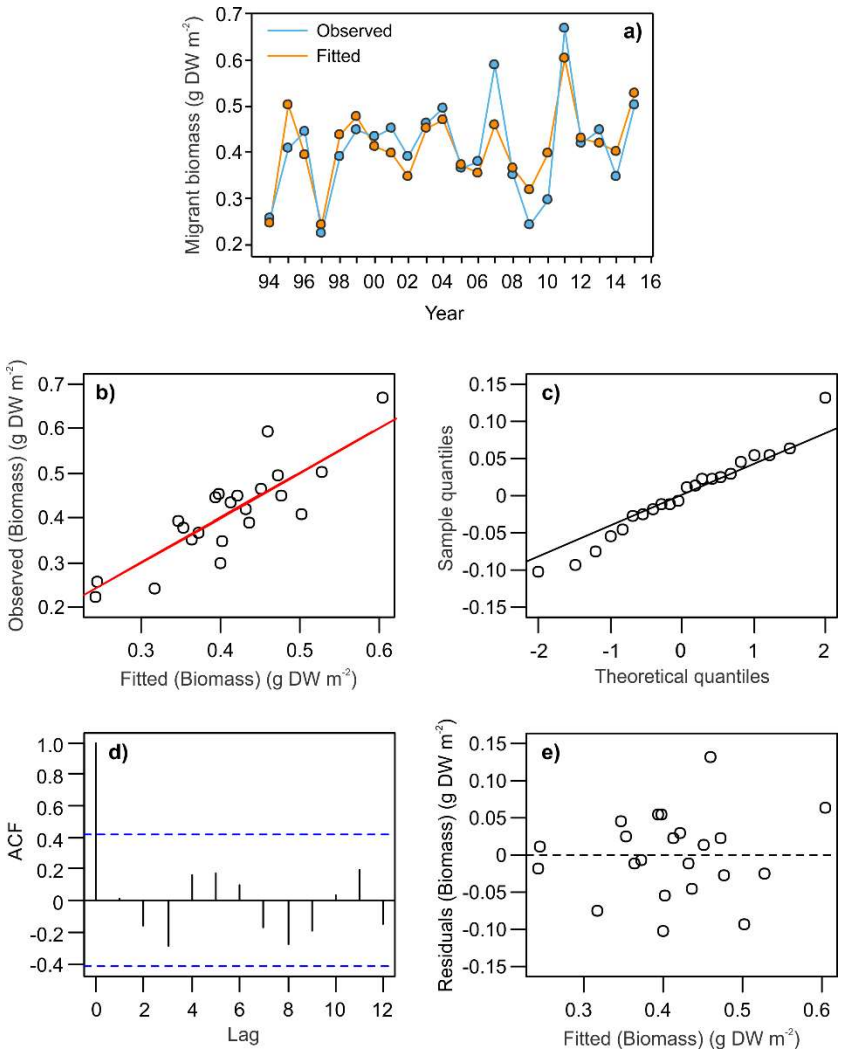

Appendix Figure S2.3. Model validation of the GAM evaluating the effect of the environmental factors on migrant mesozooplankton biomass at station ALOHA. Assumptions of the models were evaluated using the deviance residuals. a) and b) Model fit was assessed by plotting the observed versus fitted values. c) Deviation from the normal distribution was assessed by quantile-quantile plots. d) Autocorrelation in the residuals was assessed by the plot of the autocorrelation function (ACF). e) Homogeneity of variances was assessed by plotting the residuals versus fitted values.

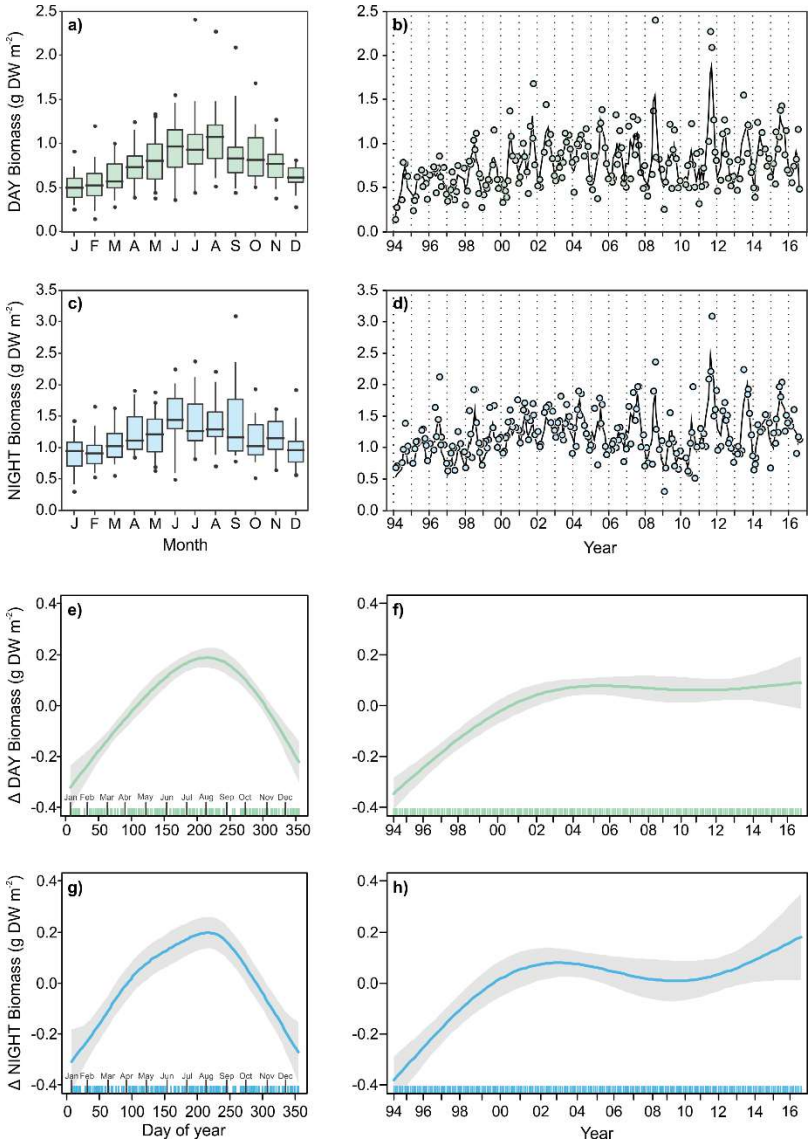

Appendix Figure S2.4. Temporal trend of day and night mesozooplankton biomass at station ALOHA from 1994 to 2016 evaluated by GAMs. a, c) Monthly variability of day and night biomass. Boxes and whiskers correspond to 25-75th and 5-95th percentiles, respectively. Circles represent outliers. b, d) Interannual variability of day and night biomass. Circles represent mean per cruise (usually n = 3) for the combined size classes. Curved fit is a three-point moving average. e-h) Partial regression plots represent the modeled seasonal and long-term trends of biomass using GAMs (see Table S3). X-axes are the model covariates (day of year and date) and the tick marks represent each observation. Y-axes represent the effects of covariates on predicted mesozooplankton biomass. Y-axes values are deviations from mean biomass and thus are centered. Numbers in parentheses are the effective degrees of freedom. Solid lines are the modeled trends and shaded areas are the 95% confidence intervals. Predicted values of biomass are obtained by adding the deviations from each smooth function to the mean biomass.

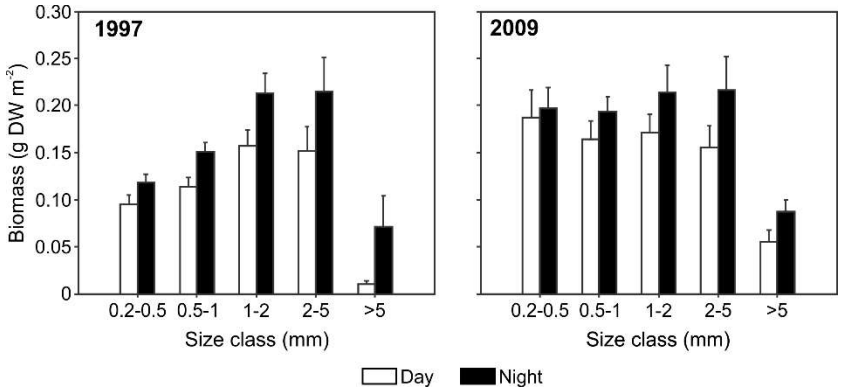

Appendix Figure S2.5. Day and night mesozooplankton biomass in each size class at station ALOHA. The change in the structure of the community in 1997 and 2009, both El Niño years, were reflected in a lower migrant biomass. Mean ± SE.

		0.2 - 0.5 mm	0.5 - 1 mm	1 - 2 mm	2 - 5 mm	> 5mm
C:DW (mg:g)	Day (n = 512)	355.0 ± 2.0	357.5 ± 1.7	359.5 ± 1.7	320.0 ± 2.1	321.7 ± 7.1
	Night (n = 514)	365.5 ± 1.9	365.6 ± 1.7	367.9 ± 1.7	348.1 ± 1.8	318.8 ± 4.4
N:DW (mg:g)	Day (n = 512)	81.1 ± 0.5	85.1 ± 0.5	87.6 ± 0.4	76.7 ± 0.6	61.1 ± 1.5
	Night (n = 514)	83.8 ± 0.5	87.4 ± 0.4	90.4 ± 0.4	85.5 ± 0.5	72.4 ± 1.1

Appendix Table S2.1. Carbon to dry weight (mg:g) and nitrogen to dry weight (mg:g) relationships of mesozooplankton at station ALOHA. Ratios were obtained for each size class from 1994 to 2016. Mean ± standard error.

	Biomass (mg C m^{-2})		Abundance (ind m^{-2})		Biomass (µg C ind^{-1})
	Night	Day	Night	Day	Mean (BW)
0.2-0.5mm	52	40	20700	16900	2.4
0.5-1.0mm	70	47	8300	7380	7.4
1.0-2.0mm	79	50	1780	1330	41.0
2.0-5.0mm	76	29	465	247	140.4
>5.0mm	15	4	4.1	2.1	2781.6

	Biomass (mg DW m^{-2})		Abundance (ind m^{-2})		Biomass (mg DW ind^{-1})
	Night	Day	Night	Day	Mean (DWI)
0.2-0.5mm	139	108	20700	16900	0.01
0.5-1.0mm	184	126	8300	7380	0.02
1.0-2.0mm	208	133	1780	1330	0.11
2.0-5.0mm	214	86	465	247	0.40
>5.0mm	48	11	4.1	2.1	8.47

	Migrant Biomass (mg DW m^{-2})	Migrant Abundance (ind m^{-2})	Migrant Biomass (mg DW ind^{-1}) (mDWI)
0.2-0.5mm	31	3800	0.01
0.5-1.0mm	58	920	0.06
1.0-2.0mm	75	450	0.17
2.0-5.0mm	128	218	0.59
>5.0mm	37	2	18.50

Appendix Table S2.2. Mesozooplankton carbon biomass and dry weight per individual at station ALOHA calculated from the carbon biomass, dry weight, and abundance per size class reported by Landry et al. (2001) in Table 2. Values of biomass per individual used in calculations of carbon cycling (section 2.3) and active flux (section 2.5) are located on the third column. BW: carbon biomass per individual, DWI: dry weight per individual, mDWI: migrant dry weight per individual.

		Parametric terms			Smooth terms				
		Estimate	SE	p-value	Covariate	edf	p-value	R^2	n
Migrants	Intercept	0.368	0.028	< 0.001	Day of year	1.88	0.07	0.04	213
	Time	0.003	0.002	0.13					
Day	Intercept	0.770	0.016	< 0.001	Day of year	2.89	< 0.001	0.55	223
					Time	2.70	< 0.001		
Night	Intercept	1.150	0.024	< 0.001	Day of year	4.39	< 0.001	0.47	223
					Time	2.76	< 0.001		
Mean									
0.2-0.5 mm	Intercept	0.140	0.010	< 0.001	Day of year	3.97	< 0.001	0.39	221
	Time	0.001	9.E-05	< 0.001					
0.5-1.0 mm	Intercept	0.229	0.006	< 0.001	Day of year	6.67	< 0.001	0.51	221
					Time	2.78	< 0.001		
1.0-2.0 mm	Intercept	0.239	0.006	< 0.001	Day of year	3.31	< 0.001	0.44	221
					Time	3.36	< 0.001		
2.0-5.0 mm	Intercept	0.188	0.010	< 0.001	Day of year	2.80	< 0.001	0.25	221
	Time	9.E-05	7.E-05	0.1940					
> 5.0 mm	Intercept	0.034	0.004	< 0.001	Day of year	2.72	< 0.001	0.40	221
	Time	3.E-04	4.E-05	< 0.001					

Appendix Table S2.3. Results of the seasonal pattern and long-term trend of mesozooplankton biomass at station ALOHA from 1994 to 2016 evaluated by GAMs. Models of migrants, day, and, night biomass were run with untransformed data including a correlation function AR1 and a variance structure VarIdent. The temporal trend of each size class of mean mesozooplankton biomass (mean of day and night) were run following the same procedure. Day of year and time represent smooth functions of the seasonal pattern and long-term trend of biomass, respectively. SE: standard error. edf: effective degrees of freedom. R2: coefficient of determination. n: sample size (cruises analyzed).

	Period	Intercept (mg DW m^{-2})	Slope (mg DW m^{-2} y^{-1})	95% CI slope	p-value	N
Day	1994 - 2003	452.6	43.4	23.1 - 63.6	< 0.001	100
	2004 - 2016	-	-	-	0.90	125
Night	1994 - 2003	740.7	61.6	36.6 - 86.6	< 0.001	100
	2004 - 2009	1351.3	-75.3	-144.8 - -5.9	0.04	59
	2010 - 2016	-	-	-	0.42	64

Appendix Table S2.4. Results of approximate periods of increase or decrease in day and night biomass that were visually identified from GAM results (Figure S1) and evaluated by GLS models. GLS models were run with untransformed data and included a correlation function (AR1) and a variance structure (VarIdent).

		Parametric terms			Smooth terms			
		Estimate	SE	p-value	Covariate	edf	p-value	R^2
Ing/PP	Intercept	0.34	0.01	< 0.01	Year	1.59	0.10	0.17
Eg/POC	Intercept	1.36	0.15	< 0.01		-	-	0.41
	Year	0.05	0.01	0.001				
DIC/POC	Intercept	0.14	0.02	< 0.001		-	-	0.04
	Year	1.4.E-03	1.7.E-03	0.42		-	-	
DIN/PON	Intercept	0.15	0.02	< 0.001		-	-	0.001
	Year	2.5.E-04	1.8.E-03	0.89		-	-	
DIP/POP	Intercept	0.36	0.03	< 0.001	Year	1.74	0.38	0.06

Appendix Table S2.5. Interannual variability of the potential contribution of mesozooplankton to carbon cycling in the euphotic zone and export flux to the mesopelagic zone at station ALOHA from 1994 to 2014. Models were initially run using GAMs. In most cases, the effective degrees of freedom (edf) were equal to 1; therefore, the models were re-run using ordinary least squares. Ing/PP: proportion of primary production potentially ingested by mesozooplankton. Eg/POC: proportion of the fecal pellets potentially produced by mesozooplankton in the euphotic zone relative to the passive flux of particulate organic carbon (POC) collected in sediment traps at 150 m. DI/PO: proportion of the active flux of dissolved inorganic carbon (C), nitrogen (N), and phosphorus (P) mediated by migrant mesozooplankton relative to the passive flux of particulate organic C, N, and P. SE: standard error. R2: coefficient of determination. n: 21 years.

	Covariate	edf	p-value	R^2	DE (%)	GCV
NB-SS slope	PP	1.00	0.174	0.04	9.03	0.0098
	SST	3.64	**< 0.001**	0.70	74.84	0.0036
	MEI.y0	2.83	0.189	0.18	28.76	0.0093
	PDO.y0	1.00	0.881	-0.05	0.11	0.0107
	NPGO.y0	1.00	0.920	-0.05	0.05	0.0107
Size diversity	PP	1.00	**0.013**	0.23	27.12	0.0009
	SST	2.37	**0.004**	0.47	52.54	0.0007
	MEI.y0	1.00	0.854	-0.05	0.17	0.0012
	PDO.y0	1.00	0.671	-0.04	0.92	0.0012
	NPGO.y0	1.00	0.959	-0.05	0.01	0.0012
Migrant biomass	PP	3.32	0.061	0.30	40.90	0.0097
	MEI.y0	1.00	0.102	0.08	12.81	0.0112
	PDO.y0	1.00	0.435	-0.02	3.07	0.0124
	NPGO.y0	1.00	0.402	-0.01	3.54	0.0124
	MEI.y1	3.57	0.065	0.31	42.52	0.0097
	PDO.y1	1.00	0.945	-0.05	0.02	0.0128
	NPGO.y1	1.00	0.286	0.01	5.66	0.0121
	MEI.y2	1.00	0.753	-0.04	0.51	0.0128
	PDO.y2	1.00	0.526	-0.03	2.04	0.0126
	NPGO.y2	1.00	0.687	-0.04	0.83	0.0127
	MEI.y3	1.00	0.423	-0.02	3.24	0.0124
	PDO.y3	1.86	0.341	0.08	16.46	0.0117
	NPGO.y3	1.00	0.088	0.10	13.84	0.0110
	MEI.y4	1.00	0.163	0.05	9.50	0.0116
	PDO.y4	1.00	0.539	-0.03	1.91	0.0126
	NPGO.y4	1.45	0.138	0.13	19.43	0.0108

Appendix Table S2.6. Two-variable GAMs evaluating the individual effect of each environmental factor on mesozooplankton biomass size structure (NB-SS slope and size diversity) and migrant mesozooplankton biomass at station ALOHA from 1994 to 2015. Significant relationships are bold highlighted. PP: primary production, SST: sea surface temperature, MEI: Multivariate ENSO Index, PDO: Pacific Decadal Oscillation, and NPGO: North Pacific Gyre Oscillation. Climate patterns are lagged 0, 1, 2, 3, and 4 years. edf: effective degrees of freedom. R2: coefficient of determination. DE: deviance explained. GCV: generalized cross validation. n: 22

	Covariate	edf	P value	R^2	DE (%)	GCV
NB-SS slope	PP	1.00	0.097	0.75	82.51	0.0035
	SST	3.59	**< 0.001**			
	MEI.y0	1.83	0.244			
	PP	1.00	0.189	0.70	77.88	0.0040
	SST	3.64	**< 0.001**			
	PDO.y0	1.00	0.816			
	PP	1.00	0.140	0.70	78.19	0.0040
	SST	3.61	**< 0.001**			
	NPGO.y0	1.00	0.506			
Siz diveristy	PP	1.10	**0.015**	0.59	67.68	0.0006
	SST	2.32	**0.005**			
	MEI.y0	1.00	0.445			
	PP	1.00	**0.016**	0.59	67.77	0.0006
	SST	2.53	**0.005**			
	PDO.y0	1.00	0.536			
	PP	1.00	**0.006**	0.68	79.22	0.0005
	SST	3.16	**0.003**			
	NPGO.y0	3.02	0.266			

Appendix Table S2.7. Effect of environmental factors on mesozooplankton biomass size structure and migrant mesozooplankton biomass at station ALOHA from 1994 to 2015 evaluated using GAMs. The effect of both local environmental factors and large-scale climate forcing were considered in these models. n: 22

	Covariate	edf	P value	R^2	DE (%)	GCV
Migrant biomass	PP	3.30	0.143	0.30	44.24	0.0103
	MEI.y0	1.00	0.337			
	PP	3.21	0.100	0.25	40.20	0.0109
	PDO.y0	1.00	0.952			
	PP	3.14	0.115	0.25	39.89	0.0108
	NPGO.y0	1.00	0.931			
	PP	3.65	0.105	0.50	67.13	0.0090
	MEI.y1	3.65	0.139			
	PP	2.73	0.065	0.26	39.03	0.0105
	PDO.y1	1.00	0.337			
	PP	3.18	0.129	0.25	40.08	0.0109
	NPGO.y1	1.00	0.852			
	PP	3.63	**0.027**	0.39	56.70	0.0100
	MEI.y2	2.48	0.339			
	PP	3.67	**0.039**	0.35	51.95	0.0102
	PDO.y2	1.77	0.459			
	PP	2.92	0.087	0.25	38.76	0.0108
	NPGO.y2	1.00	0.540			

Appendix Table S2.7. Continued

	Covariate	edf	P value	R^2	DE (%)	GCV
Migrant biomass	PP	3.26	0.096	0.25	40.53	0.0109
	MEI.y3	1.00	0.946			
	PP	3.98	**0.002**	0.61	72.92	0.0066
	PDO.y3	2.50	**0.020**			
	PP	3.14	0.168	0.28	42.85	0.0104
	NPGO.y3	1.10	0.418			
	PP	3.40	0.078	0.36	52.86	0.0102
	MEI.y4	2.19	0.459			
	PP	3.33	0.069	0.28	42.70	0.0107
	PDO.y4	1.06	0.666			
	PP	3.33	0.159	0.30	44.36	0.0103
	NPGO.y4	1.00	0.320			

Appendix Table S2.7. Continued

APPENDIX 4

Supplementary Information

Microbial communities associated with sinking particles across an environmental gradient in the California Current System

Bellineth Valencia[1], Michael R Stukel[2], Andrew E Allen[1,3], John P McCrow[3], Ariel Rabines[3], Brian Palenik[1] and Michael R Landry[1]

[1]Scripps Institution of Oceanography, University of California San Diego, La Jolla, CA, USA; [2]Earth, Ocean, and Atmospheric Science Department, Florida State University, Tallahassee, FL, USA and [3]Microbial and Environmental Genomics, J Craig Venter Institute, La Jolla, CA, USA

Materials and Methods

Cruise plan

Samples and environmental data were collected at four sites in the southern California Current System (CCS) on the R/V Sikuliaq as part of the California Current Ecosystem – Long-Term Ecological Research (CCE-LTER) process cruise P1604 (19 April - 12 May 2016). The aim of the cruise was to evaluate the effects of the anomalously warm conditions on the pelagic ecosystem due to the 2015-2016 El Niño event. At each site, we conducted experimental cycles following water parcels over 3-5 days by a surface drifter with holey sock drogue at 15 m. Sampling began at midnight with the deployment of a sediment trap and an additional experimental drifter array (Ohman *et al.,* 2013). As we followed the arrays, the euphotic zone (0.1% surface irradiance) was characterized by taking profiles twice a day (02:00 and 12:00) with a Conductivity Temperature Depth (CTD) in a Niskin-bottle rosette, collecting discrete water samples at 6-8 depths for chlorophyll (Chl*a*), nutrients, primary production (PP), and metabarcoding. Sampling ended with the recovery of the experimental (~ 02:00) and sediment trap arrays (~ 06:00). Due to bad weather, sampling at the offshore site (OO) was interrupted, and the sediment trap array drifted for a longer period of time (Table S1).

Environmental factors

Samples were collected and processed following the protocols of the CCE-LTER program (http://oceaninformatics.ucsd.edu/datazoo/catalogs/ccelter/datasets). Chlorophyll was determined by filtering 282 ml of seawater through glass fiber filters (Whatman GF/F), extracted in 90% acetone for 24-48 hours, and the fluorescence was read on a Turner Designs 10AU fluorometer. Water for dissolved inorganic nutrients (nitrate, silicate, and phosphate) was filtered directly from the Niskin bottle through a 0.1-µm cartridge filter and frozen (50 ml) until they were analyzed by a colorimetric assay at the University of California, Santa Barbara Analytical Facility. Primary production was determined by ^{14}C uptake in 250-ml samples in on-deck incubators that simulated selected ambient light levels in the euphotic zone.

Sediment traps

Sinking particulate matter was collected at each site in VERTEX-style sediment traps that were attached below the drogued drifter array (Table S1, Figure 1). Trap arrays consisted of 12 replicate particle interceptor traps deployed at each of two depths, the base of the euphotic zone and 150 m. Each particle interceptor trap had an inner diameter of 70 mm, an aspect ratio of 8:1 (height:diameter), and baffle tubes on top to minimize resuspension during recovery (Knauer *et al.,* 1979; Stukel *et al.,* 2013b). At each depth, two particle interceptor traps were assigned for metabarcoding samples of the microbial communities (prokaryotes: 16S rRNA and *Synechococcus* ITS; eukaryotes: 18S rRNA) and the tubes were filled before deployment with either 2.2 liters of a brine or a RNA later solution (Table S1). The brine solution consisted of 0.1 µm filtered seawater and 50 g l^{-1} of NaCl, creating a density interface to prevent mixing with in situ water (Stukel *et al*., 2013b). The RNA later, made following the protocol described by

Fontanez *et al*. (2015), was used to reduce DNA degradation in the traps. Briefly, 40 ml 0.5M of EDTA, 25 ml 1M sodium citrate, and 700 grams of ammonium sulfate were combined with ultrapure water. The solution was heated and stirred until the ammonium sulfate was dissolved. The pH of the solution was adjusted to 5.2 using sulfuric acid and particles were removed from the solution by filtering through a Sterivex filter (0.2 µm) with a peristaltic pump. We filled the entire particle interceptor traps with the RNA later solution.

After recovering the trap array, sample processing followed the protocol described by Stukel *et al*. (2013b): the depth of the salinity interface was stablished, the overlying water was gently removed with a peristaltic pump, and the water was filtered through a 47-mm diameter Nitex screen (200-µm pore size) to remove mesozooplankton swimmers that were carefully checked under a dissecting microscope. Non-swimmer particles larger than 200-µm were kept in the Nitex screen, placed in a 2-ml screw-cap cryogenic vial, flash-frozen in liquid nitrogen, and stored at -80°C. The remaining water and particles were filtered through Sterivex filters (0.2 µm) with a peristaltic pump, flash frozen, and stored at -80°C. The mean volume of water filtered was 1.7 liters (range: 1.37 – 2.10 liters) for tubes filled with the brine solution and 1.8 liters (range: 1.32 – 2.10 liters) for tubes filled with the RNA later solution.

Water column

Samples for metabarcoding were collected from the mixed layer, the base of the euphotic zone, and at 150-m depth to evaluate what microbes from the water column contributed to sinking particles exported from the euphotic zone (Table S1). At each depth, 280 ml (200-µm Nitex screen) or 650 ml of seawater (500-µm Nitex screen) were pre-screened to remove mesozooplankton prior to filtration through a 25-mm diameter 0.2-µm Supor membrane filters (Pall Corporation). Once the water was filtered, the filters were folded in half, placed in 2-ml screw-cap cryogenic vials, flash-frozen in liquid nitrogen, and stored at -80°C until analysis.

Library construction and sequencing

Environmental DNA from the water column and sediment trap samples was extracted using the NucleoMag 96 Plant kit (Macherey Nagel) following the manufacturer's instructions. Supor membrane filters (water column samples) and Nitex screen filters (particles > 200 µm) were placed directly in the lysis buffer. In the case of the Sterivex filters (sediment trap samples), the cartridges were opened using pliers and the filters were cut using sterilized blades in approximately 16 pieces (8 longitudinal and 1 horizontal cut). For this step, the cartridges were placed on sterilized aluminum foil on top of dry ice to prevent the material from defrosting. Filter pieces were then transferred using sterilized forceps (ethanol-flamed) into 1.5 ml Eppendorf tubes that contained the lysis buffer. Then, the protocol of the kit was followed; DNA was eluted to 50 µl and was stored at -80°C until amplification (typically within 1-5 days). Although DNA was extracted separately for the particles <200 µm and >200 µm, these were pooled for subsequent analysis.

Once DNA was extracted, amplification was done by Polymerase Chain Reaction (PCR). The prokaryotic community was characterized by amplifying the V4-V5 regions of the 16S small subunit ribosomal RNA gene (SSU-rRNA) using primers 515F and 926R (Table S2). The eukaryotic community was characterized by amplifying the V9 region of the18S rRNA gene using primers 1389F and 1510R (Table S2). Primers contained the Illumina adaptors, the linker, and the barcoded indices. Amplification was done using the Q5 high-fidelity PCR kit (New England Biolabs) in a 25-µl reaction volume. The PCR thermal protocol consisted of an initial denaturation of 30 s at 98°C, 30 amplification cycles of 10 s at 98°C, 30 s at 56°C, and 30 s at 72°C, followed by a final extension of 2 min at 72°C, and a final holding of 4°C. The band size of the amplicons was visualized on a 1% agarose gel. Because sediment trap samples did not amplify during PCR, likely due to the organic matter present in sinking particles, we used the OneStep™ PCR Inhibitor Removal Kit (Zymo Research) following the manufacturer's instructions to remove the substances that were inhibiting amplification. PCR was then carried out using 1 µl of diluted template (1:10). PCR products were purified using Agencourt AMPure Beads XP and the concentration was quantified using PicoGreen dsDNA Quantitation Reagent.

The PCR products were pooled in equimolar amounts (~ 10 ng μl^{-1}) in 1.5 ml Eppendorf tubes and were sequenced using a dual-barcode index on an Illumina MiSeq platform at the Institute for Genomic Medicine (IGM, University of California, San Diego). Demultiplexed raw reads were provided by IGM and are available in the Archive under Accession Number.

Bioinformatic analyses

Initial quality control of the raw sequence reads (fastq files) was done using the workflow for read filtering, swarm Operational Taxonomic Unit (OTU) clustering, and taxonomic classification of the SSU-rRNA written by JP McCrow (https://github.com/allenlab/rRNA_pipeline). Briefly, paired-end reads were aligned using PEAR (Zhang *et al.,* 2014) and quality trimmed to Phred score 30 (Q30 minimum average in sliding window of size 2 bp) for 18S V9 amplicons or Q20 for 16S amplicons due to lower maximum quality scores. Possible chimeras were found and filtered using USEARCH (Edgar 2010). Amplicons were clustered using SWARM into OTUs (Mahé *et al.,* 2014) and taxonomic assignment was done by the best hit from GLSEARCH36 (Pearson, 2016) against the appropriate reference database: Silva v128 (Quast *et al.,* 2013) and phytoRef (Decelle *et al.,* 2015) were used for prokaryotes and potential plastid sequences, respectively, whereas PR2 with the taxonomic updates from the Tara Oceans-W2 was used for eukaryotes (de Vargas *et al.,* 2015). Total number of sequence reads and OTUs per sample from the initial filtered OTU tables are summarized in Tables S3-S6.

The initial filtered OTU table for each library were processed further before multivariate analyses. An additional qualitative control was done following the next steps: 1) For the 18S, non-eukaryote sequence reads were removed (archaeal, bacterial, organelle, and unassigned), whereas for the 16S, only bacterial and archaeal sequence reads were kept (eukaryotes were omitted). 2) OTUs with only 1 sequence read in the entire data set (singletons) were removed. 3) OTUs that were assigned to the same species, but that occurred multiple times in the OTU table were merged to have each species only once (merge of over-split OTUs). 4) The taxonomy

of each OTU down to the genus level was examined based on the information available in the World Register of Marine Species (WoRMS, www.marinespecies.org/) using the "Match taxa" function. This step helped to fill the gaps in the taxonomic information and to correct misassignations. 5) OTUs assigned only to a supergroup level (e.g., Opisthokonta_X, Stramenopiles_X) were removed. 6) For the 18S OTU table, OTUs assigned to the Class Streptophyta (land plants) were removed. These final OTU tables (Tables S3-S6, "working OTU table") were used for analyzing the microbial communities of the sediment-trap and water-column samples.

Synechococcus *sequence analysis and classification*

The different *Synechococcus* strains were classified by sequencing the 16S-23S rRNA internal transcribed spacer (ITS) using primers ITS1F and ITS4R (Table S2). Amplification, sequencing, and bioinformatics processing (denoising, chimera detection, and OTU clustering) of *Synechococcus* sequences was carried out at RTL Genomics (Lubbock, Texas). The OTUs were assigned at a 97% cutoff. OTU classification was carried out using MOTHUR (Schloss *et al*., 2009) and a *Synechococcus* ITS database from Choi *et al*. (2014). OTUs that were assigned to the same strain were merged. The total number of sequence reads and OTUs per sample from the initial and working OTU tables are summarized in Tables S3 and S5.

Multivariate analyses of metagenomic data

Multivariate analyses of the microbial communities were done at the genus level for each OTU table. Prior to analyses, the relative abundances per sample were calculated from the sequence reads of each genus. Because most microbes occur rarely, only the genera that contributed >1% to the relative abundance in any sample were considered for analyses. After this step, the relative abundances per sample were recalculated and square-root transformed to reduce the effect of the most abundant genera.

To identify the similarity/dissimilarity of the structure of the microbial communities between sites and to characterize the microbes that differentiate those communities, we applied a set of multivariate analyses that included hierarchical clustering, similarity profile (SIMPROF), non-metric multidimensional scaling (nMDS), and similarity percentage (SIMPER). All these analyses are based on the Bray-Curtis dissimilarity index, which evaluates the structure of the communities by comparing the compositions and relative abundances of the genera among samples. The dissimilarity of the microbial communities among samples was evaluated by means of a hierarchical cluster analysis with a group average linkage, and the significance of the clusters was defined by the Simprof analysis (alpha level < 0.05). Ordination plots based on the nMDS analysis were also used to represent in few dimensions the relationship of the communities between samples. The groups of samples that were significantly clustered by the Simprof analysis were examined further by means of the Simper analysis, in order to establish the genera that differentiated each group. However, samples that were not clustered to any group (significantly different than any other sample) were joined to the closest cluster if the type of

samples were similar (e.g., a sediment trap sample joined to a group of sediment traps samples from the same sampling site).

All multivariate analyses were done using the package ‘vegan’ in R (Oksanen *et al.,* 2017). Simprof analysis was done using the package ‘clustsig’ in R (Whitaker and Christman, 2015).

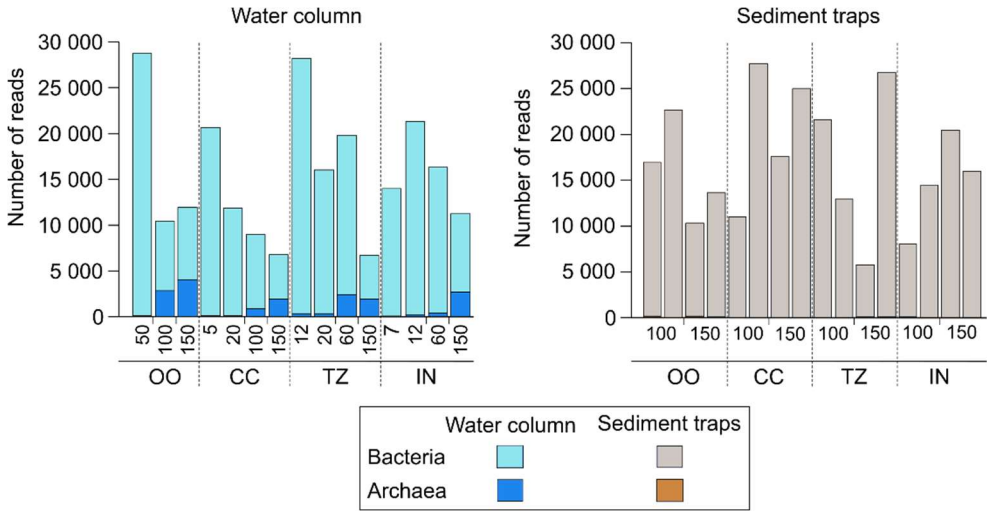

Appendix Figure S4.1. Number of sequence reads of prokaryotes (16S rRNA) in water-column and sediment-trap samples across an environmental gradient in the California Current System. OO: oligotrophic offshore, CC: California Current, TZ: transition zone, IN: inshore.

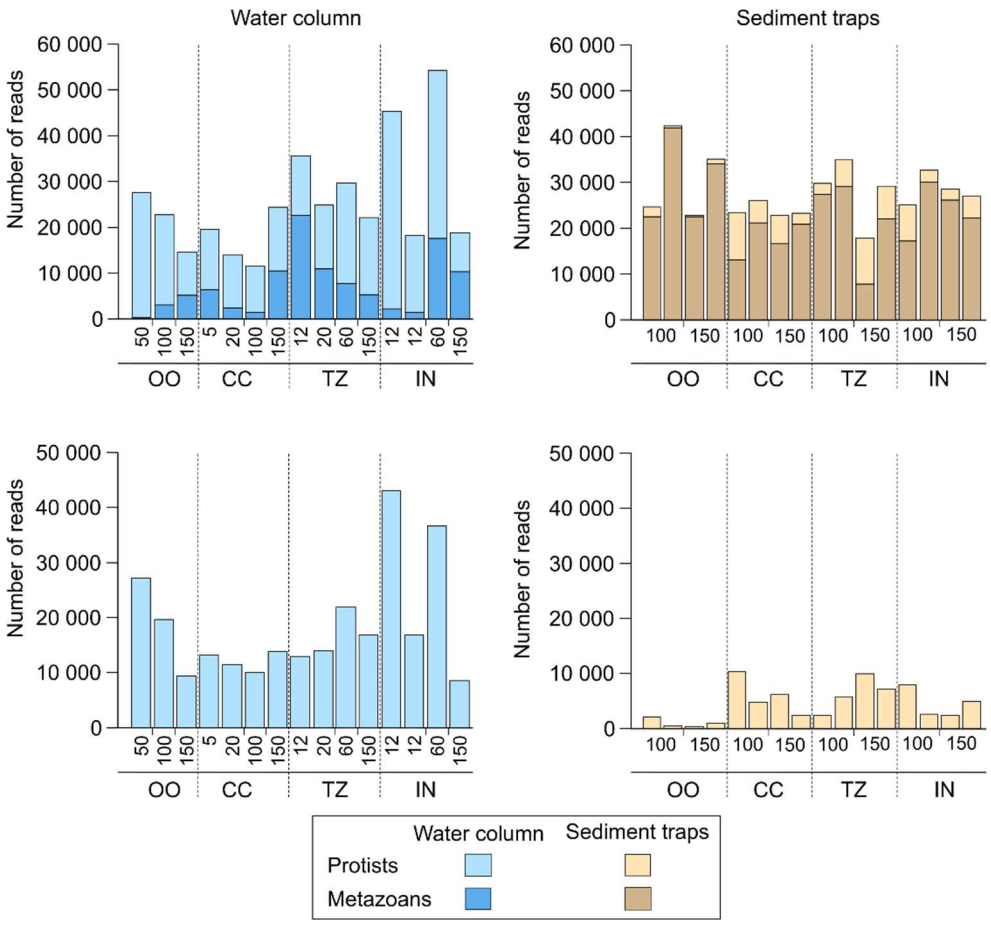

Appendix Figure S4.2. Number of sequence reads of eukaryotes (18S rRNA) in water column and sediment trap samples across an environmental gradient in the California Current System. OO: oligotrophic offshore, CC: California Current, TZ: transition zone, IN: inshore.

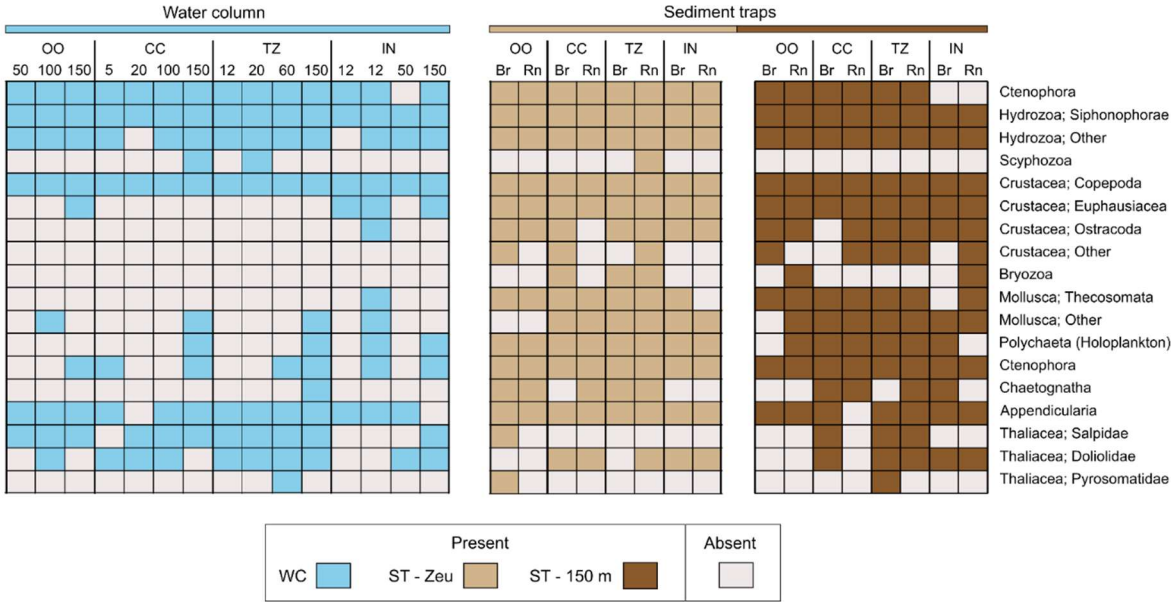

Appendix Figure S4.3. Presence-absence of metazoans in metagenomic samples from the California Current System (CCS). Samples were collected at three depths in the water column (mixed layer, base of the euphotic zone, and 150 m) and at the base of the euphotic zone (Zeu) and 150 m in sediment traps. A gradient in productivity across the CCS was followed: oligotrophic offshore (OO), California Current (CC), transition zone (TZ), inshore (IN). Except for the offshore site (OO), two water-column samples were collected in the mixed layer. In the heatmap of the water column, numbers denote the depths at which samples were collected. For the sediment trap samples, heatmps were separated by depth, and the letters on top indicate if the trap tubes were filled with a brine (Br) or RNA later solution (Rn). Some groups were omitted: Arachnida, Insecta, Vertebrata, Anthozoa, Nudibranchia, Nemertea, Platyhelminthes, Sipuncula, Ascidiacea.

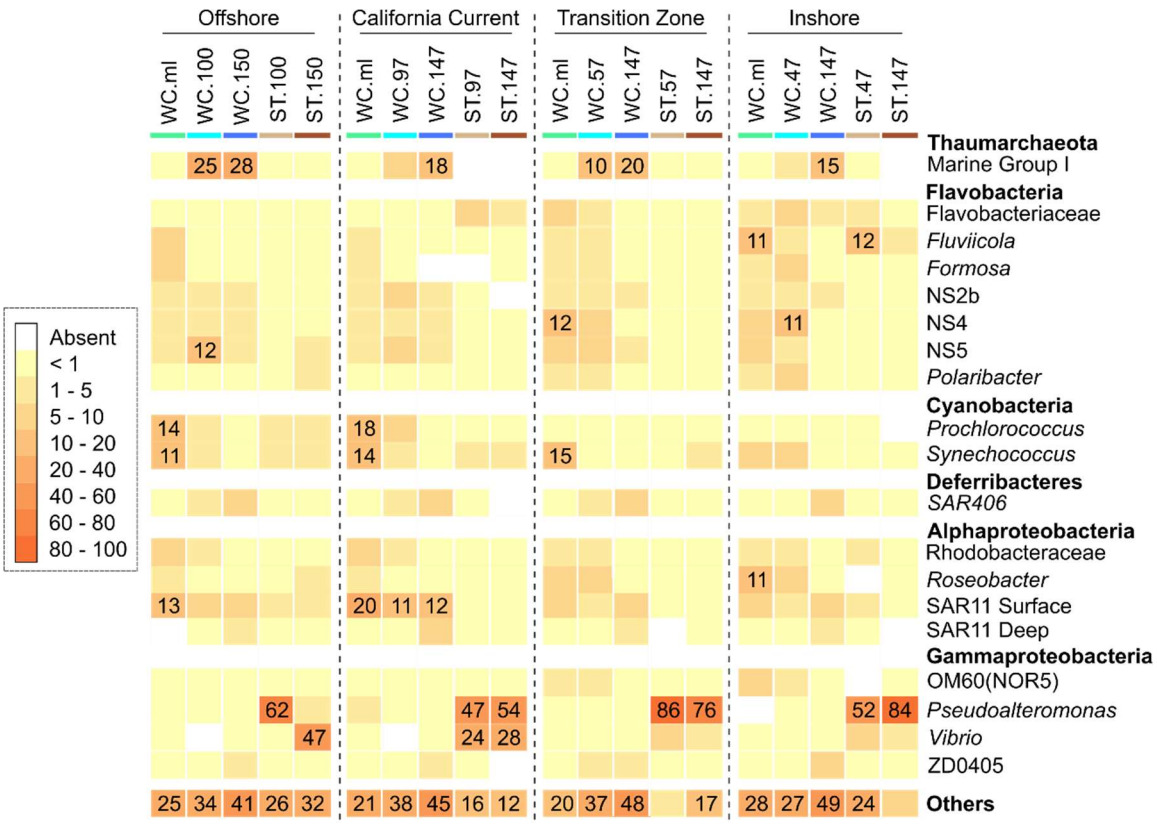

Appendix Figure S4.4. Percentages of most abundant prokaryotes (>5% in any sample) in the water column and sinking particles in the California Current System based on 16S rRNA amplicon sequencing. Percentages are shown for the genera that contributed >10% in a sample. WC: water column, ST: sediment traps.

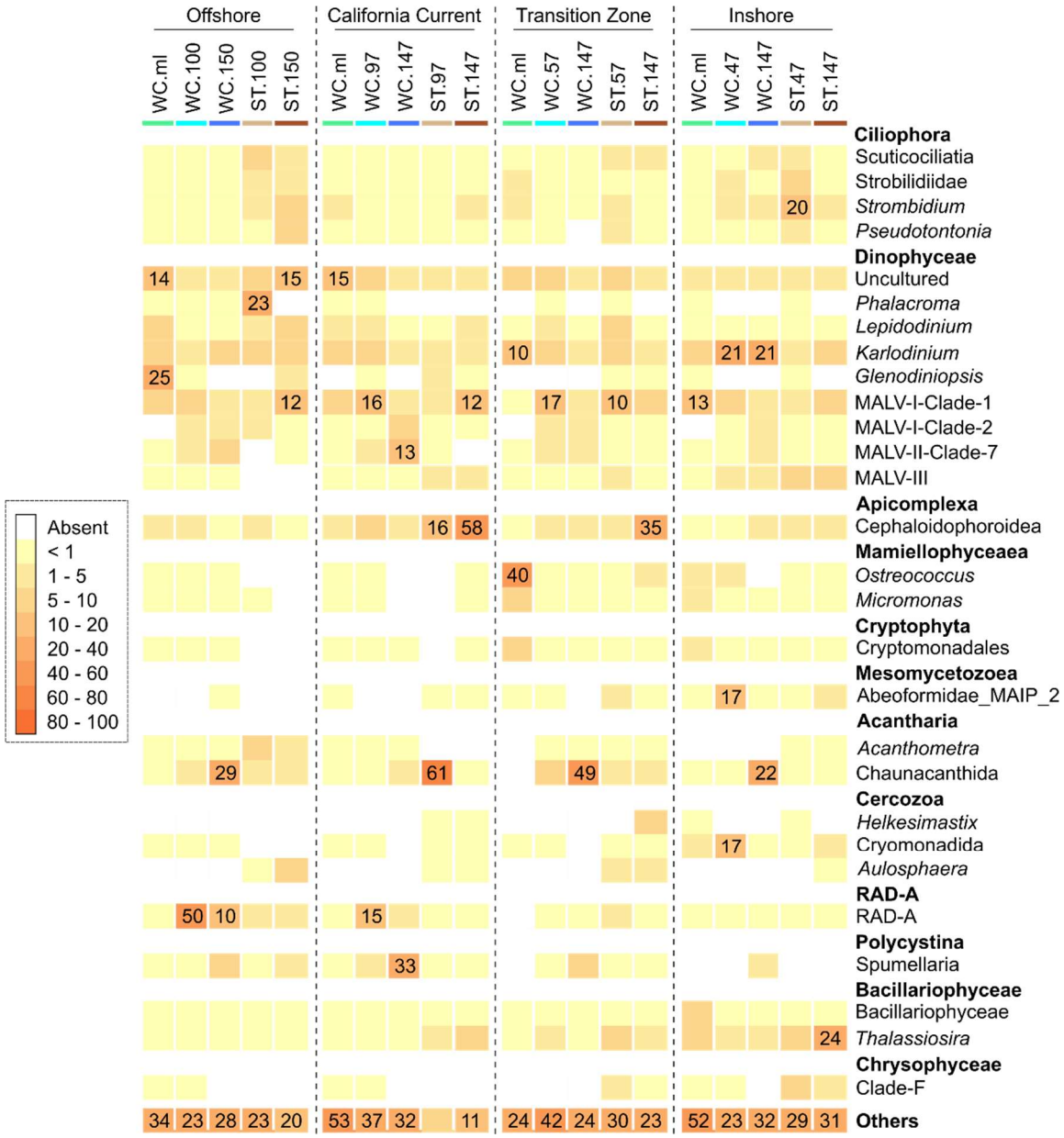

Appendix Figure S4.5. Percentages of most abundant protists (>5% in any sample) in the water column and sinking particles in the California Current System based on 18S rRNA amplicon sequencing. Percentages are shown for the genera that contributed >10% in a sample. WC: water column, ST: sediment traps.

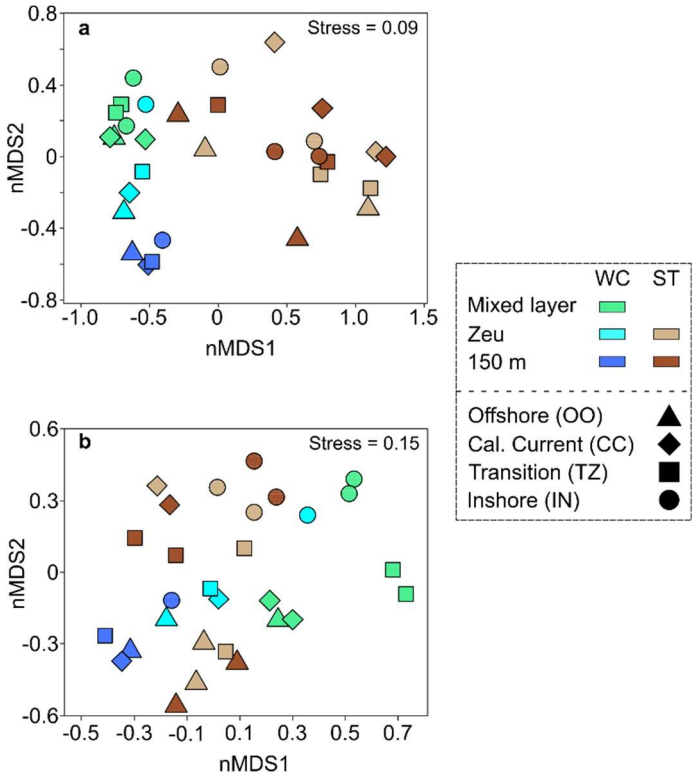

Appendix Figure S4.6. Microbial community structure in the water column and sinking particles across an environmental gradient in the California Current System evaluated by ordination analysis (nMDS). **(a)** Prokaryotic assemblages from 16S rRNA. **(b)** Protists assemblages from 18S rRNA. Colors indicate sample type (WC: water column, ST: sediment trap) and symbol shapes the sampling locations. Hierarchical cluster and SIMPER analysis for the prokaryotic and protist assemblages are presented in Figures 3 and 4, respectively.

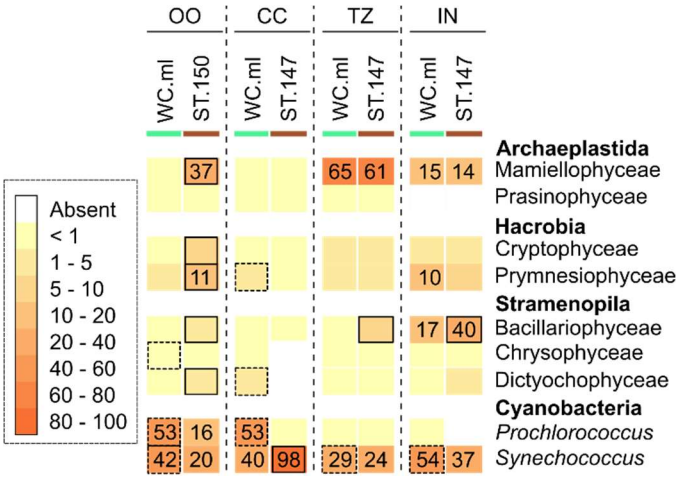

Appendix Figure S4.7. Contributions of eukaryotic phytoplankton and cyanobacteria (*Prochlorococcus* and *Synechococcus*) to sinking particles relative to their contributions in the mixed layer. Sequences of eukaryotic phytoplankton were obtained from plastid data amplified using the 16S rRNA. Only classes with relative abundance >5% in any mixed-layer sample are shown. Microbes with relative abundances significantly higher in sinking particles compared to their relative contribution in the water column are highlighted with black squares (Fisher exact test for difference between proportions greater than 1, FDR < 0.05, Table S9). Percentages are shown for the classes that contributed more than 10% in a sample. WC: water column, ST: sediment traps, B: brine solution, R: RNA later solution. OO: oligotrophic offshore, CC: California Current, TZ: transition zone, IN: inshore.

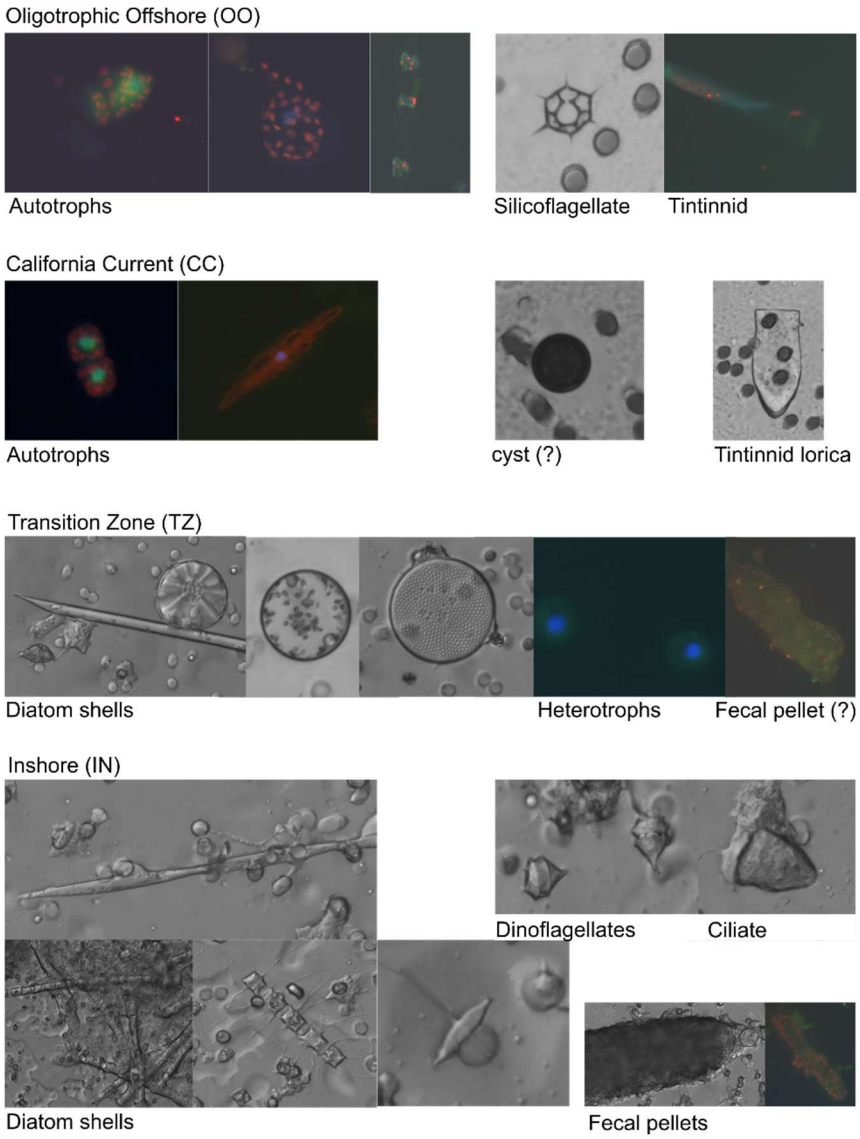

Appendix Figure S4.8. Microscopy images of some particles collected in sediment traps at four sites in the California Current System during the CCE-LTER process cruise P1604.

Sediment traps					
Zone	**Dates drifting**	**Total (days)**	**Depth (m)**	**Treatment**	**Screened (um)**
Oligotrophic	22.April.2016	5.6	100	Brine	200
Offshore (OO)	27.April.2016		100	RNA later	200
[Cycle 1]			150	Brine	200
			150	RNA later	200
	29.April. 2016	3.3	97	Brine	200
California	02.May.2016		97	RNA later	200
Current (CC)			147	Brine	200
[Cycle 2]			147	RNA later	200
	03.May.2016	3.2	60	Brine	200
Transition Zone (TZ)	06.May.2016		60	RNA later	200
[Cylce 3]			150	Brine	200
			150	RNA later	200
	07.May.2016	3.3	50	Brine	200
Inshore (IN)	10.May.2016		50	RNA later	200
[Cycle 4]			150	Brine	200
			150	RNA later	200

Appendix Table S4.1. Summary information on samples collected to evaluate the microbial communities of sinking particles in the California Current System. Dates drifting = dates of deployment and recovery of the sediment trap arrays in each zone. Total = time the trap array was drifting. Screened = pore size of the Nitex screen used to remove mesozooplankton before filtering the seawater and particles. The information in brackets refers to specific experimental cycles of CCE-LTER Process cruise P1604.

		Water column			
Zone	**Date collected**		**Depth (m)**	**Volume (ml)**	**Screened (um)**
Oligotrophic	22-April-2016	-	50	650	500
Offshore (OO)	22-April-2016	-	100	650	500
	22-April-2016	-	150	650	500
	02-May--2016	-	5	280	200
California	30-April-2016	-	20	650	500
Current (CC)	30-April-2016	-	100	650	500
	30-April-2016	-	150	650	500
	05-May--2016	-	12	280	200
Transition Zone (TZ)	04-May--2016	-	20	280	200
	04-May--2016	-	60	650	500
	04-May--2016	-	150	650	500
	10-May--2016	-	7	650	500
	08-May--2016	-	12	280	200
Inshore (IN)	09-May--2016	-	12	280	200
	10-May--2016	-	50	650	500
	10-May--2016	-	150	650	500

Appendix Table S4.1. Continued

Forward	Reverse	Amplicon size
Prokaryotes – 16S		
515F	926R	
GTGYCAGCMGCCGCGGTAA	CCGYCAATTYMTTTRAGTTT	~ 527 bp
Synechococcus		
ITS1F	ITS4R	
CTTGGTCATTTAGAGGAAGTAA	TCCTCCGCTTATTGATATGC	~ 350 bp
Eukaryotes – 18S V9		
1389F	1510R	
TTGTACACACCGCCC	CCTTCYGCAGGTTCACCTAC	~ 290 bp

Appendix Table S4.2. Primer information.

	Original OTU table		Working OTU table	
	No. of reads	OTUs	No. of reads	OTUs
16S	507494	11233	502169	984
18S	1300965	6543	826592	720
ITS	441630	414	441628	14

Appendix Table S4.3. Number of sequence reads and Operational Taxonomic Units (OTUs) obtained for each primer set used. Working OTU table: we further processed the original OTU table by removing the singletons and by merging the sequence reads of the over-split OTUs (multiple OTUs assigned to the same species) to have each species only once.

			Sediment traps						
			Original OTU table - 16S rRNA						
			No. of reads				No. of OTUs		
Site	Depth (m)	Treatment	Archaea	Bacteria	Eukaryota	Total	Archaea	Bacteria	Total
OO	100	Brine	145	16809	547	17501	24	729	753
	100	RNA later	2	22632	527	23161	2	258	260
	150	Brine	119	10209	0	10328	18	1163	1181
	150	RNA later	8	13592	9	13609	4	454	458
CC	97	Brine	4	10925	15	10944	1	482	483
	97	RNA later	0	27669	2	27671	0	470	470
	147	Brine	1	17506	0	17507	1	368	369
	147	RNA later	0	24950	57	25007	0	698	698
TZ	57	Brine	2	21533	1032	22567	2	243	245
	57	RNA later	0	12960	8	12968	0	471	471
	147	Brine	36	5736	36	5808	11	652	663
	147	RNA later	12	26663	1	26676	5	626	631
IN	47	Brine	18	8018	4	8040	8	692	700
	47	RNA later	5	14438	5	14448	4	563	567
	147	Brine	2	20449	11	20462	2	670	672
	147	RNA later	1	15960	5	15966	1	708	709

Appndix Table S4.4. Number of sequence reads and Operational Taxonomic Units (OTUs) per sample of the prokaryotic microbial community as evaluated by 16S rRNA. Working OTU table: we further processed the original OTU table by removing the singletons and by merging the sequence reads of the over-split OTUs (multiple OTUs assigned to the same species) to have each species only once. OO: oligotrophic offshore, CC: California Current, TZ: transition zone, IN: inshore.

			Sediment traps					
			Working OTU table - 16S rRNA					
			No. of reads			No. of unique OTUs		
Site	**Depth (m)**	**Treatment**	**Archaea**	**Bacteria**	**Total**	**Archaea**	**Bacteria**	**Total**
OO	100	Brine	145	16804	16949	11	360	371
	100	RNA later	2	22630	22632	2	154	156
	150	Brine	119	10145	10264	9	430	439
	150	RNA later	8	13585	13593	2	261	263
CC	97	Brine	4	10904	10908	1	216	217
	97	RNA later	0	27665	27665	0	171	171
	147	Brine	1	17506	17507	1	129	130
	147	RNA later	0	24932	24932	0	245	245
TZ	57	Brine	2	21529	21531	2	136	138
	57	RNA later	0	12948	12948	0	190	190
	147	Brine	36	5708	5744	7	336	343
	147	RNA later	12	26657	26669	5	259	264
IN	47	Brine	18	7979	7997	5	331	336
	47	RNA later	5	14419	14424	4	236	240
	147	Brine	2	20431	20433	2	256	258
	147	RNA later	1	15924	15925	1	269	270

Appndix Table S4.4. Continued

Water column											
			Original OTU table - 16S rRNA								
			No. of reads				No. of OTUs				
Site	Depth (m)		Archaea	Bacteria	Eukaryota	Total	Archae	Bacteria	Total	Bacteria	Total
OO	50	-	15	28740	0	28755	6	1613	1619	281	284
	100	-	2757	7653	0	10410	101	929	1030	265	279
	150	-	3958	7898	0	11856	247	1009	1256	272	292
CC	5	-	41	20672	1	20714	15	1416	1431	299	306
	20	-	9	11866	0	11875	8	1160	1168	236	241
	100	-	844	8121	0	8965	76	947	1023	259	271
	150	-	1837	4860	2	6699	196	832	1028	235	254
TZ	12	-	269	28667	0	28936	20	2942	2962	295	303
	20	-	242	15930	1	16173	33	1225	1258	223	228
	60	-	2344	17660	0	20004	129	2080	2209	388	403
	150	-	1840	4827	4	6671	178	818	996	245	263
IN	7	-	4	14275	0	14279	3	1758	1761	240	242
	12	-	162	21375	0	21537	28	1467	1495	269	276
	50	-	342	16458	0	16800	62	2280	2342	331	341
	150	-	2600	8557	0	11157	200	978	1178	293	315

Appndix Table S4.4. Continued

			Water column					
			Working OTU table - 16S rRNA					
			No. of reads			No. of unique OTUs		
Site	Depth (m)		Archae	Bacteria	Total	Archae	Bacteria	Total
OO	50	-	15	28611	28626	3	281	284
	100	-	2757	7614	10371	14	265	279
	150	-	3958	7888	11846	20	272	292
CC	5	-	41	20552	20593	7	299	306
	20	-	9	11775	11784	5	236	241
	100	-	838	8075	8913	12	259	271
	150	-	1836	4855	6691	19	235	254
TZ	12	-	267	27970	28237	8	295	303
	20	-	236	15739	15975	5	223	228
	60	-	2340	17399	19739	15	388	403
	150	-	1840	4824	6664	18	245	263
IN	7	-	4	13914	13918	2	240	242
	12	-	157	21067	21224	7	269	276
	50	-	340	15988	16328	10	331	341
	150	-	2600	8539	11139	22	293	315

Appndix Table S4.4. Continued

Sediment traps							
				Original OTU table		Working OTU table	
Site	Cycle	Depth (m)	Treatment	Reads	OTUs	Reads	OTUs
Oligotrophic Offshore	C1	100	Brine	14989	232	14989	13
		100	RNA later	15075	240	15075	14
		150	Brine	13861	215	13861	12
		150	RNA later	28434	264	28434	13
California Current	C2	97	Brine				
		97	RNA later	17145	217	17145	10
		147	Brine	24326	235	24326	8
		147	RNA later	12113	129	12113	6
Transition Zone	C3	57	Brine	19769	215	19769	10
		57	RNA later	19606	282	19606	8
		147	Brine	14813	231	14813	8
		147	RNA later	18236	264	18236	7
Inshore	C4	47	Brine	12719	169	12719	6
		47	RNA later	11397	216	11396	8
		147	Brine	12744	247	12744	6
		147	RNA later	6760	103	6760	6

Appendix Table S4.5. Number of sequence reads and Operational Taxonomic Units (OTUs) per sample of *Synechococcus* as evaluated by the ITS. Working OTU table: we further processed the original OTU table by removing the singletons and by merging the sequence reads of the over-split OTUs (multiple OTUs assigned to the same clade) to have each clade only once.

Water column							
				Original OTU table		Working OTU table	
Zone	**Cycle**	**Depth (m)**		**Reads**	**OTUs**	**Reads**	**OTUs**
Oligotrophic		50	-	21493	308	21492	14
Offshore	C1	100	-	7736	217	7736	9
		150	-	24413	168	24413	8
California		20	-	7669	145	7669	9
Current	C2	100	-	18680	268	18680	9
		150	-	17635	212	17635	10
		20	-	16665	207	16665	6
Transition	C3	60	-	23331	244	23331	7
Zone		150	-	19120	172	19120	8
		7	-	10814	187	10814	6
Inshore	C4	50	-	22356	270	22356	6
		150	-	9731	140	9731	6

Appendix Table S4.5. Continued.

			Sediment traps				
			Original OTU table - 18S rRNA				
			No. of reads			No. of OTUs	
Site	Depth (m)	Treatment	Porkaryotes	Unid	Eukaryota	Metazoans	Microbes
OO	100	Brine	150	2	25274	84	339
	100	RNA later	328	0	42809	90	151
	150	Brine	4	0	23007	71	102
	150	RNA later	143	0	35311	111	193
CC	97	Brine	25	4	28226	94	153
	97	RNA later	3596	1	29387	103	232
	147	Brine	3423	3	27206	97	262
	147	RNA later	309	0	24478	67	66
TZ	57	Brine	679	4	29736	105	416
	57	RNA later	3758	27	35140	129	489
	147	Brine	2991	27	17784	92	598
	147	RNA later	4370	5	29245	107	362
IN	47	Brine	641	27	25150	126	559
	47	RNA later	617	1	32700	73	272
	147	Brine	539	3	28596	98	279
	147	RNA later	1376	2	27057	86	311

Appendix Table S4.6. Number of sequence reads and Operational Taxonomic Units (OTUs) per sample of the eukaryotic community as evaluated by 18S rRNA. Working OTU table: we further processed the original OTU table by removing the singletons and by merging the sequence reads of the over-split OTUs (multiple OTUs assigned to the same species) to have each species only once. OO: oligotrophic offshore, CC: California Current, TZ: transition zone, IN: inshore. Unid: unidentified.

			Sediment traps					
			Working OTU table - 18S rRNA					
			No. of reads			No. of unique OTUs		
Site	Depth (m)	Treatment	Metazoans	Microbes	Total	Metazoans	Microbes	Total
OO	100	Brine	22425	2136	24561	34	120	154
	100	RNA later	41906	454	42360	37	78	115
	150	Brine	22443	364	22807	31	45	76
	150	RNA later	34070	991	35061	37	70	107
CC	97	Brine	13061	10334	23395	44	71	115
	97	RNA later	21164	4787	25951	41	113	154
	147	Brine	16663	6109	22772	46	108	154
	147	RNA later	20783	2405	23188	33	36	69
TZ	57	Brine	27356	2368	29724	35	132	167
	57	RNA later	29118	5759	34877	58	210	268
	147	Brine	7815	9923	17738	49	212	261
	147	RNA later	22055	7166	29221	45	155	200
IN	47	Brine	17258	7850	25108	45	223	268
	47	RNA later	30070	2616	32686	34	138	172
	147	Brine	26196	2389	28585	40	158	198
	147	RNA later	22168	4817	26985	37	174	211

Appendix Table S4.6. Continued

			Water column				
			Original OTU table - 18S rRNA				
			No. of reads			No. of OTUs	
Site	Depth (m)		Porkaryotes	Unid	Eukaryota	Metazoans	Microbes
OO	50	-	41247	27	27569	19	1132
	100	-	19121	3807	22629	24	1003
	150	-	21393	4131	14470	23	788
CC	5	-	22536	26	19643	27	947
	20	-	35904	26	13946	19	967
	100	-	24894	1833	11413	22	944
	150	-	34671	4409	24296	40	921
TZ	12	-	18571	143	35522	38	339
	20	-	19575	291	24786	38	454
	60	-	62211	8638	29675	46	1108
	150	-	33941	4823	22088	43	795
IN	12	-	9388	242	45403	13	976
	12	-	12108	113	18184	69	772
	50	-	32330	1005	54181	37	786
	150	-	15421	1420	18754	32	799

Appendix Table S4.6. Continued

			Water column					
			Working OTU table - 18S rRNA					
			No. of reads			No. of unique OTUs		
Site	Depth (m)		Metazoans	Microbes	Total	Metazoans	Microbes	Total
OO	50	-	286	27223	27509	14	280	294
	100	-	2999	19603	22602	15	262	277
	150	-	5059	9402	14461	15	201	216
CC	5	-	6291	13152	19443	15	250	265
	20	-	2434	11472	13906	13	260	273
	100	-	1366	10006	11372	17	249	266
	150	-	10396	13872	24268	28	195	223
TZ	12	-	22499	12997	35496	16	149	165
	20	-	10799	13930	24729	15	177	192
	60	-	7669	21922	29591	27	288	315
	150	-	5231	16839	22070	30	195	225
IN	12	-	2117	43111	45228	9	293	302
	12	-	1272	16803	18075	36	272	308
	50	-	17499	36632	54131	12	273	285
	150	-	10159	8533	18692	21	246	267

Appendix Table S4.6. Continued

	OO		CC	
	WC-ml vs. ST-150m		WC-ml vs. ST-147m	
	Difference	p-value	Difference	p-value
Bacteroidetes				
Flavobacteriaceae	-6.3	**< 0.0001**	-59.3	**< 0.0001**
Fluviicola	3.5	< 0.0001	2.0	< 0.0001
Formosa	7.3	< 0.0001	4.4	< 0.0001
NS4	1.4	0.017	4.0	< 0.0001
NS5	-4.3	**< 0.0001**	4.5	< 0.0001
Cyanobacteria				
Prochlorococcus	4.0	< 0.0001	24.9	< 0.0001
Synechococcus	-4.7	**< 0.0001**	-17.9	**< 0.0001**
Proteobacteria				
Rhodobacteraceae	8.0	< 0.0001	7.1	< 0.0001
Roseobacter	-9.5	**< 0.0001**	3.0	< 0.0001
SAR11 Surface 1	6.2	< 0.0001	27.8	< 0.0001
OM60(NOR5)	-5.7	**< 0.0001**	-0.4	ns

Appendix Table S4.7. Contributions of prokaryotes to sinking particulate matter (ST-150 m) relative to their contributions to the water column (WC-ml: mixed layer) across the California Current System. Negative differences between proportions indicate that the relative abundance of the microbes was higher in sinking particles than in the water column. The difference between relative contributions was evaluated by pairwise comparisons using the Fisher exact test. Only genera with relative abundances >5% in any mixed-layer sample were included in the analysis. Microbes with relative abundances significantly higher in sinking particles relative to their contributions in the water column are highlighted in bold (FDR < 0.05). OO: oligotrophic offshore, CC: California Current, TZ: transition zone, IN: inshore.

	TZ		IN	
	WC-ml vs. ST-147m		WC-ml vs. ST-147m	
	Difference	p-value	Difference	p-value
Bacteroidetes				
Flavobacteriaceae	-11.6	**< 0.0001**	-9.5	**< 0.0001**
Fluviicola	-6.6	**< 0.0001**	-11.4	**< 0.0001**
Formosa	4.8	< 0.0001	1.4	ns
NS4	13.1	< 0.0001	4.6	< 0.0001
NS5	4.4	< 0.0001	3.8	< 0.0001
Cyanobacteria				
Prochlorococcus	-0.4	**0.020**	0.0	ns
Synechococcus	-2.3	ns	8.4	< 0.0001
Proteobacteria				
Rhodobacteraceae	-1.6	ns	-3.2	**< 0.0001**
Roseobacter	1.1	ns	1.4	ns
SAR11 Surface 1	-0.7	ns	-1.0	ns
OM60(NOR5)	-0.3	ns	5.5	< 0.0001

Appendix Table S4.7. Continued

	OO		CC	
	WC-ml vs. ST-150m		WC-ml vs. ST-147m	
	Difference	p-value	Difference	p-value
Dinophyceae_Uncultured	-10.3	**< 0.0001**	28.8	< 0.0001
Lepidodinium	-10.4	**< 0.0001**	5.8	< 0.0001
Karlodinium	-4.0	ns	15.4	< 0.0001
Glenodiniopsis	36.5	< 0.0001	-3.0	**< 0.0001**
MALV-I Clade I	-11.9	**< 0.0001**	-22.4	**< 0.0001**
Ostreococcus	0.0	ns	-0.1	ns
Micromonas	0.1	ns	1.1	0.001
Cryptomonadales	0.1	ns	0.2	ns
Bacillariophyceae	0.3	ns	0.3	ns
Thalassiosira	-0.5	**< 0.0001**	-26.2	**< 0.0001**

Appendix Table S4.8. Contributions of protists to sinking particulate matter (ST-150 m) relative to their contributions to the water column (WC-ml: mixed layer) across the California Current System. Negative differences between proportions indicate that the relative abundance of the microbes was higher in sinking particles than in the water column. The difference between relative contributions was evaluated by pairwise comparisons using the Fisher exact test. Only genera with relative abundances >5% in any mixed-layer sample were included in the analysis. Microbes with relative abundances significantly higher in sinking particles relative to their contributions in the water column are highlighted in bold (FDR < 0.05). OO: oligotrophic offshore, CC: California Current, TZ: transition zone, IN: inshore.

	TZ		IN	
	WC-ml vs. ST-147m		WC-ml vs. ST-147m	
	Difference	p-value	Difference	p-value
Dinophyceae_Uncultured	-8.6	**< 0.0001**	-1.0	ns
Lepidodinium	-2.0	**< 0.0001**	-0.7	**< 0.0001**
Karlodinium	-6.6	**< 0.0001**	-1.6	ns
Glenodiniopsis	-0.1	ns	0.0	ns
MALV-I Clade I	-27.9	**< 0.0001**	9.2	< 0.0001
Ostreococcus	47.1	< 0.0001	2.8	< 0.0001
Micromonas	7.3	< 0.0001	8.5	< 0.0001
Cryptomonadales	6.8	< 0.0001	3.1	< 0.0001
Bacillariophyceae	-1.1	**< 0.0001**	16.4	< 0.0001
Thalassiosira	-14.9	**< 0.0001**	-36.7	**< 0.0001**

Appendix Table S4.8. Continued

	OO		CC	
	WC-ml vs. ST-150m		WC-ml vs. ST-147m	
	Difference	p-value	Difference	p-value
Mamiellophyceae	-37.1	**< 0.0001**	0.6	ns
Prasinophyceae	0.2	ns	0.1	ns
Cryptophyceae	-7.9	**< 0.0001**	-0.1	ns
Prymnesiophyceae	-7.6	**< 0.0001**	3.6	< 0.0001
Bacillariophyceae	-4.5	**< 0.0001**	-0.2	ns
Chrysophyceae	0.5	0.021	0.5	ns
Dictyochophyceae	-1.7	**< 0.0001**	1.7	0.001
Cyanobacteria; *Prochlorococcus*	37.0	< 0.0001	52.4	< 0.0001
Cyanobacteria; *Synechococcus*	21.1	< 0.0001	-58.6	**< 0.0001**

Appendix Table S4.9. Contributions of eukaryotic phytoplankton and cyanobacteria to sinking particulate matter across the California Current System. For this analysis, sequences of eukaryotic phytoplankton were obtained from the plastids amplified with the 16S primers. Only classes with relative abundances >5% in any mixed-layer sample were included in the analysis. Negative differences between proportions indicate that the relative abundance of phytoplankton was higher in sinking particles than in the water column. The difference between the relative contributions was evaluated by pairwise comparisons using the Fisher exact test. Phytoplankton with relative abundances significantly higher in sinking particles relative to their contributions in the mixed layer are highlighted in bold (FDR < 0.05). OO: oligotrophic offshore, CC: California Current, TZ: transition zone, IN: inshore.

	TZ		IN	
	WC-ml vs. ST-147m		WC-ml vs. ST-147m	
	Difference	p-value	Difference	p-value
Mamiellophyceae	3.2	ns	1.0	ns
Prasinophyceae	-0.1	ns	0.0	ns
Cryptophyceae	-1.5	ns	2.1	ns
Prymnesiophyceae	-1.3	ns	4.7	ns
Bacillariophyceae	-5.1	**< 0.0001**	-22.7	**< 0.0001**
Chrysophyceae	-0.1	ns	0.0	ns
Dictyochophyceae	-0.1	ns	-1.5	ns
Cyanobacteria; *Prochlorococcus*	-0.3	ns	0.1	ns
Cyanobacteria; *Synechococcus*	5.3	0.003	16.1	0.001

Appendix Table S4.9. Continued

	OO		CC	
	WC-ml vs. ST-150m		WC-ml vs. ST-147m	
	Difference	p-value	Difference	p-value
Syn_CRD1	-0.7	**< 0.0001**	0.0	ns
Syn_CRD2	2.2	< 0.0001	4.2	< 0.0001
Syn_I_CC9311	0.5	< 0.0001	-0.7	**< 0.0001**
Syn_I	-30.6	**< 0.0001**	-42.8	**< 0.0001**
Syn_II	0.8	< 0.0001	1.7	< 0.0001
Syn_III	0.6	< 0.0001	0.0	ns
Syn_IV_CC9902	0.6	< 0.0001	-0.1	ns
Syn_IV_RHCU13	6.2	< 0.0001	4.3	< 0.0001
Syn_IV	23.8	< 0.0001	35.7	< 0.0001
Syn_MS2	0.2	< 0.0001	0.0	ns
Syn_UC_A	0.1	< 0.0001	0.0	ns
Syn_WPC1	0.3	< 0.0001	0.9	< 0.0001
Syn_XVII	0.5	< 0.0001	-0.1	**0.014**
Syn_XXX_GLB64471	-4.6	**< 0.0001**	-3.1	**< 0.0001**

Appendix Table S4.10. Contributions of different *Synechococcus* strains to sinking particulate matter (ST-150 m) relative to their contributions to the water column (ml: mixed layer) across the California Current System. Negative differences between proportions indicate that the relative abundance of a clade was higher in sinking particles than in the water column. The difference between the relative contributions was evaluated by pairwise comparisons using the Fisher exact. Clades with relative abundances significantly higher in sinking particles relative to their contributions in the mixed layer are highlighted in bold (FDR < 0.05). OO: oligotrophic offshore, CC: California Current, TZ: transition zone, IN: inshore.

	TZ		IN	
	WC-ml vs. ST-147m		WC-ml vs. ST-147m	
	Difference	p-value	Difference	p-value
Syn_CRD1	-0.1	**< 0.0001**	0.0	ns
Syn_CRD2	0.0	ns	0.0	ns
Syn_I_CC9311	-1.4	**< 0.0001**	-0.2	ns
Syn_I	-33.9	**< 0.0001**	-20.2	**< 0.0001**
Syn_II	0.0	ns	0.0	ns
Syn_III	0.0	ns	0.0	ns
Syn_IV_CC9902	0.2	ns	-0.7	0.001
Syn_IV_RHCU13	5.7	< 0.0001	1.6	< 0.0001
Syn_IV	32.6	< 0.0001	19.6	< 0.0001
Syn_MS2	0.0	ns	0.0	ns
Syn_UC_A	0.0	ns	0.0	ns
Syn_WPC1	0.0	ns	0.0	ns
Syn_XVII	0.0	ns	0.0	ns
Syn_XXX_GLB64471	-3.0	**< 0.0001**	0.0	ns

Appendix Table S4.10. Continued